Wax removal using pipeline pigs

Southgate, Jonathan

Wax Removal Using Pipeline Pigs

By

Jonathan Southgate

School of Engineering

University of Durham

A thesis submitted to the University of Durham

for the degree of Doctor of Philosophy

June 2004

ABSTRACT

The deposition of paraffin wax solids in pipelines and risers represents a continuing challenge to flow assurance in offshore installations. Wax deposits reduce product throughput, requiring increased energy expenditure to re-establish flow levels. In severe cases, wax deposits can completely block a pipeline. Preventative solutions to the problem such as pipeline insulation, active heating of pipes or chemical dosing with wax inhibitors are not always economically viable, so mechanical removal using a device known as a 'pig' remains an economical solution to the problem of wax removal. A pig is a cylindrical tool that is driven through the pipe by the flow of product, scraping deposits from the pipe wall as it travels.

Despite the importance of pipeline pigging to the oil and gas industry, the effectiveness of pigs in removing wax is poorly understood and it is this problem that is addressed by this thesis. One of the first necessities in undertaking this work has been to define the mechanical properties of wax deposits. This has required critical analysis of published material on the subject of wax deposition along with practical experimentation to create representative models of wax deposits that require mechanical removal from pipelines.

Previously, studies of wax removal using pigs have assumed the mechanics of the process to be adequately represented by uniaxial compression or simple shear load models. In this work wax removal is analysed using the orthogonal cutting model. This provides a more accurate description of the process as it includes the effect of material after yielding (the chip) on the net wax removal force. Experiments were designed to allow testing of the validity of the orthogonal cutting theory to the pigging process under a variety of conditions. An original contribution from this work is through experimental and theoretical results that are given context through comparison with established metal cutting theory. Through experimentation a *specific cutting energy* is obtained for wax removal. The results of the wax cutting experiments have identified particular differences between wax cutting and metal cutting regarding the homogeneity of chip formation. These observations have important implications in predicting wax removal forces using mechanical removal tools.

Although the affect of removed wax chips on pigging forces has been neglected in theory, it is well known in practice. The fluid used to drive cleaning pigs is often used to produce a jet radiating centrally from the front of the pig intended to blast wax chips away from the pig body, avoiding formation of a 'plug' of wax ahead of the pig. In this study a novel variation of this process in the form of an *annular* bypass jet is experimentally studied. A semi-empirical model of wax removal using an annular bypass jet has been developed and empirical constants obtained to allow prediction of removal rates for different waxes under various conditions. The new model introduced here allows balancing of pig velocity with wax removal velocity so that a non-contacting wax removal system is obtainable. The bypass-jetting model has been validated using a full-scale trial of the process by industrial sponsors.

To Abigail and Dolly.

ACKNOWLEDGEMENTS

I would like to sincerely thank Professor Ernest Appleton for his supervision, guidance and support.

I would like to thank the technical staff at Durham University, particularly Roger Little, for manufacturing the experimental rigs that made this research possible.

I would like to thank my sponsors, Pipeline Engineering Ltd, without whom I would not have had this opportunity.

Enormous gratitude to my wife, Vicki, for her steadfast support.

Finally, thanks to Bill and Joan for all their support over the years.

DECLARATION

This thesis is the result of my own work. No part of the thesis has been submitted for any other degree in this or any other University.

Jonathan Southgate
Durham
2004

TABLE OF CONTENTS

		Page
Title Page		**i**
Abstract		**ii**
Dedication		**iv**
Acknowledgements		**v**
Declaration		**vi**
Table of contents		**vii**
List of figures		**xii**
List of tables		**xvii**
Notation		**xviii**
Glossary		**xx**
Chapter 1	**Introduction**	**1**
1.1	**Background**	**1**
1.2	**Solutions to the problem of wax deposition**	**3**
1.21	Pipeline burial	**3**
1.22	Pipeline Insulation	**4**
1.23	Pipeline heating	**6**
1.24	Chemical treatment of wax deposition	**7**
1.25	Prevention of wax deposition through process design	**10**
1.26	Thermal remediation of wax deposits	**11**
1.27	Miscellaneous treatments for wax deposition	**12**
1.28	Pigging to remove wax deposits	**13**
1.3	**Objectives and methodology for proposed research**	**17**
Chapter 2	**Literature review**	**18**
2.1	**Wax Deposition**	**19**
2.2	**Wax removal using pipeline pigs**	**24**
2.3	**Review of Metal Cutting Theory**	**26**
2.4	**Jet Cutting**	**30**

2.5 Conclusions from Literature Survey 32

Chapter 3 Wax Deposition & Consolidation 33

3.1 The nature of crude oil 34

3.2 The nature of wax deposits 37

3.3 Wax deposition 39

3.31 Molecular diffusion 39

3.32 Brownian diffusion 40

3.33 Gravity settling 40

3.4 Effect of deposition process on the physical properties of wax deposits 41

3.5 Age hardening and consolidation of wax deposits 48

3.6 Laboratory testing of paraffin wax 50

3.61 Tri-axial compression test 50

3.61.1 Objectives of tri-axial compression test 50

3.61.2 Procedure for tri-axial compression test 50

3.61.3 Results of tri-axial compression test 52

3.62 Uni-axial consolidation test 54

3.62.1 Objectives of uni-axial consolidation test 54

3.62.2 Procedure for uni-axial consolidation experiment 55

3.62.3 Results of uni-axial consolidation experiment 55

3.63 Conclusions from consolidation tests 56

3.7 Wax model development 57

3.71 Tensile strength test for pure wax sample 58

3.72 Conclusions from tensile strength tests 63

3.73 Tensile strength test for solid wax/oil mixtures 64

3.74 Adhesion tests 67

3.75 Results and observations from adhesion tests 69

3.8 Conclusions 71

Chapter 4 Mechanical Removal 72

4.1 Introduction 72

4.2 Orthogonal cutting theory 78

4.3 Quasi-static orthogonal cutting tests 83

4.31 Purpose of quasi-static orthogonal cutting tests 83

4.32 Description of experiment 83

4.32.1 Equipment 83

4.32.2 Sample Preparation 85

4.32.3 Test Procedure 85

4.33 Results of quasi-static orthogonal cutting tests 87

4.33.1 Observed shear angle and comparison with metal cutting theory 87

4.33.2 Cutting forces and chip formation 90

4.33.3 Effect of tool rake and depth of cut 92

4.33.4 Chip formation 94

4.4 Second test series - Increased cutting speed 100

4.41 Introduction to increased cutting speed tests 100

4.42 Procedure for increased cutting speed tests 100

4.43 Results of increased cutting speed tests 103

4.44 Conclusions from increased cutting speed tests 106

4.5 High speed cutting tests –effect of strain rate on cutting forces 108

4.51 Introduction to high-speed cutting tests 108

4.52 Procedure for high-speed cutting tests 110

4.53 Results of high-speed cutting tests 112

4.54 Conclusions from high-speed cutting tests and discussion 116

4.6 Thermal imaging tests 119

4.61 Prediction of shear plane temperature using metal cutting theory 120

4.62 High-speed cutting test with thermal imaging 122

4.62.1 Equipment and experimental procedure 122

4.62.2 Results and conclusions from thermal imaging 124

4.7 **Conclusions from wax cutting experiments** 126

Chapter 5 Wax removal using annular bypass 128

5.1 Introduction 128

5.2 Existing jetting devices 131

5.3 Proposed jetting system for wax removal 134

5.4 Theoretical model of annular bypass jetting system 135

5.5 Experiment to verify annular bypass wax removal concept 144

5.51 Preparation of test pieces 144

5.52 Description of test rig for annular bypass experiment. 146

5.53 Test procedure for annular bypass tests 148

5.54 Results and observations from initial annular bypass tests 149

5.6 Plane strain jetting experiments 151

5.61 Objectives of plane strain jetting experiments 151

5.62 Description of plane strain jetting test rig 151

5.63 Plane strain jetting test procedure 155

5.64 Pre-test calibration for plane strain annular bypass jetting tests 157

5.65 Results of plane strain jetting tests 161

5.66 Observations from plane strain tests 169

5.7 Conclusions from annular bypass jetting tests 171

5.8 Computational Fluid Dynamics (CFD) 174

Chapter 6 Annular Bypass Pig Trials 178

6.1 Introduction 178

6.2 Equipment for annular bypass pig trials 179

6.3 Sample preparation 183

6.4 Test procedure for annular bypass pig trials 186

6.5 Results of annular bypass trials 189

6.6 Conclusions from annular bypass pig trials and discussion 198

Chapter 7	Conclusion	202
7.1	Evaluation of wax removal research	202
7.2	Limitations of research	204
7.3	Future work	205
References		209
Appendix A	Example of flow reduction due to wax deposition	218
Appendix B	Heat loss from a buried pipeline	221
Appendix C	Tabulated values obtained experimentally for the specific cutting energy of pure paraffin wax	224
Appendix D	High speed cutting rig - Drawings and Specifications	225
Appendix E	Trial test procedures (Commercial Document)	245
Appendix F	Pitot tube measurements	262
Appendix G	Intermittent annular bypass jetting concept	265
Appendix H	Data sheet for Shell Vitrea oil	268

LIST OF FIGURES

Figure 1.22.1	Pipe-in-pipe insulation system.	4
Figure 1.22.2	Graph illustrating finite increase in oil transport distance (δl) before wax precipitation for insulated pipelines.	5
Figure 1.28.1	Typical 'metal-bodied' cleaning pig.	15
Figure 1.28.2	Foam pigs.	16
Figure 2.31	Piispanen's idealised 'card-model' of the cutting process	26
Figure 2.32	Merchant's composite cutting force circle	27
Figure 2.33	Comparison of theoretical and experimental angle relationships for orthogonal metal cutting (Pugh, 1958)	28
Figure 3.21	Structural formula of paraffin (alkane) series	37
Figure 3.41	Deposition of solid particles of wax on a pipe wall	42
Figure 3.42	Wax deposition pattern predicted by multi-solid theory	43
Figure 3.43	Carbon number distribution for sample wax	46
Figure 3.44	Cooling curves for oil, wax and a wax in oil solution	47
Figure 3.61.2	General arrangement of a tri-axial frame in a load frame	51
Figure 3.61.3	General dimensions of 'consolidated' wax sample	52
Figure 3.61.4	Section through 'consolidated' wax sample	53
Figure 3.62.1	Consolidation test piston and 'cup' showing drainage pipe	54
Figure 3.71	Loading configuration for 'Brazil' test	60
Figure 3.73	Load vs. extension graph for various oil content wax samples tested using 'Brazil' test method	66
Figure 3.74	Adhesion test	68
Figure 3.75	Plot of maximum removal stresses for various oil content waxes	70
Figure 4.1	Petrobras' load model for wax removal	72
Figure 4.12	Typical force vs distance behaviour for wax removal during pigging (Wang & Sarica, 2001)	76
Figure 4.21	Schematic of orthogonal cutting operation	79

Figure 4.22	Pig removing wax from pipe wall	80
Figure 4.23	Piispanen's idealised model of the cutting process	80
Figure 4.24	Merchant's model of metal cutting	81
Figure 4.32.1	Plane strain cutting box	84
Figure 4.32.3	Arrangement of load cell and 'cutting box'	86
Figure 4.33.1	Observed shear angle during the cutting of wax with a neutral rake tool , 1mm depth of cut	88
Figure 4.33.2	Load vs displacement for 1mm deep cut, pure paraffin wax	91
Figure 4.33.3	Predicted and experimentally derived specific cutting energy values for positive, neutral and negative tool rakes	93
Figure 4.34.1	Comparison of wax chip formed during orthogonal cutting tests and titanium chip from Shaw, 1984	94
Figure 4.34.2	Paraffin wax cut at 1mm depth, neutral tool (back of chip)	95
Figure 4.34.3	Wax chips, 6mm depth of cut and illustration of chip formation by cracking	96
Figure 4.34.4	Comparison of wax chip formed during orthogonal cutting tests and polystyrene chip from Kobayashi, 1981	96
Figure 4.34.5	Plot of load vs displacement for wax cut with a 45 degree rake tool at a depth of 6mm	98
Figure 4.34.6	Comparison of surface area; orthogonal shear type chip and 'cracking' type chip	99
Figure 4.41.1	Frictional force vs tool displacement for wax cutting box	101
Figure 4.43.1	Wax cut at a depth of 6mm using a positive rake tool at a velocity of 8.3mm/sec	104
Figure 4.43.2	Specific cutting energy vs depth of cut using positive, neutral and negative rake tools	105
Figure 4.51.1	Graph of cutting pressure against cutting speed for mild steel (Boothroyd, 1965)	108
Figure 4.51.2	Graph of cutting force against speed for polyester resin (Kobayashi, 1981)	109
Figure 4.52	High speed orthogonal cutting rig	110
Figure 4.53.1	Photograph showing paraffin wax cut at 0.5 m/s using a positive rake tool at a depth of 5mm	112

Figure 4.53.2	Sample plot of amplified output from strain gauge 'A' (Horizontal orientation)	114
Figure 4.53.3	Graph of force against cutting speed for 2.5mm deep cut in pure , refined paraffin wax	115
Figure 4.54	Hodograph for orthogonal cutting	117
Figure 4.62.2	Thermal image of refined wax cut a depth of 5mm using a neutral rake tool at a speed of 0.5 m/s	125
Figure 5.1	Wax deposition rate plotted against oil flow rate, Hamouda (1995)	129
Figure 5.21	Conventional arrangement for bypass holes in pig seals	131
Figure 5.22	Rotating jetting nozzles (Shell Oil Company, 1999, US patent No. 5875803)	132
Figure 5.23	Pipeline pig using circumferential grooving to provide jetting (US patent No. 2003/0056309 A1,2001)	133
Figure 5.3	Proposed non-contacting annular bypass pig	134
Figure 5.41	Diagram showing pig within pipe	136
Figure 5.42	Wall jet	142
Figure 5.51	Casting apparatus for annular bypass wax removal tests	145
Figure 5.52	Test loop for annular bypass wax removal tests	147
Figure 5.53	Annular jetting test pig	148
Figure 5.54	Wax deposit failing under the action of annular jet	149
Figure 5.62.1	Plane strain rig	152
Figure 5.62.2	Wax sample plate and mould	153
Figure 5.62.3	Plane strain test rig	154
Figure 5.63.1	'Screen shot' from analysis using video capture/animation software	156
Figure 5.64.1	Experimental model for plane strain bypass tests	157
Figure 5.65.1	Length of wax removed (distance) plotted against time	162
Figure 5.65.2	Time plotted against length of wax removed (distance) for 5mm thick samples	163
Figure 5.65.3	Time plotted against length of wax removed (distance) for 30% wax samples.	164

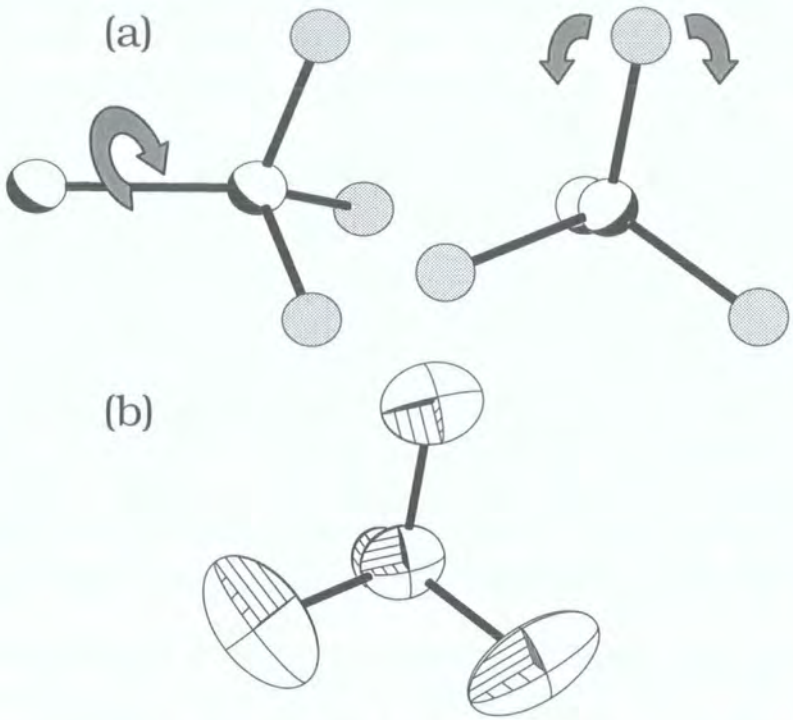

Figure 1.2-1 (a) A CF_3 group is expected to librate about the C-C bond. The result, (b), is large ADPs in the direction of circular motion about the C-C bond.

The simple one parameter model has been used to good effect to calculate [15, 16] force constants and potential barriers for the torsional motion of various groups. By assuming that the terminal group behaves as a simple harmonic oscillator, the barrier to rotation per mole, B, is related to the potential by:

$$V(\phi) = \frac{B(1-\cos n\phi)}{2} \qquad \text{Equation 1.2-6}$$

Where n is the periodicity and Φ is the librational amplitude. Providing Φ represents a small deviation from the equilibrium (i.e. $\Phi \approx 0$) and the potential

Figure 6.6	Plot of velocity against differential pressure across 12 inch pig for 30% wax sample at 5mm thick and 2mm annular gap	199
Figure 7.31	Pig and oil velocity as a function of pipeline diameter for a constant bypass velocity and annular gap	208

LIST OF TABLES

Table 3.71.2	Results of tensile and shear tests for sample wax	61
Table 3.72	Various material strengths	63
Table 5.64.2	Results from annular bypass calibration tests	158

NOTATION

A	area, m^2
b	width of cut in orthogonal cutting, m
C	specific heat capacity, J/(kg K)
C	constant, dimensionless
C	solute concentration, kg/m^3
C_c	coefficient of contraction, dimensionless
C_d	coefficient of discharge, dimensionless
C_D	coefficient of drag, dimensionless
D	diameter, m
E	Young's modulus, N/m^2
F	force, N
h	head, m
l	length, m
l_c	deformed chip length
l_a	*apparent* deformed chip length
L	Length, m
N	rotational speed, revs/s
P	pressure, N/m^2
Q	volumetric flow rate, m^3/s
r	radius, m
t	undeformed chip thickness (depth of cut in orthogonal cutting), m
t_c	deformed chip thickness
t_a	*apparent* deformed chip thickness
t	time, s
T	torque, Nm
T	temperature, K
u	specific cutting energy per unit volume, J/m^3
U	wall jet velocity, m/s
V	velocity, m/s
V	volume, m^3
x	distance, m
y	distance, m

z	distance, m
α	tool rake angle
β	friction angle
η	kinematic viscosity, m^2/s
μ	coefficient of friction, dimensionless
μ	dynamic viscosity, Ns/m^2
ρ	density, kg/m^3
σ	direct stress, N/m^2
τ	shear stress, N/m^2
ϕ	shear angle
ω	angular velocity, rads/s

Glossary of Terms

Asphaltene - Asphaltenes are complex, heavy hydrocarbon molecules and their definition is based on their solubility. Generally, Asphaltene is the component of crude oil that is insoluble in n-heptane or n-pentane and soluble in benzene/toluene.

Chip – Material removed from the workpiece by shearing.

Cloud Point – Temperature at which an oil/fuel begins to appear hazy on cooling due to the initial formation of wax (ASTM 2500-02. Standard test method for cloud point of petroleum products).

Congealing Point – defined by ASTM (American Society for the Testing of Materials) D938 as "the temperature at which molten petroleum wax, when allowed to cool under prescribed conditions, ceases to flow".

Flow Assurance - A multi-disciplinary activity concerned with maintaining the flow of oil & gas from reservoir to reception facilities. The term is thought to have originated with Petrobras in the early 1990s as 'Garantia de Fluxo', literally translated as 'Guarantee the Flow', or Flow Assurance.

Isomerism – the occurrence of two or more compounds with the same molecular formulae, but having one or more different physical or chemical properties (Wood and Holliday, 1968)

Melt Point - ASTM D87 defines this as the temperature at which most of a wax sample changes from a solid to a liquid.

Neutral (rake) – tool rake perpendicular to direction of cutting (i.e. 0° rake).

Pour Point - of an oil/fuel (as defined by the ASTM) is 3°c above the level at which the oil appears to be completely frozen, and ceases to move on tilting the container to the horizontal for 5 seconds.

Shear Angle – angle at which a thin *shear plane* is assumed to lay during orthogonal cutting.

Shear Plane - A plane assumed to separate the workpiece from the chip in orthogonal cutting along which plastic deformation occurs.

Specific Cutting Energy – the total energy per unit volume of material removed during orthogonal cutting (J/m^3).

Thrust Force – Force exerted on tool perpendicular to the direction of cutting.

Tubular Goods – The tubing and associated hardware that conduct oil or gas to the well-head at ground/sea-bed level.

WAT – Wax Appearance Temperature (sometimes WAP – Wax Appearance Point) is the temperature at which wax first starts to appear as oil is cooling.

Chapter 1 Introduction

1.1 Background

The oil and gas reserves in the North Sea are critical to the economy of the United Kingdom. Not only do they provide a net self-sufficiency in oil and gas production, Brooks (2001), but the technology and engineering excellence developed in their exploitation is a global export. The recent £300 million AMEC contract for the design and construction of production facilities destined for the Bonga field, Nigeria, testifies to this fact.

It is now 37 years since off-shore exploration commenced in the North Sea and the oil industry faces new challenges. Innovative technology is required to exploit undeveloped discoveries in the North Sea, representing some 2 billion BOE (barrels of oil equivalent) in total, [DTI 2001]. As these reserves are currently considered below the economic threshold, technology must provide greater production efficiency to make their recovery viable. Precedents do exist for such a transformation in economic feasibility. By way of example, the Captain field lay dormant for 20 years before technical innovation (Horizontal drilling) allowed economical exploitation of its viscous crude oil reserves. Further exploration of the UKCS (United Kingdom Continental Shelf) is likely to occur in the Atlantic Margin at challenging water depths, again demanding technical innovation and the offshore experience already gained in the North Sea.

A major issue in off-shore oil production is that of wax deposition within flow lines and risers. The causes of this phenomenon are well documented and are primarily related to temperature gradients through the pipe. The cooler temperatures encountered offshore exacerbate this phenomenon. The consequences of wax deposition are always

undesirable. At the very least reduced pipe diameter and increased surface roughness creates a larger pressure drop and reduced throughput; at the worst, wax deposits can be so severe that the pipe is blocked and production ceases completely. The maintenance of a profitable throughput is not the only incentive for removing wax deposits. Inspection of pipelines for integrity is more important than ever, especially where extending the life of existing infrastructure is a priority, as is the case in many sub-sea installations, Hopkins (2002). Here, the cleaning of pipes is an essential prerequisite for inspection using 'intelligent' pigs. Not only can wax deposits hinder inspection, they can also facilitate corrosion by trapping brine against the pipe wall.

An example is useful to illustrate the detrimental effect of wax deposition on flow through a pipeline. It is assumed that an operator is transporting crude from an offshore field to a reception facility on land. The pipe is 0.3m in diameter and is 50km long. Oil is to be transported at an average flow velocity of 3m/s, giving a volumetric flow rate of $0.212m^3/s$. The oil's density is $900kg/m^3$and dynamic viscosity is $0.05Ns/m^2$. The pipe is new, steel un-lined pipe, having a roughness value of 50 microns. Using Darcy's formula a total pressure loss of 16.2 Mpa along the pipe is calculated (see appendix A for calculation). At this pressure a 5mm wax deposit will reduce the volumetric flow rate to 0.195 m^3/s, a reduction of approximately 9%. Clearly, such a reduction in throughput could have a profound impact on the viability of a marginal production facility.

Not only does wax deposition have a direct effect on profit, it also impinges on production control. Continual reductions in pipe bore and resultant flow rates due to wax deposition necessitate the use of quasi-steady state models to predict process performance with an inevitable detriment to accuracy.

1.2 Solutions to the problem of wax deposition

A number of methods are used to tackle the problem of wax deposition. Some attempt to prevent wax from depositing and others are aimed at removing wax after it has deposited. In some cases prevention and remediation are both possible using the same method. Although this thesis will subsequently focus on removal of wax using pigs, a brief review of alternative solutions is important to set pigging in context.

1.21 Pipeline Burial

An effective method of preventing wax deposition is to ensure that the crude oil is kept above its Wax Appearance Temperature (WAT). This can be achieved by conserving the heat within the pipeline using insulation. The simplest way to insulate a steel pipe is to bury it. This ensures that a large thermal mass is available to slow the cooling of the oil as it progresses through the pipeline. A calculation for temperature loss from a buried pipeline, due to Dunstan [1938], is shown in Appendix B.

Factors that determine heat flow rate from a buried oil pipeline are the thermal conductivity of the soil and the pipeline burial depth. The benefits of burying a pipe diminish exponentially with depth and will be rapidly outweighed by cost. The thermal conductivity of soil varies enormously depending on its composition and water content. A dry soil is a much more effective insulator but is not available in the case of an offshore pipeline. On-shore, terrain will not always favour the burial of pipelines and this approach is therefore opportunistic from the operator's standpoint as well as being limited in efficacy.

1.22 Pipeline Insulation

Pipeline insulation offers advantages over burial as a means for conserving heat within the transported oil, though the governing physical principles are the same. Firstly, the cost and inflexibility of burial is negated. Secondly, heat flow rates are further reduced by the use of modern polymeric insulating materials.

Wet insulation coatings are polymer materials that are tough enough to be exposed to the environment and are often used in subsea pipelines. Polyurethane and Polypropylene foams used for these coatings have thermal conductivities as low as 0.16 W/m/K. Where possible, pipeline burial is used in conjunction with insulation to further reduce thermal conductivity.

Even more effective insulation is provided by *pipe- in-pipe* systems. With these systems a flowline is mounted concentrically in a carrier pipe. The annular space between the two is filled with insulating material [Figure 1.22.1]. As the material is not required to endure the harsh environments that wet coatings are exposed to, fibreglass wools can be used that offer thermal conductivities as low as 0.02 W/m/K.

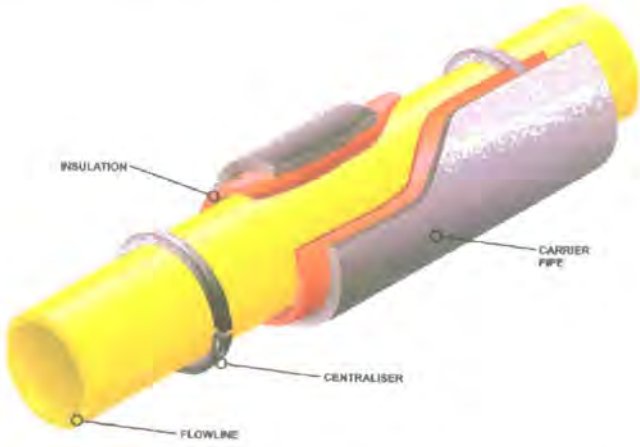

Figure 1.22.1. Pipe-in-pipe insulation system *courtesy of Technip-Coflexip*

The length of the pipeline limits the use of pipe insulation, in general terms. Without using an insulating material with *zero* thermal conductivity, oil flowing through a long insulated pipeline will eventually reach a temperature below its WAT. In this respect, insulating a pipeline merely moves the appearance of wax from one location to another further downstream. To illustrate this, Figure 1.22.2 shows theoretical oil temperature plotted against distance from wellhead for steel, dry and wet insulated pipelines. Although the gradient of the curves reduces in the case of the insulated pipelines, it can be seen that all of the curves eventually intersect the horizontal line representing the oil's WAT. Both types of insulated pipe are considerably more expensive than bare steel pipe and represent a large capital expenditure for operators.

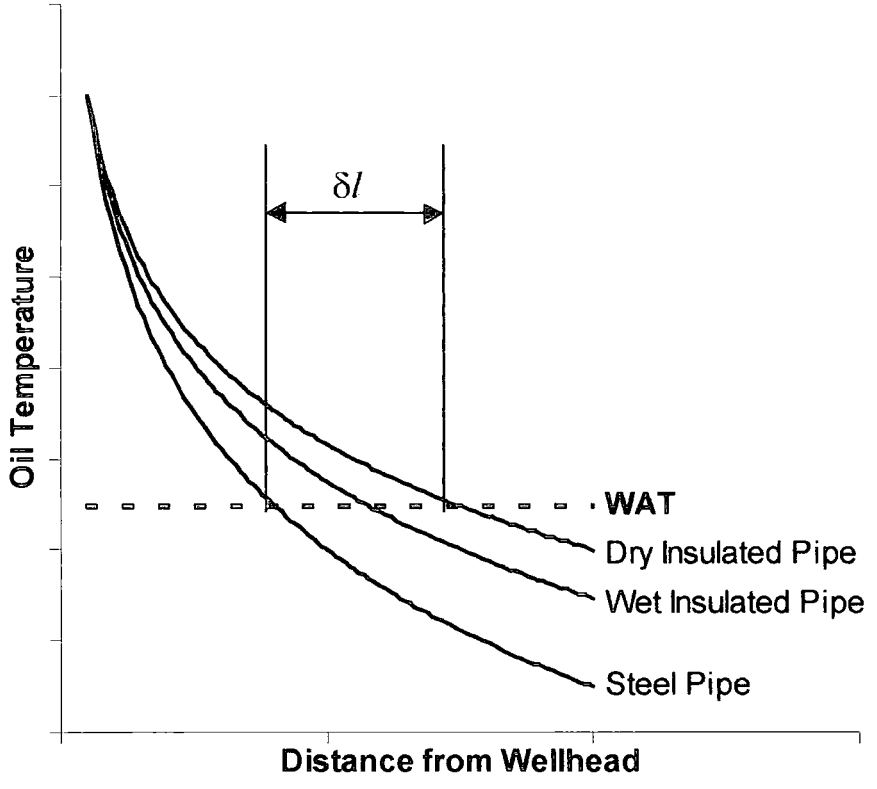

Figure 1.22.2. Graph illustrating finite increase in oil transport distance (δl) before wax precipitation for insulated pipes (author).

1.23 Heated Pipes

Heated pipes are generally of similar construction to the pipe-in-pipe systems previously described. Heat can be added to the pipeline by circulating hot fluid or by heating it with an electrical element. Hot fluid is circulated either through an annulus around the flowline or through pipes bundled in with the flowline within a 'multi-cored' pipe-in-pipe system. These active heating systems have distinct advantages over passive insulation. In the case of a passively insulated system, a transient state exists during start-up, where the thermal mass of the pipe system must be heated to the operating temperature by the oil itself. During this time deposition can occur due to the radial temperature gradient in the pipe. With an active heating system the pipeline can be brought up to temperature *before* flow commences and no deposition occurs.

Any waxes deposited during a shut down can be effectively 're-melted' on start up. The temperature of the heating fluid or element can be adjusted for seasonal variation. Theoretically, a heated flow line will allow the oil to remain above its WAT indefinitely.

The main disadvantage of heated pipelines over insulated pipelines is their greater cost owing to their increased complexity. The high capital expenditure required when installing heated pipes includes provision of plant for heating the fluid and pumping it through the pipeline. Also, unlike insulated pipelines, heated pipelines have an operating cost associated with the thermal energy required for the system.

1.24 Chemical treatment of wax deposition

A variety of chemicals are available to pipeline operators that are generally referred to as *Flow Improvers*. One group of chemicals that fit into this category are *wax inhibitors* or *Pour Point Depressants (PPDs)*. Wax inhibitors contain *crystal modifiers* that prevent the formation of large wax molecules by bonding to the wax crystal and hindering further growth. These polymers need to be added to the crude oil before the wax begins to crystallize but are not universally effective, Garcia (1998, 2000), Chanda et al (1998). Inhibitors must be matched to the composition of the crude oil, and as composition may vary from one well to another (even from the same reservoir) and will also vary over time, periodic sampling and testing is necessary to ensure the chemical's effectiveness. The problem is exacerbated where a number of wellheads feed into a common riser and process facility, as is often the case in offshore production.

Laboratory studies of the effectiveness of chemical inhibitors by the California Institute of Technology and Chevron Texaco revealed even greater concerns [Wang et al, 2003]. They found that in some instances the deposition of low molecular weight paraffins ($>C_{34}$) was reduced but the amount of high molecular weight paraffins actually *increased*. Given the general correlation between molecular weight and strength, this is a most undesirable outcome.

In one laboratory study a 'natural' inhibition of wax crystallization was observed. This was explained by a tendency for *asphaltenes* present in the crude to 'coat' wax nuclei and prevent further crystallization, Chanda [1988]. Asphaltenes themselves affect rheological behaviour of crude oil and Chanda also looked at the addition of solvents such as benzene and hexane to dissolve the asphaltene and act as flow improvers.

Whether flow was improved by the dissolution of asphaltene or by the fact that the addition of solvent produced a net reduction in viscosity is unclear. Because crystal modifiers are carried in aromatic solvents and suppliers recommend dosing of up to 2000 ppm (Parts Per Million) an ineffective crystal modifier may similarly be masked by the effect of its carrier fluid.

Aromatic hydrocarbons such as toluene and xylene are used, often remedially, to dissolve wax deposits. If they are used preventatively they are added to the crude to maintain the paraffins in solution. One criticism of solvent treatment, apart from the cost of the chemicals and time-consuming application, is their ineffectiveness in breaking down hardened deposits. Also, large amounts of solvents are required and, in an offshore setting, the storage of large quantities of aromatic hydrocarbons may pose problems, certainly given the stringent safety regulations in place for such facilities. Another caveat for offshore operators using flexible pipes is the fact that organic solvents can damage some rubber hoses.

Dispersants have a similar effect to crystal modifiers in that they prevent paraffin crystals binding to each other. One end of the dispersant molecule attaches to the paraffin and the other is soluble in oil or water. In this way wax molecules are dispersed and prevented from agglomerating. Sulfonates, alkyl phenyl derivatives and polyamides are all used to manufacture dispersants.

Other chemicals aimed more specifically at flow improvement are *Drag Reducing Agents* (DRA). The phenomenon on which DRAs are based was discovered some fifty years ago and can be more specifically described as *Polymer Induced Drag Reduction*, Toms (1949). These polymers have a specific action at the boundary layer. *Polymer*

Induced Drag Reduction can be defined as 'any modification to a turbulent fluid-flow system which results in a decrease in the normal rate of frictional energy loss and which leaves the resulting flow turbulent', Sellin (1982).

Not all inhibitors and flow improvers are supplied in liquid form. Some are waxy solids under normal conditions, and the method of application becomes an issue. Some are applied in solid, pellet form and are actually 'dropped' down the well, Valer Popp [1998]. More often, however, chemicals are injected in an aromatic solution, most effectively upstream of the deposition area, i.e. before crystallization occurs. They can be pumped in via an umbilical or 'batched' in using pigs.

Anecdotal evidence suggests that a combination of chemical and mechanical wax removal is usually employed at present, Hennessy [1999], providing confirmation that wax inhibition is not always completely effective, even once the most suitable chemical additive has been identified.

1.25 Prevention of wax deposition through process design

Sluggish movement of crude oil will tend to favour wax deposition in a pipeline, as there is little stress imposed on the incipient deposit by the flow of the oil, Hamouda [1995]. Correct design of a pipeline process, to maintain a minimum velocity will therefore help to avoid the problem of wax deposition.

Low friction internal pipe surfaces will also discourage deposition, if not precipitation, as wax crystals can only adhere to pipe walls if they have a sufficiently large coefficient of friction. However, polymer coatings intended to reduce friction at the pipe wall can be counter-productive if damaged. If these coatings become heavily scratched they can attract tenacious wax deposits, Jorda, [1966].

Transporting oil as an emulsion can have beneficial effects. Mixing the crude with a large quantity of water will lower its viscosity and improve flow. Also, precipitation tends to occur at the oil/water interface in an emulsion. These wax precipitates disperse less readily to the pipe wall and deposition is reduced, Li et al [1997]. A disadvantage of transporting crude oils with large water content is that the water must be removed, cleaned and disposed of or recycled at the process facility.

Some schools of thought suggest that it is quite futile to attempt to prevent the deposition of wax, Lawson [2002]. Rather, operators should seek to control when and where the deposition takes place. This has led to the proposal that wax should be deliberately precipitated from the oil by means of a large subsea intercooler and dealt with on the seabed. Although there are some very practical engineering problems to address, the concept of phase separation this close to the wellhead is very appealing.

1.26 Thermal remediation of wax deposits

In addition to using solvents, hot oils can be flushed into pipelines to remove wax. This method is almost exclusively employed where pigging is impossible in the tubular goods and manifolds at the wellhead. Although effective over short distances, this method has a definite disadvantage in terms of downtime and costs. More importantly, the hot oil will inevitably cool and the removed wax will be 're-deposited'.

The Nitrogen Generating System or SGN (after the original Portuguese expression 'Sistema Gerador de Nitrogenio'), developed by Petrobras, is a hybrid thermal/chemical method. This uses the localised mixing of 2 chemicals to produce an exothermic, effervescent reaction that removes deposits. Two nitrogen salt-containing aqueous solutions are mixed in the affected area of the pipeline to produce Nitrogen gas and heat. It is claimed by Petrobras in their promotional literature, that the process is environmentally friendly as the only by-products of the reaction are common salt and pure water (i.e. brine). In common with other chemical methods, however, a means of batching the 2 products into position and then mixing them is required. Delayed action chemical catalysts have been suggested to achieve the latter.

1.27 Miscellaneous treatments for wax deposition

Magnetic fluid conditioning (MFC) is said to alter the growth pattern of paraffin crystals and inhibit their adhesion to pipeline walls. In 1996, Deepstar[1] funded research at the University of Florida looking into the feasibility and science of using magnets to prevent paraffin blockage. The simple goal of this research was to determine if a magnet could be used to alter the cloud point of oil. The results of this research were inconclusive, although in tests the cloud point of a sample crude oil was lowered by 2°F.

A number of companies have recently started to offer microbial treatment of paraffin deposits. Proprietary brands such as *Oilzym*™ and *Para-Bac*™ are said to be bacteria that feed on Paraffins, breaking them down into smaller components. The bacteria are introduced at the wellhead and establish a living colony in the pipeline. Not only does this offer the potential of removing wax deposits, but also the possibility of a partial refinement that occurs while the crude is in transit. The claims of these manufacturers have yet to be fully tested.

[1] The DeepStar Project is a joint industry technology development project focused on developing technologies needed to drill and produce hydrocarbons in water depths of up to 3 km.

1.28 Pigging to remove wax deposits

The traditional answer to the problem of wax deposition has been to mechanically clean the pipeline using a *pig*. A pig is effectively a moving piston that is driven through the pipe by a pressure differential. During production the driving pressure for a cleaning pig is provided by the oil and the pig is *launched* near the well head and is driven to a *receiver* at or near the nearest downstream facility, a separator or storage facility for example.

In offshore situations, if a pig is to be launched from (near) the wellhead the operation must occur underwater. This requires divers and/or ROVs (Remotely Operated Vehicles) to load a pig into the launcher. Because such an operation is expensive, magazine style launchers have been developed that allow operators to load a number of pigs at one time to reduce costs. They still require periodic loading, however, and represent a considerable capital expenditure in themselves. It is more convenient to launch a pig from the rig and send it towards the wellhead. In this case production is suspended and fluid is pumped from the rig to drive a (bi-directional) pig to the wellhead. In this case a pipe loop is required for the fluid to travel back to the rig. This type of operation is generally referred to as TFL (Through Flow Line) pigging. As the pig travels through the pipeline it scrapes wax from the pipe wall. It is also possible to operate tools within a live pipeline using a 'wireline' or 'slickline', but these are generally used for working on the tubular goods at the wellhead.

The architecture of a modern pig is basically that of at least two seals either end of a mandrel giving a 'dumb bell' shape, as shown in figure 1.28.1. Where this central mandrel is steel the pig is termed *metal-bodied*. This configuration will often clean a

pipe quite effectively. To assist in wax removal many different tools and scrapers have been developed that can be attached to these metal bodied pigs. In this way, a thoughtfully designed pig can be a flexible tooling station and they have even been used to accommodate data logging devices and signallers.

Pigs can also be moulded in polyurethane foams of various densities. This type of pig is usually bullet shaped and, if a more aggressive cleaning operation is required, bristles or studs can be moulded into a hard gel coat (figure 1.28.2). Very hard deposits such as hard wax and scale require a very aggressive tool. This usually takes the form of a metal-bodied pig with tooling attached. Brushes, ploughs, scrapers and pin-wheels are all available to increase the effectiveness of metal-bodied pigs.

In its hundred year history the pigging process has changed very little, with the exception being the development of intelligent pigs for inspection. Because pigging is a 'blind' operation it is performed according to rules of thumb which have developed historically. These rules of thumb dictate pig design, pig speed and cleaning frequency. Caution is exercised in the process as over aggressive cleaning can remove too much deposit and *plug* the line, causing the pig to become stuck. Where a large build-up of wax is suspected a common approach is to pig the line using progressively harder foam pigs until the operator has sufficient confidence to introduce a full-bore metal-bodied pig.

The risk of plug formation can be reduced by introducing bypass through a pig. This is usually achieved by using a hollow mandrel or by placing holes in the pig seals or discs. Bypass has the effect of slowing the pig down and promoting a turbulent jet ahead of it to allow the removed deposits to be transported away in the bulk flow of the oil.

Currently, there is no scientific evidence to prove how effective bypass flow is in deterring plug formation, only field experience. For this reason, sizing and placement of bypass holes is largely intuitive on the part of manufacturers.

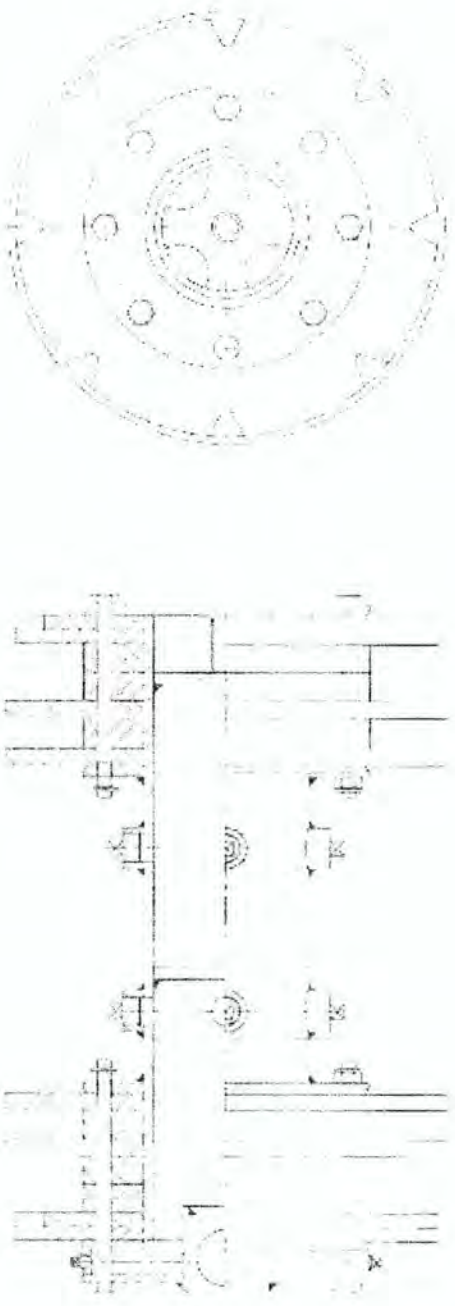

Figure 1.28.1. Typical 'metal-bodied' cleaning pig. *Courtesy of Pipeline Engineering Ltd*

Figure 1.28.2. Foam pigs. *Courtesy of Pipeline Engineering Ltd*

1.3 Objectives and methodology for proposed research

The primary objective of the research was to develop a deeper understanding of the mechanisms by which wax is removed by pipeline pigs. This was achieved by a combination of laboratory experimentation and detailed study of the existing work in this area. The second objective was to use this understanding to develop a semi-empirical model of wax removal that could be used to optimise the process and stimulate innovation. Further experimentation has allowed evaluation of proposed concepts and refinement of theoretical models.

The structure of this thesis is divided into three major parts. The previous introduction to pigging has been deliberately brief, as the relevant elements of pig design and function will be more fully introduced in subsequent chapters. One of the difficulties in developing a model of wax removal has been the definition of the deposited waxes, so chapter 3 concentrates on providing a better definition of these, based on extensive research of established theory on this topic. Chapters 4 and 5 examine mechanical and jet cutting methods respectively, evaluating their effectiveness in removing wax deposits.

It is intended that the research findings presented in this thesis will be used by the sponsors in their product development. Commercial application of one of the concepts described is already underway and chapter 6 describes field trials of a pig that employs an annular bypass concept as analysed in chapter 5. The findings from the mechanical removal experiments described in chapter 4 will be used to optimise tool design in the case of scrapers, discs and ploughs.

Chapter 2 Literature Review

Although there are few published studies of the pigging process itself, recent offshore driven interest in *Flow Assurance* has generated a large quantity of research into wax deposition. This work is reviewed here, and is discussed in more detail in Chapter 3. The more important milestones in the development of machining technology are reviewed to provide context to the subsequent analysis of mechanical wax removal. Literature is also identified that provides a theoretical framework for the analysis of the novel wall jetting technique described in chapter 6.

It should be noted that although published material describing research into pigging is scarce, this by no means implies that this is not a fertile area for research. The service provision market for the oil industry is a fiercely competitive one and publication of research findings is not always appropriate.

2.1 Wax Deposition

During the early years of the oil industry, easy profits meant that pipeline operators could afford to be ambivalent about wax deposition and there was little incentive to analyse the phenomena. Although the cooling of oil was, self evidently, the cause of wax deposition, there were few studies of the various parameters that control deposition rate and severity until mitigation of these deposits started to become prohibitively expensive, largely due to the move towards offshore oil recovery.

Most of the theoretical models underpinning studies of wax deposition are based on oil-wax equilibria and equations-of-state. Essentially, these models are semi-empirical and require experimental measurements of WAT (Wax Appearance Temperature) to allow their application to specific crude oils. Won [1989] considered wax to be a solid solution of hydrocarbons into which all components of the crude oil could enter. He based oil-wax phase equilibria on the cooling curves of simple hydrocarbon mixtures. Subsequent studies have shown this model to over predict wax deposition when tested against 'real' crude oil samples, Pedersen et al [1991]. Also, WAT obtained from stock tank oils (STO's) has been shown to vary considerably depending on measurement method, Hammami [1997]. This raises the possible danger of an over-predictive model calibrated using inaccurate WAT values.

Faroozibadi [1995] proposed that a more accurate model of wax deposition would take into account the range of solidification temperatures for different molecular weight waxes and suggested that they do not form a solid solution, but rather de-mix on solidification. This 'multi-solid' model for wax deposition was tested against the

more traditional solid-solution model by Coutinho [2002]. Although Coutinho acknowledged that a 'multi-solid' model was more realistic, the de-mixing of wax on solidification is supported by experimental evidence, he concluded that the solid-solution model's simplicity outweighed any limitations imposed by idealisation.

Regardless of how idealised solutions are based on phase equilibria, they cannot accurately predict deposition without considering the dynamic environment in which these phase changes occur. Not only must the thermodynamics of deposition be understood but also the *kinetics* of the process. To this end, experimental studies have analysed mechanisms of wax deposition in flowing pipelines. In a study by Burger et al [1981] a laboratory flow circuit was set up to allow cooling of oil as it was circulated through ½ inch pipes. From his observations and measurements of deposition rate Burger proposed mechanisms for deposition and identified controlling factors. The mechanisms for wax deposition he proposed were molecular diffusion, Brownian diffusion, gravity settling and shear dispersion. The controlling factors identified were radial temperature flux, the oil's WAT and the flow velocity and regime.

Burger's observations and theoretical predictions are confirmed by later experimental studies by, amongst others, Hamouda and Davidsen [1995] and Creek et al [1998]. All of these experimental studies observed that in addition to the controlling factors affecting deposition rate, they also affected the deposit's physical structure. In terms of removing wax, knowledge of the physical structure of the deposit is equally as important as predicting its deposition rate.

The mechanical properties of wax deposits are a function of the distribution of different molecular weight hydrocarbons and the amount of oil entrained within the wax's crystalline structure. Once a deposit establishes itself on a pipe wall these parameters change over time and *age hardening* takes place. This phenomenon is of particular interest, as imposing time dependency on the deposit's mechanical properties can have a profound impact on remediation issues such as pigging frequency.

Singh [2000, 2001] has performed a series of laboratory experiments to develop a model describing the aging and morphological changes in wax deposits. He proposed the existence of a critical carbon number within the wax-oil system above which wax molecules diffuse into the deposit and below which oil diffuses out into the bulk flow. The rate of this diffusion process is controlled by the radial temperature gradient within the deposit and the flow regime in the pipe. Also, in an experimental study, Cordoba and Schall [2001] provided confirmation of this theory, concluding from their own experiments that hardening of the wax deposit occurs due to solvent migration. Again, it is proposed that this solvent migration (or diffusion) occurs due to a temperature gradient between the cool pipe wall and the flowing oil.

A major problem researchers have encountered is full-scale validation of wax deposition models. This is ideally achieved by comparison of theoretical predictions with the results of field trials. Validation of deposition models is an important stage before integration into flow simulation packages such as OLGA[1]. One such attempt, described by Kleinhans [2000], exemplified this problem perfectly. In this study the

pressure required to drive a TFL (Through Flow Line) pig was monitored to allow measurement of wax removal forces. These forces were then used in a force balance equation to quantify the wax removed by the pig and this quantity compared with the thickness of the wax deposit predicted by theory. Kleinhans equated the wax removal force to the force driving the pig as follows,

$$\pi D_{pig}^2\left(\frac{\Delta P}{4}\right)=\left(D_{pipe}-D_{wax}\right)\pi D_{pig}L_{pig}\frac{S}{2} \qquad \textit{equation 2.1}$$

and wax thickness was calculated thus,

$$T_{wax}=\frac{\left(D_{pipe}-D_{wax}\right)}{2} \qquad \textit{equation 2.2}$$

Where,

D_{pipe}= Internal diameter of pipe.

D_{pig}= Diameter of pig.

D_{wax}= Inner diameter of wax deposit.

ΔP = Pressure differential across pig.

L_{pig} = Length of pig.

S = Shear strength *per unit length.*

T_{wax}= Thickness of wax deposit

Equations 2.1 and 2.2 can be combined as follows,

[1] OLGA 2000 is a computer simulation program for transient multiphase flow of oil, water and gas in wells and pipelines with process equipment.

$$\pi D_{pig}^2\left(\frac{\Delta P}{4}\right) = T_{wax}\pi D_{pig}L_{pig}S \qquad \textit{equation 2.3}$$

This equation can be simplified further to the following, where F_{pig} is the force acting to drive the pig through the pipeline,

$$F_{pig} = T_{wax}\pi D_{pig}L_{pig}S \qquad \textit{equation 2.4}$$

Although equation 2.4 is dimensionally correct, the physical model it describes is ambiguous. In the first case equation 2.4 might be interpreted as describing a resistive force due to the pig's contact area with the wax along its length (the term $\pi D_{pig}L_{pig}$). In this case, the resistive force would be independent of wax thickness and the equation incorrect. In the second case, the resistive force might be due to the cross sectional area of wax confronting the pig, described by the term $T_{wax}\pi D_{pig}$. In this case, the resistive force would be independent of the length of the pig. It is therefore the author's opinion that equation 2.4 is of no use in determining the thickness of wax deposits removed by a pig.

2.2 Wax removal using pipeline pigs

A recent study entitled 'The mechanics of wax removal' was carried out at Penn State University, [Wang and Sarica, 2001]. This study, sponsored by Deepstar, aimed to experimentally measure the effectiveness of established pig designs against deposits of varying thickness and consistency. Refined waxes and oils were blended and cast into a length of pipe to a desired thickness. Pigs were dragged through the pipe using a winch and the load was measured. Tests were carried out on metal-bodied pigs with a scraper disc and with cup seals only. A tapered foam pig was also tested.

The results of this parametric study showed that removal forces were affected by pig geometry, wax consistency and thickness. They also observed that the wax removal process was not steady state. Four distinct phases were identified as: compression of the wax, failure of the wax and plug formation, growth of the plug and decay of the plug. The fourth stage can be interpreted as an irrelevant transient imposed on the process by the limited scale of the laboratory rig and can be ignored.

Wang and Sarica provide no analysis of their results other than the observation that the variation in results due to the pig's shape indicates the possibility of tool optimisation using geometric parameters. The results also indicate a need to better understand the contribution of the removed wax to the net 'cutting force'. Both of these issues are addressed within this thesis.

Brazil's state owned oil company, Petrobras, have collaborated with the University of Rio de Janeiro to produce a predictive model of pig dynamics. It followed the premise

that pig motion could be evaluated as an equilibrium state between hydrodynamic driving forces and resistant forces generated by friction. By extension, the report included wax removal forces in the resistive component of the force balance. These resistive forces were modelled in isolation using FEA software and physical measurements taken of waxes reclaimed from subsea pipelines to provide values for deposit strength [Mendes et al, 1999].

The Petrobras model of wax removal, based on these assumptions, has some important limitations. Although this work aimed to create a dynamic model of pigging, the wax removal component of the model represents a transient state. It takes no account of the forces that accumulate due to friction as the wax flows along the tool face and accumulates to form a plug. In this respect, use of the model is likely to result in an under-estimation of resistive forces. Indeed, Mendes et al conclude that despite good qualitative agreement with field observations,

"... the numerous idealizations adopted should severely limit the accuracy of the predictions"

Again, this indicates a need to better understand the actual mechanisms by which the wax is removed from the pipe wall by the pig tool.

2.3 Review of Metal Cutting Theory

In this work, the orthogonal machining model has been used to analyse wax removal. As this model was developed to provide analysis of metal cutting a vast amount of material has been published on the topic. Metal cutting models take full account of the frictional forces produced by the removed chip and can address the limitations of the model described in the previous section. The following is a brief review of metal cutting theory, focusing on the more significant and fundamental developments over the latter half of the last century.

One of the earliest studies of the mechanics of the cutting process is by Ernst and Merchant [1941]. This work built on earlier studies that rejected the idea of a crack propagating ahead of a tool, as is seen when working wood, and proposed that the chip is produced by shearing. This concept is well illustrated by Piispanen's earlier 'card model' (Figure 2.31).

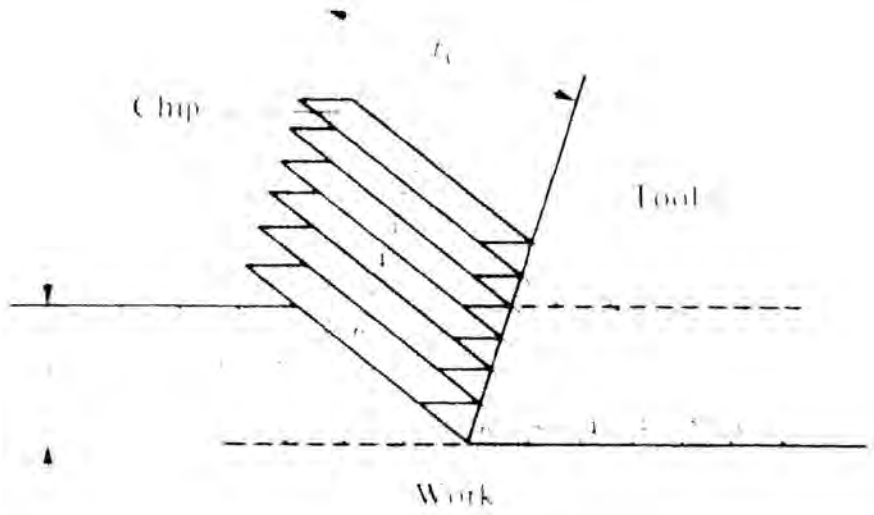

Figure 2.31 Piispanen's idealized 'card-model' of the cutting process.

By treating the chip as a free body and assuming a shear angle that gives a minimum energy requirement, Merchant produced the composite cutting force circle shown in figure 2.32. It resolves the forces at the shear zone (F_s) between the work-piece and chip and those at the chip's interface with the tool (F_c) into a resultant cutting force (R). This orthogonal model is highly idealised and requires a known shear angle or deformed chip thickness to allow prediction of forces. It takes no account of the affects of strain rate and assumes a perfectly sharp tool. The various parameters shown in figure 2.32 are not described here but are examined in more detail in chapter 4.

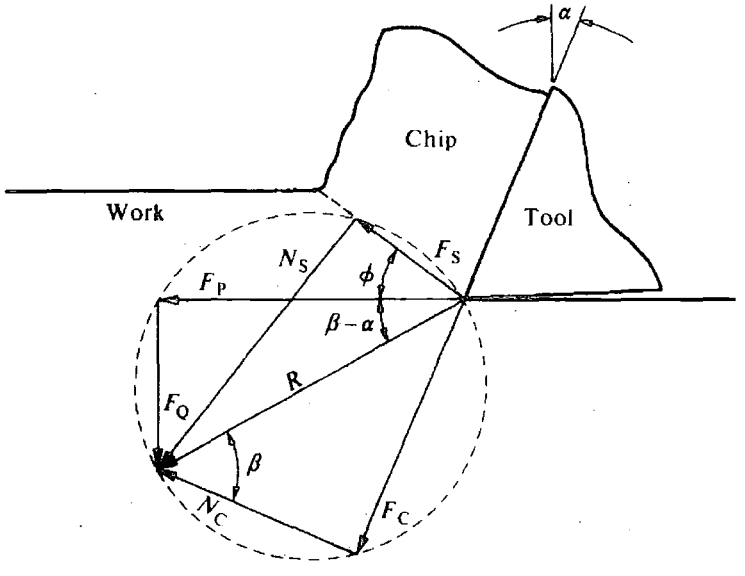

Figure 2.32. Merchant's composite cutting force circle (notation as used in Merchant's analysis).

Lee and Schaffer (1951) provided further refinement of the idealised orthogonal model. They applied plasticity theory to the problem of orthogonal cutting. By assuming the material to behave as a rigid-plastic material and constructing a slip-line

field between the primary shear zone, tool face and resultant chip, Lee and Shaffers' model more fully described the transfer of forces from the cutting tool to the shear plane.

Despite the limitations of both of the models described, Pugh (1958) demonstrated a qualitative agreement with experimental results [figure 2.3] and the models still form the basis of metal cutting analysis to this day. By way of example, modern Finite Element Analysis (FEA) techniques have recently been used explain the underestimation of the energy consumed in new surface formation [Atkins, 2002].

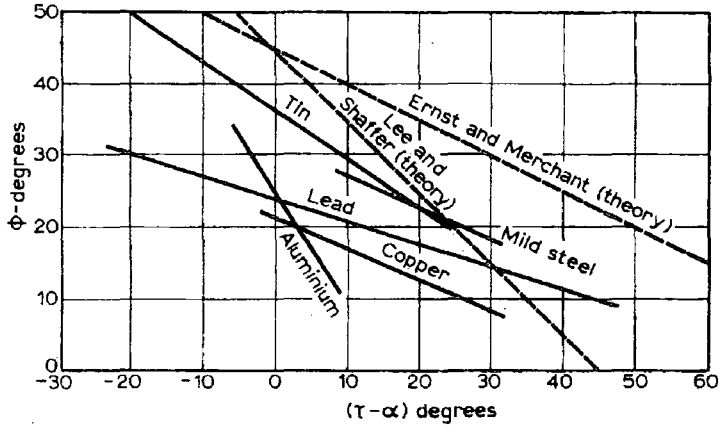

Figure 2.33. Comparison of theoretical and experimental angle relationships for orthogonal metal cutting (Pugh, 1958)

The models described in the previous section are based largely on texts that describe *metal* cutting. If the principles of metal cutting are to be used as a basis for understanding wax removal it is important to discern behaviour that is not common to both materials. Fang[2], at Nanjing University, has done some work in this area, although it was by nature rather incidental. Fang's interest was in simulating metal cutting using paraffin wax, purely from a practical standpoint, in that he proposed that

this method would allow the use of acrylic resins to manufacture cheap experimental tools for his research into chip formation.

Fang's experimental observations showed a similarity between chips produced when cutting steel and wax, using the same tool. However, he presents no theoretical explanations for his findings and describes the chip deformation mechanism of cutting paraffin wax as a 'completely unknown field'. In addition, the similarities that Fang found were under specific conditions, i.e. at specific cutting speeds and feed rates. For example, at high speeds, wax chips were subjected to what Fang described as a 'shock force' resulting in their fragmentation, unlike the steel chips produced.

Fang's findings serve to illustrate the necessarily empirical nature of machining theory. In his work, a simple 'scaling up' of wax cutting forces to represent the behaviour of steel when machined by tools of similar geometry was not possible. The fragmentation of wax during high-speed cutting suggests sensitivity to strain rate that is unique to the material. Rather than attempting to predict the behaviour of wax during machining based on its intrinsic properties, thorough experimentation is required that can mitigate the complex interactions that might be expected in a dynamic process such as machining.

2.4 Jet Cutting

The idea of using a wall jet to remove wax deposits stems from the fact that critical velocities are identified in many pipeline processes that will determine movement or settlement of solid phases. Studies into deposition identified minimum velocities that sheared off wax deposits before they became fully established, Hamouda [1995]. This observation is interpreted to mean that a flow velocity exists at which point the rate of removal due to fluid shear exceeds the rate of settlement of the wax. Although the processes of settlement and removal occur simultaneously and share common physical parameters it is expedient to examine the removal mechanism in isolation. In this way a model of wax removal can be formed that has application as a remedial process.

Examples of similar shearing processes can be found in other industries. In the water industry, settlement, removal and transport of solids (slime) are predicted by flow velocities at different points in a sewage system, Michelbach [1995]. This allows engineers to design sewage systems that are periodically self-cleaning by ensuring that increased flow velocities, for example during heavy rains, will remove settled debris and slime.

It should be noted that the process described in this thesis is distinct from the high-pressure jet cutting processes used in machining. These jets are delivered through fine bore nozzles at pressures of up to 1000 Bar and are often at supersonic velocities, Tikhomirov [1992]. To obtain such a pressure differential across a pipeline pig would

be impossible and the fine bore nozzles would be prone to blocking due to the extraneous matter present in crude oil.

The jetting process under consideration in this work uses an annular jet bypassing the pig to provide sufficient shear stress to remove soft wax deposits. The behaviour of such a jet has been described theoretically by Glauert [1956], and experimentally by Bakke [1957]. Excellent agreement was obtained between these theoretical and experimental studies and they provide a useful framework for subsequent analysis.

A 'jet' is a stream of fluid that is moving at a velocity greater than the surrounding fluid and interaction with a solid boundary will accelerate its decay due to the frictional resistance encountered. Glauert showed that the change in the velocity of the wall jet at a distance x from its origin could be expressed by simple power laws. It is this change in velocity at incremental distance from the jet's origin that is of interest as it will determine the shear stress at the pipe wall and the resulting removal rate of wax deposits.

2.5 Conclusions from Literature Survey

There is an abundance of published literature regarding wax deposition. An understanding of the deposition process must be gleaned from this material, not for the specific purpose of refining existing models, but in order to help define the physical nature of wax deposits.

To date, models of wax removal have been limited by their description of a transient state of material removal immediately prior to chip formation. Metal cutting theory is well established and can provide a simple model for mechanical removal that is one step more advanced than the existing pigging studies due to its dynamic nature.

While no work exists in the novel area of removing wax from the pipe wall with a fluid jet, the fundamental principles underlying such a process are well understood. The annular bypass system proposed utilises a wall jet, the behaviour of which has been described by Glauert and Bakke. Although it is possible to approximate jet velocity at axial positions in a pipe using such theory, the resultant stresses at the fluid/wax interface cannot be reliably predicted and an experimental approach is required. The provision of an empirical model of wax removal using a wall jet will be an original contribution to the pigging industry.

Chapter 3 Wax Deposition & Consolidation

Before exploring methods for the removal of wax deposits it is necessary to develop an understanding of their physical nature. Direct evidence of the nature of wax deposits is provided in the form of material retrieved from pig traps and filters during cleaning operations. In more extreme circumstances, pipe sections retrieved from abandoned facilities can provide material for examination. In a more predictive manner, the testing of crude oils for properties such as cloud point or WAT can yield information regarding the likely composition of wax deposits.

The prediction of wax deposition is an important task when planning oil transportation and a number of theoretical models are available to assist engineers to do so. Despite the apparent abundance of evidence, there is little convincing validation of these deposition theories. Quantitative proof of deposition is difficult to obtain, as removed deposits cannot be accurately measured. Even if it were possible to retrieve 100% of removed material, it cannot be guaranteed that this represents all of the available deposit as removal efficiencies for pigging operations are not certain. Nevertheless, the considerable research that has been carried out in this area has been used in this work to develop a qualitative understanding of the physical nature of the deposits encountered during pigging. The following chapter describes the development of a suitable model of a wax deposit for experimentation based on this understanding. Also described are some simple laboratory experiments that assisted in the development of the wax model.

3.1 The Nature of Crude Oil

The A.S.T.M. (American Society for Testing and Materials) define Crude oil as,

A naturally occurring mixture, consisting predominantly of hydrocarbons, and/or sulphur, nitrogen, and/or oxygen derivatives of hydrocarbons, which is removed from the earth in liquid state or is capable of being so removed.

Extraneous substances such as water, inorganic matter and gas often accompany crude oil but the removal of these alone does not alter the substance's status as *crude* [Dunstan, 1938]. It is worth noting that the A.S.T.M. describe crude oil as a *mixture.* In fact, a crude oil can exist as a mixture of mutually soluble hydrocarbons, or a suspension if prevailing conditions cause the precipitation of some constituents. It is often found mixed with water (brine) and existing as water in oil emulsion or oil in water emulsion.

Crude oil can be straw coloured, green, brown or black in appearance. Densities range between 0.75 g/ml and 0.97 g/ml and viscosities from 0.7 centipoises to over 42,000 centipoises. Crude oils generally behave in a Newtonian fashion but, some heavy viscous and waxy crude oils can be Non-Newtonian, behaving as 'Bingham Fluids'. Flow behaviour of crude oils will also alter from Newtonian to Non-Newtonian as solid precipitates appear, such as waxes or asphaltenes.

Crude oils were originally separated into three broad classifications, describing their 'base'; paraffin, intermediate or naphthene. Because of the complex nature of crude

oil the USBM (United States Bureau of Mines) refined this classification method in the 1930's by introducing the measurement of two 'key fractions' of the crude[2]. The first key fraction is the material that boils between 482 °F and 527 °F (250 °C and 275 °C). The second key fraction is the material that boils between 527 °F and 572 °F (275 °C and 300 °C). Following the test, the crude oil is named after the base of the first and second key fractions respectively. Also, if the cloud point of the second key fraction is above 5°F the term 'wax-bearing' is added and if the pour point is below 5°F, it is termed 'wax-free'. Hence, a crude oil that has paraffinic characteristics in its lighter ('gasoline') portion, intermediate characteristics in its heavier ('lube') portion and contains little wax is referred to as 'Paraffin-intermediate-wax-free'.

This information appears on Assay tests of crude oils, classifying their properties as feedstock for refineries. Other information that appears on these assay reports are sulphur content, viscosity, specific gravity and carbon residue. A crude oil's classification using this data will determine the type of products that can be extracted from it. Napthenic oils, for example, will generally yield better quality gasoline, while paraffinic oils produce good quality lubricating oils. Perhaps the most important property a crude oil possesses, in terms of wax deposition, is its cloud point or WAT; the temperature at which wax solids will start to appear in a sample of the oil. It should be noted, however, that as WAT is determined on a *static* laboratory sample, it is a property value that cannot be relied upon in isolation to predict wax deposition from a flowing crude oil.

[2] USBM, Report 3279 (September 1935)

The complex nature of crude oil means that during production and transportation a number of materials can be deposited in addition to waxes. Other deposits from crude oils include asphaltenes, diamondoid (adamantine), resins, sands and sediments. As an example, Valer Popp [1998] provides the following description of a deposit recovered from a Romanian oil field producing viscous, asphaltic oil,

"(The deposit consisted of) 40% by weight water and minerals and around 60% by weight organic mass, of which 50% paraffins, 17% resins and asphaltenes, the remainder being liquid hydrocarbons incorporated in the lattice."

Clearly, wax deposits do not always manifest themselves in isolation. Nevertheless, for the purpose of this experimental research, wax deposition is the focus of study. In most of the published work on deposition, wax has been considered in isolation to reduce the number of problem variables. Likewise, a model of solids removal must isolate wax to reduce problem variables. The interaction of other solid deposits with wax during removal must be considered as a separate matter, and one that can only be analysed once an understanding of the behaviour of the individual components is attained.

3.2 The nature of wax deposits

Wax deposits consist mainly of normal paraffins (or alkanes) having the chemical formula C_nH_{2n+2}. The term *paraffin* deposition is often used in place of *wax* deposition without changing the meaning. Structurally, paraffins consist of chains of carbon atoms with each of their spare valencies joined to hydrogen atoms, as illustrated by figure 3.21. As each valency is used to the greatest combining power, these hydrocarbons are said to be *saturated.*

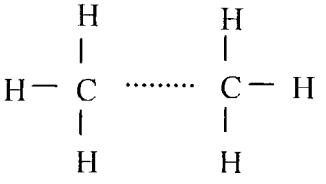

Figure 3.21. Structural formula of paraffin (alkane) series.

As the carbon number, and therefore molecular weight of the paraffins increase so do their boiling point and mechanical strength. In basic terms, this is attributable to the increase in the net attractive force between molecules as the number of atoms is increased. On this basis, deposits containing a greater quantity of HMW (High Molecular Weight) paraffins might be expected to offer greater resistance to pigging.

The relationship between molecular weight and mechanical strength is not quite as simple as might first be supposed from the foregoing discussion. With increasing carbon chain length in the paraffin molecule comes the increasing probability of *isomerism.* In the paraffin series, branched chain isomers exhibit different boiling points to their corresponding normal paraffins due to the greater compactness of the

molecules. These structural differences are used to differentiate the two main types of (refined) paraffin wax. *Macrocrystalline* waxes have an observable crystallinity on a macroscopic level and tend to behave visco-elastically. Microcrystalline waxes, sometimes referred to as *amorphous*, have no such order on a macroscopic level and can have profoundly different mechanical responses ranging from high ductility to extreme brittleness. Microcrystalline waxes contain more HMW iso-paraffins and macrocrystalline wax consists mainly of normal paraffins with carbon numbers up to approximately C40. In their refined form, they also contain more oil than macrocrystalline varieties.

The crystalline structure of waxes is not solely determined by chemical content. Cooling rate from the melt will affect the type and size of crystals present and, in turn, the mechanical properties of the solid wax. Rapid cooling tends to favour the formation of finer crystals with greater strength.

Clearly, if a wax deposit contains paraffins with lower carbon numbers (<40) it might be expected to behave like a macrocrystalline wax and if it predominantly consists of hydrocarbons with higher carbon numbers (>40) it might display the properties of a microcrystalline wax. However, this simple predictive method is complicated by the fact that the characteristics of a wax deposit are predominantly influenced by its oil content. Oil trapped in the crystalline wax matrix can represent up to 90% of the deposit by volume [Burger et al, 1981]. Oil content and carbon number distribution are influenced by a variety of factors and a description of the deposition process will facilitate a better understanding of these factors.

3.3 Wax Deposition

Most deposition theories describe the deposition of wax as a diffusion process, driven by a temperature gradient in the pipeline. However, no single theory can be applied to all production scenarios, with crude oil type, flow regime and environmental conditions determining which mechanism predominates, if any. Researchers most commonly identify the following mechanisms.

3.31 Molecular Diffusion

Molecular diffusion occurs if a radial temperature gradient in the pipe causes a simultaneous concentration gradient. This causes a movement of dissolved wax towards the cool pipe wall where precipitation and deposition occurs [Burger et al, 1981]. This diffusion can be described by Fick's Law,

$$J = -D\frac{(C_1 - C_2)}{(x_1 - x_2)} \qquad \textit{equation 3.31}$$

Where J is the rate of wax diffusion, x_1 and x_2 are two (radial) points in the flowing oil having concentrations of paraffin wax C_1 and C_2 respectively and D is a diffusion constant. It can be seen from equation 3.31 that if a large temperature gradient produces a large concentration gradient, deposition will be accelerated. It might be assumed therefore that this mechanism predominates in close proximity to the wellhead where heat from the oil is rapidly lost to the surrounding environment, particularly in the case of un-insulated subsea flow lines. Also, the temperature of the bulk flow of oil need never drop below its WAT for wax to diffuse in a radial direction and deposit on a cool pipe wall.

3.32 Brownian Diffusion

Brownian movement (or motion) is the random movement of suspended particles caused by collisions with molecules of the surrounding medium. This movement causes the diffusion of particles from areas of high concentration to areas of low concentration. In this sense it is a more generalized, macroscopic description of the molecular diffusion process previously described. In an oil pipeline, wax crystallizes heterogeneously when its temperature drops below its WAT (Wax Appearance Temp)[1]. This solid precipitate is transported to the pipe wall by Brownian diffusion. It might be assumed this mechanism will occur in long un-insulated flow lines where the oil has reached a state of thermal equilibrium with the outside environment. A temperature gradient is not essential as a concentration gradient is set up by the wax particles 'lost' by adhesion to the pipe wall.

3.33 Gravity Settling

With paraffin solids approaching neutral buoyancy and flow rates high relative to the settling velocities of particles, this mechanism has little effect on wax deposition and operators can expect to see a near uniform circumferential deposit of wax on pipe walls. In the case where other solid precipitates might provide nucleation sites for wax crystals this mechanism may have greater dominance due to an increase in the net relative density of these 'multi-component' particles.

[1] Note that solubility is also a function of pressure. WAT will rise with increasing pressure.

3.4 Effect of deposition process on properties of wax deposits

It can be seen from equation 3.31 that with some empirically derived coefficients for diffusivity it becomes possible to produce a mathematical model of wax deposition. Such a model might predict deposition in terms of mass per unit time but reveals nothing of the structure of the deposited wax. Perhaps of more interest than deposition rate, are the physical characteristics of deposited paraffins. Anecdotal evidence from pipeline operators suggests that wax deposits can have physical properties covering a broad range. At one end of this range are the light gels formed during shutdowns giving a crude the characteristic of a Bingham fluid during start up and at the other end of the spectrum are the hard, brittle deposits that have properties approaching those of man made polymers.

The entrainment of oil in a wax deposit might be explained by the primary deposition method. If the wax precipitates out and is diffused by Brownian motion to the pipe wall as a solid particle it will adhere to the existing immobile deposit randomly orientated. This will create an oil filled porous structure, as shown in figure 3.41. This is the hypothesis put forward by Burger et al [1981], and the author's observations during laboratory experimentation lend support to this theory.

Following this theory, deposits laid down by molecular diffusion can more intimately interlock and more oil will be excluded from the deposit. This would produce a much stronger deposit with its mechanical properties dominated by the molecular weight of the solid fraction. For a process of molecular diffusion to dominate a high temperature gradient and core temperature above the oil's WAT might be expected. This theory is

supported by Hamouda's [1995] research where a large temperature gradient produced a harder deposit.

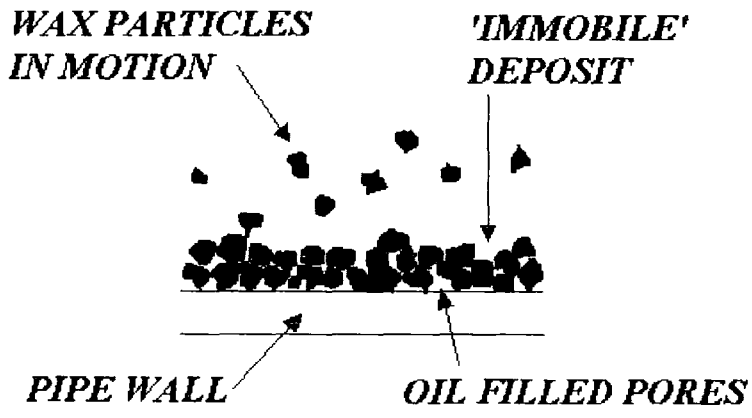

Figure 3.41 Deposition of solid particles of wax on pipe wall.

In instances where the nature of the solid fraction dominates the deposit's properties over and above oil content, the factors that determine molecular weight distribution are of prime importance. In order for high molecular weight paraffins to be deposited they must firstly exist as a component in the crude oil. Assuming that they do, two schools of thought exist regarding their deposition. If a solid solution theory is adopted, the solid that deposits will contain a mixture across the range of carbon numbers available and the deposit's properties will reflect this. If a multi-solid theory is used, the pipe's temperature will be a limiting factor for the carbon number available for deposition and the intrinsic properties of the deposit will vary with the axial temperature gradient of the pipe. In the latter case the high molecular weight hydrocarbons will deposit first, so a graduation from hard to soft wax might be expected through the length of the pipeline. If a temporal aspect is introduced, a pattern of wax deposition as shown in figure 3.42 might emerge. As insulation increases with deposit thickness, so the gradation will be offset by the extended conservation of heat at the pipe-wall.

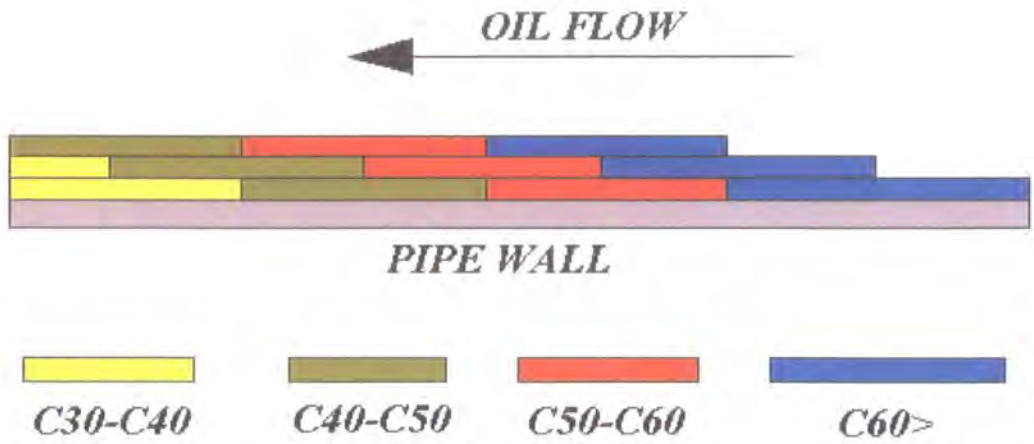

Figure 3.42. Wax deposition pattern predicted by multi-solid theory.

This concept provides another explanation for changes in deposit properties throughout thickness. Ultimately, a process such as this would produce a deposit with a hard, high molecular weight shell and a soft, low molecular weight substrate.

In order to test the multi-solid theory a simple laboratory test was conducted to see if individual components of wax would precipitate out at different temperatures as a sample of oil cooled. A sample of refined macrocrystalline paraffin wax was dissolved in hot paraffinic oil and the resultant liquid was left to cool in a glass beaker with the temperature monitored using a thermistor and data logger. If the cooling curve obtained showed a number of 'steps' or 'plateaus' it would indicate phase changes at different temperatures, confirming the multi-solid theory. The refined wax consists of a range of hydrocarbons from C21 to C47 distributed around a median of C26 (figure 3.43).

Figure 3.44 shows the cooling curves from these tests. Tests were conducted using pure oil and pure wax in order to provide a baseline for comparison with the wax in oil solution. Notice that the y-axis on these plots displays electrical resistance in

Ohms as a thermistor was used to monitor temperature changes. The curve showing the pure oil's temperature against time is a smooth one, as might be expected. As the pure wax cools, however, a step can be seen. This is due to the liquid-solid phase change that occurs at a constant temperature. As there is only one step on this curve it can be assumed that all of the wax solidifies at this single temperature. This indicates that all of the wax undergoes a phase change (solidifies) at the same temperature and the solid solution theory holds true under these circumstances.

It would appear then that if a multi-solid theory is true for real deposition in real pipes then solidification might not occur at discrete temperatures for individual species of wax. Rather, solidification might occur at different temperatures for *groups* of hydrocarbon species. In this sense, real deposition may produce a number of de-mixed solid solutions and the multi-solid model can be applied in the manner indicated by figure 3.42.

Researchers have also identified flow regime as a factor that influences deposition rate. In the case of turbulent flow, deposition is more rapid than in the case of laminar flow. This can be explained by the turbulent flow's radial velocity component accelerating transport of wax particles to the pipe-wall. Even in the case of high viscosity crude oil production, laminar flow can rarely be expected. Due to the relatively small bore of the flow line from a subsea wellhead, the modest flow rates sometimes encountered may allow the prediction of a low Reynolds number.

However, in these flow lines the transition from laminar to turbulent flow may be caused by a rough pipe surface, so general corrosion and aging of the pipeline is also a factor to consider. Moreover, in subsea flow-lines, regardless of flow regime, the large temperature gradients encountered as the oil emerges into the cool underwater environment will tend to cause high molecular diffusion rates. Crude oil flow will almost certainly be turbulent in the 'trunk' pipelines that transport the oil collected from a number of fields. In these large bore pipelines (For example, oil is transported to Phillip's Teeside receiving facility in a pipe approximately 1m in diameter) the large volumetric flow rate produces a high Reynolds number and turbulent flow can be expected.

For wax particles to adhere to a pipe wall, it might be assumed that a rough surface is necessary. This assumption was confirmed by Jorda [1966] in tests that involved the deposition of paraffin on a variety of materials and surface topographies under laboratory conditions. However, Jorda also found that paraffinic plastic coatings, regardless of their smoothness, attracted 'massive and extremely tenacious deposits. He attributed this to chemical bonding between the (like) materials.

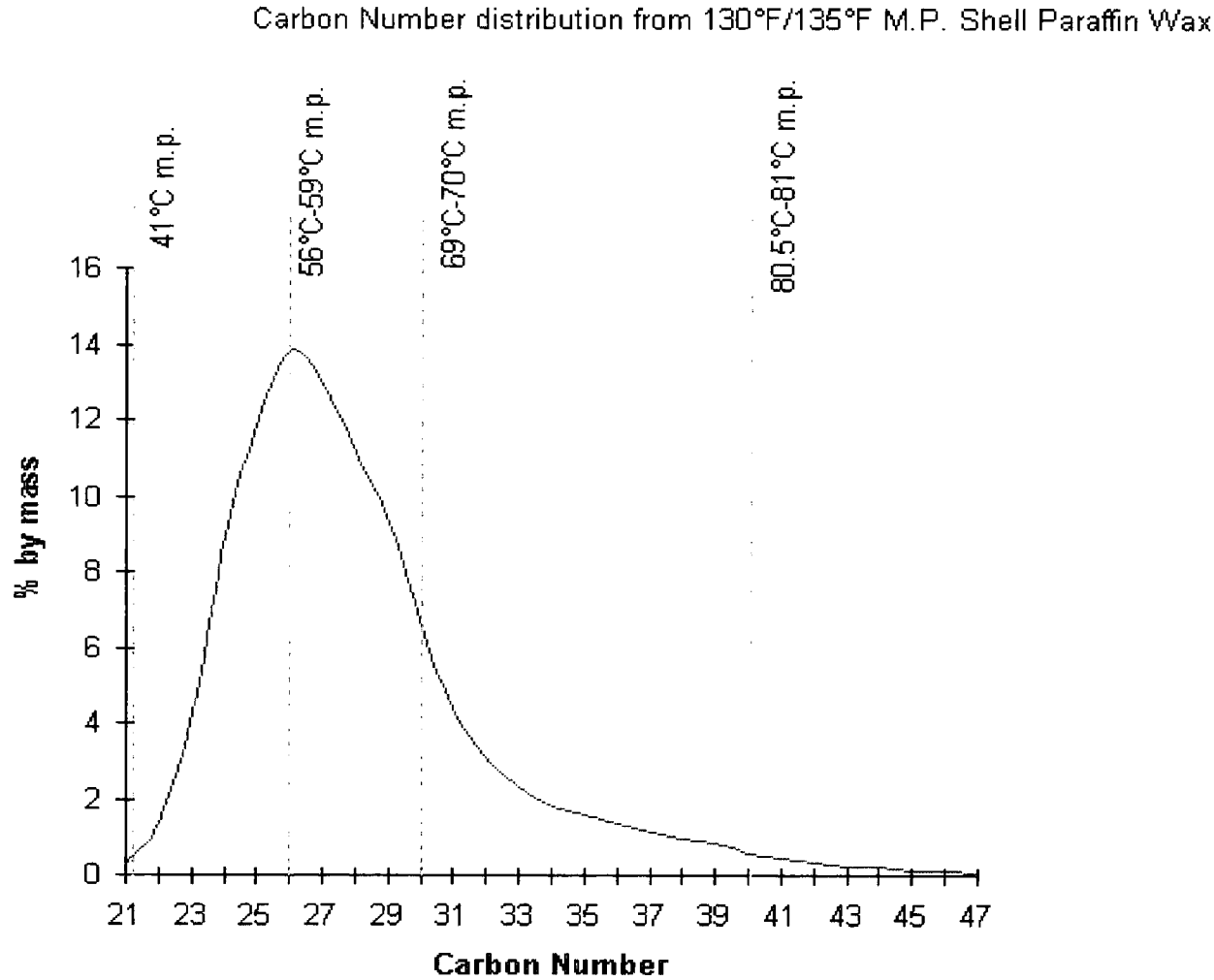

Figure 3.43 Carbon number distribution for sample wax

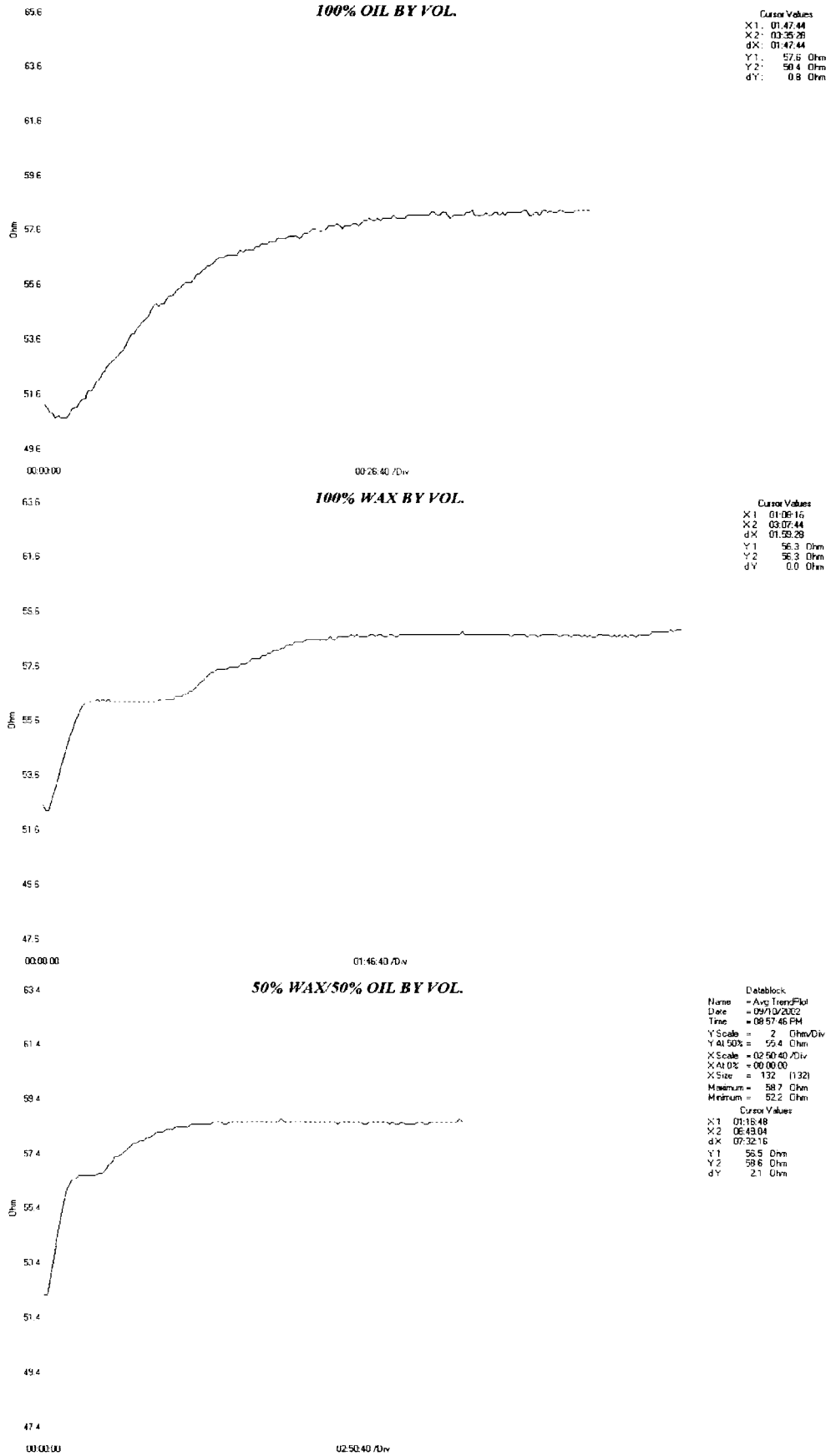

Figure 3.44. Cooling curves for oil, wax and a wax in oil solution.

3.5 Age Hardening and consolidation of wax deposits

Once a deposit has established itself on a pipe-wall, changes begin to occur that affect its physical structure. Age hardening will occur as oil is lost from the deposit and it increases in solidity. Singh [2000, 2001] and Cordoba and Schall [2001] explain decreasing oil content as a diffusive, thermodynamic process. They conclude from their own experiments that hardening of the wax deposit occurs due to solvent migration within the deposit due to a temperature gradient between the cool pipe wall and the flowing oil. In this way, the porosity of the wax is reduced and the average carbon number for its hydrocarbon content increases. However, it is proposed here that other, mechanical processes also contrive to reduce the deposit's oil content and increase its hardness. In qualitative terms, some evidential weight is provided for this hypothesis in the form of some simple laboratory experiments.

Under normal conditions, pores of oil formed in the immobile deposit will be at the same pressure as the flowing oil at any point in the pipe. There is no reason, in such circumstances, that the deposit should undergo any sort of consolidation, settling or compression due to the pressure of the fluid flowing in the pipe. If, however, a pipeline was shut down for some reason, maintenance for example, the pressure in the pipe may drop to a value near atmospheric. Isolated pores of oil within the wax will then rupture in order to obtain equilibrium with the rest of the fluid in the pipe. On restarting the pipeline, the suddenly pressurised fluid will then compress the porous deposit, forcing oil out towards the surface of the deposit. In this way successive shutdowns, if no cleaning is performed between them, will act to consolidate a wax

deposit until its oil content is negligible, or else the wax structure is able to support the pressure differential across it.

In addition to the methods of age hardening described, it is possible that an erosion process causes wax deposits to evolve in a Darwinist or 'survival of the fittest' manner. In such a process a cycle of deposition and shearing due to instability would leave only the strongest deposits adhered to the pipe wall. If such a mechanism occurred in parallel with the diffusive and mechanical processes already described, it might be expected to have a 'polishing' effect that might give the deposit a hard 'skin'.

3.6 Laboratory testing of paraffin wax

In order to investigate the possibility of pressure consolidation as a realistic mechanism for deposit hardening, two laboratory experiments were undertaken by the author.

3.61 Tri-axial Compression Test

3.61.1 Objectives of tri-axial compression test

The tri-axial compression test is most often employed in civil engineering to determine physical properties of soils, sands and clays. The pressure of fluid expelled from the sample (pore pressure) is usually measured, but in this test the objective was to allow free drainage of the sample's oil content to atmospheric pressure. The objective was to prove that the application of a hydrostatic pressure to the porous sample would 'squeeze' all of the oil from the sample pores.

3.61.2 Procedure for tri-axial compression test

In order to prepare a sample for the test a mixture of 50% Oil and 50% wax was heated to a temperature of 66°C ensuring that all of the wax was melted. The wax/oil mixture was then cast into a plastic mould with a steel base, ø100mm and height 100mm. Having cooled to room temperature (21 °C) the sample was transferred to a refrigerator and cooled overnight to allow easy ejection from the mould. The easy removal of the cooled specimen is attributable to the large coefficient of thermal expansion of wax. The sample was then tested in the apparatus shown in figure 3.61.2. A pressure of 7 bar was applied to the tri-axial cell for the duration of the test.

The wax sample was sheathed with a soft latex cover to prevent penetration of the sample with fluid. Liquid (in this case oil) removed from the sample was 'vented' to atmosphere through a drainage line. The sample was compressed vertically at a rate of 4.7mm (3/16 inch) per day for 7 days.

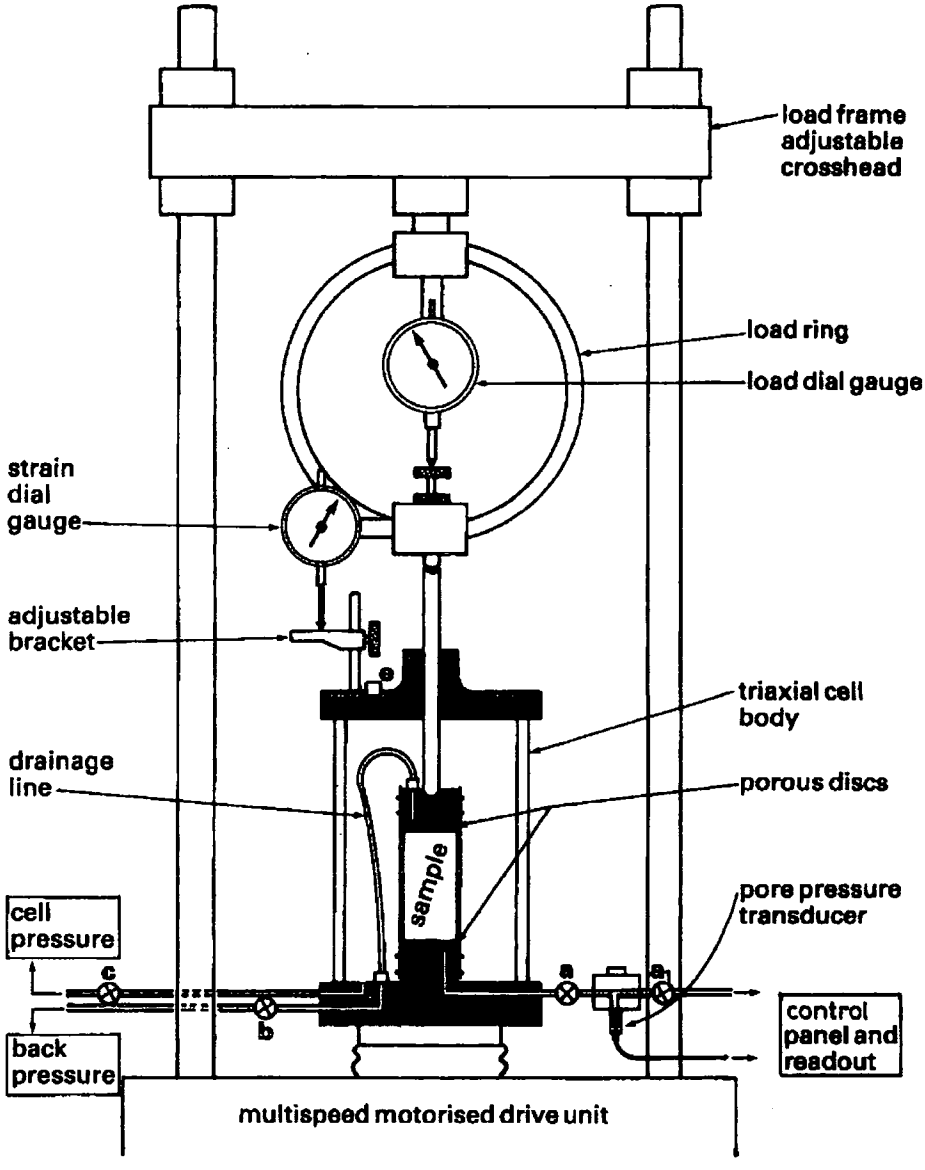

Figure 3.61.2. General arrangement of a tri-axial frame in load frame.

3.61.3 Results of tri-axial compression test

At the end of seven days the tri-axial cell was depressurised and the sample removed and measured. The approximate dimensions of the sample removed are shown in figure 3.61.3. These dimensions give a volume of 4.036×10^{-5} m^3, just over 51% of the original volume.

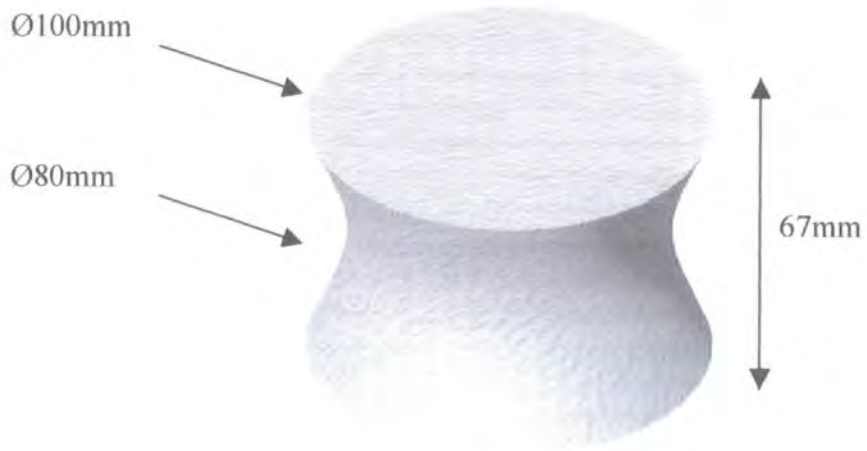

Figure 3.61.3. General dimensions of 'consolidated' wax sample

A sectional view of the actual sample is shown in figure 3.61.4. It can be seen that the edges of the material are more opaque than the centre, indicating less oil content. This was confirmed by tactile inspection of the sample, with the outer edges of the sample proving more brittle than the centre.

Figure 3.61.4. Section through 'consolidated' sample

3.62 Uni-axial consolidation test

3.62.1 Objectives of uni-axial compression test

Again, the objective of this test was to prove that the application of a hydrostatic pressure to the porous sample would 'squeeze' all of the oil from the sample's pores. In this case, the wax sample is higher in oil content and a piston and cup (cylinder) arrangement was used as illustrated in figure 3.62.1. With this arrangement the wax sample, even if it is a weak gel, is constrained by the steel cup which doubles as the sample mould.

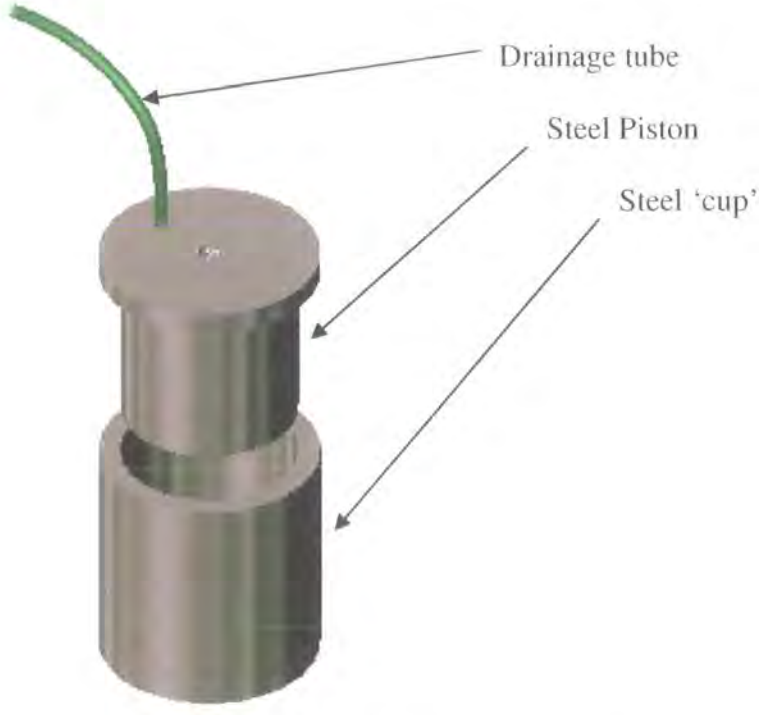

Figure 3.62.1 Consolidation test piston and 'cup' showing drainage tube.

3.62.2 Procedure for uni-axial compression test

The steel piston and cup assembly was designed and manufacture such that it would produce an effective seal to prevent oil bypass around the piston skirt, without generating large frictional forces on displacement of the piston. A wax sample with 75% oil by weight content was prepared by heating the wax and oil mixture until all of the wax had melted. The mixture was then cast into a steel cylinder and allowed to cool to room temperature (21°C). The flat-bottomed steel piston was lowered into the cylinder to allow compression of the wax sample. A hole drilled through the piston allowed any oil to drain out. A thin layer of gauze prevented occlusion of the drainage hole.

Initially, the sample was allowed to settle overnight with only the weight of the piston acting on the sample. The piston was then loaded daily in increments of 25 kg. On the fifth day with a weight of 100kg acting on the piston, all (75g) of the oil had been recovered and the sample was removed.

3.62.3 Results of uni-axial compression test.

The oil recovered from the test, though apparently pure and clear, contained some dissolved wax. This became evident when the oil was allowed to cool below room temperature and clouding was observed. Also, the solid tablet of wax produced by the test had a hard skin and a softer, oilier, core.

3.63 Conclusions from consolidation tests

In both tests the wax samples could be separated into their two base components by the application of pressure. The fact that most of the wax could be recovered by mechanical separation lends support to the 'solid-solution theory' described in section 3.4. Conversely, the clouding of the recovered oil on cooling suggests the retention of some wax in solution, so some agreement is also found with the multi-solid theory. More importantly, the results of the test prove that the hardening of wax deposits due to a reduction in oil content is not only due to a thermodynamic process. Consolidation of the deposit due to the fluid pressure in the pipeline may also occur, provided fluctuations in pipeline pressure occur that produce a pressure differential at the deposit/oil interface.

3.7 Wax model development

It is evident from the foregoing chapter that operators might expect to encounter any number of different wax deposits in different production facilities. Although the exact nature of the deposit can only be discovered by sampling, a qualitative prediction of its physical characteristics might be made with some knowledge of the crude's assay properties and some basic production parameters. For the purpose of the research described in this thesis it has been important to identify a suitable wax or range of waxes that are physically, if not chemically, representative of those encountered in real pipe lines. Operators' physical descriptions of deposits compare them to 'Swarfega' at one end of the spectrum, through to 'boot-polish' and at the other end of the spectrum, 'candle wax'.

As the physical properties of a wax deposit are dominated by its oil content, percentage oil content has been used as a variable in the wax model for experimentation. The oil used is a highly refined 'white' lubricating oil (Shell Vitrea 22). A data sheet for this oil can be found in appendix H. This oil contains no additives such as detergents that might cause unwanted interactions. It is also non-toxic and safe to handle, an important consideration for the experiments undertaken.

The solid fraction of the wax deposit has been represented by a 130/135 °F melting point refined paraffin wax. As it has been fully refined, it has no more than 0.2% by weight of oil content. This macrocrystalline wax is of the type used to manufacture candles and, in its pure form, is used to represent the 'hardest' deposits encountered in

a pipeline. Oil was added in 25% (by weight) increments down to a mixture of 25% wax and 75% oil representing the softer, incipient deposits.

The analogous descriptions of the wax models' physical properties are, on first impression, rather unscientific. Undoubtedly, research and development could proceed in a more systematic and convenient manner if a standard test was available with which to describe a wax. A standard test for hardness does exist for waxes, a needle penetration test described in ASTM D 1321. Such an empirical test is of limited value when making comparisons of wax removal operations with other processes. Of more use are the material's shear and tensile strengths. There follows a description of tests performed on the model wax to obtain values for tensile and shear strengths.

3.71 Tensile strength tests for pure wax samples

A conventional tensile test of the material placing a sample in uniaxial tension would have proved difficult as the relatively weak material could not be readily gripped in the jaws of a tensile testing machine. For this reason the following tests were used to obtain tensile and shear strengths for the pure wax sample. As each test is a standard procedure in civil engineering, only a brief description is provided.

Firstly, a diametrical compression test was used. This test is sometimes referred to as a 'brazil' test and is commonly used in determining the tensile strength of rock or concrete (British Standards Institute, 1983). It allowed the use of a conveniently cast wax sample. In this test a circular disc of material is compressed until it fails (or

'splits') across its vertical diameter due to a uniformly induced *tensile* stress. A tensile strength is then obtained using the following formula,

$$\sigma = \frac{2F}{\pi LD} \qquad \textit{equation 3.71}$$

Where,

σ = Tensile stress in horizontal plane

F = Force in vertical plane

L = Length of sample

D = Diameter of sample

The loading configuration for this test is shown in figure 3.71. Test samples should have a diameter to length ratio of 2:1. Two different sample sizes were tested. The wax sample split cleanly along its vertical diameter, suggesting the material was sufficiently brittle for the test to be appropriate.

A Modulus of Rupture (MOR) test was also used to determine a flexural strength of the wax. In this test, the same loading frame is employed, as in the Brazil test, but the load is applied centrally to a beam of material in order to derive the effective stress from simple bending theory.

Lastly, a direct shear test was performed. This test confines a sample within a square cross-section box, split horizontally at mid-height. The two halves of the box move relative to one another until failure occurs giving the shear stress of the material. The test is actually for soils, and other considerations are; clearance between the box halves, a normal load to compress soils etc. Nevertheless, a wax sample placed in the

box will be subjected to a shearing force, and the load at failure and cross sectional area can be used to calculate the ultimate shear stress value for the material. The results of the various tests described are shown in table 3.71.2

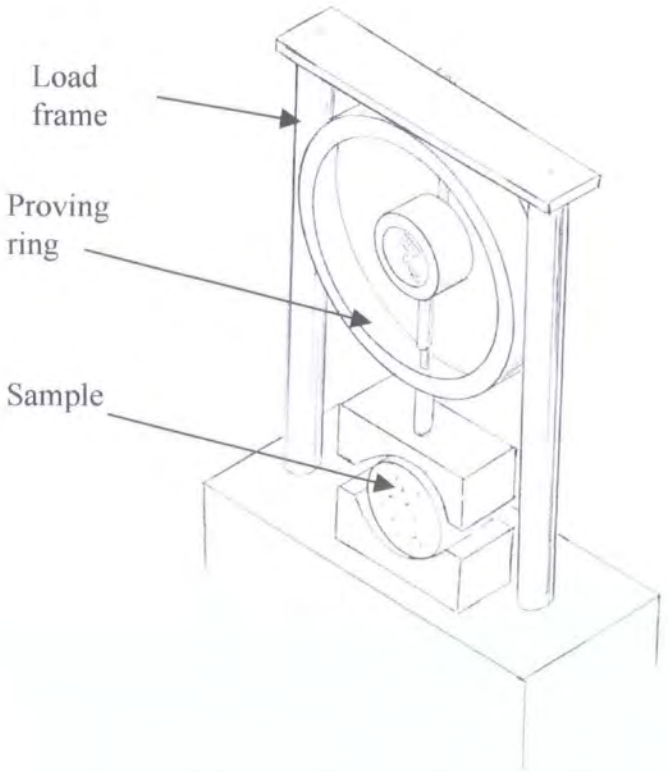

Figure 3.71. Loading configuration for Brazil test.

In order to make useful comparisons of the results of both tensile and direct shear tests, Tresca yield criterion can be applied, Edwards & Endean [1990]. The Tresca yield criterion is based on the assumption that yielding of a material occurs when the maximum shear stress reaches a critical value. In a general triaxial stress system, the magnitude of the largest maximum shear stress, τ_2, is given by,

$$\tau_2 = \frac{\sigma_1 - \sigma_3}{2} \qquad \textit{equation 3.72}$$

where σ_1 is the greatest principal stress and σ_3 is the smallest. For a tensile test, $\sigma_2 = \sigma_3 = 0$, therefore the ultimate tensile strength σ_u and maximum (critical) shear stress, τ_c, are related by the following equation,

$$\tau_c = \frac{\sigma_1 - 0}{2} = \frac{\sigma_U}{2} \qquad \textit{equation 3.73}$$

Test	Sample dimensions (mm)	Failure Stress	τ_y (Tresca)	τ_y (von Mises)
Brazil	∅50 x 25	0.676 MPa	0.338 Mpa	0.39 Mpa
Brazil	∅50 x 25	0.596 MPa	0.298 Mpa	0.344 Mpa
Brazil	∅100 x 50	0.422 MPa	0.211 Mpa	0.24 Mpa
MOR	∅26 x 100	2.21 MPa	-	-
MOR	∅26 x 100	2.47 MPa	-	-
Direct *Shear*	60x60x20	0.208 MPa	-	-
Direct *Shear*	60x60x20	0.202 MPa	-	-
Direct *Shear*	60x60x20	0.341 MPa	-	-
Shell Method	Not known (value from data sheet)	1.472 MPa	-	-

Table 3.71.2. Results of tensile and shear tests for sample wax.

An alternative analysis can be made using von Mises yield criterion, Kinloch and Young [1988]. The von Mises criterion states that yielding of a material will occur when,

$$(\sigma_1 - \sigma_2)^2 + (\sigma_2 - \sigma_3)^2 + (\sigma_3 - \sigma_1)^2 = 6\tau_y^2 \qquad \textit{equation 3.74}$$

Again, assuming the case of a tensile test where $\sigma_2 = \sigma_3 = 0$, equation 3.74 can be rewritten to give a value for a yield shear stress, τ_y, as follows,

$$\tau = \sqrt{\frac{\sigma^2}{3}} \qquad \textit{equation 3.75}$$

Both yield criterion have been used to obtain a value for the yield shear stress, τ_y, from the results of the tensile splitting tests and the results are shown in table 3.71.2. The mean average yield shear stress predicted from these results using the Tresca yield criterion and the von Mises yield criterion are $\tau_y = 0.28$ Mpa and $\tau_y = 0.32$ Mpa respectively. The mean average yield shear stress predicted using the Tresca yield criterion ($\tau_y = 0.28$ Mpa) is nearest to the actual mean average shear stress obtained in the direct shear tests ($\tau_y = 0.25$ Mpa) and the Tresca yield criterion is therefore used in subsequent analysis.

The results from the modulus of rupture (MOR) tests bear an empirical relationship with ultimate tensile strength of materials obtained using the 'Brazil' test. For example, in laboratory tests, the ultimate tensile strengths of riverbed gravel and crushed limestone have been shown to be 5/8 and 2/3 of their respective flexural strengths, Grieb and Werner [1962]. Using the results of the tensile splitting shown in table 3.71.2, the average tensile strength is 1/4 of the average flexural strength obtained by MOR test.

3.72 Conclusions from tensile strength tests

The difference between the ultimate tensile stress values from the Brazil test and the flexural strengths obtained by the MOR test is greater than that normally encountered if testing civil engineering materials such as rock and concrete. This apparent anomaly may be due to the casting method used for producing the wax samples. All of the samples were prepared by casting of the melted wax into cylinders. The 'Brazil' test used a plastic mould and the MOR test, a copper one. Rapid cooling of the wax in the MOR's thinner and more conductive mould meant that a wax sample with finer grain structure and enhanced mechanical properties may have been produced. This highlights the profound effect of cooling rates and crystal structure on the properties of waxes.

As the purpose of this testing has been to obtain a qualitative impression of the behaviour of wax, the range of the results is useful, and the mean average for the ultimate tensile strength of 1.3 MPa will be used in subsequent calculations. To put this value into context it is worth comparing it with that of a few familiar engineering materials (table 3.72). The materials properties are contrasted here against engineering materials, as data for these is readily available.

Material	Tensile strength
Paraffin wax	1.3 MPa
Polypropylene	27 MPa
Acrylic	74 MPa
Mild Steel	430 MPa

Table 3.72. Various material strengths

3.73 Tensile strength test for wax/oil mixtures

In order to determine the effect of oil content on the mechanical properties of the model wax deposit, the 'Brazil' test described in the previous section was repeated on samples containing varying percentages of oil. The results can be seen in figure 3.73 in the form of a load versus displacement graph. These tests were all performed at a crosshead speed of 2mm/min and the effects of strain rate are ignored. It can be seen from this plot that the *pure* wax sample behaves in a brittle manner, a prominent peak indicating the limit of proportionality and coinciding with failure of the sample. The apparent plastic deformation is exaggerated by contact of the two (broken) halves of the sample contacting the compression platens. As oil is added, however, the sample becomes more ductile. At 50% wax, the sample requires very little force before it begins to flow, with no discernible elastic response. There is no tensile failure and the wax/oil mixture appears to behave rather like a 'Bingham' fluid. As the wax samples with appreciable oil content do not behave in a brittle fashion, equation 3.71 no longer describes the stress state at failure. However, the presentation of the load versus displacement graph in figure 3.73 qualitatively demonstrates the ductile nature of these samples.

The fact that the behaviour of waxes with different oil contents varies not only in terms of ultimate tensile strength, but also in the nature of their visco-elastic response, has a profound impact on remediation issues and on the conduct of research. If no single model of wax failure can be used to describe the mechanical removal of wax, then it is unlikely that a universally applicable removal method can be found. This is acknowledged by the subsequent structure of the research described in this thesis.

Wax removal methods are consequently divided into mechanical and fluid jet removal systems for hard and softer (higher oil content) waxes respectively.

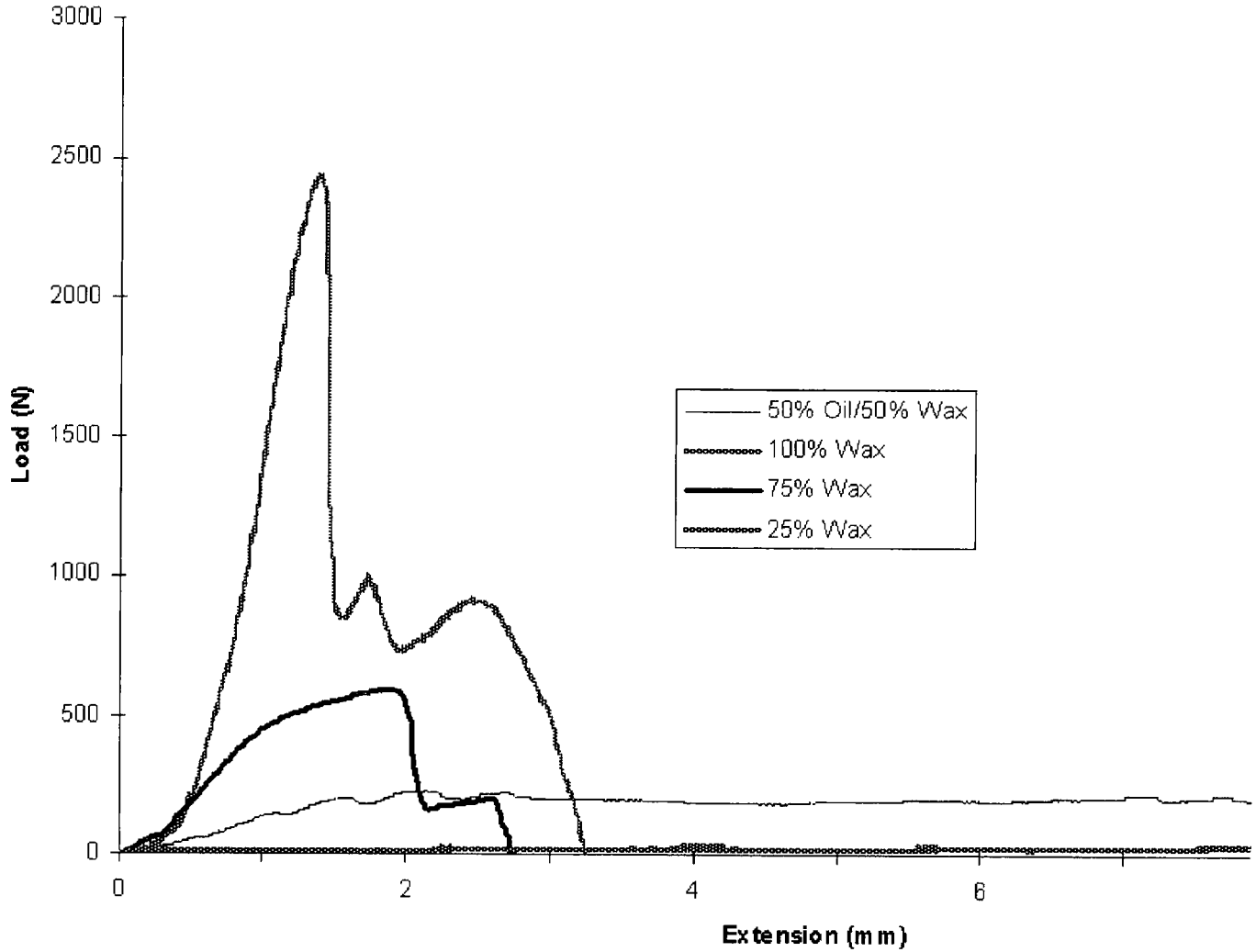

Figure 3.73. Load vs. extension graph for various oil content wax samples tested using the 'Brazil' test method.

3.74 Adhesion Tests

The cohesive strength of sample wax deposits is of little consequence if they do not adhere well to the pipe wall. Field reports suggest that wax deposits' adhesive strength is at least equal to their cohesive strength and they cling tenaciously to the pipe wall. When casting pure macrocrystalline wax onto a steel pipe wall under laboratory conditions, however, this is not the case. The wax adheres so poorly to the steel that a negligible force is required to cause gross fracture at the steel/wax interface. If a wax model is to be found that can provide robust testing of removal concepts, it needs to allow cohesive failure of simulated deposits. That is, it needs to stick well to the pipe wall.

The orthogonal cutting tests described in chapter 4 are impervious to the adhesive properties of the wax. Tests are configured such that a relatively large block of wax is cut to a certain depth and failure is always cohesive. The assumption is therefore that under real removal conditions the wax deposit will fail at the pipe wall because of the conditions enforced by tool geometry, not because the adhesive and cohesive forces are not equivalent. The jetting test described in chapter 5, however, require that the actual model wax *is* perfectly adhered to the steel pipe.

It was noted during experimentation that wax/oil mixtures adhered better to steel than pure wax. Put simply, they were *stickier*. As the force required to remove pure wax from the steel test plate, even with a textured surface of 50 microns, was negligible, a series of tests were performed measuring removal forces for varying oil content waxes. The high speed test apparatus described in chapter 4 was used to measure the

removal forces and the sample was configured such that the tool's depth was coincident to the wax/steel interface, with a slight clearance to avoid friction between the tool and steel plate (figure 3.74). In these tests the tool was driven by hand at an approximate speed of 0.1m/s.

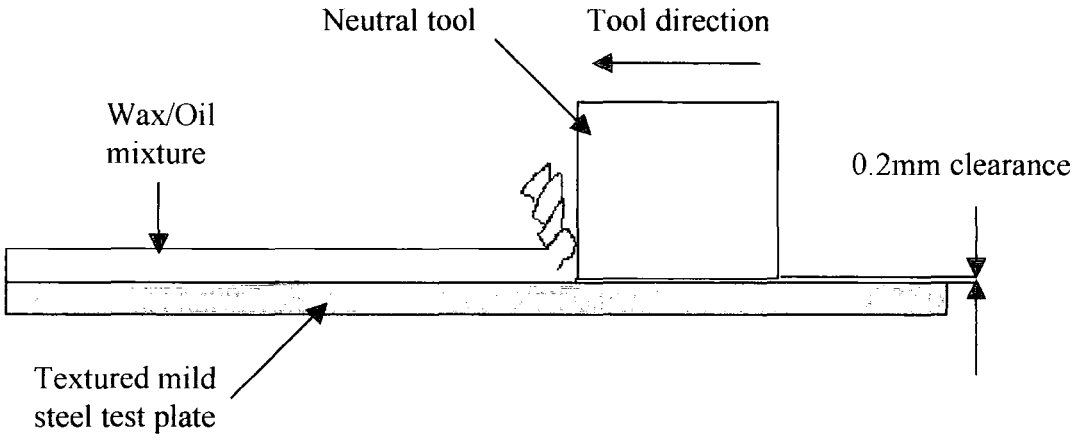

Figure 3.74. Adhesion test

3.75 Results and observations from adhesion tests

The results of these tests are shown in graph 3.75. It can be seen that the removal stress (Force divided by area of test plate) is negligible until an oil content of approximately 50% is reached. At this point the wax was removed by a shearing process rather than gross fracture at the steel/wax interface. This was confirmed by visual observations during the test.

It is deduced that there is a critical oil content that, below which, the wax/oil deposit is insufficiently ductile to endure the large strains imposed on it by cooling. Paraffin wax has a large coefficient of linear expansion, and moreover, it undergoes a solid-solid phase transition where it changes from a ductile to brittle material (Mozes et al, 1982). This transition occurs above room temperature such that further contraction of the brittle wax as it cools to room temperature ruptures the interfacial bonds with the steel plate. This property of solid-solid phase transition has been exploited by researchers who have used paraffin wax to model fundamental geophysical processes of the earth's crust (i.e. tectonics).

A sample of pure refined *micro*-crystalline wax tested using the procedure described showed perfect adhesion to the test plate. This was due to the high ductility of this type of micro-crystalline wax.

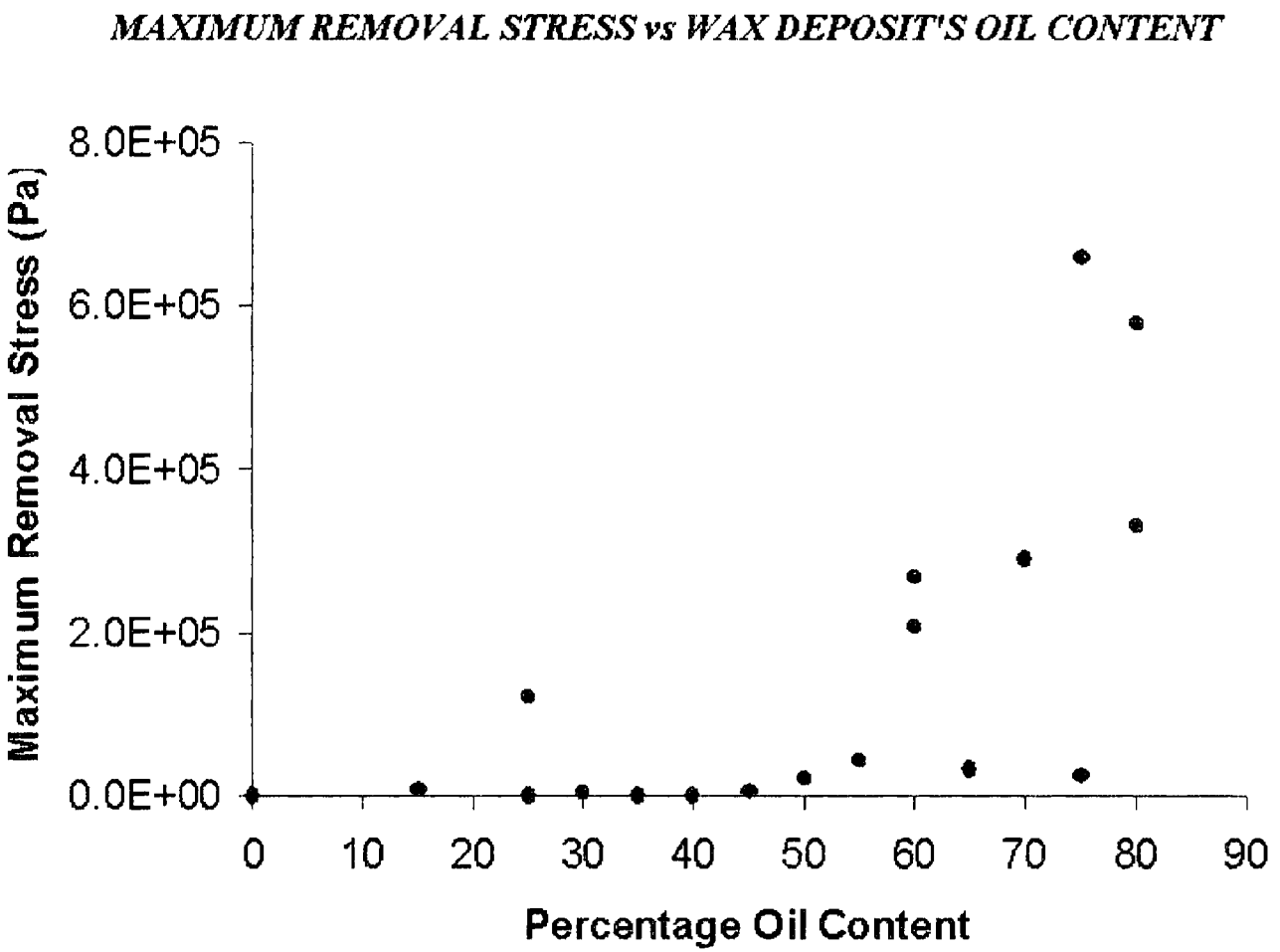

Figure 3.75 Plot of maximum removal stresses for various oil content waxes

3.8 Conclusions

The physical properties of paraffin wax deposits vary according to crude oil source, flow regime, prevailing thermal environment and age. Predictions of deposition based on thermodynamic models are likely to oversimplify and over-predict the problem. Even if a mathematical model could accurately predict a mass deposition rate for paraffin wax in a pipeline, it is unlikely to predict the physical structure and properties of the deposit.

In view of the simple consolidation experiments performed and the existing literature on the subject, it seems most likely that there will be radial variations in a deposit's physical structure and oil content and axial variations in its depth, structure and oil content.

Removal methods must be aimed at deposits with a broad spectrum of properties. In this thesis, two major techniques with corresponding experiments are described. The experiments surrounding the more traditional mechanical removal methods are mostly performed with a pure 130/135 °F melt point paraffin wax representing a hard, aged deposit. The more novel, jetting technique is modelled using a series of high oil content wax blends. These blends contain solid fractions of equal quantities of microcrystalline and macrocrystalline. The microcrystalline wax was added to ensure the most ductile (and *stickiest*) possible sample that would provide a robust challenge for the removal concept.

Chapter 4 Mechanical Removal

4.1 Introduction.

In this section the mechanics of wax removal are explored and practical experiments are presented in order to create a better understanding of the process. An immediate requirement when modelling wax removal using a pig is that a force balance equation must be satisfied. This force balance equates the driving force for the pig with the resistive force of the wax deposit. In their study of pig dynamics, Petrobras use equation 4.1 to obtain such a force balance [Azevedo et al, 1998]. Using this equation, the wax failure stress is defined as the quotient of the force exerted by the pig and the cross sectional area of the wax deposit. It ignores other forces, such as friction between the pig's seals and the pipe wall. The relevant load model is shown in figure 4.1.

$$\sigma = \frac{\Delta P}{t/D(2 - t/D)} \qquad \textit{equation 4.1}$$

Where

σ = Failure stress of wax deposit

D = Pipe diameter

t = Thickness of deposit

ΔP = Pressure differential across pig

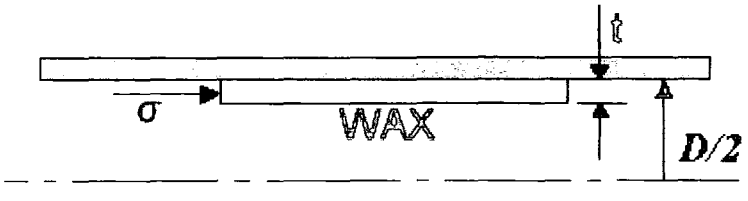

Figure 4.1. Petrobras' load model for wax removal.

Equation 4.1 is derived as follows,

It is assumed that the force exerted on the pig by the flowing oil, F_{pig}, is,

$$F_{pig} = \frac{\pi D^2}{4}\Delta P \qquad \textit{equation 4.2}$$

The load model described by Petrobras (figure 4.1) assumes that the stress on the wax deposit is compressive and aligned to the pipe axis. In this case the resistive force of the wax is a product of the deposit's failure stress and cross sectional area, as follows,

$$F_{wax} = \sigma\left(\frac{\pi D^2}{4} - \frac{\pi(D-t)^2}{4}\right) \qquad \textit{equation 4.3}$$

For equilibrium, F_{pig} must equal the resistive force of the wax deposit, F_{wax}. Therefore,

$$\sigma\left(\frac{\pi D^2}{4} - \frac{\pi(D-t)^2}{4}\right) = \frac{\pi D^2}{4}\Delta P \qquad \textit{equation 4.4}$$

Equation 4.4 can be rearranged to obtain the failure stress of the wax deposit as follows,

$$\sigma = \frac{\frac{\pi D^2}{4}\Delta P}{\frac{\pi D^2}{4} - \frac{\pi(D-t)^2}{4}} \qquad \textit{equation 4.5}$$

Simplifying equation 4.5,

$$\sigma = \frac{\Delta P}{t/D(2-t/D)} \qquad \textit{(equation 4.1)}$$

It is the author's opinion that Petrobras' equation does not correctly describe the physical load model shown in figure 4.1. It is the author's opinion that this is due to error that can be seen in equation 4.3. The cross-sectional area of the wax should be calculated using *2t*, not *t* as shown. Equation 4.1 can be shown to be incorrect by applying an end condition where the pipe is completely occluded by wax. The condition where the pig is resisted by a solid plug of wax is satisfied when the pressure acting on the pig and the stress on the wax are equal. In this case the wax thickness, *t*, is equal to *D/2* and,

$$\sigma = \frac{\Delta P}{\frac{D/2}{D}\left(2 - \frac{D/2}{D}\right)} \qquad \textit{equation 4.6}$$

Therefore,

$$\sigma = \frac{\Delta P}{0.75} \qquad \textit{equation 4.7}$$

However, if the force balance equation described by Petrobras' load model is derived using the term *(D-2t)* to describe the inner diameter of the wax deposit, the following equation is obtained,

$$\sigma = \frac{\Delta P}{t/D(4 - 4t/D)} \qquad \textit{equation 4.8}$$

Again, applying the condition where *t* is equal to *D/2*,

$$\sigma = \frac{\Delta P}{\frac{D/2}{D}\left(4 - 4\frac{D/2}{D}\right)} \qquad \textit{equation 4.9}$$

Therefore,

$$\sigma = \frac{\Delta P}{1} \qquad \textit{equation 4.10}$$

Equation 4.8 therefore correctly describes the end condition where t is equal to $D/2$ and is the correct equation to describe the load model depicted in figure 4.1.

A useful application of Equation 4.8 would be to calculate the required pressure drop across a pig to remove a given thickness of wax. However, this model oversimplifies the mechanical removal of wax as it assumes uniform properties in the deposit and ignores the forces of adhesion between the wax and the pipe wall. Also, it can be seen that this formula describes a transient state in the pigging process. As soon as wax is removed from the pipe wall it will begin to accumulate (to some degree) in front of the pig. In practice, this accumulation will lead to a plug forming and greatly increase the required driving force from the initial transient state described by equation 4.8. These limitations call the validity of this model of wax removal into question.

Wang and Saricas' [2001] experimental study of wax removal forces does not develop past the presentation of raw data obtained during wax removal tests under laboratory conditions. Nevertheless, the experiments and limited analysis are perhaps more interesting as they point towards a fuller description of the pigging process, i.e. where an accumulating plug of wax adds a further component to the force balance equation.

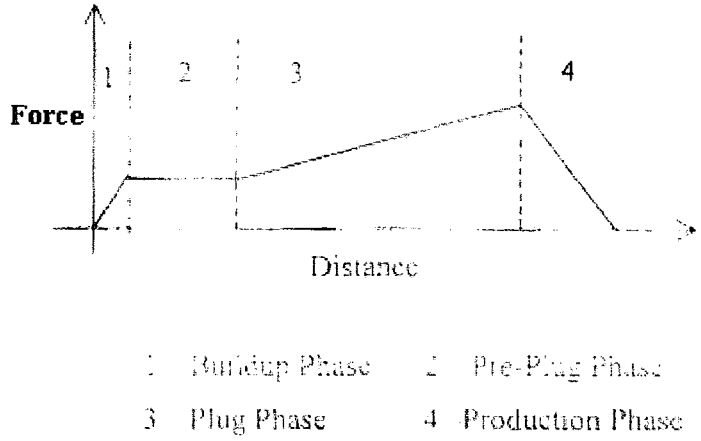

Figure 4.12. Typical force vs distance behaviour for wax removal during pigging [Wang& Sarica, 2001]

Although the trend observed by Wang and Sarica shows an accumulation of wax affecting the net driving force, limitations in their experimental design do not allow a prediction of when (if ever) these forces reach a steady state. The sudden reduction in pigging force shown in figure 4.12 (Phase 4- production) represents the point at which the wax plug begins to emerge from the end of the pipe into free space.

It can be seen that the two models briefly described represent two opposite ends of a spectrum in terms of predicting removal forces. Petrobras' model with zero plug formation represents a lower bound solution and Wang & Sarica's, assuming a constant increase in the plug component of the removal force, could be developed into an upper bound solution. In this respect, neither model offers a convincing description of the wax removal process. An ideal model of the wax removal process would encompass Petrobras' simple predictive model and Wang and Sarica's observations regarding the contribution of plug formation to the net removal force.

It should be noted that the plug formation observed in Wang & Sarica's experiments formed in a *dry* pipe. In practice, the flow of oil with and around the pig will help to alleviate this wax build up. Indeed, bypass ports are commonly included to produce a turbulent jet of fluid to remove the wax from the pig's front seal. Wang and Sarica's experimental design did not imitate the actual process of pigging because there was no fluid present. In this respect their model of wax removal is flawed.

Even an effective bypass system, however, cannot avoid the consequences of friction at the point of contact with the deposit being removed. In practice then, the incipient plug formation, before it is cleared by the jetting action of bypassing oil, can be considered in the same light as the chip formed during metal cutting. As with metal cutting, the behaviour of the wax during the removal process will depend on the geometry of the cutting tool and the mechanical properties of the deposit. With this in mind, a description of the orthogonal cutting model is provided as a basis for metal cutting theory.

Metal cutting theory can provide a wealth of knowledge that can be used to optimise the wax removal process. An experimental programme is required that can test the validity of this theory when used to predict the behaviour of wax. It is firstly useful to give a general description of the basic principles relevant in the removal of wax by 'cutting'. In order to be able to make a useful comparison with existing 'cutting' research, *orthogonal* cutting will be considered, as it is most likely to represent a practical model for workshop experimentation.

4.2 Orthogonal cutting theory

Cutting processes in the domestic environment use hard, metallic, wedge-shaped tools to cut through (relatively) soft bodies. An example is a chopping knife slicing through a carrot, its faces symmetrically forcing apart the two halves as it proceeds. During metal cutting, the large stresses imposed on the tool by the work-piece make such a process impossible. Instead, a wide angled tool is used to remove a thin layer of material from a thick body. The thin layer of material, referred to as the 'chip' is plastically deformed consuming large amounts of energy and generating heat. Energy is also consumed in producing two new surfaces.

In order to study the cutting process and chip formation a set of simplified conditions can be imposed and the resulting process is referred to as *orthogonal cutting*. In orthogonal cutting the material is assumed to deform in plane strain. In plane strain deformation the material is constrained to flow everywhere parallel to a single plane and independent of the distance from that plane (Johnson and Sowerby, 1970). For the assumption of plane strain to hold true the tool edge must be straight and normal to both the direction of cutting and also the feed direction. Also, the depth of cut must be small compared to the width, approximately $1/12^{th}$. This gives a view of the cutting process in which all flow of the material occurs in 2 dimensions. Other assumptions on which the orthogonal cutting model is based are as follows, Shaw [1984],

1. The tool is perfectly sharp and there is no contact between the workpiece and tool at the clearance face.
2. The shear surface is a *plane* extending upward from the cutting edge.
3. The depth of cut is constant.

4. Tool width is greater than that of the work piece.

5. The work moves relative to the tool with uniform velocity.

6. A continuous chip is produced with no built-up edge.

7. The shear and normal stresses along the shear plane and tool are uniform.

It can be seen from the schematic of the orthogonal cutting process shown in figure 4.21 that a turning or milling operation must be conducted in a rather contrived manner to reproduce these conditions. The conditions of a planing or shaping operation, however, match this orthogonal model very well. Furthermore, viewed in section, the mechanical removal of wax using a plain scraper disc provides a very literal interpretation of the

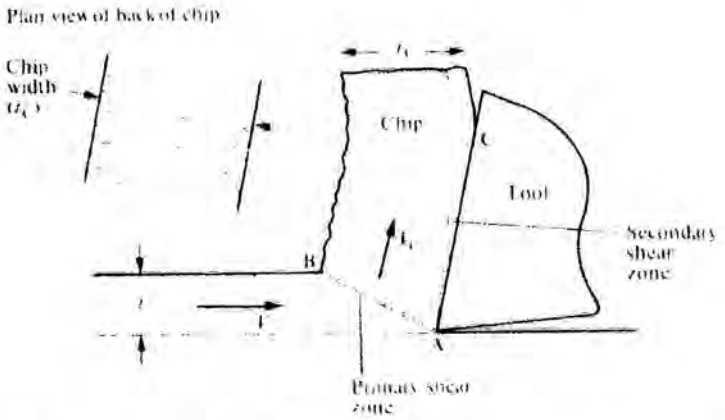

Fig.4.21. Schematic of orthogonal cutting operation.

orthogonal model (figure 4.22), especially if no differentiation is made between the adhesive and cohesive strengths of the deposit. When metal is cut under orthogonal conditions, deformation of the material occurs along a narrow shear zone, as illustrated in figure 4.21. Piispanen [1937] gives an elegant illustration of this process with his 'deck of cards' model for cutting (figure 4.23). This idealization of the cutting process shows a number of discrete shear zones representing the primary shear plane over time.

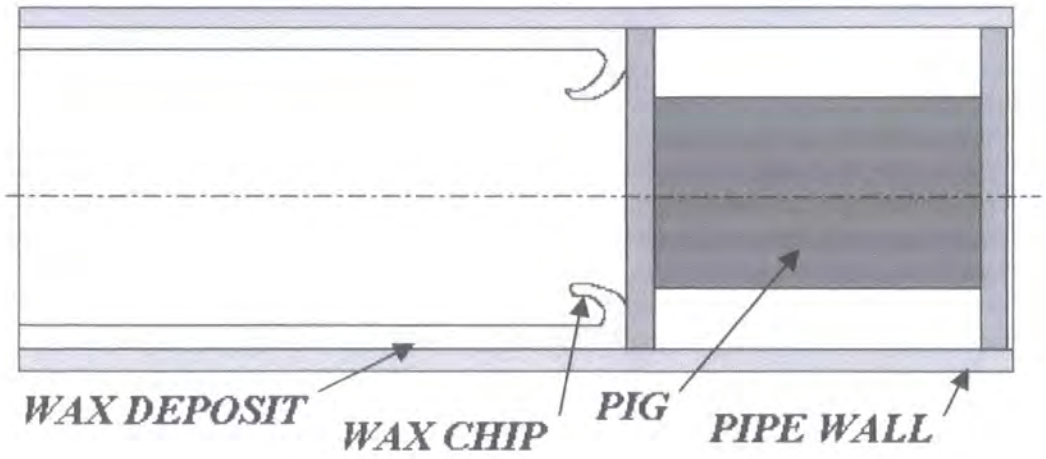

Figure 4.22. Pig removing wax from pipe wall.

During cutting, chip formation depends on a number of factors, but in general terms the material's ductility/brittleness is critical. In most metal machining processes, a smaller chip length is more manageable as waste. For this reason, 'chip-breakers' are often used. These effectively decrease the curve radius of the chips, encouraging fracture and failure of the chip.

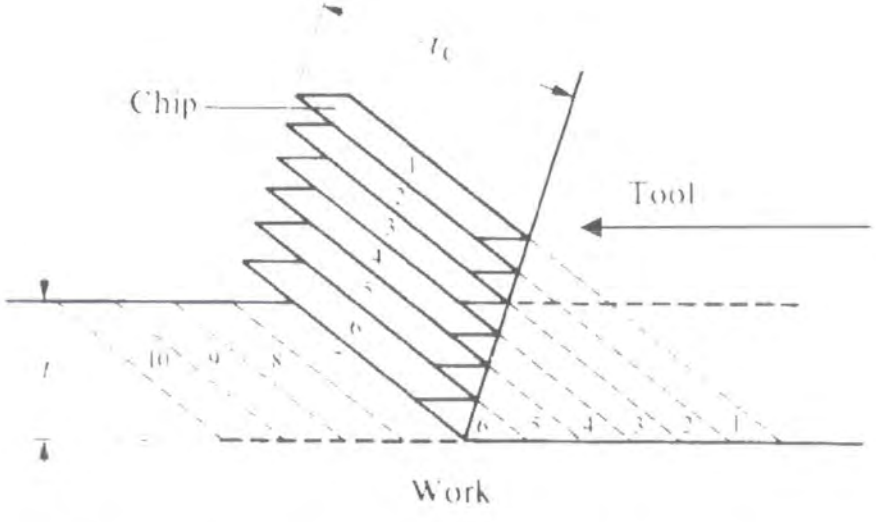

Fig.4.23. Piispanen's idealized model of the cutting process

One of the first researchers to offer a convincing model for the mechanics of cutting, based on an orthogonal model, was Merchant (1945). His model relates cutting forces to tool geometry and friction at the rake face. It requires knowledge of the specific cutting energy for the material and a shear angle in order to produce a unique semi-empirical model. Merchant suggests that considering the chip as a free body, the resultant force, R, between the tool face and the chip can be resolved graphically using the circle shown in figure 4.24.

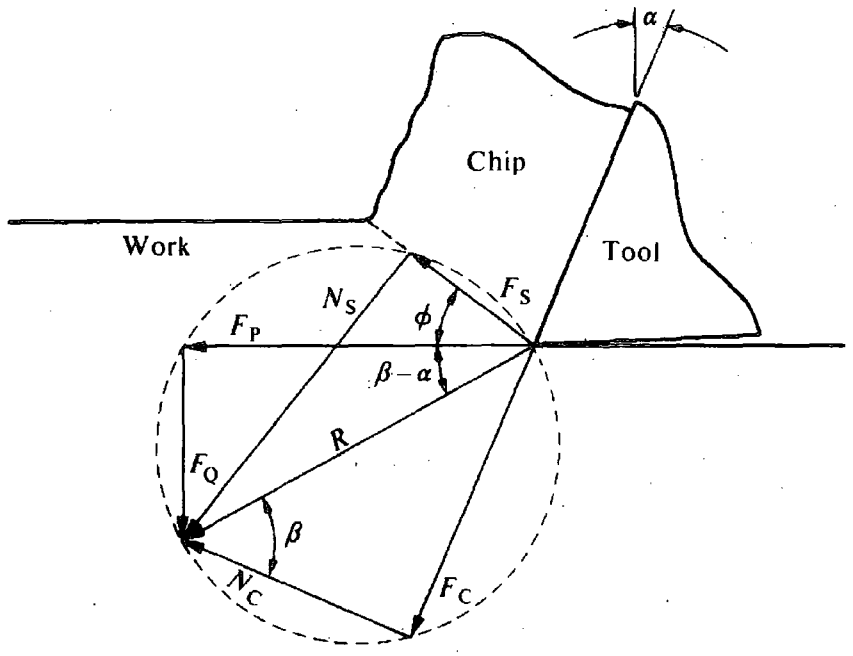

R= Resultant tool force

F_c= Friction force on rake face

F_p= Cutting force component

F_Q= Thrust force component

F_s= Shear force on shear plane

N_c= Normal force on rake face

N_s= Normal force on shear plane

α= Tool rake angle

ϕ= Shear angle

β= Mean friction angle

Figure 4.24. Merchant's model of metal cutting

Merchant's theory assumes that during cutting a shear angle (ϕ) develops that gives a minimum possible energy requirement for cutting. Merchant's description of the cutting process in terms of the magnitude and direction shear forces along two planes is far from comprehensive however. Including the forces described by Merchant's model, Shaw [1984] subdivides the total energy per unit volume for orthogonal cutting into four components as follows;

1) Shear energy per unit volume (u_S) on the shear plane.
2) Friction energy per unit volume (u_F) on the tool face.
3) Surface energy per unit volume (u_A) due to the formation of new surface area in cutting.
4) Momentum energy per unit volume (u_M) due to the momentum change associated with the metal as it crosses the shear plane.

Shaw discounts u_A and u_M as negligible however and gives the following approximation, where u is the total energy per unit volume consumed in cutting;

$$u = u_S + u_F \qquad \textit{equation 4.2}$$

Although Merchant's cutting model may only offer an approximation of the cutting forces that determine the energy consumption in equation 4.2, the fact that it differentiates between the forces generated at the shear plane and at the tool face is important. An understanding of the contribution of both components of the cutting force is crucial for the understanding of wax removal and the optimisation of pig tool geometry. The subsequent experiments described in this thesis are all conducted under plane strain conditions to allow analysis using the orthogonal cutting model described.

4.3 Quasi-Static Orthogonal Cutting Tests

4.31 Purpose of Experiments

The purpose of these initial experiments was to allow the observation of chip formation and measurement of the principle forces during the orthogonal cutting of wax. This allows comparison with predictions based on metal machining theory and evaluation of the suitability of such models in solving wax removal problems.

4.32 Description of Experiment

4.32.1 Equipment

For this experiment a 'cutting box' (figure 4.32.1) was designed to ensure the wax was cut under 'plane strain' conditions[3]. The box is constructed from mild steel with a toughened glass observation window. A tool post mounted between two parallel shafts runs between the observation window and the steel 'back-plate'. As the tool post is translated vertically along the shafts it runs parallel to a wax sample held in the box and the tool mounted to it cuts a wax sample block. The position of the wax sample within the cutting box can be varied relative to the tool-post in order to alter the depth of cut. This is achieved by the use of a removable 'jacking plate' mounted on studding that can be positioned relative to the side-wall of the box and held in position by pairs of lock nuts. The wax sample is moulded directly onto the jacking plate. Three different tools of varying rake were designed for mounting to the tool post.

[3] Under plane strain conditions flow of material occurs only in 2 dimensions parallel to the principal stresses σ_1 and σ_2. Deformation parallel to σ_3 is prevented, in this case by the 'cutting box' window and back-plate.

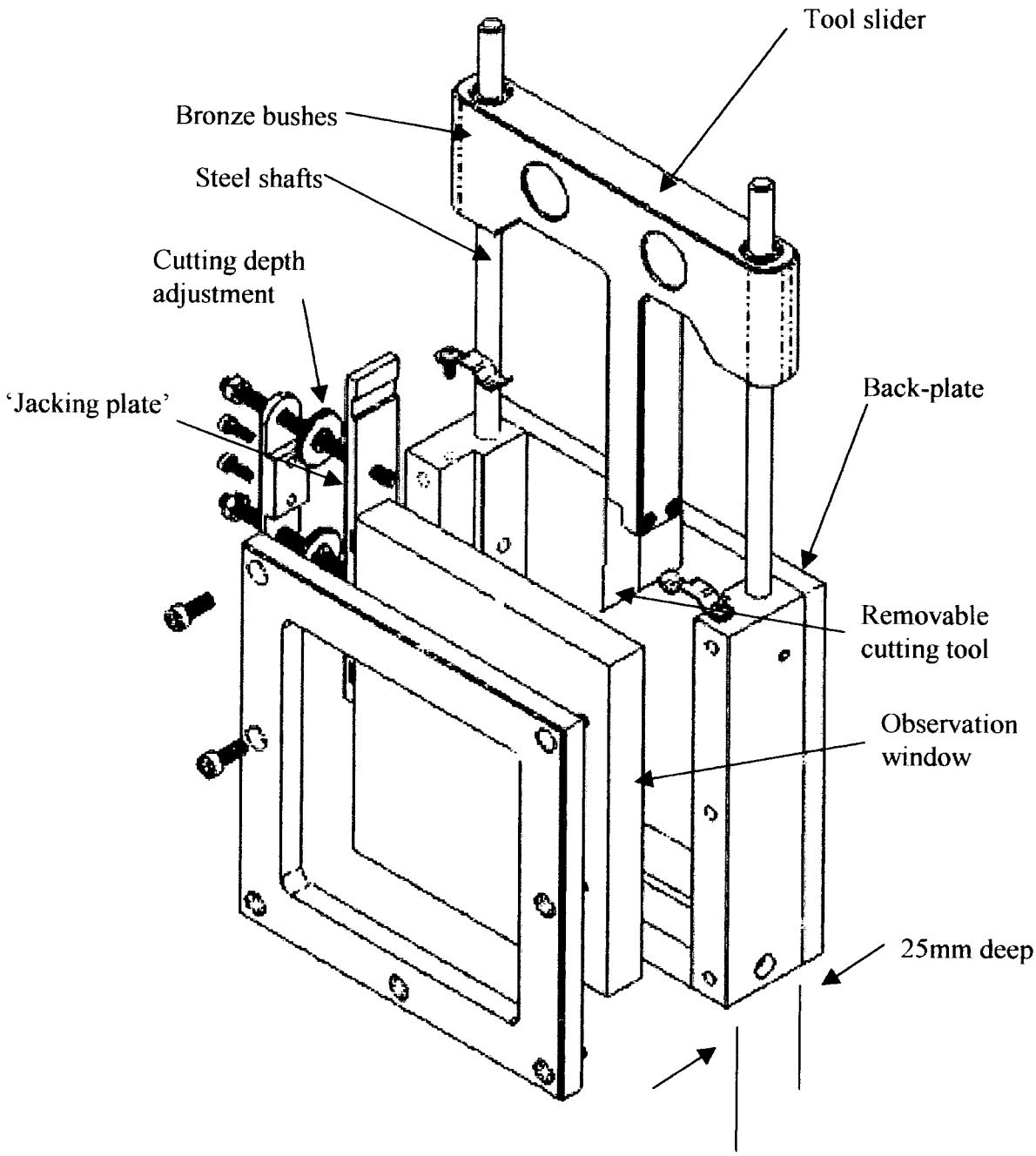

Figure 4.32.1. Plane Strain Cutting Box.

4.32.2 Sample preparation

A sample block of paraffin wax of equal width to the cutting box was cast using a gravity fed, aluminium mould. The overall dimensions of the cast wax sample were 165mm x 65mm x 25mm. This gave a sample that fitted closely into one half of the cutting box. The casting operation was achieved by heating a 130/135 °F melt point paraffin wax on an electrical hot plate until it had completely melted. The molten wax was then poured into the mould with the 'jacking plate' in place. Once the sample had cooled to approximately 20°C it was ejected from the smooth-walled aluminium mould, still attached to the 'jacking plate'. Adhesion to the jacking plate was achieved by 'keying' the plate with topographical features. Some experimentation was required to find a surface that the wax would adhere to well without fracturing from it during testing. The most successful method was to 'spatter' the steel plate's surface with an arc-welding rod. This gave a surface of random steel beads that the wax sample could adhere to by mechanical interlocking.

4.32.3 Test procedure

The cutting box was placed into a Wykeham Farrance load cell as shown in figure 4.32.3. A 200kg proving ring was placed between the cutting box's tool slider and the load-cell's cross-head to allow a measurement of the cutting force. Load was calibrated to displacement of the proving ring measured using a 0.002mm Dial Test Indicator. Having brought the tool tip into contact with the wax sample, the tool was displaced vertically by 25mm at a rate of 2.54mm per minute. The resultant 25mm cut represents the 'un-deformed' chip length. The deformed chip length was then measured to allow calculation of the cutting ratio. During the test data was collected from transducers sampling load and displacement every 7 seconds (the sampling frequency was dictated

by the laboratory's data logging equipment). Displacement of both the cutting tool and the proving ring were logged as a voltage output from Potentiometer type Linear Displacement Transducers (LDT) giving an accuracy of +/- 0.01mm. The transducers used were regularly calibrated by technicians for use in the civil engineering laboratory at the University of Durham.

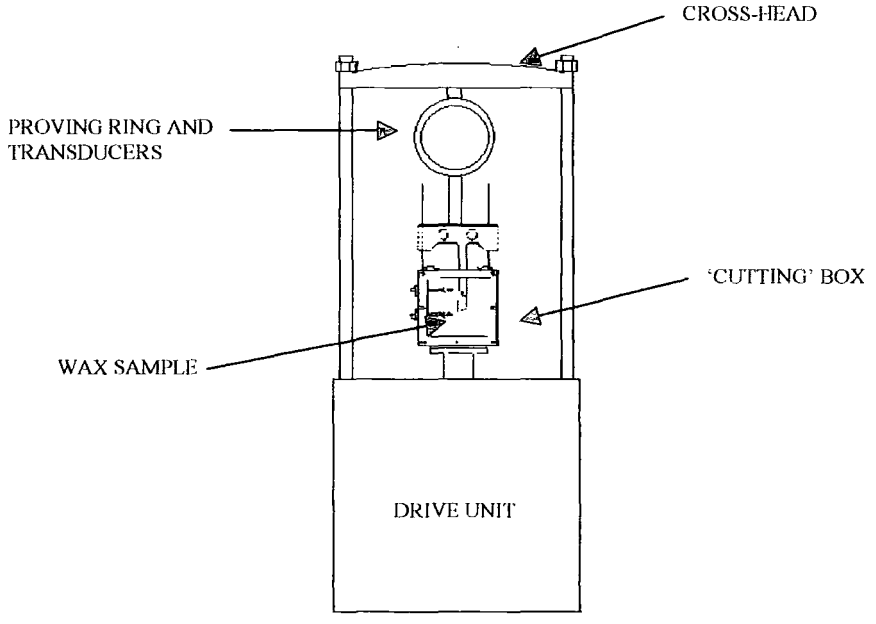

Figure 4.32.3. Arrangement of load cell and 'cutting box'.

The cutting tool in the cutting box was removable and neutral (0°), positive (45°) and negative (-45°) rake tools were used to cut wax at depth increments of 1mm. An initial series of load measurements were taken without wax present to ascertain a baseline figure for friction in the sliding mechanism to allow adjustment of the final results.

4.33 Results of quasi-static orthogonal cutting tests

4.33.1 Observed Shear Angle and Comparison with metal cutting theory

The shear angle (ϕ) formed during orthogonal cutting can be obtained trigonometrically (Merchant and Zlatin, 1945). It requires knowledge of the cutting ratio (r) and the tool's rake angle (α). The cutting ratio is the ratio of the undeformed chip (t) to deformed chip (t_c). As stated in section 4.2, one of the assumptions made for the orthogonal cutting model is that of a continuous chip. The chip produced during the wax cutting tests was *discontinuous* and the thickness of the deformed chip irregular. However, the discreet chips produced during the wax cutting tests were fused together giving the appearance of a continuous chip such that an *apparent* deformed chip length could be measured. Maintaining the assumption that cutting is a constant volume process and width of the chip does not change because of the plane strain conditions, a cutting ratio can also be obtained by comparing deformed and undeformed chip length. In this case an *apparent* deformed chip length (l_a) is used to obtain an *apparent* cutting ratio (r_a). Using measurements obtained in the test described in section 4.32, a displacement of the tool through the wax of 25mm (the un-deformed chip length, l) produced an *apparent* chip length of 40mm (the deformed chip length, l_a) and an apparent deformed chip thickness, t_c. The *apparent* cutting ratio (r_a) is therefore;

$$r_a = \frac{t}{t_a} = \frac{l_a}{l} = \frac{40}{25} = 1.6 \qquad \textit{equation 4.33}$$

Using trigonometry to obtain an apparent shear angle, ϕ_a, and substituting r for r_a,

$$\tan\phi_a = \frac{r_a \cos\alpha}{1 - r_a \sin\alpha} \qquad \textit{equation 4.33.1}$$

$$\tan \phi_a = \frac{1.6}{1}$$

$$\phi_a = 58°$$

If this result were obtained with a *continuous* chip it would be remarkable when compared to the shear angles commonly encountered during metal machining. When cutting steel under orthogonal conditions the shear plane angle is generally less between 16° and 25° for tool rakes between –10° and +10° and the cutting ratio less than 0.5 [Merchant, 1945]. The cutting process is 100% efficient when the shear angle is 45° and the shear angle would not be expected to exceed this value when plastic deformation is occurring under plane strain conditions. Figure 4.33.1 shows a photograph of the wax chip formed during the test described in section 4.32. It can be seen that the *observable* shear angle is approximately equal to 45°. Larger shear angles than those obtained when cutting metal have been produced when cutting polymers. Under orthogonal conditions cutting ratios approaching 1 can be obtained for certain thermoplastic materials and shear angles greater than 45° have been reported by Kobayashi [1981] when cutting with positive rake tools. However, in these cases chip formation may not be due to a shear process as seen when cutting metals.

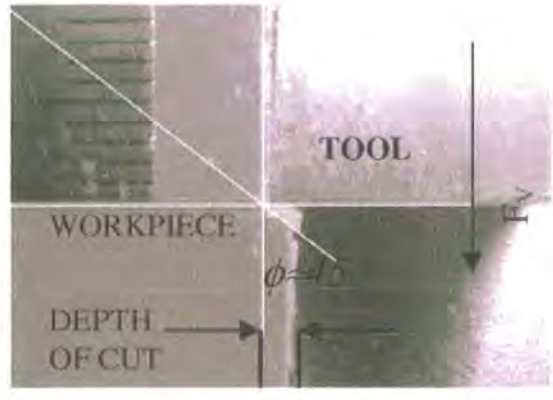

Figure 4.33.1. Observed shear angle (ø) during the cutting of wax with a neutral rake tool, 1mm depth of cut.

Notwithstanding the fact that $r_a > r$, it is assumed that r for paraffin wax might approach 1 as in the case of polymers, due to the low frictional forces at the chip/tool interface. The large shear angle observed in the wax cutting test suggests that $r \approx 1$. However, as the chip is discontinuous the cutting ratio, and therefore shear angle, may fluctuate greatly as cutting proceeds. For this reason the shear angle as observed from photographic stills may be misleading. Also, it is not possible to confirm the existence of a thin shear plane (a condition for Merchant's analysis) by mere observation. The observed opacity in the wax chip, apparently delineating strained and unstrained material, may in fact mark the boundary of a wider 'shear zone', further removing the test results from Merchant's idealised model.

4.33.2 Cutting Force and Chip Formation

A value for total specific energy (u) for paraffin wax can be calculated thus,

$$u = \frac{F_v}{bt} \qquad \textit{equation 4.33.2}$$

Where,

F_v = cutting force in direction of cutting speed vector (Note: F_p in merchant's notation)

b= width of cut

t =thickness of cut (depth)

If sample results from one of the tests carried out using a neutral rake tool at a depth of 1mm are inserted into this equation a value for u is obtained for the paraffin wax used in the experiments.

$$u = \frac{142.2N}{25mm \times 1mm}$$

$$u = 5.69MJ/m^3$$

Note that the total specific cutting energy u is sometimes referred to as a *cutting pressure* by other authors. The value used for F_v, used in equation 4.33.2, is the mean average load value obtained cutting wax to a depth of 1mm using a neutral rake tool. A plot of load against displacement is shown in figure 4.33.2 as a sample of the data format. In this instance load is the principle cutting force and displacement is the distance moved by the tool.

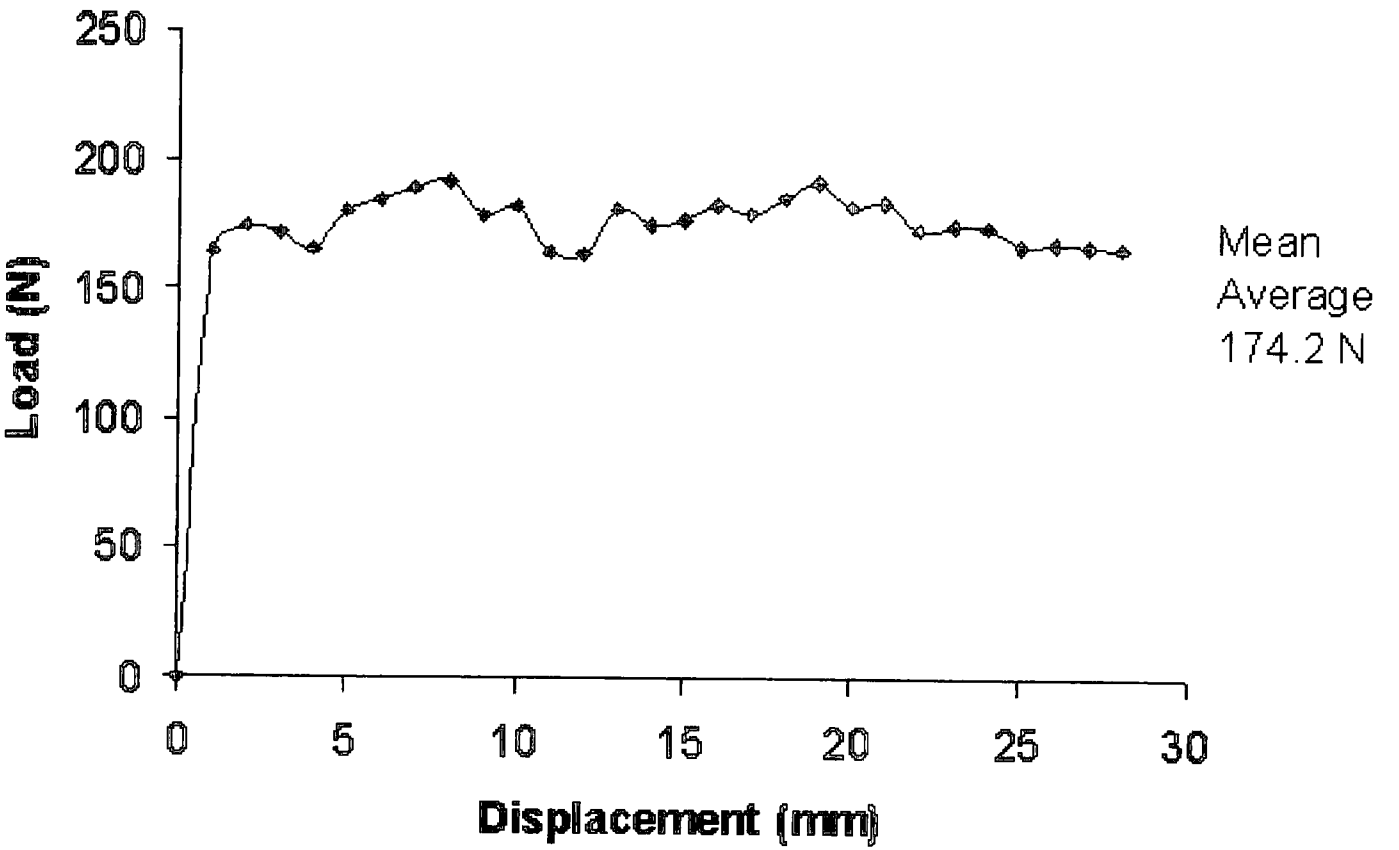

Figure 4.33.2. Load vs. displacement for 1mm deep cut, refined paraffin wax cut using a neutral rake tool at a depth of 1mm

4.33.3 Effect of rake and depth of cut

The results of the tests described in section 4.32 are shown graphically in figure 4.33.3. Figure 4.33.3 is a plot of u (specific cutting energy) against depth of cut for three different tool rakes. The results obtained experimentally are plotted alongside predicted values for u. The predicted values for u were obtained by extrapolation of the test results for a 1mm cut taken with a neutral rake tool, using equation 4.33.1. A tabulation of the tests results can be seen in Appendix C. As a 'size effect' exists and u is also influenced by tool rake, values for specific cutting energy can be calculated thus (Shaw, 1950),

$$\text{'Adjusted' } u = u\left(1-\frac{\alpha-0}{100}\right)\left(\frac{1}{t}\right)^{0.2} \qquad \textit{equation 4.33.1}$$

The first term in equation 4.33.3 provides an adjustment of u based on tool rake, α, and the second term, $(1/t)^{0.2}$, defines the effect of increasing the depth of cut, t (the 'size-effect).

The following observations can be made from the data,

- The general trend suggests agreement with orthogonal metal cutting theory.
- Measured values for u as a function of tool rake (α) agree closely with those predicted at smaller depths of cut.
- Whilst u is reduced for larger depths of cut, it appears to decline with a noticeably steeper gradient than that predicted by theory.

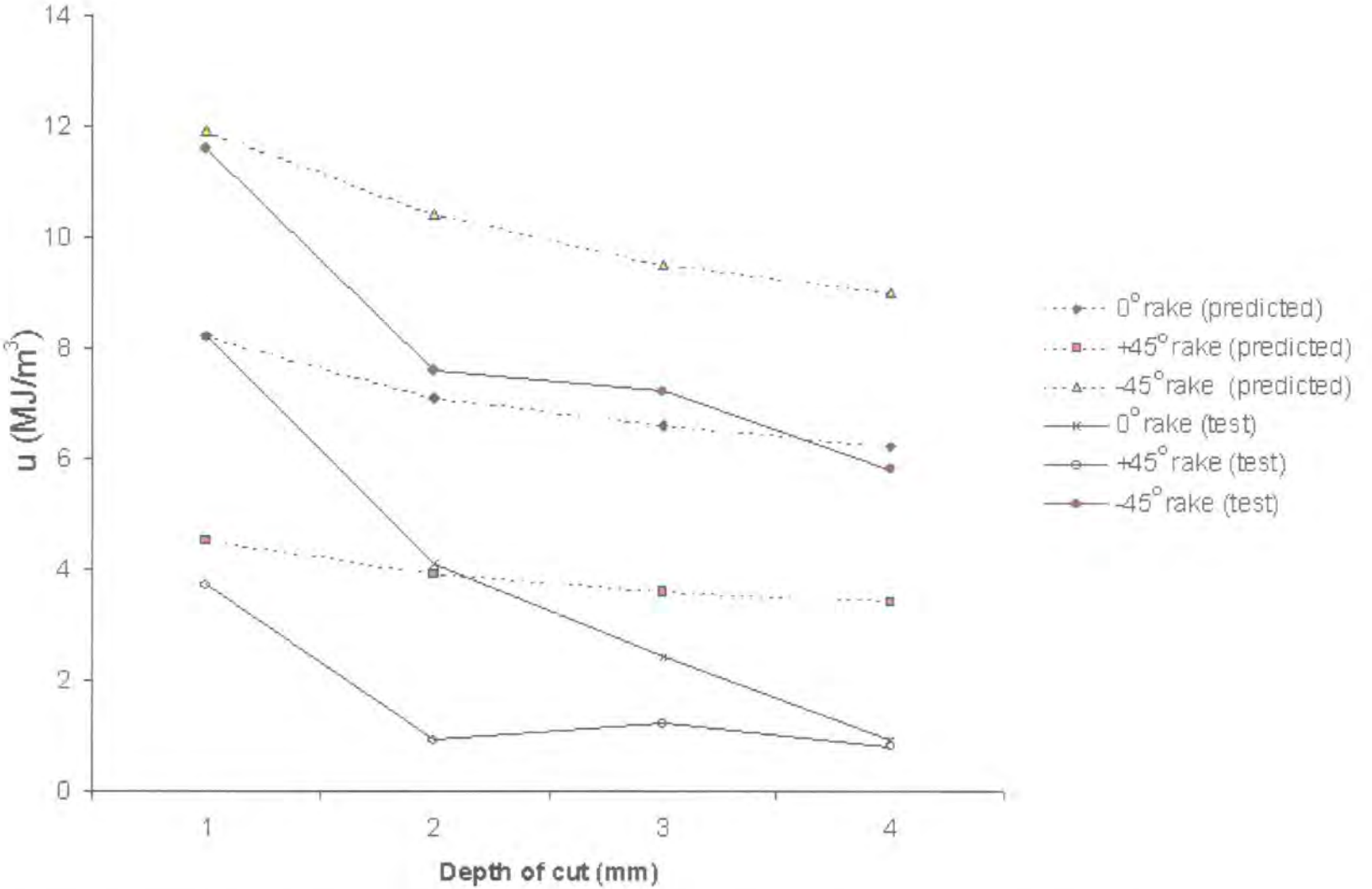

Figure 4.33.3. Comparison of predicted and experimentally derived specific cutting energy (u) values for paraffin wax cut using positive, neutral and negative rake tools at quasi-static speed.

4.33.4 Chip Formation

It can be seen from figure 4.33.2 that as a cut is made the load on the tool fluctuates between 150N and 200N. These fluctuations appear to occur in rhythm with the periodic fracture (or gross plastic deformation) of the wax, which forms a complex discontinuous chip. It can be observed that the wax plastically deforms along the shear plane until the chip reaches a certain size, at which point it appears to fracture from the work piece. Meanwhile another chip starts to form, giving the chip a segmented appearance. The chips are very loosely bonded together, suggesting that as the (separated) chip slides along the surface of the adjacent chip, it adheres to it. This process can be seen to happen in metals. Figure 4.34.1 shows a very similar chip formed in the machining of Titanium at low speed (1" per min) described by Shaw [1984] as exhibiting 'periodic fracture, gross sliding and rewelding'.

Figure 4.34.1. Left; paraffin wax chip formed during orthogonal cutting (Author's tests). Right; titanium chip (Shaw, 1984).

Shaw refers to this type of chip as *continuous with inhomogeneous shear*. The wax chip appears to suit this description too, but is friable and can be easily broken into discreet chips. Figure 4.34.2 shows the characteristically wavy back of the chip, and this too agrees with Shaw's description of *continuous inhomogeneous shear*. The term

continuous inhomogeneous shear is, in the context of the simple orthogonal cutting model, rather misleading. Inhomogeneous shear means that deformed chip thickness (and subsequently shear angle) is not uniform. In this respect the chip is not continuous, but an *apparently* continuous chip made up of a 'chain' of discontinuous chips. As stated in section 4.33.1, this type of chip cannot be easily analysed using simple orthogonal cutting theory.

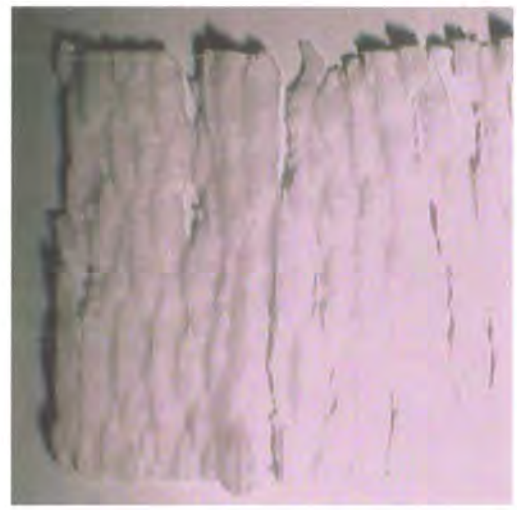

Figure 4.34.2. Paraffin wax cut at 1mm depth, neutral tool (back of chip).

At depths of cut above 2mm a pattern of chip fracture emerges that does not fit well with the concept of a shear angle. Rather, the chips now appear to form due to brittle fracture. This may explain the manner in which values for u appear to decline more rapidly as depth of cut increases than might be expected from orthogonal cutting theory. Figure 4.34.3 is a photograph of 2 chips produced by cutting paraffin wax using a positive rake tool at a 6mm depth of cut.

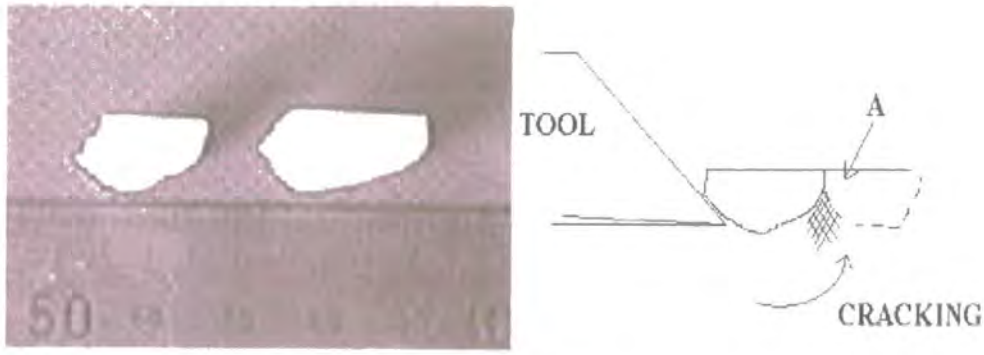

Figure 4.34.3. Wax chips, 6mm depth of cut and illustration of chip formation.

Note that despite some variance in their size, they are similarly shaped and this general shape is consistent whatever the depth of cut (above 2mm). Kobayashi (1981) refers to this mechanism of chip formation as 'discontinuous cracking'. Figure 4.34.4 shows, on the right, polystyrene cut under specific conditions during Kobayashi's experiments. On the left is a photograph of wax cut at a depth of 2.5mm during the tests described in section 4.3. A marked similarity can be observed in the geometry of the chips.

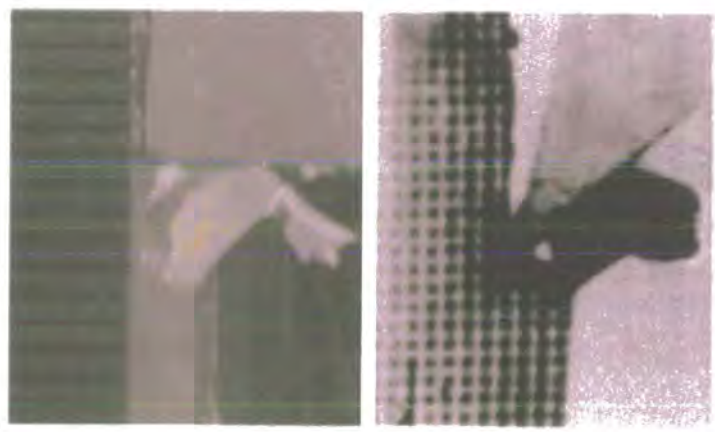

Figure 4.34.4. Left; wax chip (Author's tests) Right; polystyrene chip (Kobayashi, 1981)

Figure 4.34.5 is a graph of load against displacement for the cutting of wax samples at a depth of 6mm using a 45° rake tool. The load is a measure of the principle cutting force. Under these conditions a crack-type chip was produced and a pattern emerges in the measured load. Peak forces can be seen to occur at intervals corresponding to the

approximate length of the chips shown in figure 4.34.3. The ramp up of load immediately prior to the peak force represents compression of the wax, followed by an abrupt reduction in load as the wax fails due to cracking. Although the load is significantly reduced, it does not reach a zero value because of the frictional force as the chip slides up the tool's rake face.

The observation of a crack-type chip forming during the cutting of wax has important implications. If the chip is removed from contact with the rake face as soon as cracking occurs the peak cutting force will remain unaltered but average cutting force will be reduced. Unlike conventional orthogonal cutting where continuous shear occurs, this cutting mechanism can allow substantial displacement of the tool along the principle cutting plane under negligible load and there is therefore *no requirement for the chip and tool to be in permanent contact.* This is especially so when the cutting mechanism is placed into a 'pigging' context, where fluid bypass can be used to drive the chips away from the tool face. There are other prominent, though considerably smaller, load peaks visible in the graph. These can be attributed to the shearing off of those peaks of wax left by the fractured chip, marked 'A' in figure 4.34.3.

The size effect predicted in section 4.33.3 dictates a reduction in the specific cutting energy as depth of cut increases. Boothroyd [1965] attributes the size effect to a 'ploughing' force at the tool edge that is independent of chip thickness. The ploughing force is due to deformation of the workpiece without chip production. Even an apparently 'sharp' tool will have a slight radius at its edge and this radius creates a small negative rake face (i.e. tangential to the lower quadrant of the radius) that effectively compresses a thin layer of material. At large depths of cut the contribution of this 'ploughing' force is minimal. As depth of cut is reduced the 'ploughing' force

represents a larger percentage of the total cutting force and results in the 'size effect'. It is proposed that in the wax cutting experiments described in section 4.3 the 'size effect' observed has a different origin, explaining the variance between predicted and actual values for u during experimentation. The dramatic size effect observed when cutting wax is due to the fundamental differences in chip

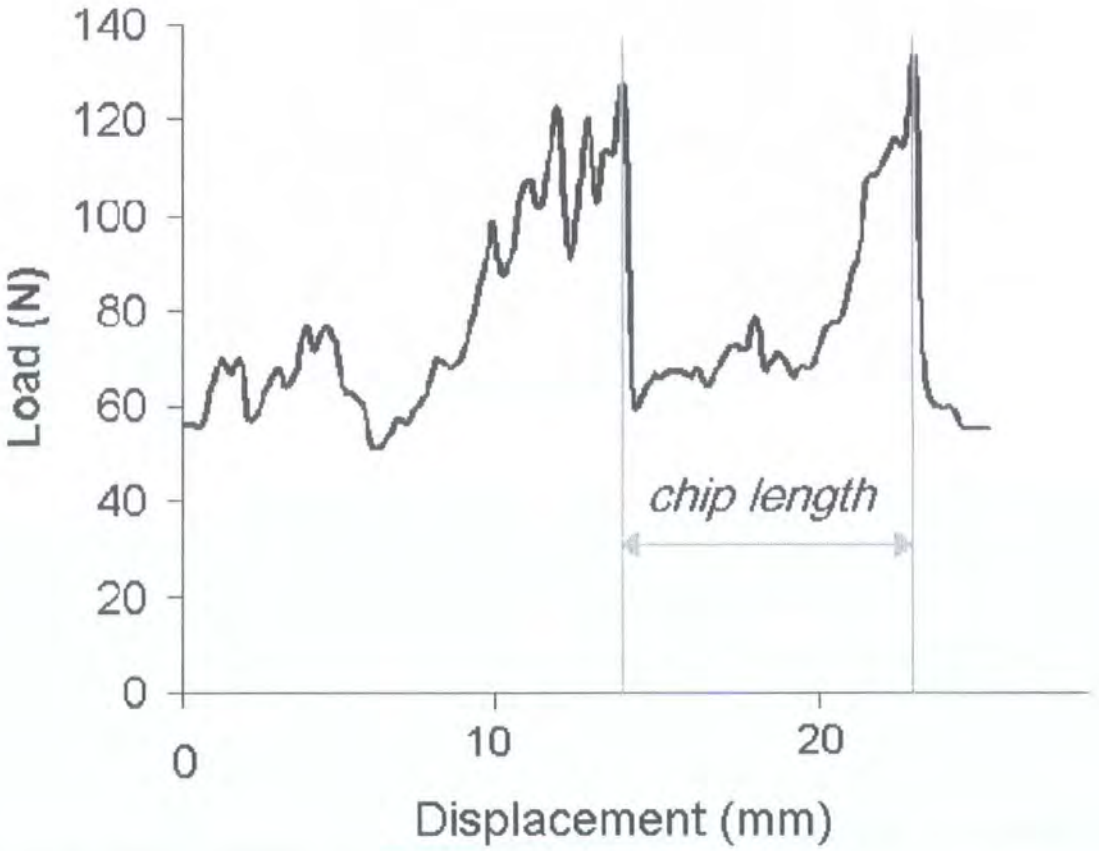

Figure 4.34.5. Plot of load vs. displacement for refined paraffin wax cut using a 45° positive rake tool at a depth of 6mm.

formation observed with different depths of cut. It can be simply illustrated by comparing the total new surface area formed per unit volume for shear type and crack type chips. It can be seen that the sum of the area of the shear planes for the shear type chip is greater than that of the crack type chip for a given volume of material (figure 4.34.6).

A simple 'efficiency ratio' for the case shown in figure 4.34.6 can be expressed thus,

$$\frac{\sum A_{shear}}{A_{cracking}} = \rangle\rangle 1 \qquad \textit{equation 4.34}$$

The formation of 'crack type' chips in wax appears, thus far, to be related to depth of cut. The depths of cut tested for the wax tests exceed those ordinarily found in metal or plastic machining, so unconventional chip formation might be attributable to this fact. However, cutting speeds have also differed largely from those normally encountered in metal machining. Therefore, in order to check that the transition to a crack type chip was not precipitated by the quasi-static load application, a second test series was performed at higher velocity.

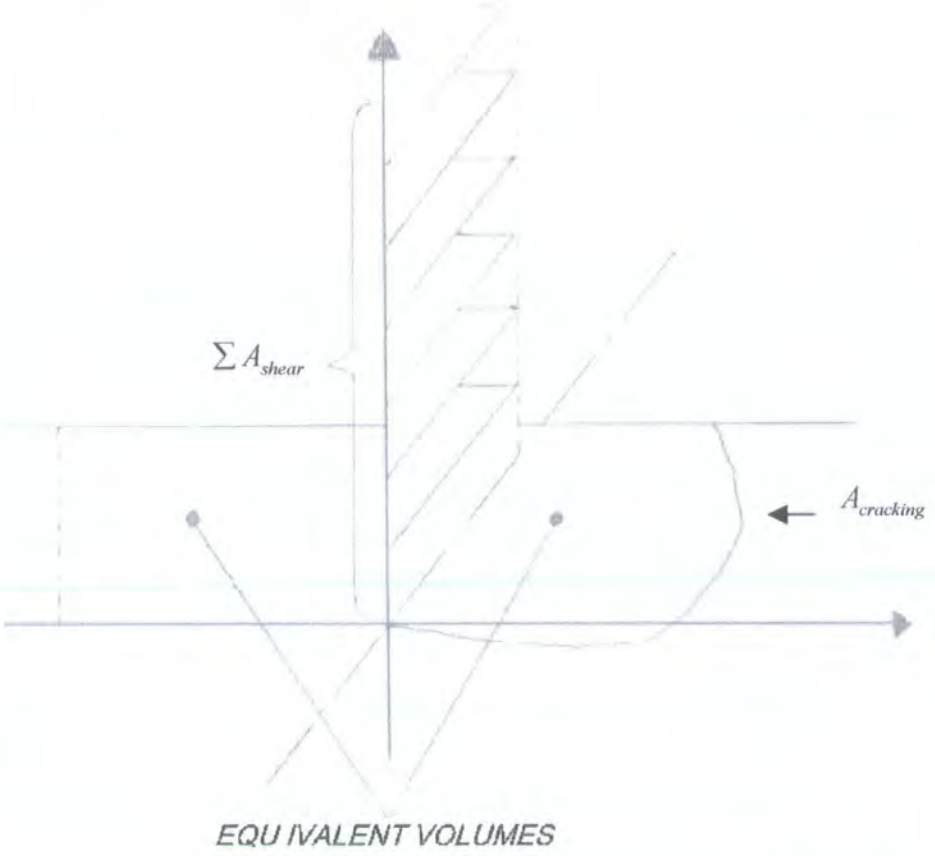

Figure 4.34.6. Comparison of surface area; orthogonal shear type chip and 'cracking' type chip.

4.4 Second Test Series – Increased cutting speed

4.41 Introduction to increased speed cutting tests

In order to analyse cutting at higher speeds a second series of tests were carried out using a Lloyd tensile test machine. This machine allows movement of the cross-head at a maximum of 8.3mm per second. The machine also has a control unit that allows it to log load and extension and output values in spreadsheet format. A second series of tests was carried out in the same manner as those described in the previous section but at a speed of 8.3mm/second. Also, the cut length was increased to 100mm allowing a more reliable average value for the measured cutting force.

4.42 Procedure for increased cutting speed tests

As in the tests described in section 4.3, wax samples were tested using the 'cutting-box' to allow a plane-strain analysis of the process. Before the testing of a wax sample was commenced, a series of measurements were taken of load along the full stroke of the tool slider in the cutting box to provide an average value for friction in the system. The results of these tests are shown in figure 4.33.1. It can be seen that the frictional force increases linearly with displacement of the tool. A frictional force was generated by engagement of the tool into the cutting box before (recorded) displacement, hence a Y-axis intercept for the plot. The mean average value for the frictional load along a 100mm stroke is 30N.

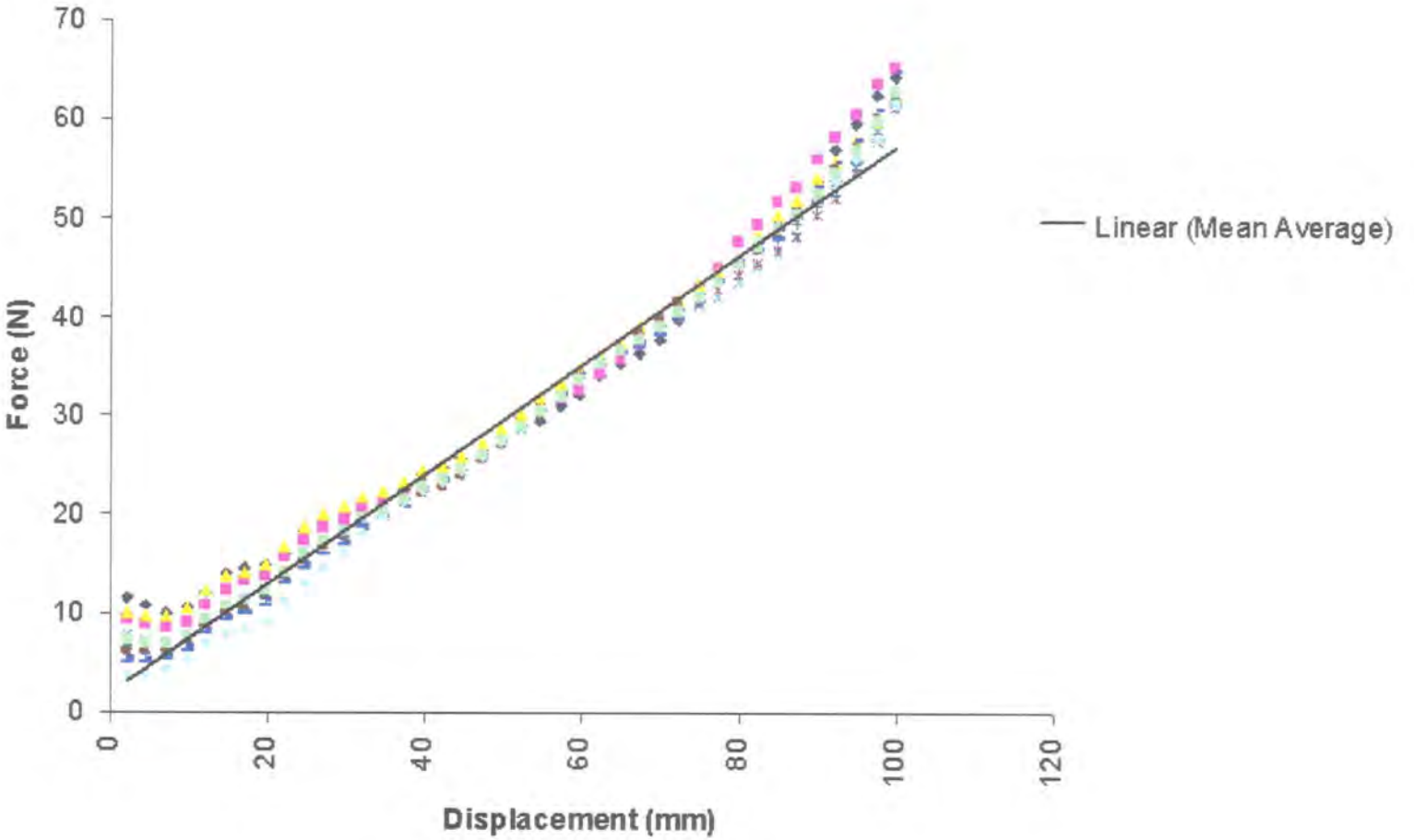

Figure 4.41.1. Frictional force vs. Tool displacement for wax cutting box. (Note: Data points are shown for 10 tests. Solid line represents mean average linear trend line for all tests.)

The linear increase in frictional resistance can be explained by slight misalignment of the slider shafts. As the tool slider moves along the shaft it encounters an increasing load perpendicularly to the shaft, resulting in greater frictional forces. Given the repeatability of this frictional resistance it was decided not to attempt to realign the shafts, but to adjust data accordingly. Samples were prepared in the same manner as described in section 4.3 and tests were carried out using various tool rakes and at various depths of cut.

4.43 Results of increased cutting speed tests

Based on an initial cut of depth 1mm using a neutral tool at the increased speed of 8.3mm/sec, the specific cutting energy for wax is significantly lower than in the initial, quasi-static test series. The expected reduction in specific cutting energy, u, due to size effect was not as pronounced as in the quasi-static tests, although such a trend was still in evidence. Tests using the negative rake tool appeared to produce an anomaly at low depths of cut in the form of values for u equivalent to those found when using a *positive* rake tool (Figure 4.43.2). Also, at depths of cut above 2mm using the negative rake tool (-45° rake), u is considerably larger than predicted. This appears to be due to a ploughing process, Boothroyd [1965].

Ploughing occurs in metal cutting, when the cutting edge of the tool, because it has a radius rather than a perfectly sharp point, deforms a small amount of the workpiece that does not contribute to the deformed chip. The 'ploughing force' generated represents a fixed contribution to the overall cutting force regardless of depth of cut and, as stated in section 4.33.4, it is the cause of the 'size effect' encountered in metal machining. 100% ploughing occurs when the shear angle coincides with the rake face of the cutting tool and no material is available for chip production. In the tests conducted in section 4.42, at depths of cut greater than 2mm using a negative rake tool, the chip/tool interaction was one of ploughing. The chip could not be relieved from the tool face due to the geometric constraints of the test set-up and so material accumulated to the full depth of the tool. The accumulated wax at the tool face effectively becomes the workpiece under these circumstances as material is constantly deforming but no chip is produced.

It was noted that the failure mechanism changed from shearing to brittle fracture as in the quasi-static tests (figure 4.43.1). This change began to occur at depths greater than 2mm for the neutral and positive rake tool. Figure 4.43.1 is a photograph from a test cutting wax at a depth of 6mm using a positive rake tool. In this test the wax chips were formed by the propagation of a crack starting at the tool tip.

Figure 4.43.1. Wax cut at a depth of 6mm using positive rake tool at a velocity of 8.3mm/sec

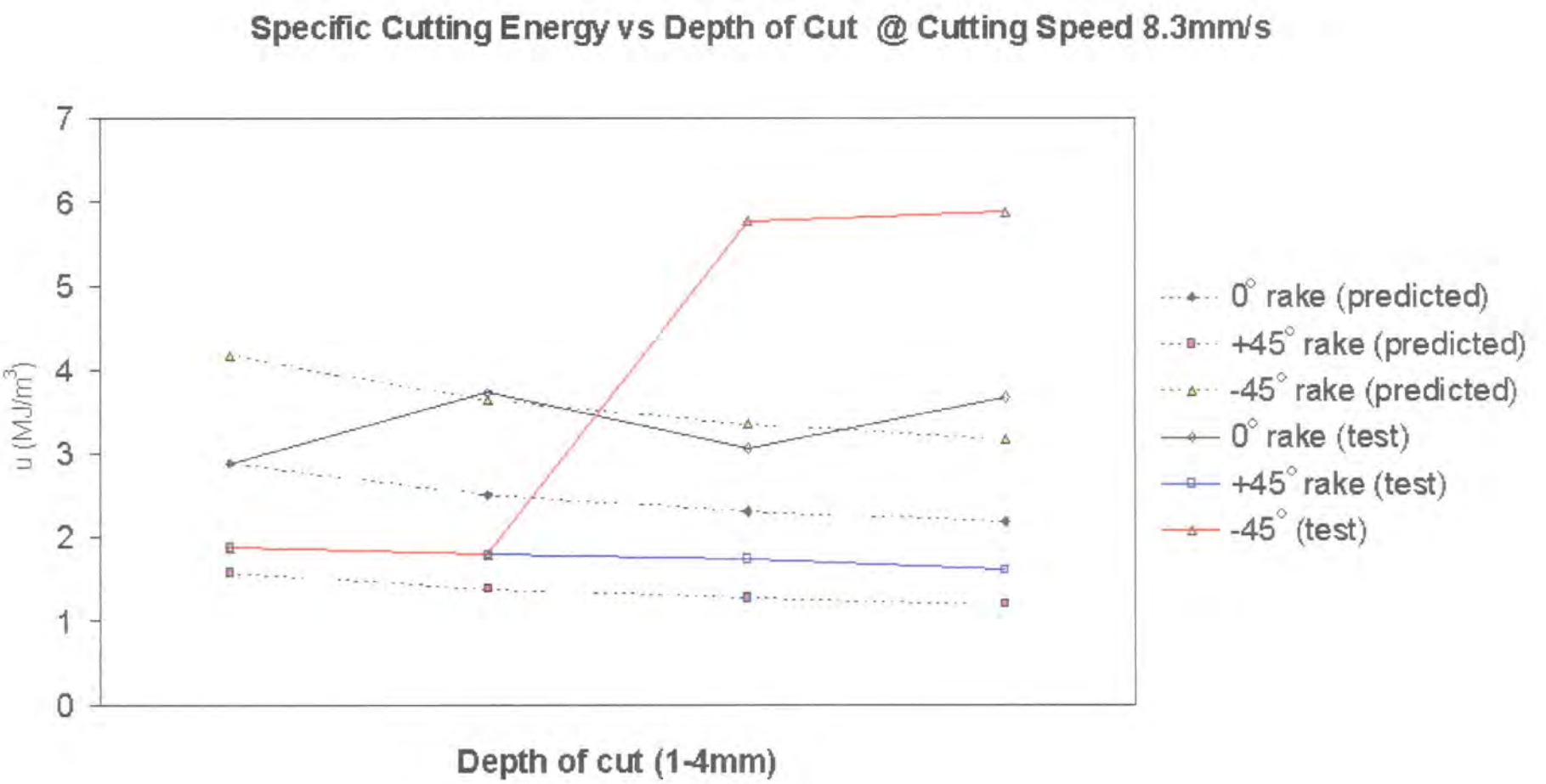

Figure 4.43.2 Specific cutting energy (u) vs. depth of cut using positive , neutral and negative rake tools.

4.44 Conclusions

The experiments so far have shown some interesting differences between the orthogonal cutting of wax and metals. The frictional component of the cutting force is very much lower for wax cutting than metal, as is found in many polymers. The lower frictional force at the chip/tool interface appears to result in high shear angles and cutting ratios. However, at greater depths of cut the process of wax cutting is less predictable and a mode of failure occurs (cracking) that cannot be readily described by conventional metal cutting theory. This limitation is perhaps unsurprising given that the depths of cut for the wax removal process are significantly larger than those that might usually be encountered in a metal cutting process.

At depths of cut under 2mm wax chips appear to form by a process of continuous inhomogeneous strain. Shaw [1984] asserts that chips produced by continuous inhomogeneous shear do not allow a cutting ratio to be obtained and, in the same way as a discontinuous chip, cannot be analysed using the simple orthogonal cutting model. However, substituting cutting ratio (r) for the apparent cutting ratio (r_a) obtained by measuring the wax chip, an analysis could be made of shear angle using Merchant's theory.

If an analysis of wax cutting forces can be made using metal cutting theory when continuous inhomogeneous shear type wax chips are formed, it is of interest to identify the key parameter effecting a transition from this type to the brittle fracture type observed. This transition would appear to relate to depth of cut and a resultant reduction in the ductility of the chip. Although the second series of tests revealed no marked difference in the behaviour of the process, it is possible that at higher speeds (perhaps

those approaching real pigging speeds above 1 m/s) significant differences may become apparent. Observations made by Shaw and Crowell [1965] do indeed relate the formation of 'crack' type chips to cutting speed. However, their findings were related very specifically to steels cut at low speed.

4.5 High Speed Cutting – effects of strain rate on cutting forces

4.51 Introduction to high-speed cutting tests

With a maximum cross-head velocity of 8.3mm per second, the compression testing machines used in the initial stages of experimentation cannot provide sufficient cutting speed to give an understanding of the effects of strain rate on wax removal. Figures 4.51.1 and 4.51.2 illustrate the fact that there is by no means a universal rule relating cutting speed and cutting force. The first graph (figure 4.51.1), due to Boothroyd [1965], clearly shows that cutting pressure, and therefore force at constant depth and feed, drops as cutting speed increases, in the case of mild steel. The second graph (figure 4.51.2), due to Kobayashi [1981], shows an initial increase in the cutting force along with cutting speed, followed by a sharp decline in the region of cutting speeds of 1 to 10 metres per minute. This sudden reduction in the cutting force is explained by Kobayashi as being due to the change in chip type at a critical cutting speed.

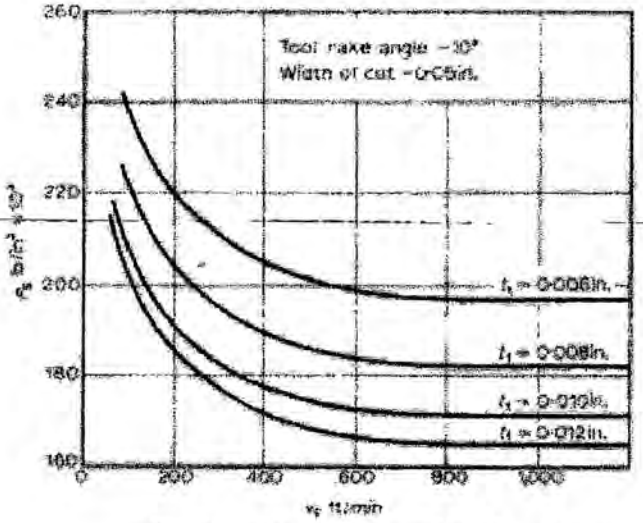

Specific cutting pressure for mild steel in turning.
p_s = specific cutting pressure
v_c = cutting speed.
t_1 = undeformed chip thickness.

Figure 4.51.1 Graph of cutting pressure against cutting speed for mild steel (Boothroyd, 1965).

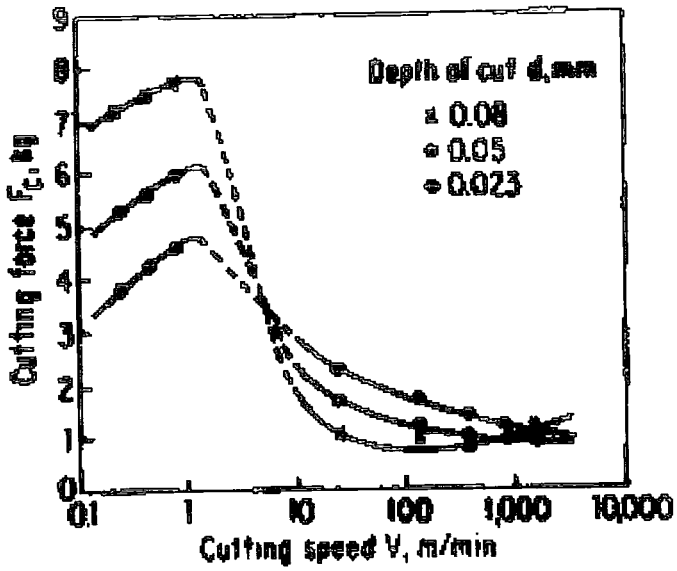

Figure 4.51.2. Graph of cutting force against cutting speed for polyester resin (Kobayashi, 1981)

As normal pigging speeds are in the order of 1 to 2 m/s, it is important to establish, qualitatively, the relationship between cutting speed, cutting forces and chip formation in the case of paraffin wax. To this end, a test rig was designed and manufactured to allow high-speed orthogonal cutting of wax. Observation of chip formation was made possible by the use of a high-speed camera and measurement of principal forces using load cells. Detail of the high-speed rig's design can be found in Appendix D.

4.52 Procedure for high-speed cutting tests

The high-speed test rig, to the author's design, uses an orthogonal tool mounted on a horizontally sliding carriage, as can be seen in figure 4.52.The tool carriage is accelerated rapidly by the instantaneous engagement of a drive pin between the carriage and a rotating flywheel. The energy stored in the flywheel ensures that the tool rapidly accelerates to a velocity dictated by the motor speed. The wax sample is secured to the machine bed, shimmed to provide an appropriate depth of cut. The tool is mounted on a post that contacts two small cantilever beams that have strain gauges to measure their deflection. These measure deflection horizontally and vertically and have been calibrated to give values for the cutting and thrust forces respectively. Output from the strain gauges' amplifier was recorded using a Fluke oscilloscope with a 100MHz bandwidth.

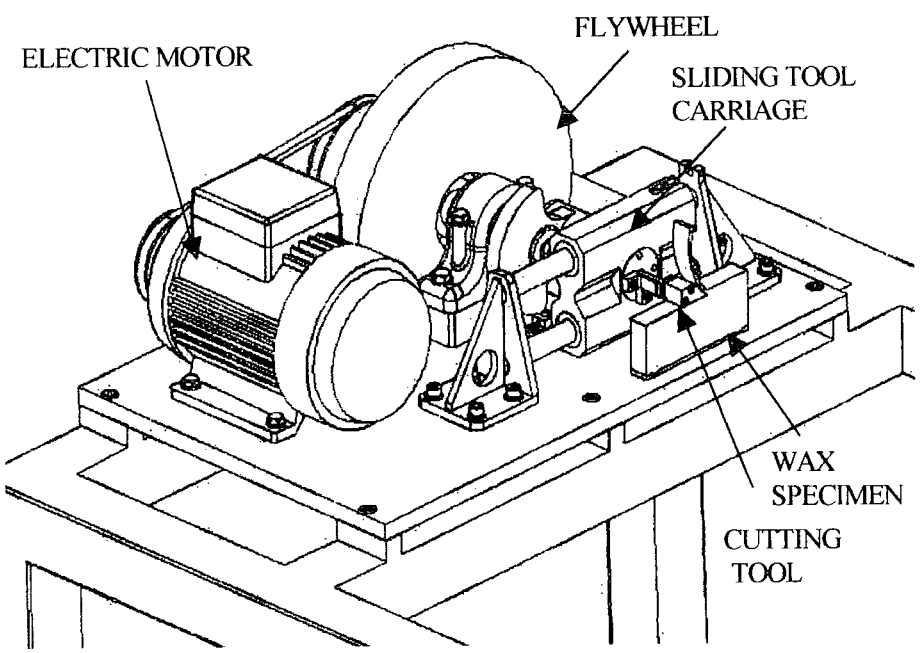

Figure 4.52. High speed orthogonal cutting rig

Using this test rig, pure paraffin wax was orthogonally cut at speeds ranging from 0.5m/s to 4 m/s using a neutral rake tool at depths of cut of 2.5mm and 5mm. Horizontal and vertical components of the cutting forces (Often referred to as 'cutting' force and 'thrust' force respectively) were measured. Chip formation was observed using a high-speed digital video camera, capable of recording at up to 500 frames per second.

4.53 Results from high-speed cutting tests

It was noted that a segmented 'discontinuous shear' type of chip was produced in all cases, with the chip becoming completely opaque indicating a large amount of strain within the material. Figure 4.53.1 shows a sample of refined paraffin wax cut at 0.5 m/s using a positive rake tool and at a depth of 5mm. At these higher speeds, no 'fracture' type chips, as observed in quasi-static testing, were produced.

Figure 4.53.1 Refined paraffin wax cut at 0.5 m/s using a positive rake tool, at a depth of 5mm

A sample of the oscilloscope's output is shown in figure 4.53.2. The X-axis on this graph represents time measured in milliseconds and the Y-axis shows the strain gauge's voltage output (note: the strain gauges measure displacement of tool post due to forces acting on it in horizontal and vertical planes). With the strain gauge calibrated to give 3.3mv per Newton, it shows the cutting force to be 124 Newtons. Figure 4.53.3 shows cutting force and thrust force plotted against tool velocity. It can be noted from the graph that the cutting force climbs proportionally with the increase in cutting speed. It

can also be noted that the corresponding thrust force remains largely static irrespective of changes in cutting speed. The cutting force reaches a maximum value at a velocity of approximately 3 m/s and to fall again as cutting velocity increases.

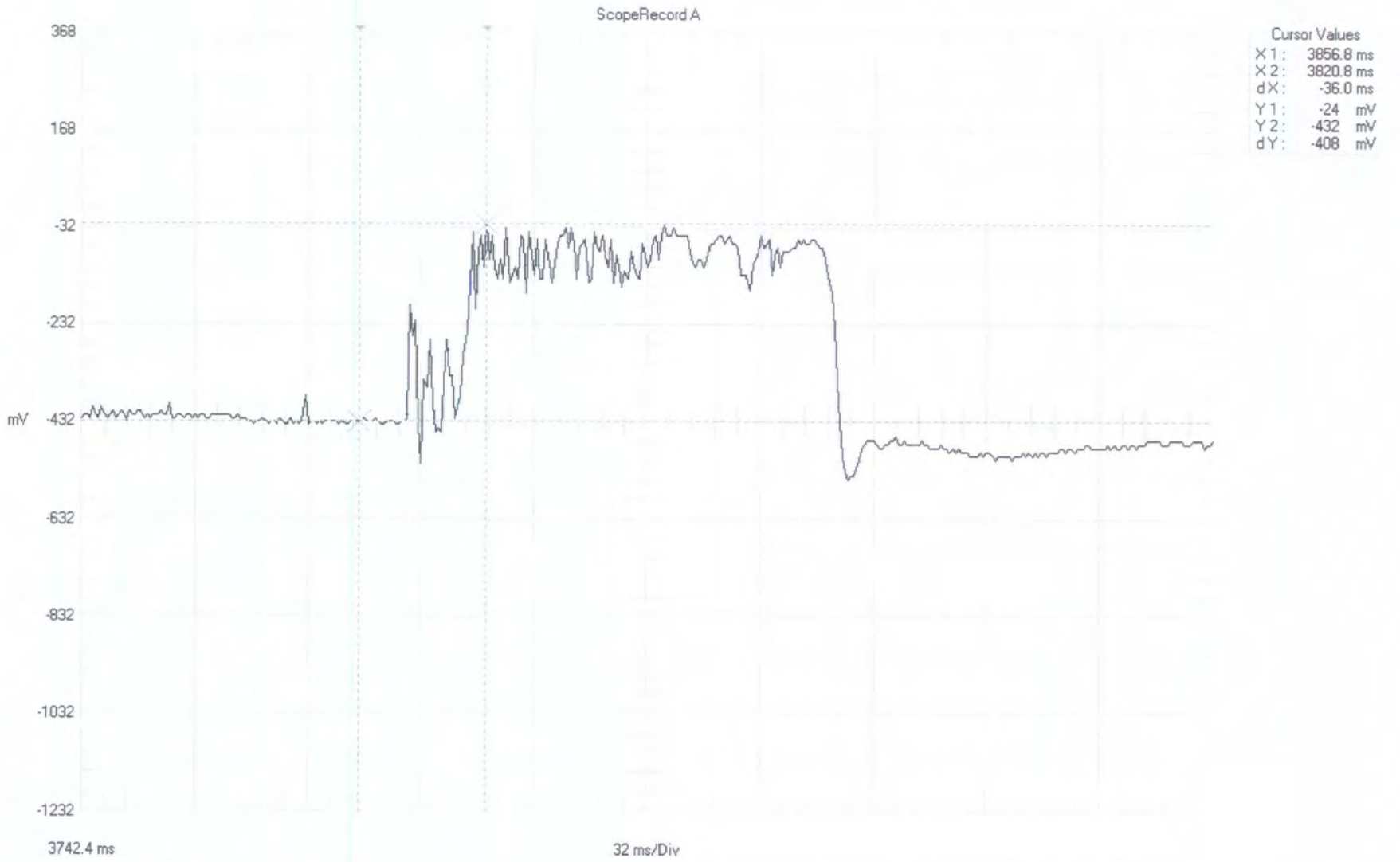

Figure 4.53.2. Sample plot of amplified output from output from strain gauge 'A' (Voltage output on Y-axis is proportional to F_v).

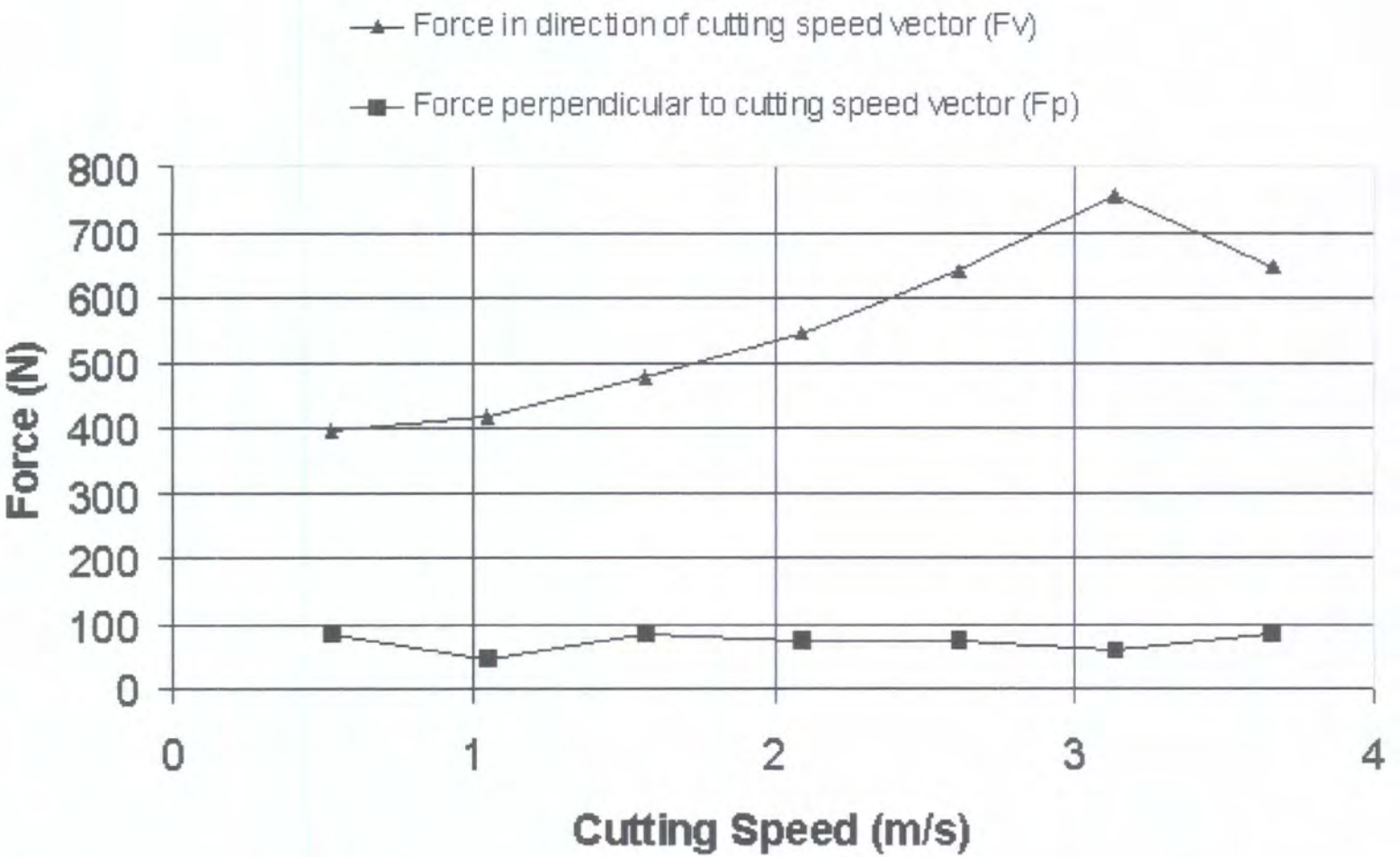

Figure 4.53.3. Plot of force against cutting speed for paraffin wax cut using a neutral tool at a depth of 2.5mm

4.54 Conclusions from high speed cutting tests and discussion

The first noteworthy observation from the high-speed cutting tests is that chip type remains consistent across the speed range. The chip type was also the same regardless of depth of cut compared to the quasi-static cutting tests that produce crack-type chips above a 2mm depth of cut. This suggests that at higher speeds chip ductility is maintained at greater depths of cut. Tool rake may also be a significant factor, with, more specifically, *sharper* tools increasing the likelihood of cracking. Such a hypothesis fits well with general fracture mechanics, in particular the stress intensity factor approach described originally by Irwin [1957].

The second point of interest is the fact that the principal cutting force climbs in relation with cutting speed, but not the vertical (thrust) component of the cutting force. The hodograph shown in figure 4.54 illustrates how chip and shear velocity relate to the cutting velocity. If the shear angle, ϕ, remains constant, vertical and horizontal velocity vectors must maintain the same ratio, regardless of cutting speed. Clearly, for this solution to remain kinematically admissible, the vertical (chip) velocity might remain static only if the shear angle, ϕ, becomes smaller with increasing cutting speed (V). As no such change in the apparent shear angle was observed, the static thrust force measurements are clearly anomalous.

The anomalous thrust force measurements can be explained by a limitation of the dynamometer design along with a peculiarity of the wax cutting process. The dynamometer's strain gauges were arranged to measure the horizontal component of force in the direction of the cutting speed vector (F_v) and the component of force perpendicular to it (F_p) but specifically in a *downwards* direction. It is proposed that the

relatively small forces involved in cutting wax, particularly the low frictional force at the tool/chip interface, result in a negligible or negative (upwards) force perpendicular to the direction of cutting. A negative force perpendicular to the direction of cutting has been recorded during experimentation with polymers where cutting ratios and shear angles are high and friction low at the chip/tool interface, Kobayashi [1981]. However, the principal cutting force measurements are not in question and have proved adequate for the analysis.

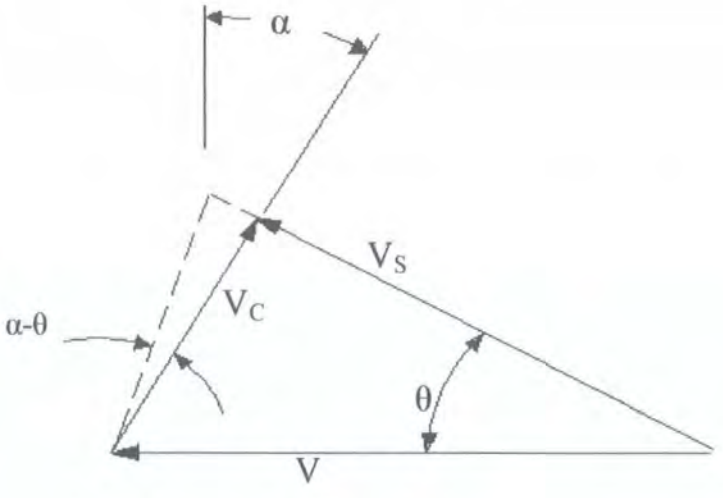

θ = Shear Angle

V = Cutting Velocity

V_C = Chip Velocity relative to tool (along tool face)

Vs = Shear Velocity relative to work-piece (along shear plane)

α = Tool rake

Figure 4.54. Hodograph for orthogonal cutting

An increase in cutting force with increased speed may be attributable to the unique strain rate sensitivity of wax. The fact that cutting forces reach a peak at 3 m/s and begin to fall away may be due to the thermal properties of the wax at the shear plane. As wax is an efficient insulator, with a relatively low specific heat capacity, localised melting

may occur at the shear plane at higher speeds. Melting might also occur at the rake face of the tool, effectively providing hydrodynamic lubrication. If a change in flow behaviour for the wax chip occurs at different velocities at the primary and secondary shear planes it may account for the results observed.

Although theory exists to allow prediction of chip temperatures in metal cutting, its validity to wax cutting has not been proven to date. In order to investigate chip temperatures during wax cutting a series of tests were performed using a thermal imaging camera. The results were compared to those obtained from predictions for cutting temperatures using metal cutting theory.

4.6 Thermal Imaging Tests

It was proposed that the decline in cutting forces for the wax sample at speeds exceeding 3 m/s might be due to a process of localised melting at the shear plane and/or tool face. Given that paraffin wax is relatively close to its melt point at room temperature this might occur with a relatively small amount of heat generated at the shear plane. Because of the insulative nature of wax, the process would approximate to adiabatic conditions and the localised melting allow viscous flow of the chip. Melting might also occur at the rake face of the tool, effectively providing hydrodynamic lubrication. Calculations based on established metal cutting theory are presented that suggest melting is unlikely. However, to check the validity of these theoretical calculations in the case of wax cutting further tests were undertaken. A thermal imaging camera was used to record images of wax undergoing high-speed cutting to see if the generated temperatures agreed with theoretically predicted values.

4.61 Prediction of temperature at shear plane using metal cutting theory

The following analysis of the temperature produced by orthogonal cutting at the shear plane is based on an approach provided by Loewen and Shaw [1954]. It assumes that all of the mechanical work done at the shear plane is converted into heat.

According to Loewen and Shaw, the heat generated at the shear zone per unit time per unit area, q, is,

$$q = \frac{F_s V_s}{tb \csc \phi} \qquad \textit{equation 4.61.1}$$

Where,

F_s = component of cutting force directed along shear plane

V_s = velocity of the chip relative to the work-piece, directed along the shear plane

t= undeformed chip thickness

b= width of work-piece

ϕ = shear angle

Loewen and Shaw's analysis predicts that the mean temperature of the chip (θ_s), in the vicinity of the shear plane, is

$$\overline{\theta_s} = \frac{Rq(bt \csc \phi)}{C\rho(Vbt)} + \theta_O \qquad \textit{equation 4.61.2}$$

C is the specific heat capacity of the material ρ is the density. Rq is the heat per unit time per unit area leaving the shear zone with the chip. $(1\text{-}R)q$ is the heat per unit time per unit area flowing into the work piece. R is a function of three non-dimensional

quantities; a geometric factor; a ratio of thermal conductivity and a velocity-diffusivity factor. In this instance R will be estimated at *0.5*. Using approximate values from the data collected in the experiments described in section 4.5, the expected increase in temperature is as follows,

From equation 4.61.1 the heat generated per unit area per unit time is,

$$q = \frac{1000N \times 5m/s}{0.005m \times 0.025m \times \csc 45^{o}}$$

$$q = 2.83 \times 10^{7}\ \mathrm{W/m^2}$$

Substituting this value into equation 4.61.2, the mean temperature of the chip in the vicinity of the shear plane is,

$$\overline{\theta_s} = \frac{0.5 \times 2.83 \times 10^{7} W\left(0.005m \times 0.025m \times \csc 45^{\circ}\right)}{2140J/kg.K \times 900kg/m^{3}\left(5m/s \times 0.005m \times 0.025m\right)} + 19^{\circ}C$$

$$\overline{\theta_s} = 21.1^{\circ}C$$

The mean increase in the temperature of the chip in the vicinity of the shear zone is therefore 2.1°C. Clearly, such a temperature change will not cause melting of the wax at the shear zone. Moreover, equation 4.61.3 does not account for the latent heat required for the phase change from solid to liquid, should the temperature be raised significantly.

4.62 High speed cutting test with thermal imaging

In order to check the validity of the calculations presented in section 4.61, a series of tests were carried out using a thermal imaging camera to record the orthogonal cutting of wax and determine the actual temperature rise around the shear zone.

4.62.1 Equipment and Experimental Procedure

An Agema 880 thermal imaging system was used to film pure refined paraffin wax being cut with a polyurethane neutral rake tool at high speed. The Agema 880 is a cryogenically cooled long wave analysis system with a temperature range of -20° to +1500°C with a sensitivity of 0.07°C at +30°C. It operates the *CATSE* thermal analysis software package and uses *IRWIN* software to convert images into formats compatible with Windows-based programs such as Word and Excel. Pipeline Engineering Ltd produced the polyurethane tools in the same polyurethane grades commonly used to manufacture wax scraping tools for cleaning pigs.

The Agema thermal imaging camera uses photovoltaic detectors that produce a signal voltage in response to infra red waves. Such a system has advantages over thermal infra red detectors in terms of response time, of particular importance when attempting to study a dynamic event such as high-speed cutting. The disadvantage of the photovoltaic sensors is their limited spectral response. Spectral response can be increased by cooling and this is achieved in the Agema system using liquid nitrogen.

Tests were performed using the high-speed cutting rig described in section 4.5. The thermal imaging camera was set up at a distance of approximately 300mm from the wax sample in the test rig and was calibrated by comparison with the ambient temperature of the sample measured using a mercury thermometer. Because only one image of the deformed chip was required for analysis, recording at 25 frames per second was satisfactory for the test.

The largest possible temperature rise was required to give the clearest thermal image and parameters were set accordingly. Referring to equation 4.61.1, cutting force (F) and cutting speed (V) must be maximised to generate the most heat at the shear plane. A neutral tool was used to make a 5mm deep cut into pure paraffin wax of width 25mm at 5 m/s.

4.62.2 Results and conclusions from thermal imaging tests

The thermal image is shown in figure 4.62.2 and shows the temperature rise to be approximately 4°K.The observed temperature rise is greater than that predicted by metal cutting theory. It is proposed that this slight discrepancy may be due to additional heat generated at the secondary shear zone (i.e. frictional heat at the tool/chip interface). Despite this slight discrepancy, the experimental result shows that the theoretical prediction for heat generated in chip formation is valid for wax cutting.

While the temperature increase observed in the wax chip during the test was not inconsiderable, it seems unlikely that localised melting could occur. However, the temperature increase may cause thermal softening that reduces the flow stress for the wax material at higher cutting speeds.

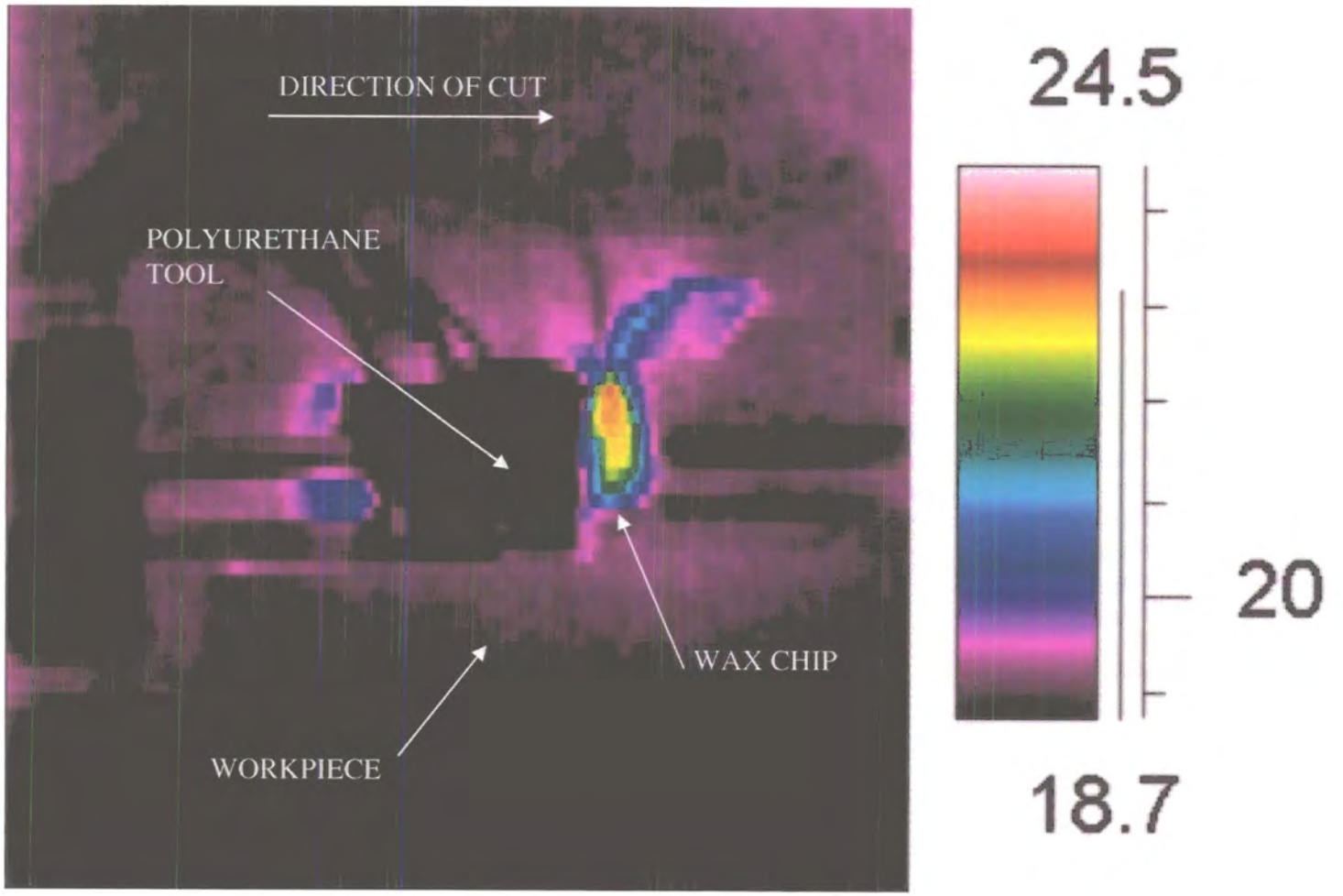

Figure 4.62.2. Infra-red image of refined wax cut at a depth of 5mm using a neutral rake tool at

4.7 Conclusions from wax cutting experiments

The experiments described in this chapter have shown that metal cutting theory can provide a useful framework for analysing the mechanical removal of wax deposits from pipelines. The semi-empirical nature of this theory means some amount of bench testing is necessary where a quantitative analysis is required. Nevertheless, predictive models based on metal cutting theory will provide more accurate results than previous models that do not account for chip/tool interaction. Values for specific cutting energy, u, measured in the tests described in this chapter are all in excess of the shear strength of paraffin wax that is obtained by the standard laboratory tests described in chapter 3. This suggests that predictive models based on simple uni-axial load models will always provide an underestimation of wax removal forces.

Analysing wax removal using metal cutting theory has confirmed the significance of tool rake to the process. This introduces the possibility of designing cleaning tools with features such as limited contact rakes and chip breakers.

It is evident that optimising tool design can not only reduce the force required to remove wax, but may also help produce wax chips of the optimum geometry for transport downstream as a suspension within the crude, avoiding plug formation. Both of these factors are highly desirable to pig operators.

All of the tests described in this chapter have been carried out on pure wax samples. In light of the findings described in chapter 3, a 'pure' wax deposit, if not a peculiarity of a specific production operation, is most likely to occur as the result of age hardening due to infrequent pigging. If a pipeline is more frequently pigged it is more likely that a

softer, gel like deposit will be encountered and this may be removed by less aggressive means, as described in the next chapter.

Chapter 5 Wax Removal Using Annular Bypass

5.1 Introduction

Many experimental studies of wax deposition have shown a critical flow velocity at which wax deposits become unstable and are sheared from the pipe-wall by the flow of oil, Bott and Gudmundsen [1977], Hamouda and Davidsen [1995], Cordoba and Schall [2000]. Figure 5.1 is a plot of wax deposition rate against oil flow velocity obtained experimentally by Hamouda. The plot in figure 5.1 illustrates how deposition rate initially increases with flow velocity, until a velocity is reached where the wax deposit becomes unstable and is sheared off (faster than it can accumulate). This process will also be affected by the crude oil's composition and the pipe's surface roughness, Jorda [1966]. Even if thermodynamic conditions favour the deposition of wax a smooth pipe wall may prevent the deposit from establishing itself on the pipe wall.

Extrapolation from the data presented in figure 5.1 is not possible, as it does not account for all of the parameters involved in the deposition process. Nevertheless, Hamouda's observations provide a qualitative indication that wax deposits *will be removed by fluid shear at a critical velocity*, the value of which is dependent on the wax's shear strength and the topographic and energetic state of the pipe wall.

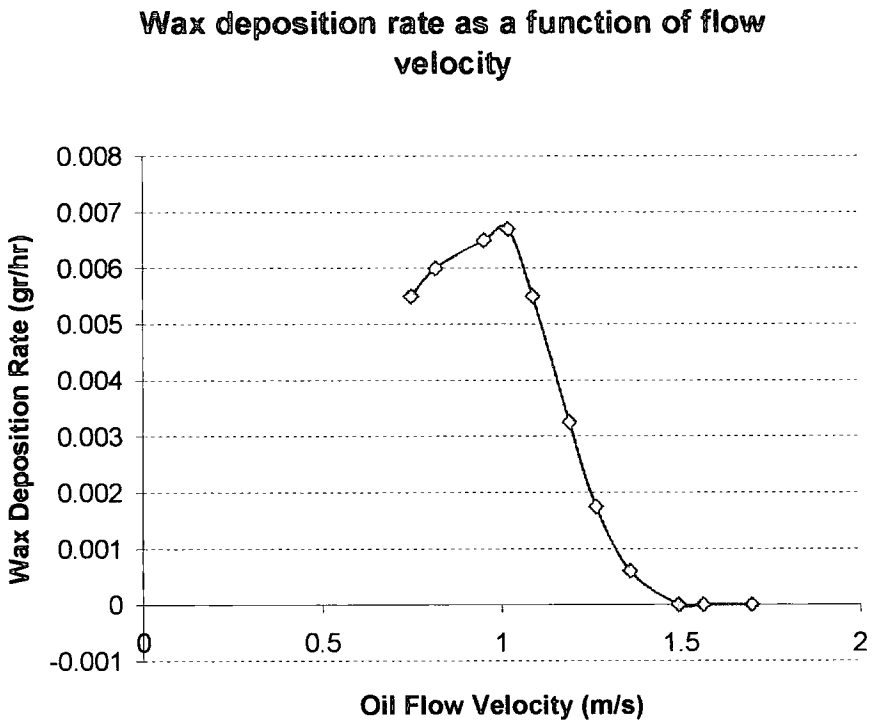

Figure 5.1. Wax deposition rate plotted against oil flow rate, from Hamouda (1995).

With a critical velocity in mind, the ideal solution to the problem of wax deposition might be to operate the pipeline above a critical velocity such that wax can never establish itself on the pipe-wall. However, even if a critical velocity could be determined for a particular crude oil, there may be too many conflicting factors for the oil to be pumped at this rate. Also, the necessity for shutdowns of oil production for various maintenance procedures means that fluctuations in oil velocity are unavoidable.

An alternative to providing the necessary shear rate for wax removal throughout the entire pipeline length is to use a pig to travel along the pipe jetting fluid at the wax deposits to remove them. Such a pig could have distinct advantages over a conventional device, in that,

i) No physical contact means no tool wear.

ii) No physical contact means no BUE (Built Up Edge).

iii) Fluid jet would assist in re-suspending removed wax to avoid plug formation.

In order to be of use over long distances in the challenging environment of an oil pipeline, such a pig would ideally be a passive, mechanical device similar in architecture to a conventional pig. Jetting would therefore be supplied in the form of fluid bypass through the pig. This chapter will describe how such a device might work and its limitations.

5.2 Existing jetting devices

The use of bypass flow in pigging is already well established. A limited amount of bypass flow can be used to control the velocity of a pig or to aid removal and re-suspension of wax ahead of the tool. At the most basic level, bypass is introduced by allowing the driving fluid to flow through the central mandrel or through holes placed in an array around the seals (figure 5.21).

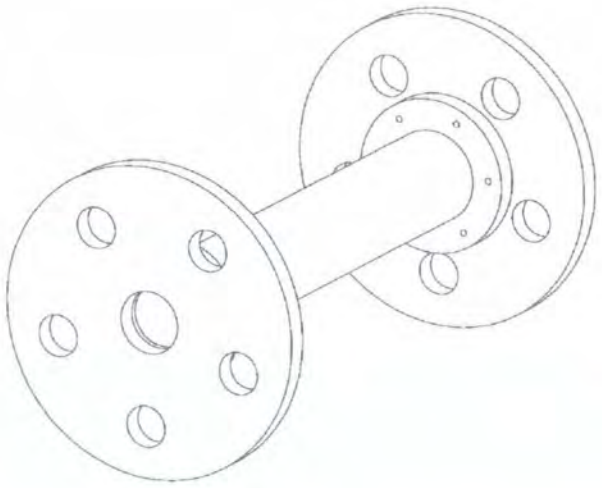

Figure 5.21. Conventional arrangement for bypass holes in pig seals.

The effectiveness of the bypass produced by these pigs in cleaning the pipe wall is not proven, although evidence does exist for some success in the control of velocity. Operators can time a pig's passage through a length of pipe to obtain its average velocity.

Although uncommon in use, patents do exist for more sophisticated jetting devices. Figure 5.22 shows a jetting pig that uses a central element with an array of nozzles that, driven by the fluid bypass, rotates and sprays fluid towards the pipe wall. In both

the turbine mechanism that provides rotation and the fine nozzles, such a device is of questionable robustness if used for any distance in a crude oil pipeline.

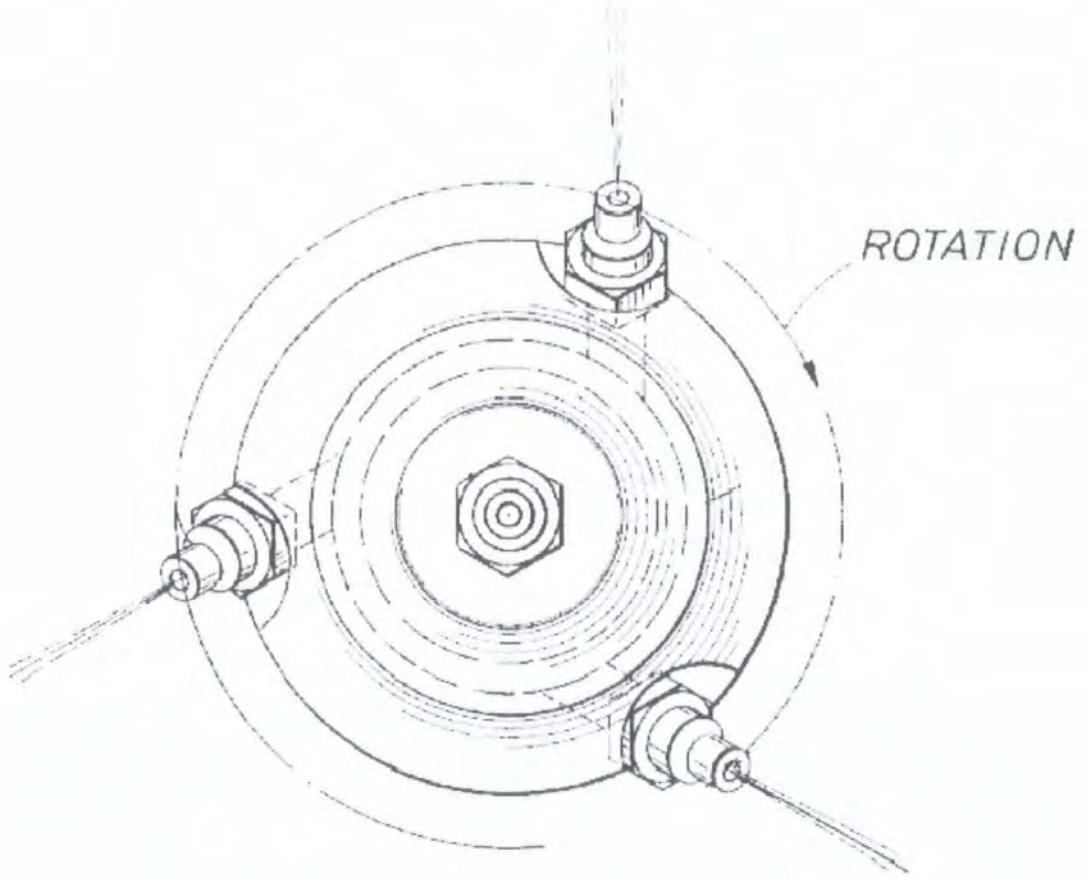

Figure 5.22. Rotating jetting nozzles, (Shell Oil Company,1999, US PAT No.5875803)

A less complicated and possibly more robust device is shown in figure 5.23. It has deep grooves cut into the circumference of the seal that allow fluid to pass through forming jets close to the pipe wall. It is assumed that these jets will assist in wax removal. Note, however, that the seal is still in contact with both the pipe wall and the wax deposit. The primary mechanism for wax removal is therefore mechanical and the pig is subject to all the problems of tool wear and sensitivity to pipe geometry that conventional pigs suffer from.

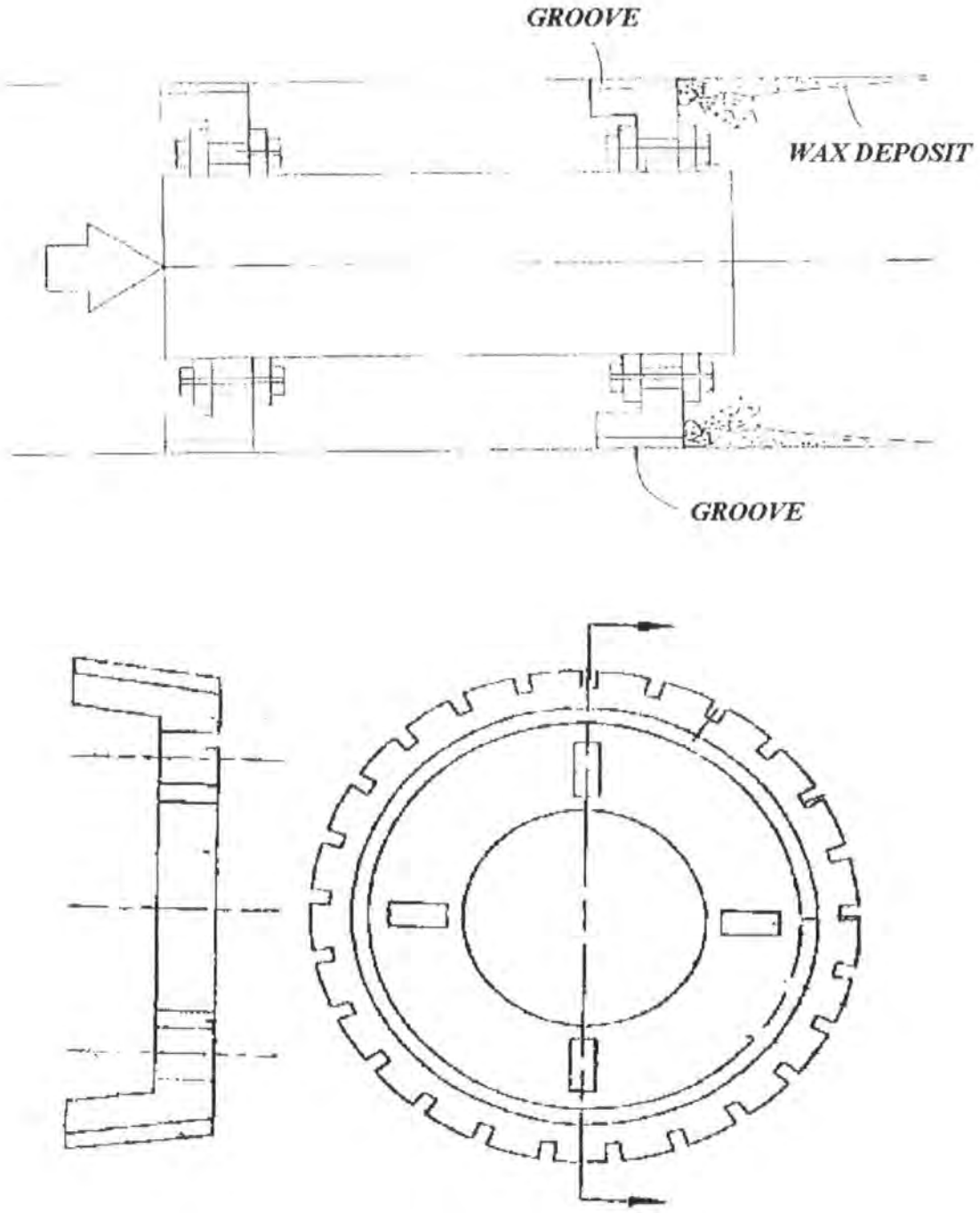

Figure 5.23. Pipeline pig using circumferential grooving to provide jetting (US pat 2003/0056309 A1, 2001).

5.3 Proposed Jetting System for Wax Removal

The system proposed for analysis in this thesis uses a plain disc at the front of the pig to produce an annular wall jet intended to remove soft wax deposits (figure 5.3). The large diameter mandrel allows free flow around the 'seals'. The seals in this instance are intended to hold the device concentrically in the pipe (and might just as easily be wheels). Drive is provided by a drag force produced as the bypass flows around the plate at the front of the pig. To maintain continuity of flow, the fluid in the area of the annulus around the plate is accelerated and a wall jet emerges. This wall jet shears wax deposits from the pipe wall and prevents the pig ever contacting the wax deposit.

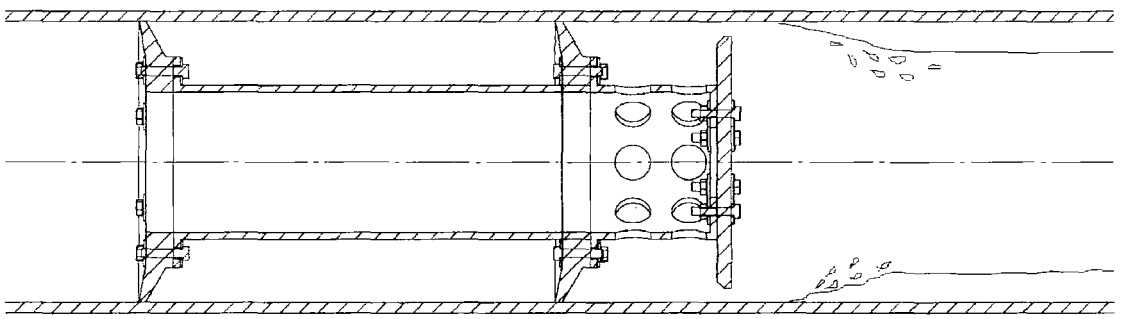

Figure 5.3. Proposed non-contacting annular bypass pig

Note that using this concept, no contact is required between the pig and the wax deposit and the risk of plug formation is greatly reduced. The wall jet should not only remove deposits from the pipe wall, but also provide sufficient turbulence to maintain a 'stand-off' distance between the pig and the removed wax.

5.4 Theoretical model of annular bypass jetting system.

In order to progress towards a theoretical model of a pig that uses an annular bypass system to remove wax, it is necessary to describe the mechanism by which a conventional pig operates. For an incompressible fluid such as oil, if no bypass is present, a pig will move at the mean velocity of the oil within the pipe. In accordance with Newton's second law of motion, for the pig to accelerate to this velocity a force must be applied to it. A pressure differential will therefore develop across the pig until the necessary force is available. A force must also be applied to the pig to overcome the friction between the pig's seals and the pipe wall. Equating the forces acting on a pig, the pressure differential across the pig is therefore;

$$\Delta P = \frac{ma + F_f}{\pi r^2} \qquad \textit{equation 5.41}$$

Where,

P = Pressure (N/m^2)

m = Mass of pig (kg)

r = Pig radius = Pipe radius (m)

F_f = Frictional Resistance (N)

Once the pig has reached the mean velocity of the fluid a steady state is achieved where only the frictional resistance needs to be overcome and the pressure differential across the pig reduces to,

$$\Delta P = \frac{F_f}{\pi r^2} \qquad \textit{equation 5.42}$$

If bypass around the pig is to be accounted for in the force balance equation, a control volume moving with the pig can be considered (figure 5.41).

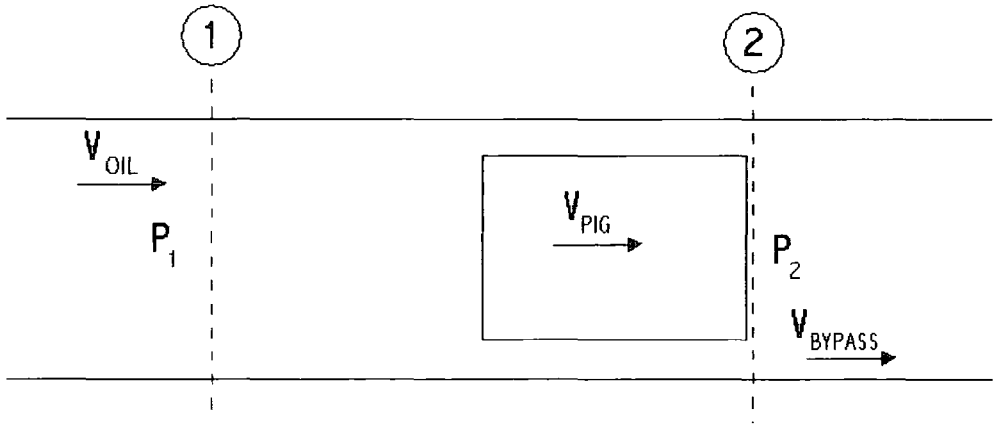

Figure 5.41. Control volume bounded by points 1 and 2 moving with a pig in a pipe.

If a steady state is considered, with the pig moving at a constant velocity, V_{PIG}, the sum of the forces acting on the pig will equal zero. Therefore,

$$\Sigma F_{pig} = (P_1 - P_2)A_{pipe} + \dot{m}(V_2 - V_1) - F_f = 0 \qquad \textit{equation 5.43}$$

Where,

$V_1 = V_{OIL} - V_{PIG}$ (m/s)

$V_2 = V_{BYPASS}$ (m/s)

$\dot{m}$ = mass flow rate = $\rho A V_1$

ρ = density (kg/m^3)

A = Area (m^2)

In order to gauge whether or not the contribution of the momentum forces are significant enough for inclusion in the analysis some typical values for V_1 and V_2 can

be considered. If V_1 is approximately 0.5 m/s, V_2 can be calculated from an assumption of continuity,

$$V_2 = \frac{A_1}{A_2} V_1 \qquad \textit{equation 5.44}$$

For the bypass system under consideration A_1/A_2 is typically in the order of 1/10 for a 160mm diameter pipe. The force due to momentum change across the pig, F_m, is therefore,

$$F_m = \rho A V_1 (V_2 - V_1) \qquad \textit{equation 5.45}$$

$$F_m = 1000 kg/m^3 \cdot 0.021 m^2 \cdot 0.5 m/s (5 m/s - 0.5 m/s)$$

$$F_m = 47 \text{ N}$$

A typical pressure differential across such a pig will be approximately 1 Bar. The percentage of the net force acting on the pig due to the momentum change (ignoring the friction force, F_f) is therefore,

$$\left(\frac{F_m}{(P_1 - P_2) A_{pipe} + F_m} \right) \cdot 100\% \qquad \textit{equation 5.46}$$

$$\left(\frac{47N}{10^5 Pa \cdot 0.021 m^2 + 47N} \right) \cdot 100\%$$

$$=2\%$$

As a simple and robust analysis of a jetting pig is required, the small contribution to the net force on the pig due to fluid momentum change will be omitted.

In the case where there is bypass through the pig, Azevedo et al (1998) provide a useful analysis. If the pig is travelling at the mean velocity of the oil within the pipe, the pig can be represented by a control volume of oil with a flow rate (Q_{pig}) equivalent to the bulk flow of oil. Hence,

$$Q_{oil} = Q_{pig} \qquad \textit{equation 5.47}$$

If oil bypasses the moving pig continuity of flow is maintained when,

$$Q_{oil} = Q_{pig} + Q_{bypass} \qquad \textit{equation 5.48}$$

In the case of annular bypass, the velocity of the bypass, V_{bypass}, is,

$$V_{bypass} = \frac{Q_{oil} - Q_{pig}}{\pi\left(R^2 - r^2\right)} \qquad \textit{equation 5.49}$$

Where,

R = Pipe radius = major radius of annulus

r = minor radius of annulus

In order to find a solution for equation 5.45 the proportion of flow as bypass must be determined at any given oil flow rate. This is possible if both the pressure differential across the pig and a discharge coefficient for the annular orifice are known. The pressure differential across the pig relates to the frictional resistance at the seals and is described by equation 5.42. An equation for flow through the annular gap can then be

obtained using Bernoulli's equation. Applying the equation to points 1 and 2, axial positions immediately before and after the pig respectively,

$$\frac{P_1}{\rho g}+\frac{V_1^{\,2}}{2g}+z_1=\frac{P_2}{\rho g}+\frac{V_2^{2}}{2g}+z_2 \qquad \textit{equation 5.50}$$

Where,

P = Pressure (N/m^2)

ρ = Density (Kg/m^3)

V= Velocity (m/s)

g = acceleration due to gravity (m/s^2)

z = potential energy (m)

Using the pig as a reference frame, in a horizontal pipe,

$$\frac{P_1}{\rho g}+\frac{V_1^{2}}{2g}=\frac{P_2}{\rho g}+\frac{V_2^{2}}{2g} \qquad \textit{equation 5.51}$$

Also, continuity is still assumed, as in equation 5.44, so

$$V_2=\sqrt{\frac{2(P_1-P_2)}{\rho\left[1-\left(d_2/d_1\right)^4\right]}} \qquad \textit{equation 5.52}$$

Equation 5.52 gives the theoretical discharge velocity at the orifice. The term $(1-(d_2/d_1)^4)$ approaches unity for the bypass system under analysis and is subsequently

omitted for clarity. Frictional losses mean that the actual velocity at the orifice is slightly less than the theoretical velocity and a coefficient of discharge must be applied to obtain an accurate prediction of flow. If A_{bp} is the orifice area, through which bypass is discharging,

$$Q_{BP} = A_{BP} C_d \sqrt{\frac{2\Delta P}{\rho}} \qquad \textit{equation 5.53}$$

Where,

Q_{bp} = Bypass flow (m^3/s)

C_d = Discharge coefficient for annular orifice $\approx$ 0.8

Assuming that ΔP provides sufficient force for the pig to overcome friction between the seals (or wheels) and the pipe-wall, a maximum value for ΔP, and therefore the bypass flow rate can be found. Equations 5.44 and 5.49 can therefore be combined to allow calculation of a minimum flow rate, Q_{oil}, that will drive the pig at a velocity, V_{pig}, dependent on the frictional force between the pig and the pipe wall, F_f and subsequent bypass flow rate,

$$Q_{oil} = \left(V_{pig} \times A_{pipe}\right) + \left(A_{BP} C_d \sqrt{\frac{2\left(\frac{F_f}{\pi r^2}\right)}{\rho}} \right) \qquad \textit{equation 5.54}$$

Assuming a gel-like wax deposit behaves like a Bingham fluid, any bypass flow velocity above a critical value will remove the deposit. In order for a non-contacting, annular bypass pig to work effectively, the wax removal *velocity* must be greater than the pig's velocity. If the wax removal velocity is less than the pig velocity, the pig will 'catch-up' with the wax deposit and plug formation will begin. If wax removal

velocity is exactly equal to the pig velocity the system will lack robustness. If the wax removal rate drops briefly for any reason, for example if a slightly stronger area of deposit is encountered, the pig will contact the deposit and there is a risk of plug formation.

Equation 5.48 gives the maximum bypass velocity based on the principle of continuity and predicts the velocity of the fluid at a point a small distance from the orifice known as the *vena contracta.* At some point further downstream of the orifice the jet issuing from the orifice will disintegrate and the velocity distribution in the pipe will resume the same profile as before the orifice. The exact position of the vena contracta can be determined experimentally and will depend on the profile of the orifice in question. If a critical velocity (for wax removal) is obtained at the vena contracta, it is important to understand the rate of decline of this velocity so that the point at which the jet's velocity is no longer greater than or equal to the wax removal velocity can be identified. This point will effectively determine a stand-off distance for the wax removal front ahead of the pig. A large stand-off distance is desirable as it will give a more robust removal process that can accommodate inconsistencies in the deposit's mechanical properties and slight irregularities in the pig's velocity.

Equation 5.48 is most commonly applied to orifices issuing into a fluid medium. In the proposed system the orifice is an annular ring and the subsequent jet will be bounded by fluid on one side and a solid wall on the other. In order to understand the decay of the jet as it issues from the annular orifice it can be analysed as a classical wall jet (Figure 5.42). Launder and Rodi (1981) define a wall jet as,

"a shear flow directed along a wall where, by virtue of the initially supplied momentum, at any station, the stream-wise velocity over some region within the shear flow exceeds that in the external stream."

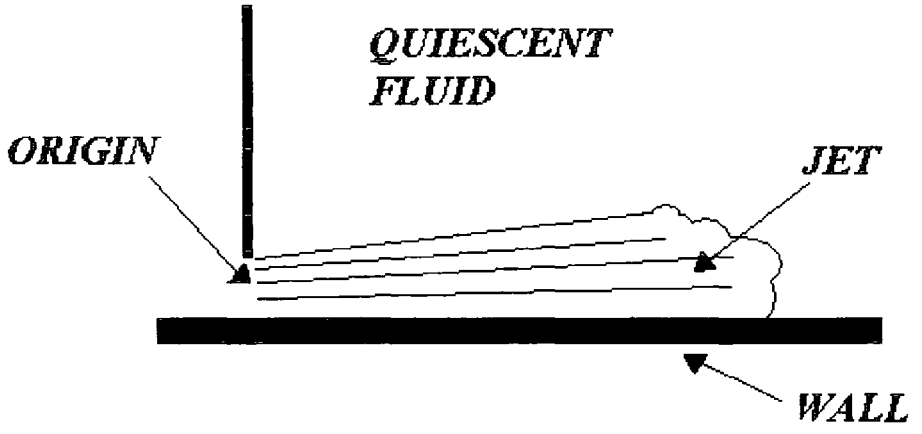

Figure 5.42. Wall jet.

Considering the annular bypass as a wall jet is useful as it takes into account the loss of energy in the jet due to viscous eddies both at the pipe wall and the boundary with the quiescent fluid. The wall jet theory, originally described by Glauert (1956), allows prediction of the rate of decay of the annular bypass jet and the axial position, relative to the pig, at which wax removal velocity and pig velocity are in equilibrium. According to Glauert's wall jet theory, the relationship between maximum jet velocity (U_m) and distance from the origin (x) is approximately,

$$U_m \propto x^{-1.12} \qquad \textit{equation 5.55}$$

As the pipe wall is moving in an opposite direction to the wall jet with a velocity equal to the pig, the jet's velocity profile will be distorted in comparison to that of a jet bounded by a static wall. This might cause a faster rate of decay of the wall jet than in the case of a static wall. However, pig velocity is small compared with that of the jet, so the effect will be negligible. Assuming the fluid jet obeys Newton's law of viscosity, the shear stress at the wax deposit will be proportional to the jet's velocity and the wax removal velocity will also vary according to axial distance from the jet origin. Assuming the gel-like wax deposit behaves plastically, the wax removal velocity will have the following relationship to jet velocity

$$V_R = C + kV_J^{\,n} \qquad \textit{equation 5.56}$$

Where C, k and n are constants and V_J is jet velocity. It is necessary to empirically derive values for these constants that will allow prediction of wax removal rates based on a known jet velocity. To this end an experimental rig was designed that would allow measurement of jet and removal velocities for waxes of different thickness and composition. Before this series of experiments was carried out an initial test of the concept was performed to allow a qualitative observation of the process and assess feasibility.

5.5 Experiment to verify annular bypass wax removal concept

To test the concept of wax removal using a non-contacting pig providing an annular jet, a laboratory experiment was designed. The aim of the experiment was to determine whether or not a soft wax deposit applied to the wall of a circular pipe could be removed by the action of an annular jet. At this stage only qualitative results were necessary, and an accurate measurement of the rate of removal of the wax deposit was not necessary.

5.51 Preparation of test pieces.

It was anticipated that the annular bypass system of wax removal would only be effective where the wax deposit was in the form of a gel. Although a gel with a low shear strength was desirable to test the removal concept, the gel required sufficient rigidity to maintain structural integrity against the effects of gravity when cast onto the pipe wall. Some initial experiments with ratios of wax to oil suggested that a blend of 30% macrocrystalline wax and 70% white oil would give the best results. The oil and wax were heated in a glass beaker using an electrical hot plate. The mixture of wax and oil was heated to 70 °C (slightly above the melt point of the wax) to ensure the wax was completely melted and the mixture cast into a test spool as shown in figure 5.51. Once the liquid had been poured into the spool between two end-stops the spool was rotated on a cradle at approximately 30 rpm until the mixture had solidified sufficiently such that 'slumping' did not occur when the spool was left stationary. Cooling was aided by the use of an 'ice-pack' around the spool. The wax was cast to a

depth of approximately 5mm. With the end stops set a distance of 200mm from each other a volume of approximately 0.5 litres of the wax/oil mixture was required.

Figure 5.51. Casting apparatus for annular bypass wax removal tests.

5.52 Description of test rig for annular bypass experiment

The sample wax was cast into the pipe spool, and then inserted into the pipe loop shown in figure 5.52. This rig comprises of approximately 5m of transparent PVC 6" (162mm) pipe emptying into a 400 litre break tank and fed by a centrifugal pump delivering water at up to $100m^3/hr$. Flow rate can be throttled by a 3" (75mm) gate valve mounted to the pump delivery flange[3].

The upstream closure plate of this rig is fitted with a seal to allow a 6mm plastic coated steel cable to run from the test pig within the pipe to a pulley assembly behind the pump. This allows drag forces on a stationary pig to be measured and compared to prevailing flow conditions in order to determine specific drag coefficients. Forces were measured using a 0-100kg spring balance. Flow rate was measured using an orifice plate with a discharge coefficient ≈ 0.62, designed in accordance with British Standard 1042 (1964).

The test pig used in this experiment is shown in figure 5.53. It consists of a 10mm thick circular PVC plate mounted on an aluminium shaft. The shaft is held concentrically in the pipe by two sets of spokes that radiate out to thin-sectioned rims, 300mm apart. These support rims are a sliding fit in the pipe such that the frictional force resisting axial movement of the pig is negligible. The PVC plate has 10mm of clearance to the pipe bore.

[3] Note that the components used in this rig are described by the nominal imperial sizes given by the manufacturers. Actual dimensions in SI units are shown in brackets. This reflects industry practice in pipeline engineering.

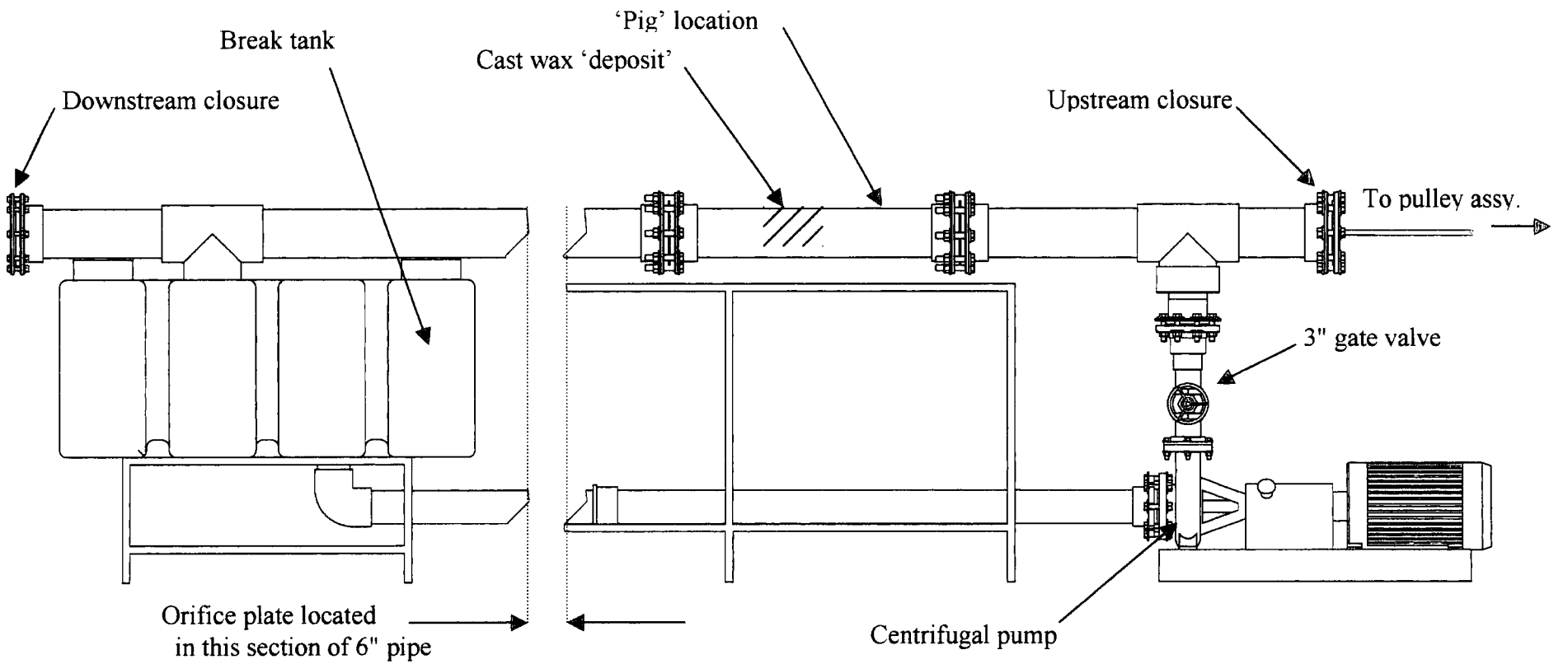

Figure 5.52. Test Loop for annular bypass wax removal tests.

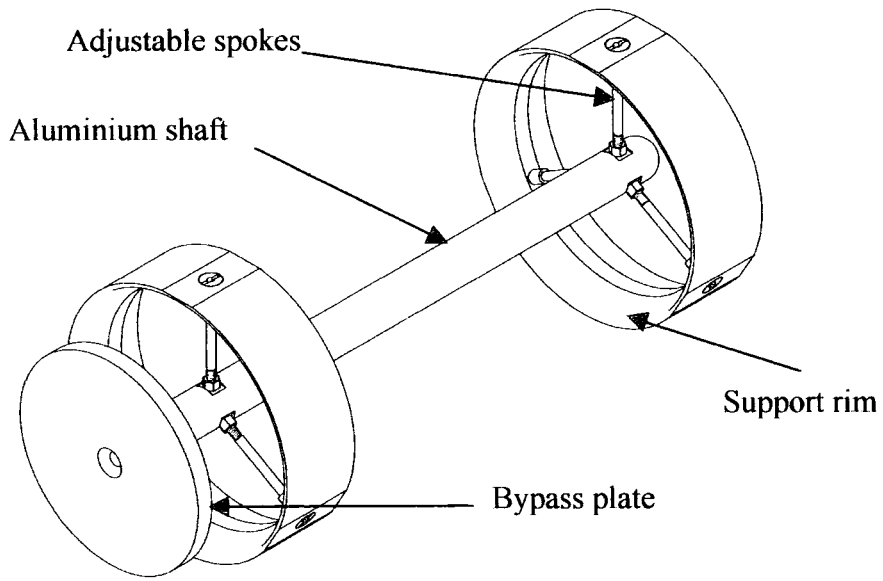

Figure 5.53. Annular jetting test pig

5.53 Test procedure for annular bypass tests

With the wax spool in position as indicated in figure 5.52, the test 'pig' was inserted and held, using the steel cable, at a distance of approximately 0.5m upstream of the wax. With the gate valve three quarters closed, the pump was started and the pipe loop slowly filled with water. With the pipe loop full of water, the gate valve was gradually opened and the pressure differential across the orifice plate was recorded. The pig was then slowly introduced to the wax by winding out the restraining cable. This process was repeated at increments of throttle opening until the jet of fluid bypassing the test pig removed the wax in the spool.

5.54 Results and observations from initial tests

With a wax deposit of approximately 5mm depth, removal could be observed at a volumetric flow rate of 11.5 litres per second. At this flow rate the mean velocity of the fluid in the pipe is 0.56 m/sec. For continuity of flow, the velocity of the fluid emerging through the annular gap around the plate must be 2.4 m/sec. The test was conducted with a 1.5 Bar pressure differential across the pig.

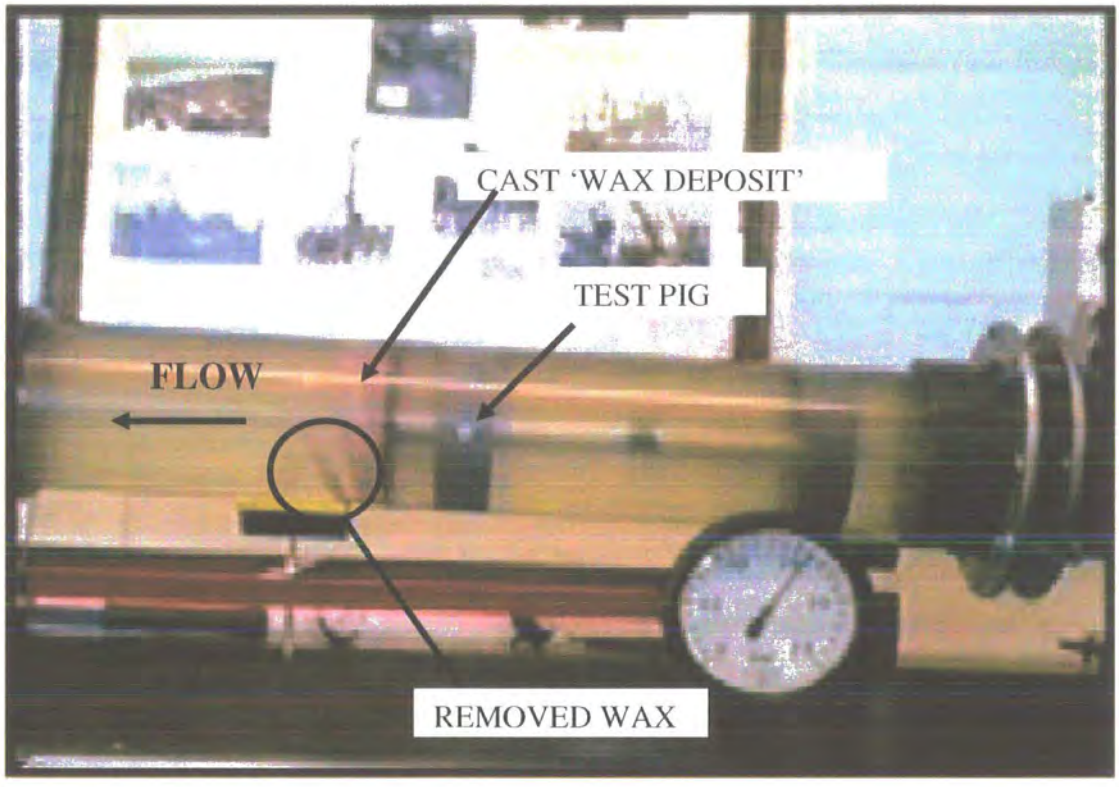

Figure 5.54. Wax deposit failing under the action of annular jet.

Although the wax was removed under the conditions described, it was impossible to provide a quantitative analysis of the observations. The wax broke off in lumps in some places, indicating adhesive failure. In other places the wax slid down the pipe

wall axially as a rigid body (figure 5.54). Moreover, observation of the exact failure mechanism was made difficult because of the cylindrical presentation of the deposit.

In light of the observations described, it was decided to carry out further investigation into the casting process used to simulate deposition in order to better understand the factors that determine the adhesive or cohesive failure of the deposit. These investigations are described in section 3.74. To improve visualisation and simplify analysis it was decided to use a plane strain experimental rig for further experimentation.

5.6 Plane Strain Jetting Experiments

5.61 Objectives of plane strain jetting experiments

The objectives for this series of experiments were,

a) To allow observation of the removal of wax deposits from a pipe wall so that a qualitative description of the process could be made.
b) To allow measurement of the forces and velocities acting on the wax during the jetting process.

5.62 Description of plane strain jetting test rig

The rig used for the plane strain tests was a modification of the existing flow loop described in section 5.52 and was designed by the author. A two metre length of the circular section pipe was replaced with two 1 metre long 'flat' pipes constructed from 200mm wide aluminium channel extrusions (figure 5.62.1 & 5.62.3). The root radii of the extruded sections were machined out to provide a perfectly rectangular cross section and flanges were welded to the ends to allow the use of adapter plates to connect the rectangular channels to each other and to the existing 6" circular section pipe. An acrylic window was made for each channel and was secured with a heavy steel frame. Sealing between the channel and window was achieved by using 6mm thick, cork impregnated rubber strips, mitred and glued to form a rectangular gasket. The flat pig, shown fitted to the rig in figure 5.62.1, was constructed from 10mm PVC plate. Two parallel plates separated by round aluminium pillars supported an

spanned the full width of the channel but left a gap at the top and bottom from which the wall jet could emerge. The rectangular plate could be replaced to give different gap sizes. Positioning of the pig was made possible by attaching the end of a cable to a round pin that could be dropped into holes drilled at increments of 50mmm along a box section steel tube mounted at the upstream end of the rig.

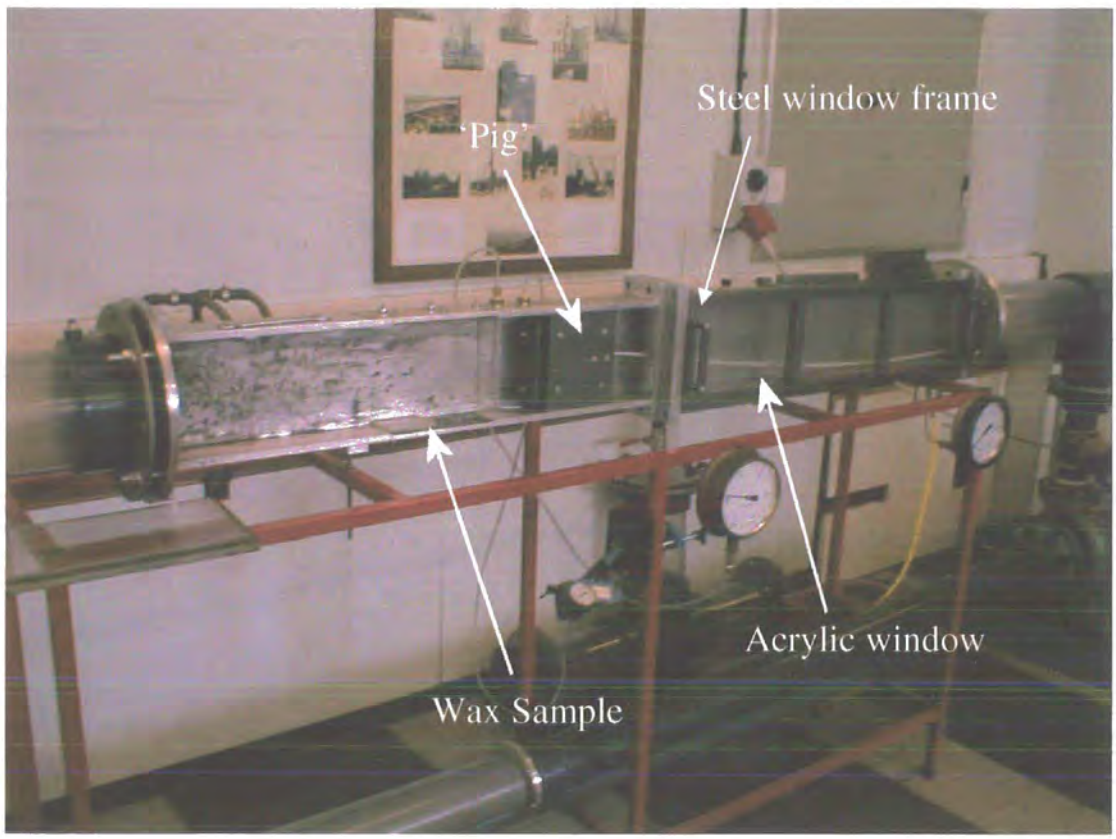

Figure 5.62.1. Plane strain rig

Wax samples were prepared using the casting equipment shown in figure 5.62.2. The mixture of oil and wax was heated until all the wax had melted (approximately 60°C). With the steel test plate mounted in the wooden mould, the molten wax was poured in to the required depth and allowed to cool to room temperature. The mould was constructed from wood to provide insulation to slow cooling of the wax mixture. It was found that without insulation the samples were highly sensitive to the steel test

plate's temperature and rapid cooling would occur at the wax/steel interface producing a gel-like sample with a hard substrate. Slowing the cooling of the wax promoted a more homogenous structure in the sample. A sheet of grease-proof paper was inserted between the mould and plate to prevent the wax sticking to the wood and breaking up on removal.

Figure 5.62.2 Wax sample plate and mould.

The test plate shown in figure 5.62.2 was constructed from mild steel and its top surface was milled to give a surface roughness of approximately 50μm. This texture was applied to simulate the surface roughness of a new, unlined steel pipe.

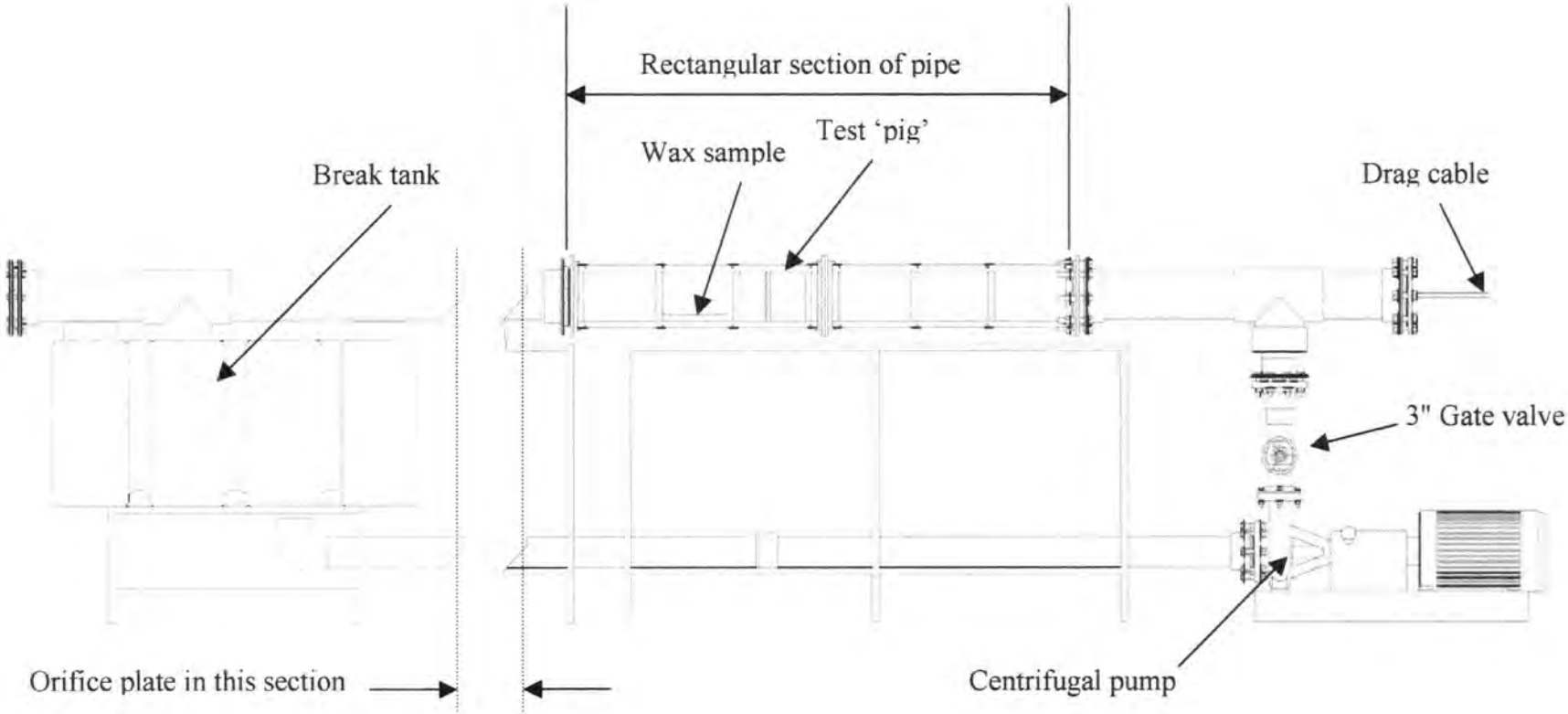

Figure 5.62.3. Plane strain test rig

5.63 Plane Strain Jetting Test procedure

Using the test rig described in section 5.62 a clear, 'sectional' view of the wax could be obtained as it was removed from the steel test plate by the jet of water directed along the pipe wall. Having cast a wax sample of the desired thickness, the steel test plate was secured into the 'pipe' wall and the observation window fitted. The pig was held back 0.5m from the deposit and the pump turned on. With the pump heavily throttled by the gate valve, the pipe loop was slowly filled with water. A video camera was placed at the observation window to record the test and the pig was moved to within an inch of the deposit while raising the pressure across the annular plate to 0.5 Bar. At this pressure a wall jet emerged from the gap between the plate and the 'pipe' wall with sufficient velocity to shear the wax from the steel plate. When all of the wax had been removed, or else removal had slowed to a barely discernible rate, the pump was shut off and the video footage was taken away for digitalisation and study.

The analogue video recordings of individual tests were converted to digital format on a personal computer using Adobe Premiere software. Using JASC Animation Shop software, the test footage was studied frame-by-frame to allow plotting of the length of wax removed against time. Two frames from a test are shown in figure 5.63.1 to illustrate how these measurements were made. A pixel count was used to determine lengths a and b for each frame studied. Length 'a' is the length of remaining sample and length 'b' is the original length of the sample. The ratio of these lengths, $(b-a)/a$ was multiplied by the actual plate length of 200mm to give the length of wax removed at each second of the test period, given by the frame number $F/25$ (note that the tests

were filmed at 25 fps). *F* denotes frame number, counted from the first frame in which movement of the wax sample can be discerned.

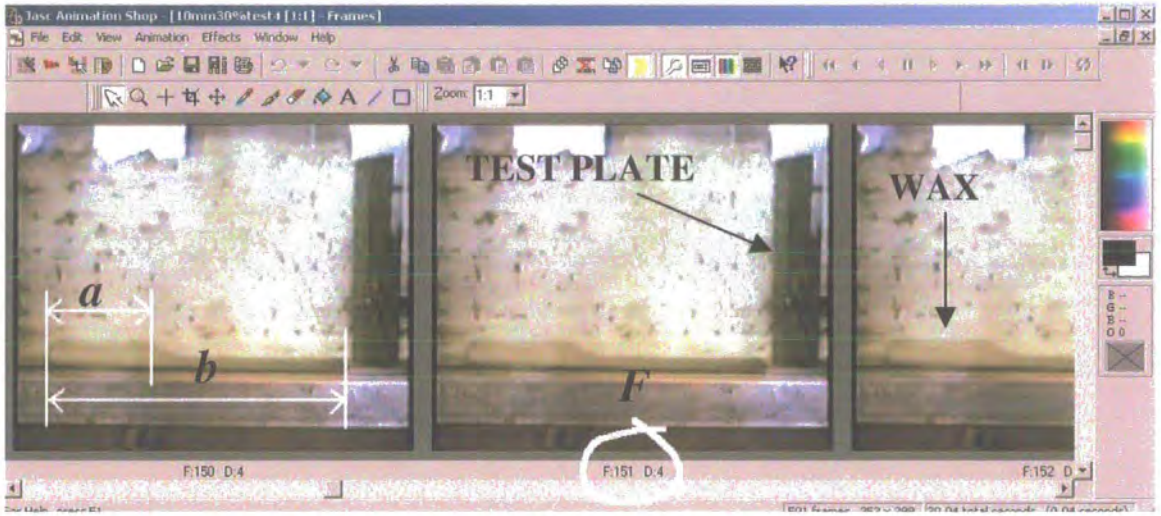

Figure 5.63.1. 'Screen shot' from analysis using video capture/animation software.

Tests were carried out for three different compositions of wax and for three different depths of wax. The gap and pressure differential across test plate were kept constant for all of the tests. The gap and pressure were determined by running a series of 'pre-tests', as described in the following section.

5.64 Pre-test calibration for plane strain annular bypass jetting experiment

A set of 'pre-tests' were performed to estimate the best annular gap to use in the subsequent experimental work. The test rig employed a centrifugal pump so it was important to match the system head to the pump's performance curve to obtain an optimum combination of volumetric flow rate and flow velocity at the jetting orifice. The experimental model used for the plane strain jetting tests is shown in figure 5.64.1 along with the relevant experimental parameters.

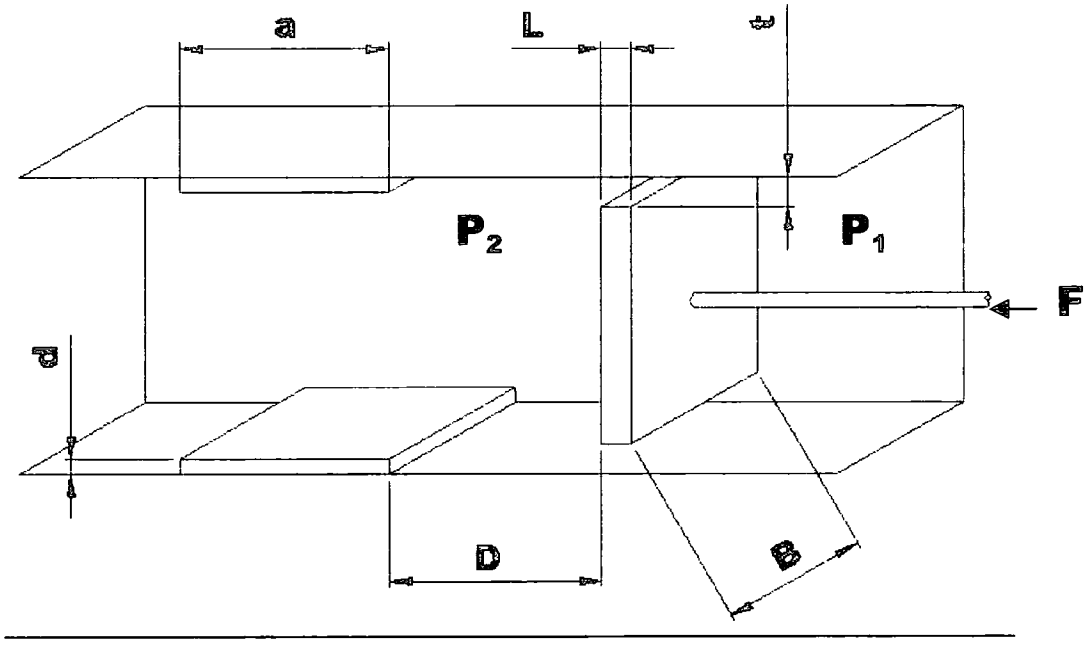

a=sample length (m)	L=length of test plate (m)
d=sample thickness (m)	t=gap (m)
D=stand-off distance (m)	F=force (N)
P=pressure (Pa)	B=width of channel (m)

Figure 5.64.1 Experimental model for plane strain bypass tests.

	Parameter levels			Length of wax removed (mm)					
RUN No.	A	B	C	1	2	3	4	5	MEAN
1	1	1	1	45	8	50	55	52	42.0
2	1	2	2	10	14	10	13	2	9.8
3	2	1	2	2	12	25	35	27	20.2
4	2	2	1	15	35	14	5	5	14.8

		L1	L2
A	ANNULAR GAP	5mm	15mm
B	D	75	175
C	WAX THICKNESS	5mm	10mm
	(WAX VOLUME)	(66ml)	(132ml)

Table 5.64.2. Results from annular bypass calibration tests

The calibration tests were carried out using the same procedure as described in section 5.63, with the exception that they were not filmed. Instead of filming, the tests were timed for 60 seconds and then the pump was stopped and the length of wax removed was measured. The tests indicated that the fastest and most consistent wax removal rate using this system was obtained using a 5mm gap to produce the wall jet.

During the tests flow was measured through the pipe loop using an orifice plate mounted approximately 3 metres downstream of the test area in a section of 6" round pipe. All tests were conducted with a constant pressure of 1.5 bar recorded immediately upstream of the test pig (indicated P_1 in figure 5.64.1). When a 5mm gap was used at the test 'pig' a pressure differential of 0.5 bar was recorded across the orifice plate. Equation 5.48 can be used to calculate the flow rate through the orifice plate. The subsequent fluid velocity at the test section and at the origin of the bypass around the test pig can be obtained by application of the principle of continuity. The

flow rate obtained in these tests was used in subsequent experimentation, so it is useful to obtain values for the flow velocity at key points in the test loop,

Inserting values for the pressure differential measured across the orifice plate (during the calibration tests) into equation 5.48 gives the volumetric flow rate through the test loop,

$$Q = 0.0011m^2 \times 0.62\sqrt{\frac{2 \times 50000N/m^2}{1000kg/m^3}} \qquad \textit{equation 5.52}$$

$$Q = 6.82 \times 10^{-3} m^3/s$$

Assuming continuity,

$$Q = V_C A_C = V_R A_R \qquad \textit{equation 5.64.1}$$

Where Q is volumetric flow rate, V is velocity, A is area and the subscripts C and R denote circular and rectangular pipes respectively. The mean velocity of the fluid within the rectangular section of test pipe will therefore be,

$$V_R = \frac{V_C A_C}{A_R} \qquad \textit{equation 5.64.2}$$

$$V_R = \frac{6.82 \times 10^{-3} m^3/s}{0.0108m^2}$$

$$V_R = 0.63m/s$$

The mean fluid velocity as it emerges from the test plate, V_J, is therefore,

$$V_J = \frac{6.82 \times 10^{-3} m^3 / s}{6 \times 10^{-4} m^2}$$

$$V_J = 11.4 m/s$$

5.65 Results of plane strain jetting tests

All tests were carried out at a flow rate of 6.8 litres per second with a gap of 5mm at the test 'pig', giving a theoretical velocity of 11.4 m/s at the jet's origin. Figure 5.65.1 shows a plot of distance (length of wax removed) against time for wax/oil mixtures of 50%, 40% and 30% wax, all at 5mm sample thickness. Plotted on the same graph is distance against time for 10mm and 15mm thickness of waxes for the 30% wax mixture. The 'distance' plotted is the mean average value of length of wax removed obtained from 6 tests for each respective sample type. All of the curves fitted to the data show that the length of wax removed is a natural logarithmic function of time. The data is plotted in figures 5.65.2 and 5.65.3 in inverse form as time against length of wax removed. Figure 5.65.2 shows the results of the tests on the 5mm thick wax samples and figure 5.65.3 the results of the tests on the 10 and 15mm thick samples. Considered in this form, it can be seen that time is an exponential function of length of wax removed and all of the curves have the form,

$$y = ae^{kx} \qquad \textit{equation 5.65.1}$$

Where y represents time, x represents length of wax removed, e is the base of the natural logarithm and k and a are constants. This exponential function can be differentiated with respect to x (length of wax removed) in order to obtain a ratio of time/distance at any given distance,

$$\frac{dy}{dx} = ake^{kx} \qquad \textit{equation 5.65.2}$$

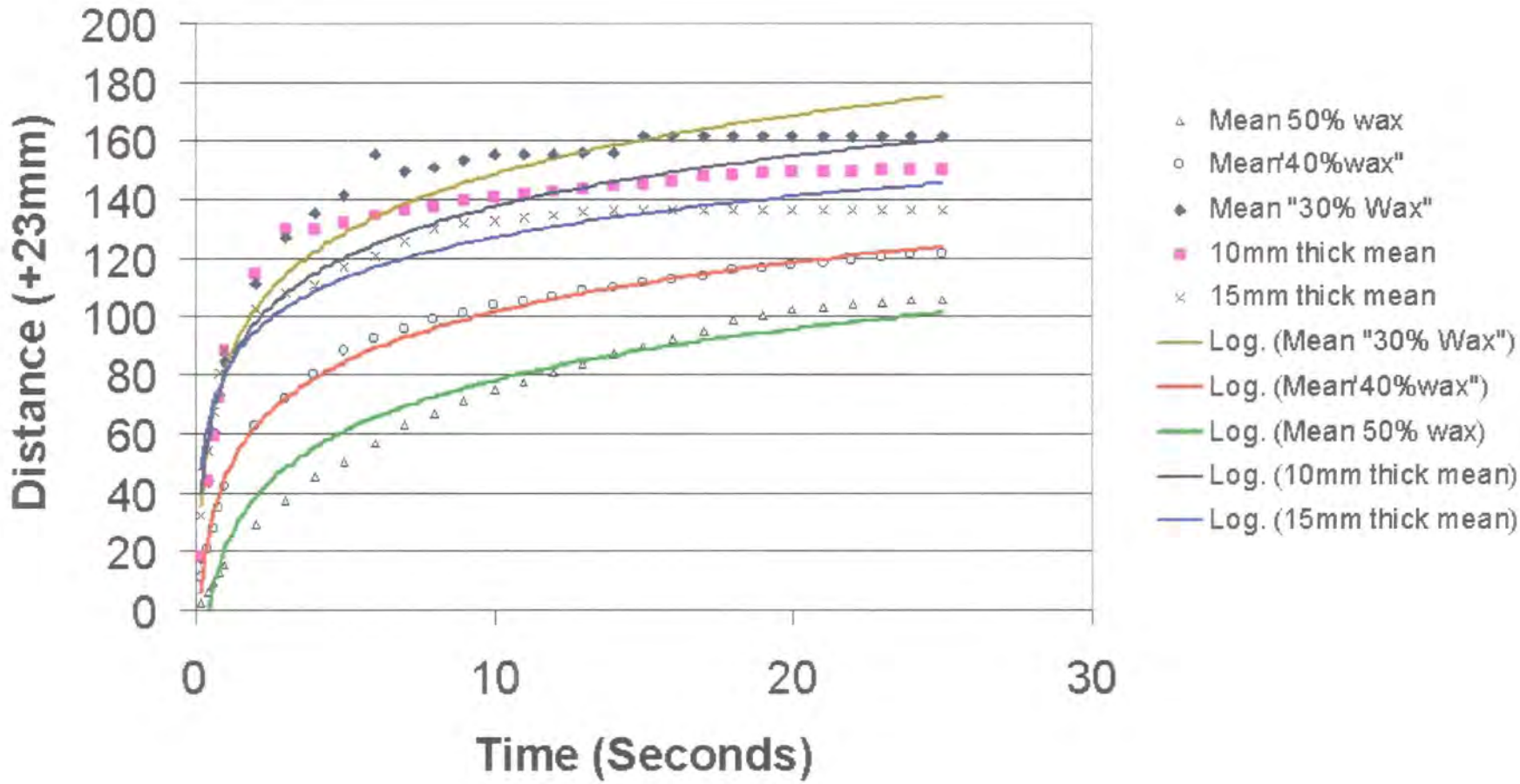

Figure 5.65.1. Length of wax removed (Distance) plotted against time.

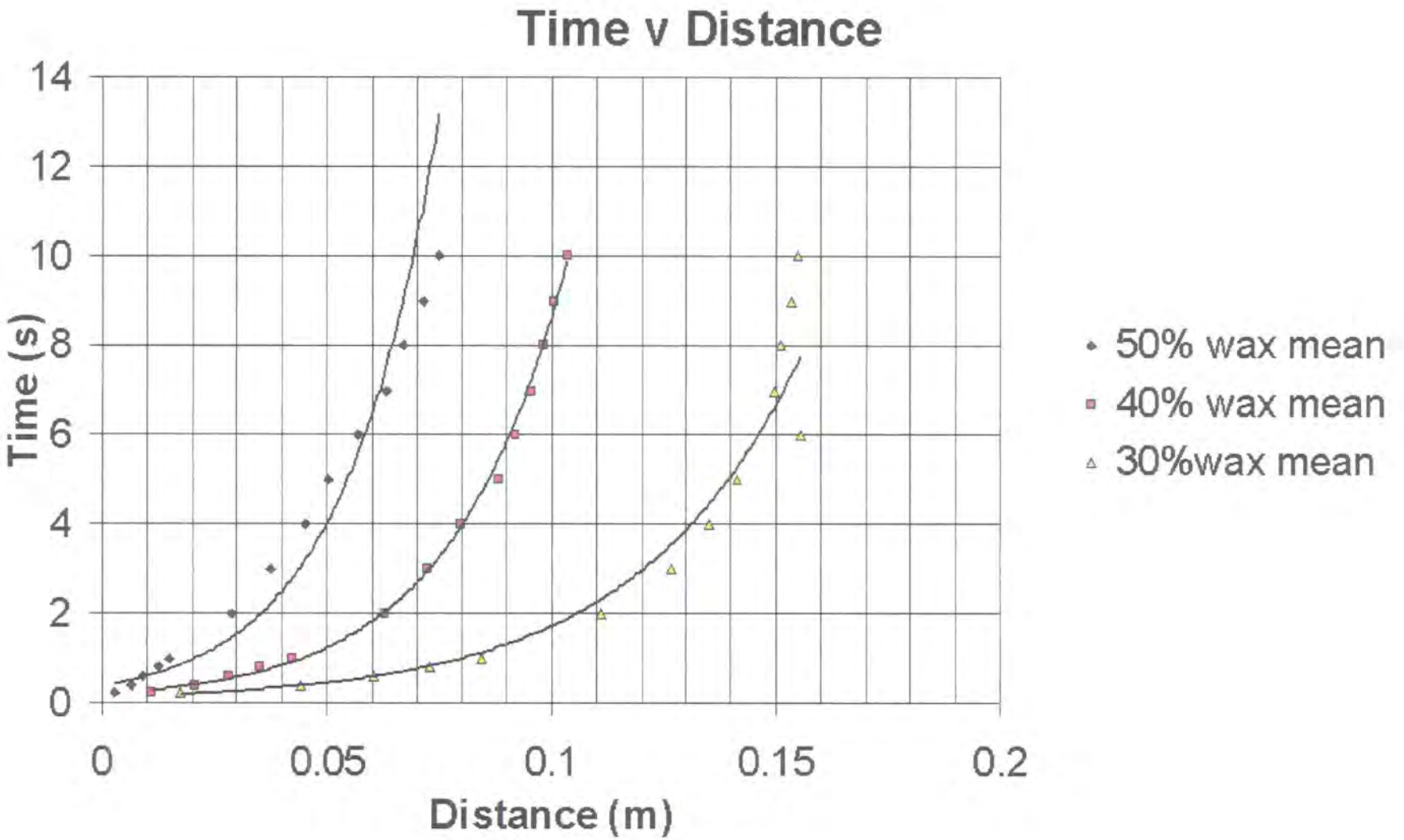

Figure 5.65.2. Time plotted against length of wax removed (Distance) for 5mm thick samples.

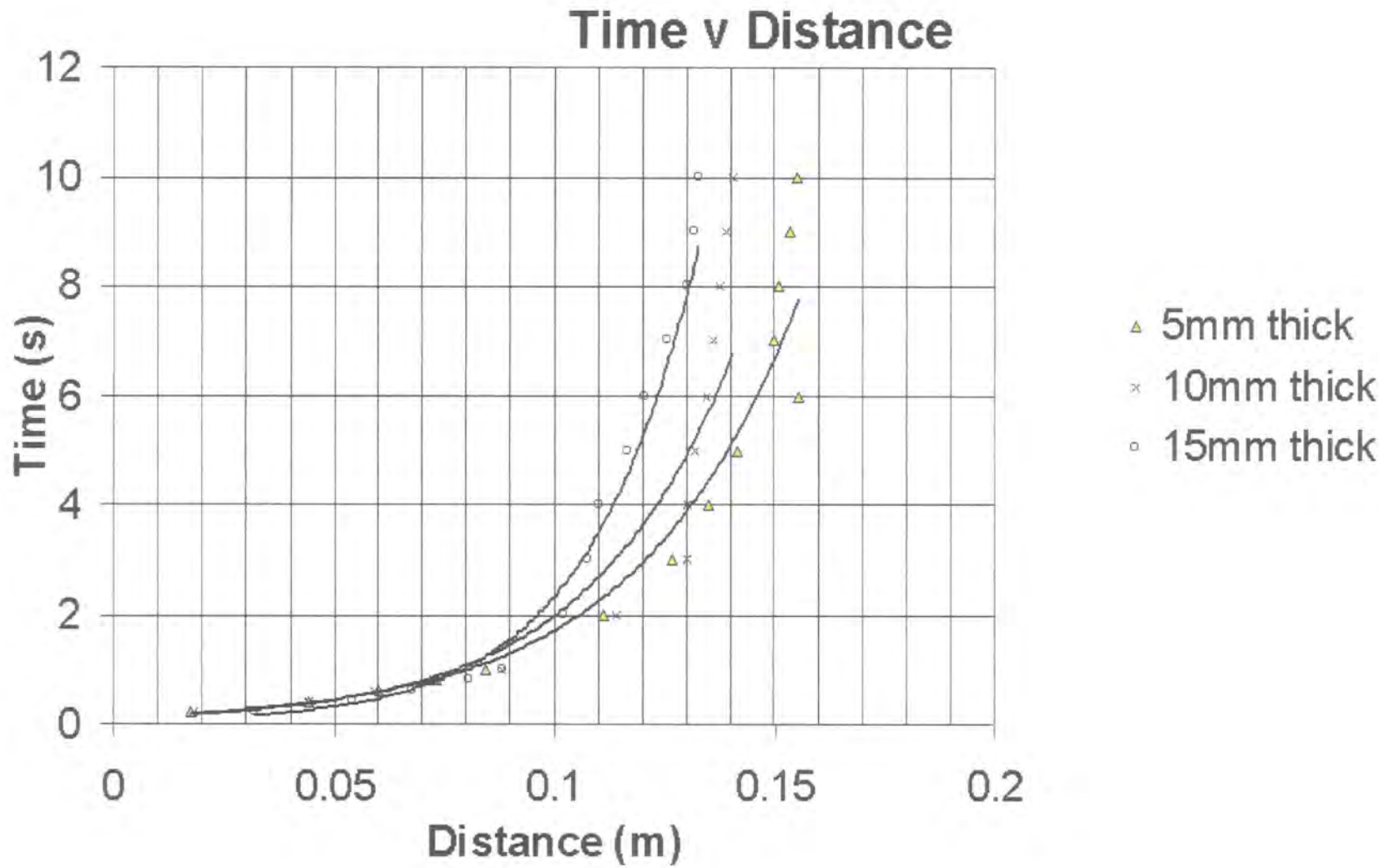

Figure 5.65.3. Time plotted against length of wax removed (Distance) for 30% wax samples.

The term *dy/dx* represents the reciprocal of the wax removal velocity, V_R, therefore,

$$V_R = \frac{1}{ake^{kx}} \qquad \textit{equation 5.65.3}$$

Using empirically derived values (from graphs 5.65.2 and 5.65.3) for the constants *a* and *k*, equation 5.65.3 was used to obtain values for wax removal velocity at increments of axial distance from the jet origin. Wax removal velocity is shown plotted against distance in figure 5.65.4. A formula for wax removal velocity with respect to an offset distance *x* is certainly useful, but is unique to this particular pig geometry and flow rate. An expression relating wax removal velocity to jet velocity is more useful. This would allow a prediction of removal rates in any circumstances, provided the flow rate and pig dynamics are understood.

In order to produce a graph of wax removal velocity against jet velocity, readings of the flow velocity were taken at several points along the axis of the pipe to measure the rate of decline of the wall jet velocity at its boundary with the pipe wall. These measurements were taken using a Pitot tube and the tests are described in Appendix F. The results of the pitot-tube measurements are shown in figure 5.65.5. It can be seen that the fluid velocity is inversely proportional to distance from the jet origin, in agreement with the wall jet theory described in section 5.4.

Jet velocity is plotted against removal velocity in figure 5.65.6. Straight-line curves have been fitted to the data points and it can be seen that the x- axis (jet velocity) is intercepted by all of the curves at approximately 7 m/s. This suggests that in all cases

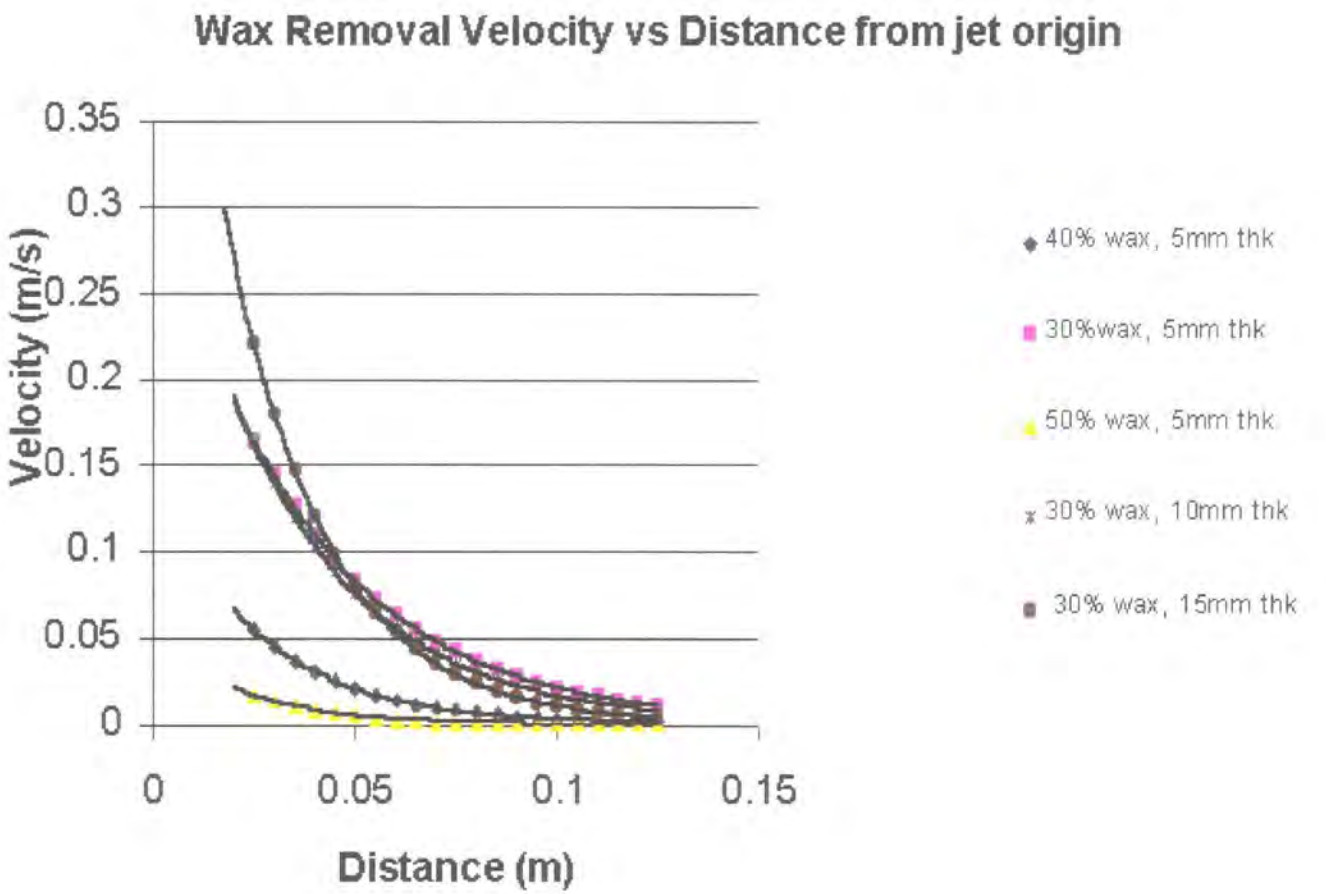

Figure 5.65.4. Wax removal velocity plotted against distance from jet origin

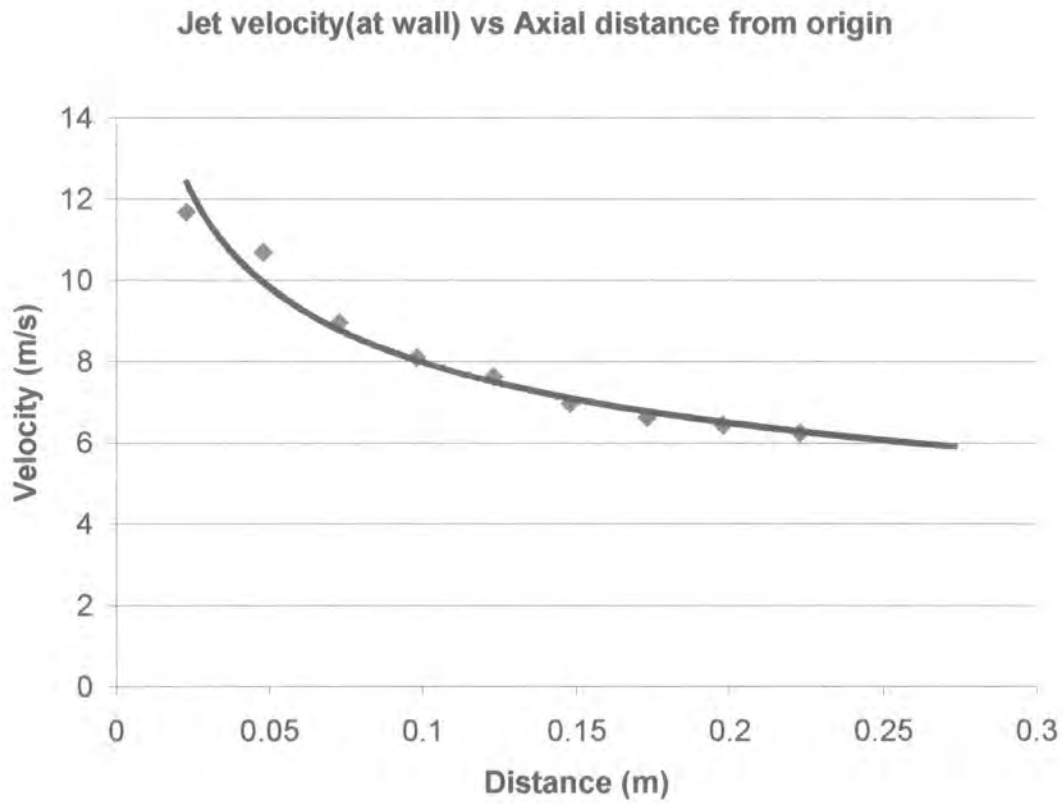

Figure 5.65.5. Graph showing velocity of wall jet, measured adjacent to the wall, plotted against axial distance from jet origin using measurements taken using a pitot tube.

wax removal does not begin until a critical velocity of approximately 7m/s is reached. Once removal of the wax commences, at jet velocities greater that 7 m/s, the gradient of the curves varies in proportion to oil content. The steepest gradient is for the 30% wax sample and the smallest gradient is for the 50% wax sample.

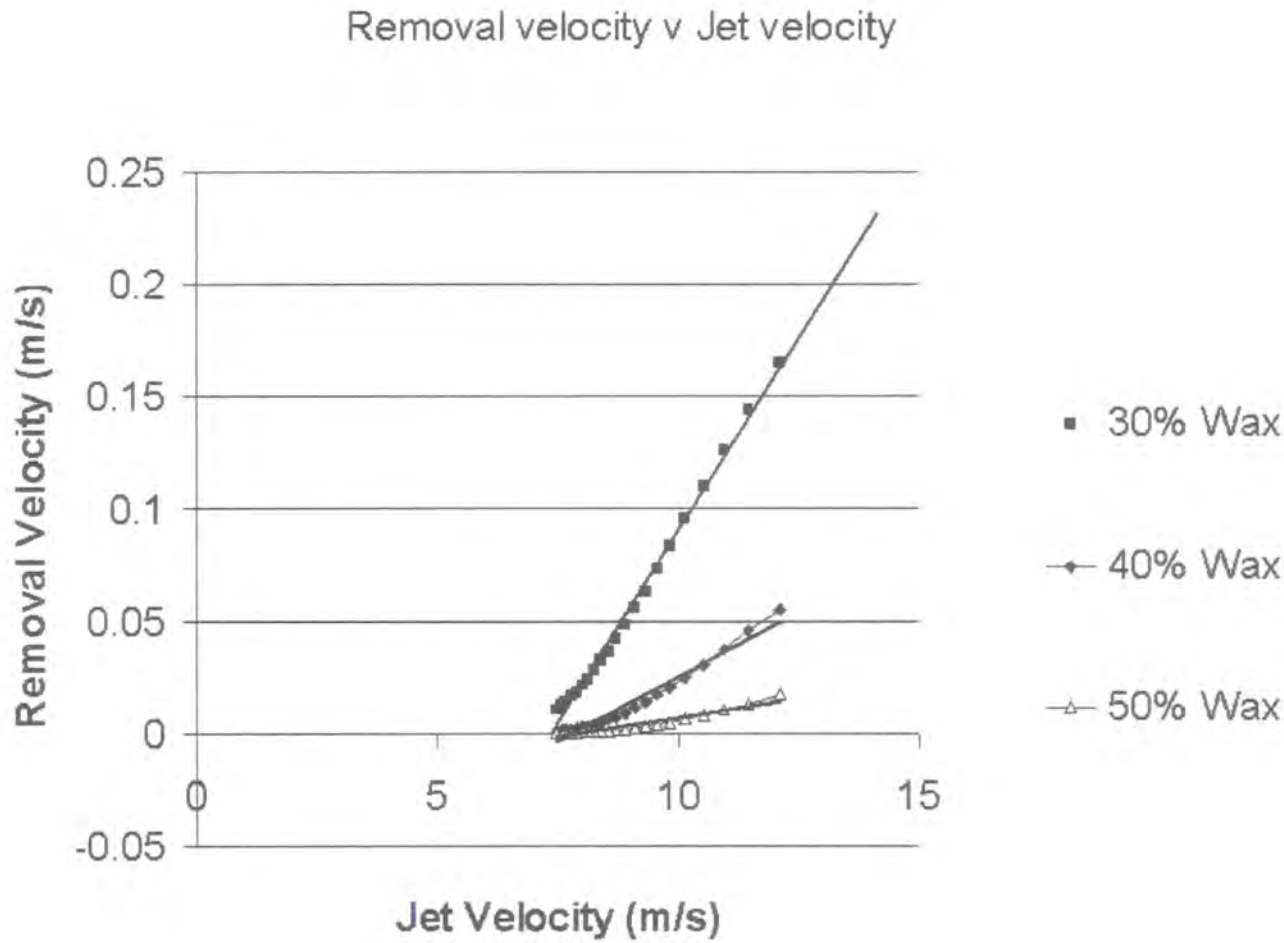

Figure 5.65.6. Wax removal velocity plotted against distance from jet origin

5.66 Observations from plane-strain jetting tests

It was noted that during removal of the wax deposit by the wall jet an area of re-circulating water developed immediately downstream of the test plate. This re-circulating water transported the removed wax back towards the pig. To visualise this phenomena clearly, a high-speed camera recording at 250 frames per second was used to film a test. The wax used in this test was a 32mm thick sample of 30% wax/70% oil. The sample was particularly thick to allow clearer visualisation of its flow path on removal.

During the test, the flow of material was constant along the breadth of the sample with no transverse movement of the material indicating that the assumption of *plane strain* conditions was valid. Figure 5.66 shows the 32mm thick wax sample being removed by the wall jet. The five frames were selected from a time span of approximately 0.7 seconds to best illustrate the pattern of re-circulation.

It can be seen in figure 5.66 that the action of the wall jet on the wax sample 'knocks off' the square edge of the sample. As flow of the wax sample continues, an angle of approximately 45 degrees establishes at the front of the wax. This occurred in all of the tests, suggesting that the physical mode of failure for the wax is that of shearing.

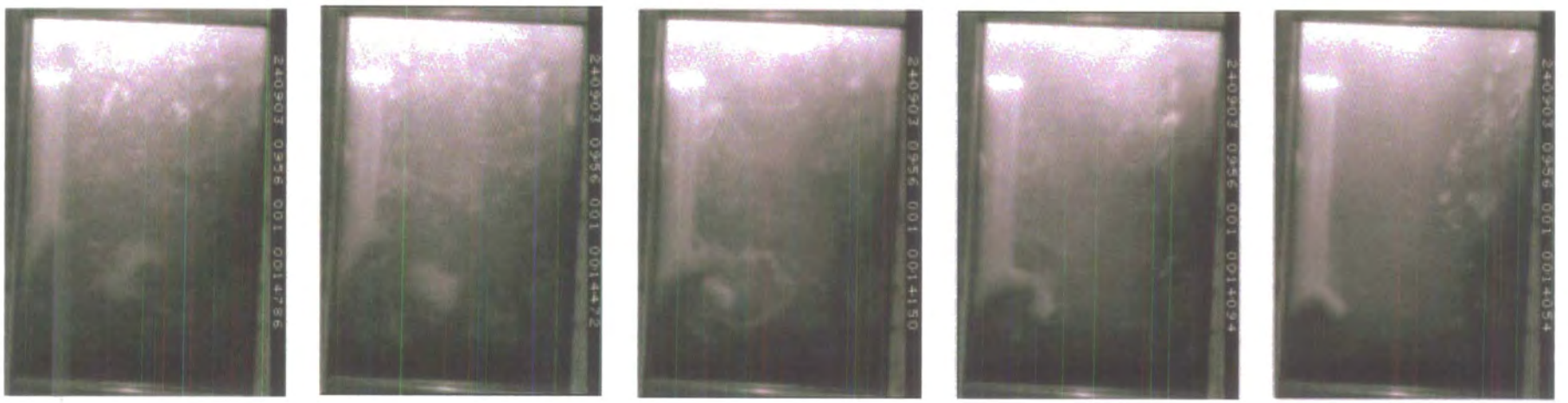

Figure 5.66. Wax removal test showing re-circulation of removed deposit.

5.7 Conclusions from jetting tests

Having obtained a linear relationship between jet velocity and wax removal velocity for a specific wax consistency and depth (Figure 5.65.6), it is possible to extract constants for gradient and y axis intercept from the resultant curves. These constants can be inserted into the equation that predicts pig velocity based on bypass area, discharge coefficient and pressure drop in order to determine appropriate parameters for successful wax removal. For the annular bypass method of removal to work, the velocity of wax removal must always exceed the pig velocity, or the pig will collide with the deposit and removal will occur mechanically with the attendant risk of plug formation. Therefore, for a given pig geometry and total flow rate, pig velocity and removal velocity are described by equations 5.71 and 5.72 respectively. Note that equation 5.71 is a variation of that describing pig velocity, already stated in equation 5.54.

$$V_{pig} = \frac{\left(V_{oil} \times A_{pipe}\right) - \left(C_d A_{BP} \sqrt{\frac{2P}{\rho}}\right)}{A_{pipe}} \qquad \textit{equation 5.71}$$

$$V_{removal} = K \times V_{bp} + C \qquad \textit{equation 5.72}$$

These two equations can be combined to determine the required flow rate to allow effective use of any given pig to remove a specified deposit. The resulting equation gives a value for V_{oil} where V_{pig} and $V_{removal}$ are equal.

$$V_{oil} = \frac{C_d \sqrt{\frac{2P}{\rho}} \left(A_{oil} K + A_{bp} \right) + A_{oil} C}{A_{oil}} \qquad \textit{equation 5.73}$$

Figure 5.7 shows a plot of flow velocities against differential pressure across the pig, obtained using equation 5.73. The wax removal constants, K and C, were those obtained from the 30% wax removal tests where a 5mm thick sample was used. The first curve (circular data points) shows the flow velocity that produces a pig velocity equal to wax removal velocity. Above this maximum flow velocity, $V_p > V_R$ and a collision will occur between the pig and wax precipitating mechanical removal and plug formation. The second curve (square data points) shows the velocity of the pig when the system is optimised and $V_p = V_R$. If the flow rate is below that shown by the first curve, $V_p < V_R$ a stand-off distance will begin to establish itself between the pig and wax removal front. Reducing the flow rate further will ultimately lead to a point where there is insufficient flow through the annular orifice to create a pressure differential large enough to overcome friction. At this point the pig will stall, as indicated by the third line on the graph (triangular data points).

The differential pressure across the pig is a design parameter that can be honed experimentally by altering friction at the seals and the discharge coefficient for the pig's annular bypass orifice. The flow rate, however, is usually an operational constraint. With this in mind, it is clear that 'tuning' an annular bypass pig to operate in the (narrow) wax removal zone shown in figure 5.7 is a considerable practical challenge. Possible solutions to this problem are discussed in chapter 7.

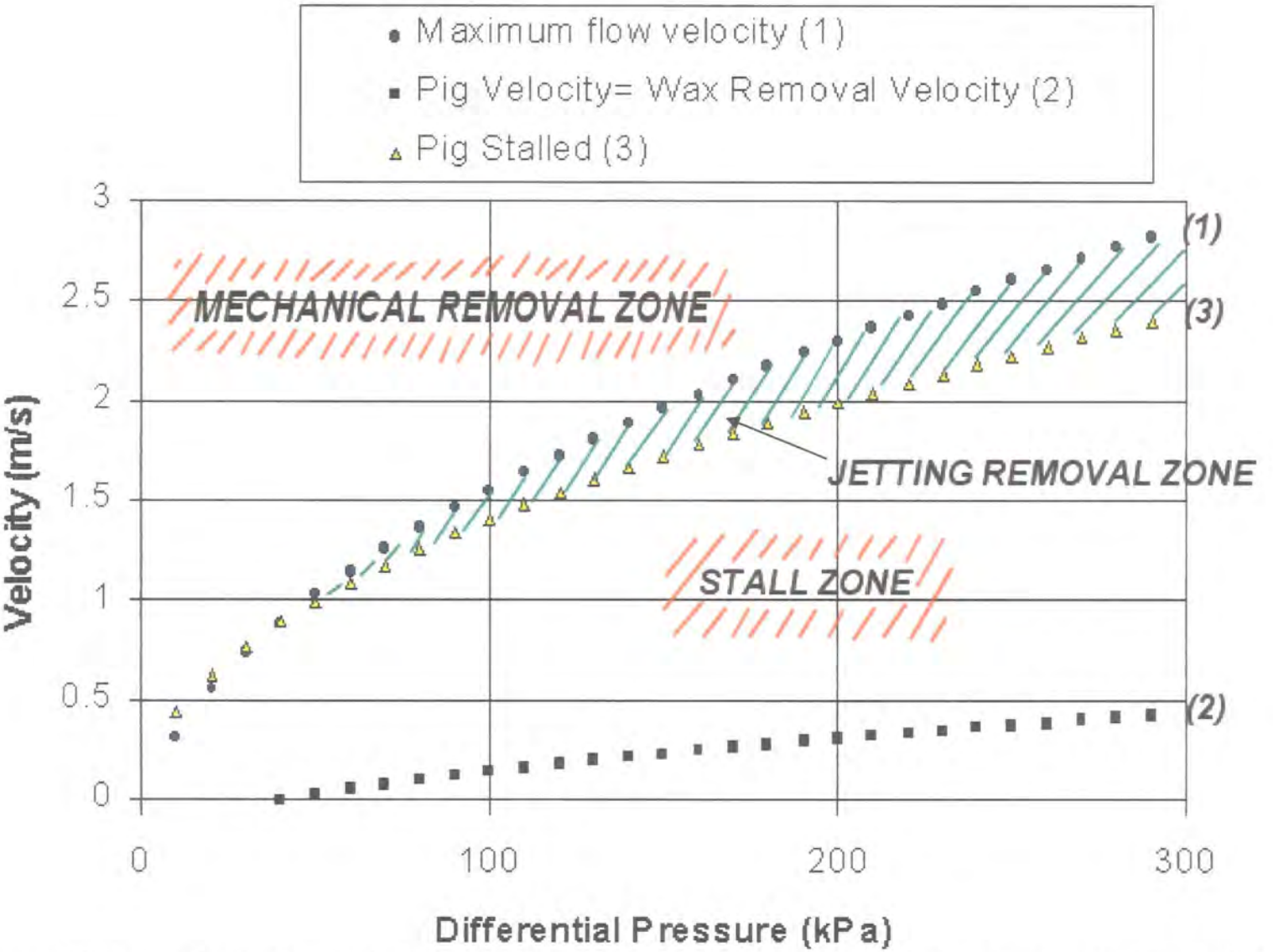

Figure 5.7 Plot of velocity against differential pressure across pig for 30% wax sample, 5mm thick. 5mm annular gap in a 6" pipe.

5.8 Computational Fluid Dynamics

The foregoing test procedure has shown that an approximate prediction can be made of the performance of an annular bypass pig, based on simple continuity theory and some empirically derived constants for wax removal rates. In order to improve the likelihood of successful wax removal however, it is necessary to optimise the design of the annular bypass tool. A powerful tool in this optimisation process is Computational Fluid Dynamics (CFD). The following section describes computations made using *Fluent* software that illustrate how CFD can be used to model the annular jetting system.

Having obtained agreement between theory and experimental results for the basic flow pattern in question, a CFD model of the annular bypass experiment was made based on the experimental conditions and a series of simulations were performed. The *Fluent* software operated in 2D mode, reflecting the plane strain conditions of the experiment. A step was included in the solid boundary of the CFD model, to represent the wax deposit to be removed. The leading edge of this step was chamfered to represent the 'shear angle' that formed at the retreating wax removal front during the tests described in section 5.66. The distance between the origin of the wall jet and the 'wax sample' in the CFD model was set at 23mm, as in the practical experiments.

Figure 5.81 shows a plot of the contours of maximum flow velocity generated by the CFD program for these conditions. The maximum velocity of 13.5 m/s compares favourably with the simple prediction based on continuity of 11.4 m/s and the measured value from the pitot tube of 11.7 m/s. Accuracy of the solution provided by

the CFD software can be improved by increasing the number of iterative calculations performed by the program. In this case 200 iterations were made, taking less than an hour to compute using a typical desktop PC (Personal Computer). Because so few iterations were used in the calculation, accuracy is limited. For example, it can be seen from figure 5.81 that the jet widens and maintains velocity, suggesting an *increase* in momentum. Nevertheless, the acceleration of the jet as it enters the slot and the general flow pattern both appear correct. Figure 5.82 shows the pattern of recirculation predicted by the software model and it is an accurate reflection of the pattern observed and illustrated in figure 5.66.

Although beyond the remit of this thesis, the CFD model described could be exploited, in conjunction with the empirical data gathered, to optimise a commercial annular bypass, jetting tool. The design of the bypass plate could be optimised by minimising the re-circulation illustrated in figure 5.82. A series of computations could be made using the CFD software and changing the profile of the bypass plate to determine which produces the least re-circulation without sacrificing the compactness of the jet. It may also be desirable to produce a maximum discharge coefficient for the annulus by streamlining the tool. A discharge coefficient can be obtained from the *Fluent* computations.

Clearly, optimisation of the jetting tool design can be rapidly and cost effectively achieved using CFD software modelling. Once an optimised design has been finalised a physical model could be built and tested using the equipment described in section 5.5 to provide validation of the design.

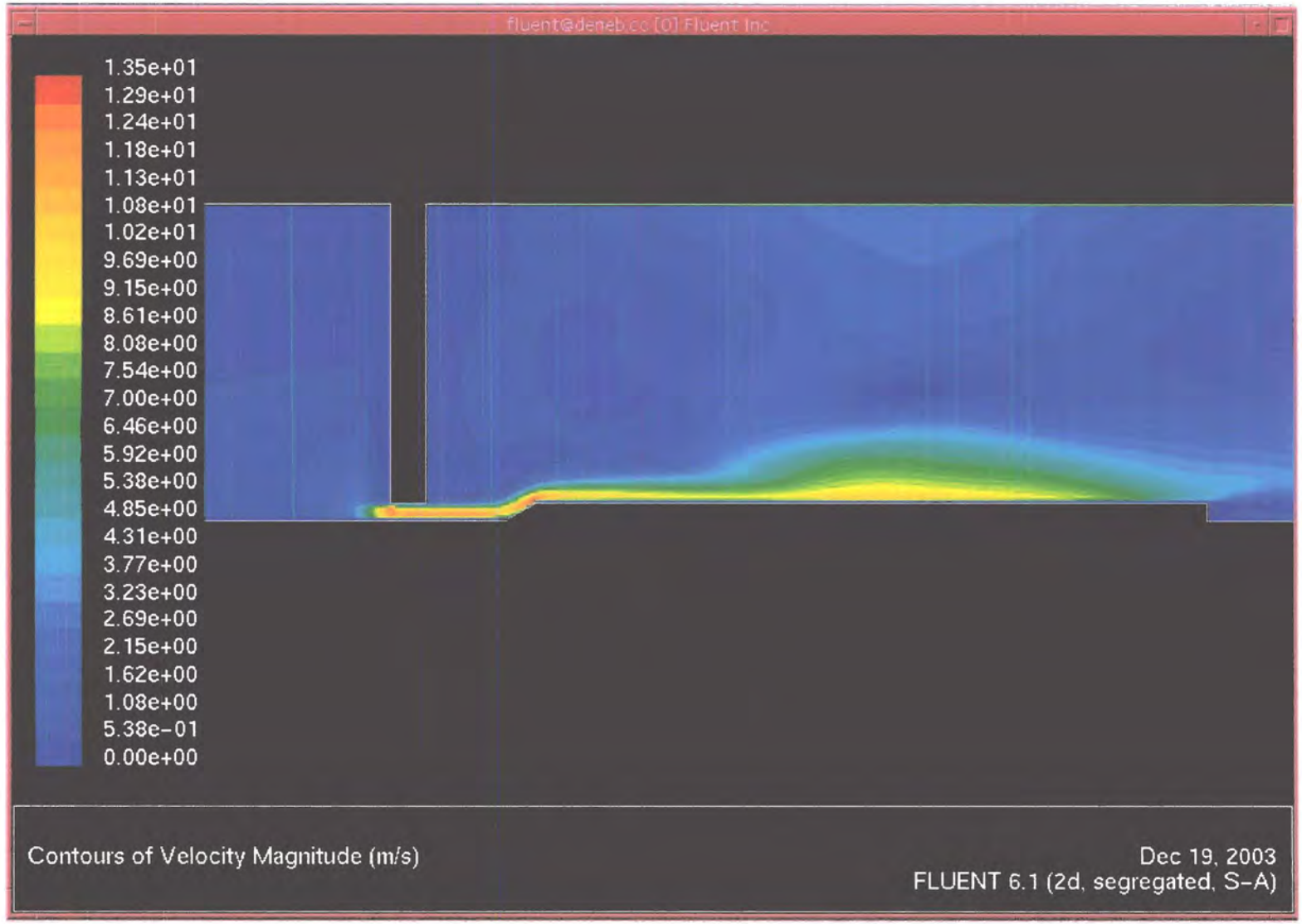

Figure 5.81 Plot of contours of maximum velocity, generated using *Fluent* CFD program

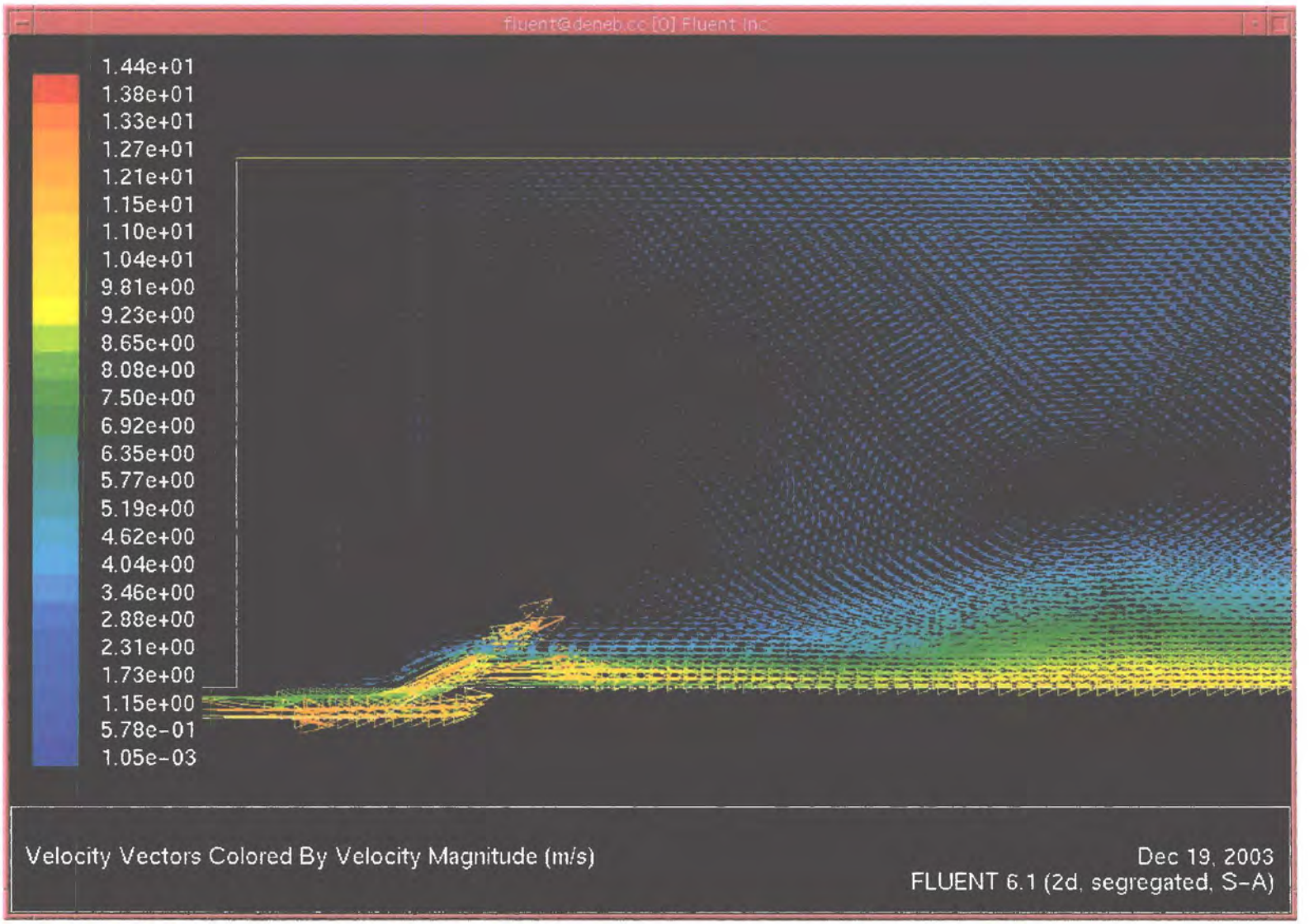

Figure 5.82 Plot of velocity vectors, generated using *Fluent* CFD program

Chapter 6 Annular Bypass Pig Trials

6.1 Introduction

Complimentary to the laboratory based research described in chapter 5 has been a programme of trials by Pipeline Engineering Ltd. The design and development of these trials was influenced by the progress of the author's laboratory work, and in turn, the field trials have helped to validate the laboratory results. These trials were undertaken at Pipeline Engineering Ltd's test facility in Catterick, North Yorkshire. The trials were used to determine the practical feasibility of employing an annular bypass pig to remove wax from the wall of a gas condensate pipeline. The tests were carried out at full scale using 40 metres of 12 inch steel pipe to represent a section of the Shah Deniz gas condensate transport pipeline, soon to go 'online' in the Caspian Sea.

A prototype pig, manufactured by Pipeline Engineering, was used to remove wax samples from a clear polycarbonate test spool inserted into the pipe loop. The efficiency of the pig's annular bypass system was assessed by observation of the pig's interaction with the sample in the clear spool. Observation was made possible by the use of the same high-speed camera as used in the tests described in chapter 4.These observations were analysed with reference to other data gathered during the trials, such as pressure measurements, flow measurements and the physical configuration of the trial pig. Analysis of the results was based on the model developed by the author and described in chapter 5. The tests were organised and run by Pipeline Engineering LTD in conjunction with BP. Their full test procedure is detailed in Appendix F.

6.2 Equipment for annular bypass pig trials

A 90hp Sykes-Weir centrifugal pump was used to pump potable water through the test loop, shown in figure 6.21. A schematic of the test loop is shown in figure 6.22. At either end of the length of 12" pipe was a launching/receiving unit for the pig. The trial pig is shown in figure 6.23. The trial pig was constructed in a similar manner to a conventional metal-bodied pig, with a hollow steel mandrel connecting two sets of polyurethane drive seals. The annular bypass pig, however, differs from a normal pig in that there is flow through the steel mandrel and around a 'bypass plate' fixed to the front of the pig. The plate at the front of the pig is slightly below the nominal size of the pipe bore to give a 2mm annular gap. The bypass emerges from this annular gap in the form of a wall jet, as described in chapter 5 of this thesis.

Figure 6.21. 12" Pipe loop at Pipeline Engineering's test facility

A clear spool inserted into the pipe loop allowed observation and video recording of wax removal (Figure 6.24). The tests were filmed, by the author, using a high-speed video camera on loan from the EPSRC (*Engineering and Physical Sciences Research Council*) instrument pool. The camera used was an NAC 500 analogue high-speed video camera system, capable of recording at 500 frames per second (fps). This system uses standard VHS or S-VHS tapes and a recording time of 43 minutes is available from a single 180 cassette. The system has a P4 2.5GHz PC, to allow image capture via a National Instruments card. The files are generated in AVI (*Audio Video Interlaced*) format.

Pressure was recorded by transducers and logged electronically. Flow rate was recorded using a turbine flow meter. Average pig velocity was calculated by timing the pig between mechanical pig signallers, distributed along the test loop. A more accurate pig velocity was obtained by timing its passage through the clear spool by studying the camera footage.

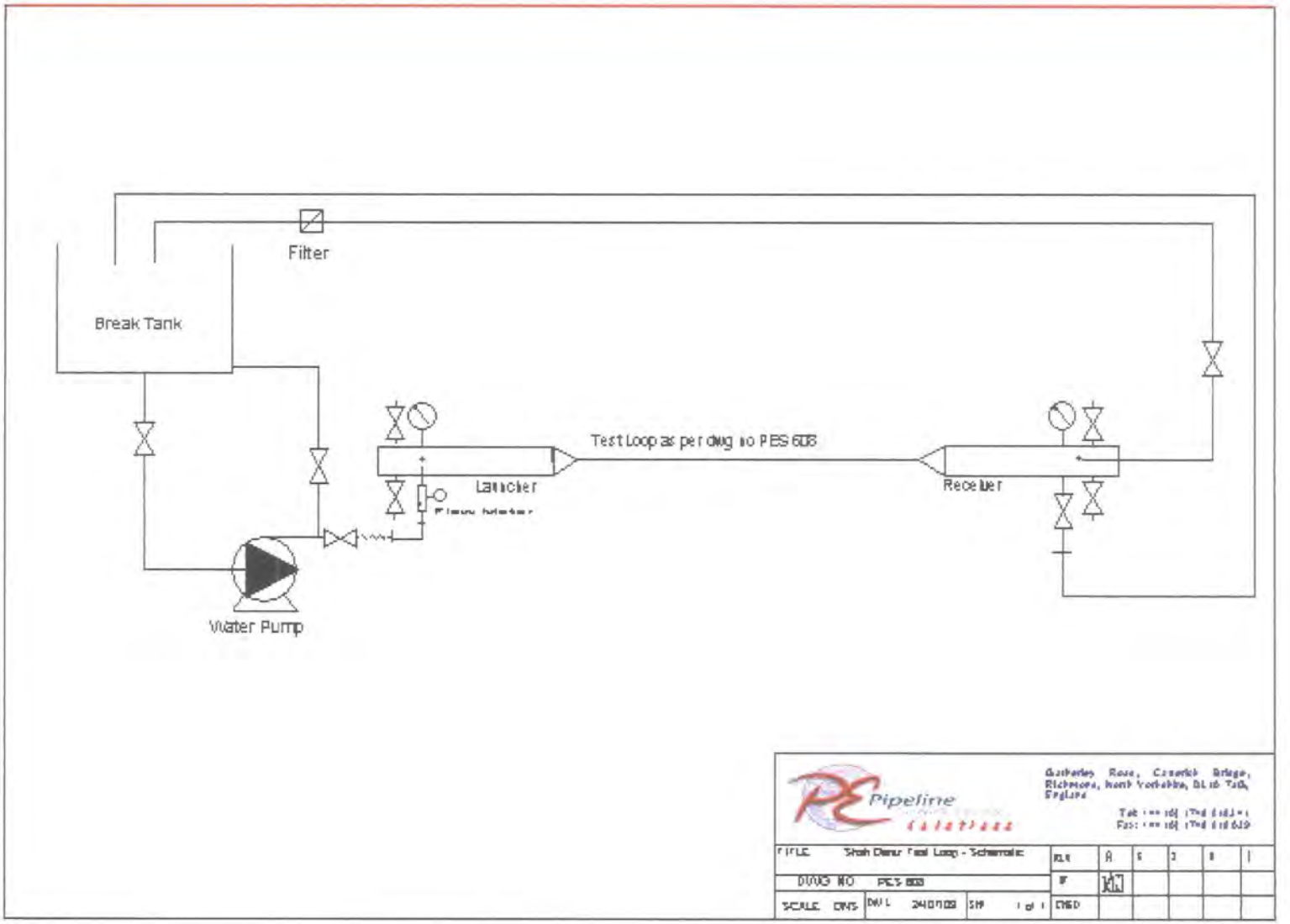

Figure 6.22. Schematic diagram of trial test loop

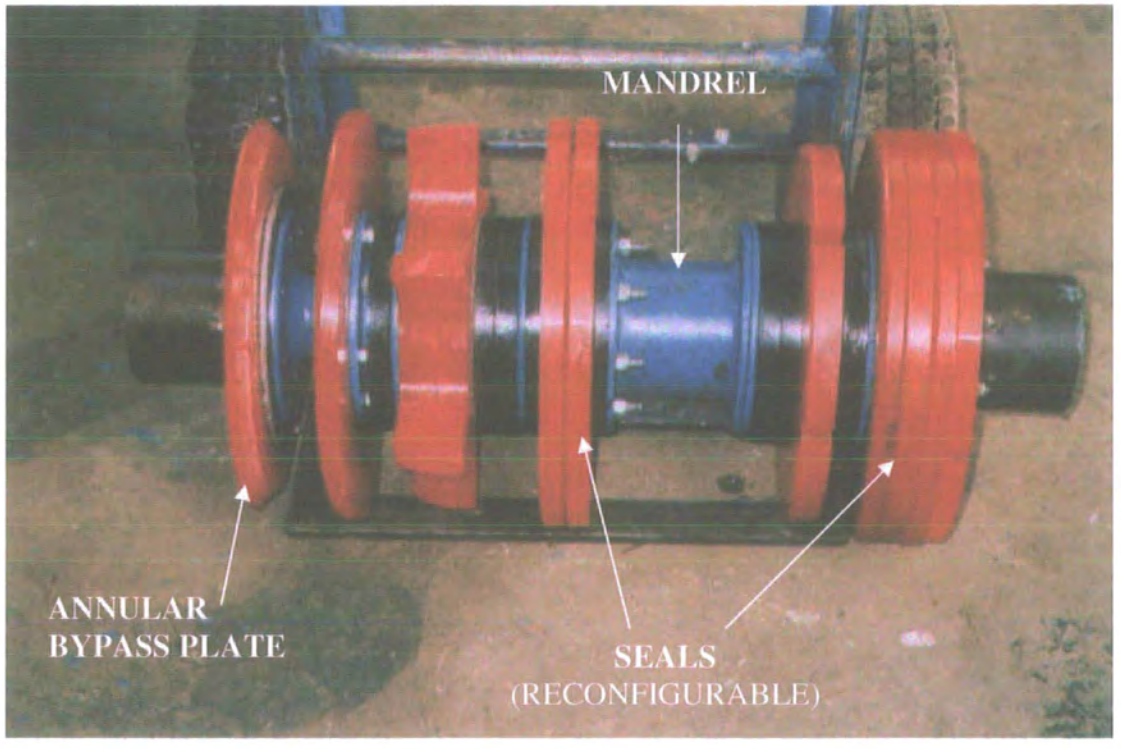

Figure 6.23. Annular Bypass Trial Pig

Figure 6.24. Observation spool and high-speed camera

6.3 Sample Preparation

The wax samples used in the trials were prepared from a mixture of refined paraffin wax and oil, as in the laboratory experiments described in chapter 5. The wax was a 130/135 °F macro-crystalline paraffin wax. The oil was a highly refined 'white oil' – Shell Vitrea. During the trials, a lower percentage of wax was used in samples than during the laboratory tests. This was requested by Pipeline Engineering's clients who predicted a very light gel would form in the pipe-line carrying gas condensate. The mixture was prepared using 10% by volume of wax melted into the oil using an acetylene torch as shown in figure 6.31.

Figure 6.31. Mixing of oil and wax for sample preparation.

Once the mixture had reached a uniform temperature of approximately 70° C and all of the wax had melted, the mixture was poured into the test spool. Polyurethane bungs at either end of the spool prevented the mixture escaping before it had set. In the same manner as the author's sample preparation described in section 5.5, the spool was slowly (< 20r.p.m.) rotated on a purpose built 'cradle' to ensure that the wax mixture formed a layer on the pipe wall of uniform thickness (figure 6.32).

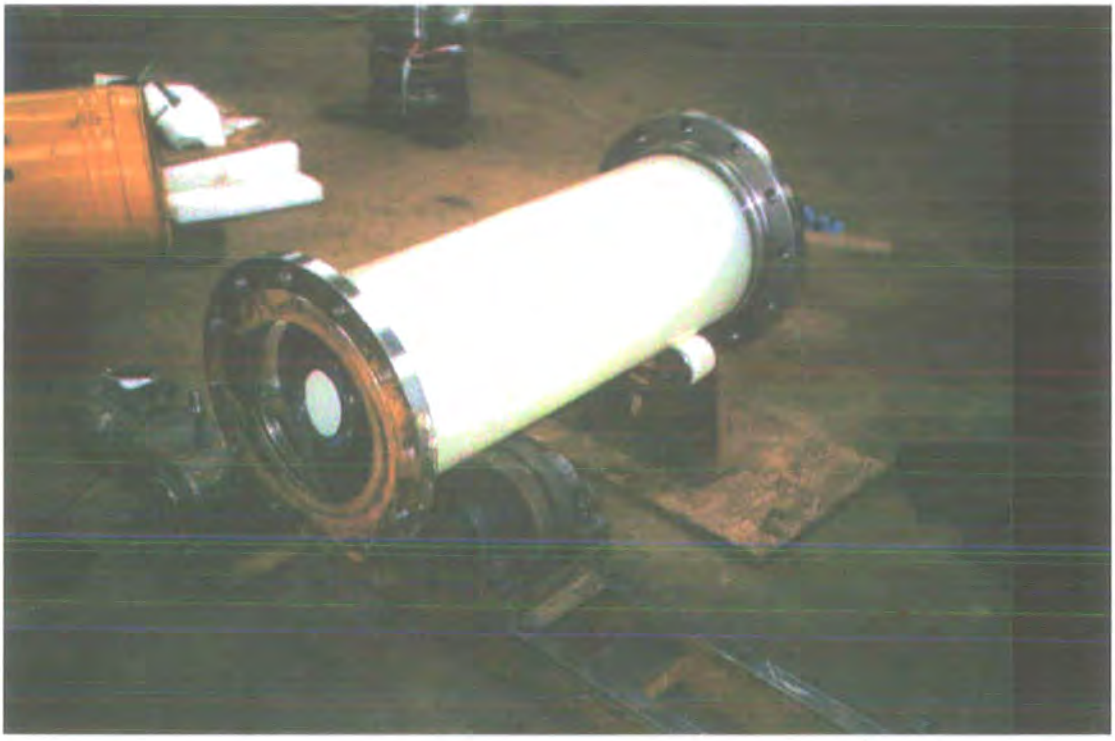

Figure 6.32. Rotating casting 'cradle'.

Determining the exact speed of rotation for the spool required some experimentation. If the spool rotated too slowly, 'slumping' of the sample would occur as the initial layer of set mixture would be covered with the still molten mixture at the bottom of the spool and would itself melt again. This would cause the molten mixture to 'roll' back along the pipe-wall under the force of gravity. If the spool was rotated too fast, a

similar result occurred because the mixture was never lifted out from the molten pool at the base of the spool for long enough to solidify fully.

The adhesion of the wax/oil mixture to the pipe wall was also improved by adding the molten wax mixture in small increments. The thickness of the solidified mixture was periodically checked using a depth gage until the required thickness of 15mm was obtained. A fully set sample is shown in figure 6.33. Once the cast sample had solidified and cooled to the ambient temperature it was transported using slings to the test area and inserted into the pipe.

Figure 6.33. Wax/oil gel cast into test spool.

6.4 Test procedure for annular bypass pig trials

Over fifty test runs were made during the annular bypass trials. The trial pig was driven through the pipe at various velocities to test its general performance and ability to remove wax using bypass jetting. The configuration of seals on the test pig was altered to vary frictional drag and therefore pressure drop across the pig.

The trial runs tested the ability of the pig to remove wax from the 1 metre spool in the centre of the test loop. In some tests, wax was cast directly into this spool so that removal could be observed, in others wax was cast into the preceding steel spool so that the removed wax could be observed mixing with the bypass and general flow. This steel spool could be removed in the same manner as the polycarbonate spool and the same casting process employed to prepare the sample (figure 6.41).

Figure 6.41. Steel spool removed ready for sample casting

For each test run, the average velocity of the trial pig was obtained by timing it between pig signallers. The trial pig could be observed passing through the clear test spool (figure 6.42) and the time taken for it too pass through could be obtained from the high-speed video footage. Using the video-recordings in this way allowed a more accurate, instantaneous measurement of the pig's velocity at the test spool.

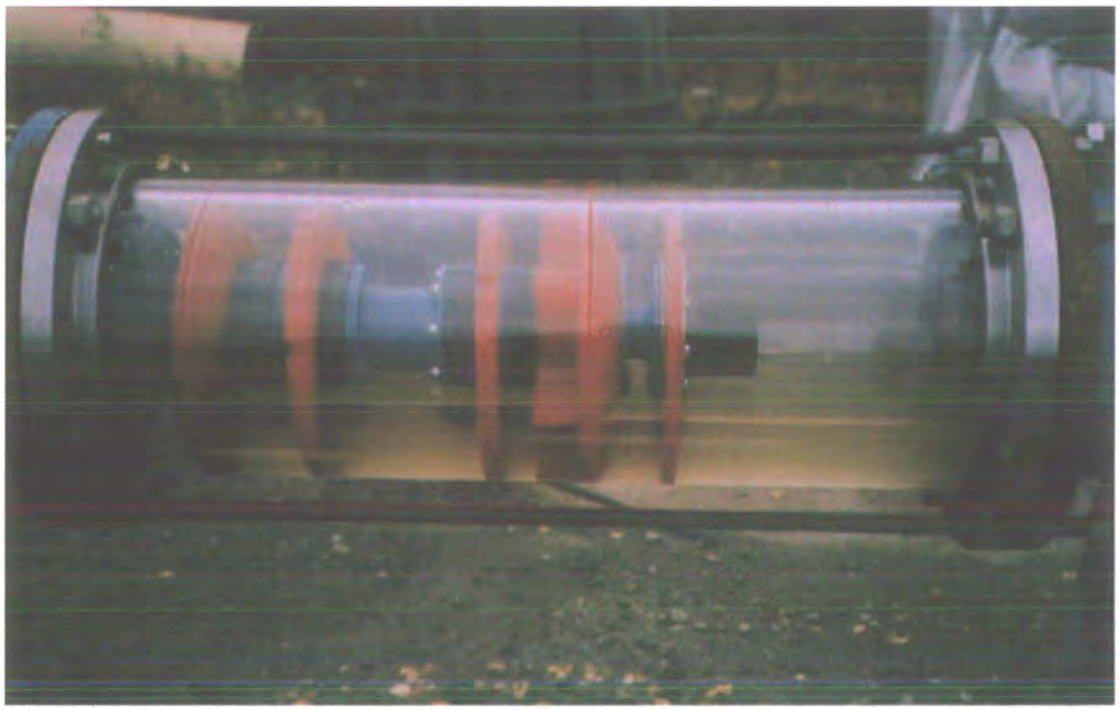

Figure 6.42. Trial pig viewed through clear test spool (no wax sample).

Each test run was recorded using the high-speed video camera. The footage was studied after each run in order to decide how best to change the test parameters in order to optimise the removal process. The trial pig was removed from the receiver at the end of each run ready for reconfiguration (if necessary) and reloading (figure 6.43).

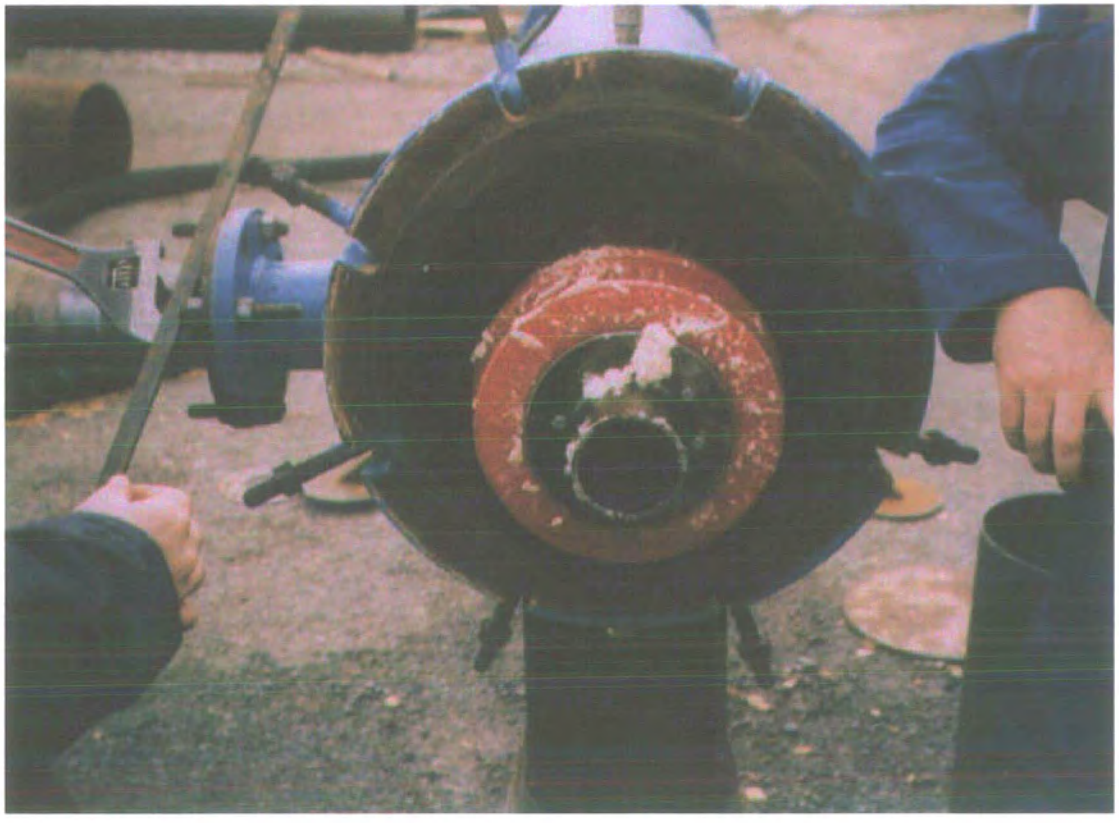

Figure 6.43. Removal of trial pig from receiver.

6.5 Results of annular bypass trials

Only the test runs that provided useful information regarding the process are presented in this section. The results are numbered according to the sequence of the trials.

Run 1.4a

In this test a 15mm deep deposit of 10% wax/90% oil was cast into the polycarbonate spool. At a flow rate of 0.4 m/s and a differential pressure of 0.3 Bar measured across the pig, the annular jet failed to remove the wax deposit. It can be seen from figure 6.51 however, that some wax was stripped away by the jet (area circled), with the bulk of the deposit making contact with the first drive seal.

Figure 6.51. Initial contact between wax and pig in run 1.4a.

Figure 6.52 shows that wax was also jetted away from the pipe wall towards the end of the pig's journey through the test spool. This suggests that the wax removal in these areas is not just an anomaly, but that the correct conditions for successful removal of the wax by jetting are almost satisfied. Again, the area of wax removed by jetting is circled. Whether the bulk of the wax that has been mechanically removed is being jetted away from the pig cannot be seen as the spool has wax cast along its entire length.

Figure 6.52. Pig exiting test spool during run 1.4a.

Run 1.6a

For this test run, a 15mm deep deposit of 10% wax/90% oil was cast into the 1 metre long steel spool immediately preceding the polycarbonate spool. This allowed any wax removed and jetted away from the pig to be viewed clearly as it passed through the clear spool. The pressure drop across the pig was 0.3 bar and the flow rate was 0.4 m/s. It can be seen in figure 6.53 that a plug formed on the front of the pig, extending back to the first seal. The wax's conical shape suggests definition by the pattern of re-circulation highlighted in chapter 5. The annular bypass did not remove any wax from the pipe wall, but did have some effect in 'shaping' the wax plug.

Figure 6.53. Plug formation- failure of the annular bypass jetting system

Run 2.3a

For this test a further 3 seals were added, over and above the pig's original configuration, increasing the pressure drop across the pig to approximately 0.85 bar. So that any removed wax could be viewed, wax was cast into only three quarters of the length of the test spool. With flow at approximately 0.4 m/s it can be seen in figure 6.44 that the wax removal process is more successful.

Figure 6.54. Removal of wax sample by annular bypass

Wax can clearly be seen downstream of the pig as it enters the test spool and no deposit reaches the first seal this time. It would appear that a combination of mechanical and jetting removal is occurring. It is proposed that, because the deposit is deeper than the annular gap, the wax contacts the edge of the annular plate and is

broken away or weakened by this mechanical contact. Once this occurs it is instantly jetted away by the bypass. Although this does not exactly correspond to the envisaged mechanism, in that there is no 'stand-off' distance between pig and wax, it is a definite improvement over pure mechanical removal where the wax will form a plug at the tool.

Figure 6.55. Pig approaching end of wax sample during run 2.3a

It can be seen in figure 6.55 that as the pig approaches the end of the wax deposit, the wax begins to slide axially along the spool as a rigid body (circled). This raised concerns over the adhesion of the deposit to the smooth plastic spool. These concerns were addressed in run 5b by using the same system parameters, but casting the wax into the steel spool, where adhesion was known to be excellent.

Run 5b

To test whether a pig operating under the same conditions as in run 2.3a could successfully remove wax from a steel surface, a test was set up using identical parameters, but with the wax cast into the steel spool preceding the observation spool. The pig was identical to that used in run 2.3a, with a pressure differential of 0.85 bar measured across it, and the flow rate was the same at 0.4 m/s. There was no evidence of removed wax in the flow ahead of the pig, and it emerged in the form of a plug (figure 6.56). These results confirmed that adhesion of the wax mixture to the steel surface was stronger than that of the wax to the polycarbonate spool.

Figure 6.56. Pig emerging from steel spool with wax plug attached

Run 21b

It was decided to repeat the test using the same parameters as in run 5b, but with a weaker wax mixture. The 10% wax/90% oil mixture previously used had represented a particularly robust challenge and it was felt that a 5%wax/95% oil mixture would better match the physical properties of the actual deposit anticipated in the Shah Deniz pipeline, described by BP as having a consistency rather like 'Swarfega'. Again the sample was cast into the steel spool so that removed wax could be viewed through the clear spool. The same pig was used, with a 0.85 bar pressure differential across it, and the flow rate was kept at 0.4 m/s. This test proved successful, as can be seen in figure 6.57. Again, no 'stand-off' distance is established between the wax and the pig, suggesting a combination of jetting and mechanical removal.

Figure 6.57. Run No. 21B

Standard bypass pig

In order to compare the annular bypass system of wax removal with a more conventional pig, a test was performed at the same flow rate (0.4 m/s) using a pig equipped with a standard jetting 'spider'. This is effectively a 'shower head' that fits over the hollow mandrel to direct jets of fluid towards the pipe wall. The pressure differential across the standard pig was approximately 0.85 bar. A standard jetting pig is not intended to remove wax from pipe walls by its jetting action, rather to prevent the wax that has been mechanically removed from settling at the nose of the pig and forming a plug.

Figure 6.58. Plug formation with standard pig

With wax cast into the steel spool no wax could be observed in the flow ahead of the pig as it approached the polycarbonate observation spool. The pig emerged with wax packed around its front seals (figure 6.58). However, this did not represent conclusive proof that a plug would form. Because there was sufficient room for the volume of wax available to pack in behind the jetting head, the jets' ability to clear or prevent a plug could not be tested. There is no doubt, however, that the standard jet did *not* remove wax from the pipe wall.

6.6 Conclusions from annular bypass pig trials and discussion

It is useful to compare the data obtained from the annular bypass pig trials with the laboratory results described in chapter 5. In order to do this, a plot of flow velocity against differential pressure across a 12 inch pig is shown in figure 6.6. This plot assumes the wax removal coefficients k and C (see equation 5.73) are identical to those obtained in the laboratory for a 5mm thick deposit containing 30% wax. Given that a softer deposit was used in the trials (5% wax by volume), it can be assumed that the performance of the system predicted by this plot will be conservative.

The flow velocity and differential pressure across the pig for test runs 1.6a and 21b are plotted in figure 6.6. It can be seen that run 1.6a, an unsuccessful run in the trials, falls in the 'mechanical removal zone'. It is assumed that in this zone the pig is travelling faster than the wax can be removed by the annular jet, so there is contact between the pig and wax deposit and mechanical removal occurs. On this basis, run 1.6a provides agreement between the empirical theory developed from the laboratory tests and the trials data.

It can be seen in figure 6.6, that run 21b is plotted on the border between the mechanical and jetting zones. This indicates that the pigging conditions provide an approximate equilibrium between wax removal velocity and pig velocity. In this case, wax removal occurs at or near the origin of the annular bypass jet, where the fluid velocity is greatest. Again, the actual performance of the annular bypass jetting system in the trial run confirms the performance predicted by theory. Wax, removal

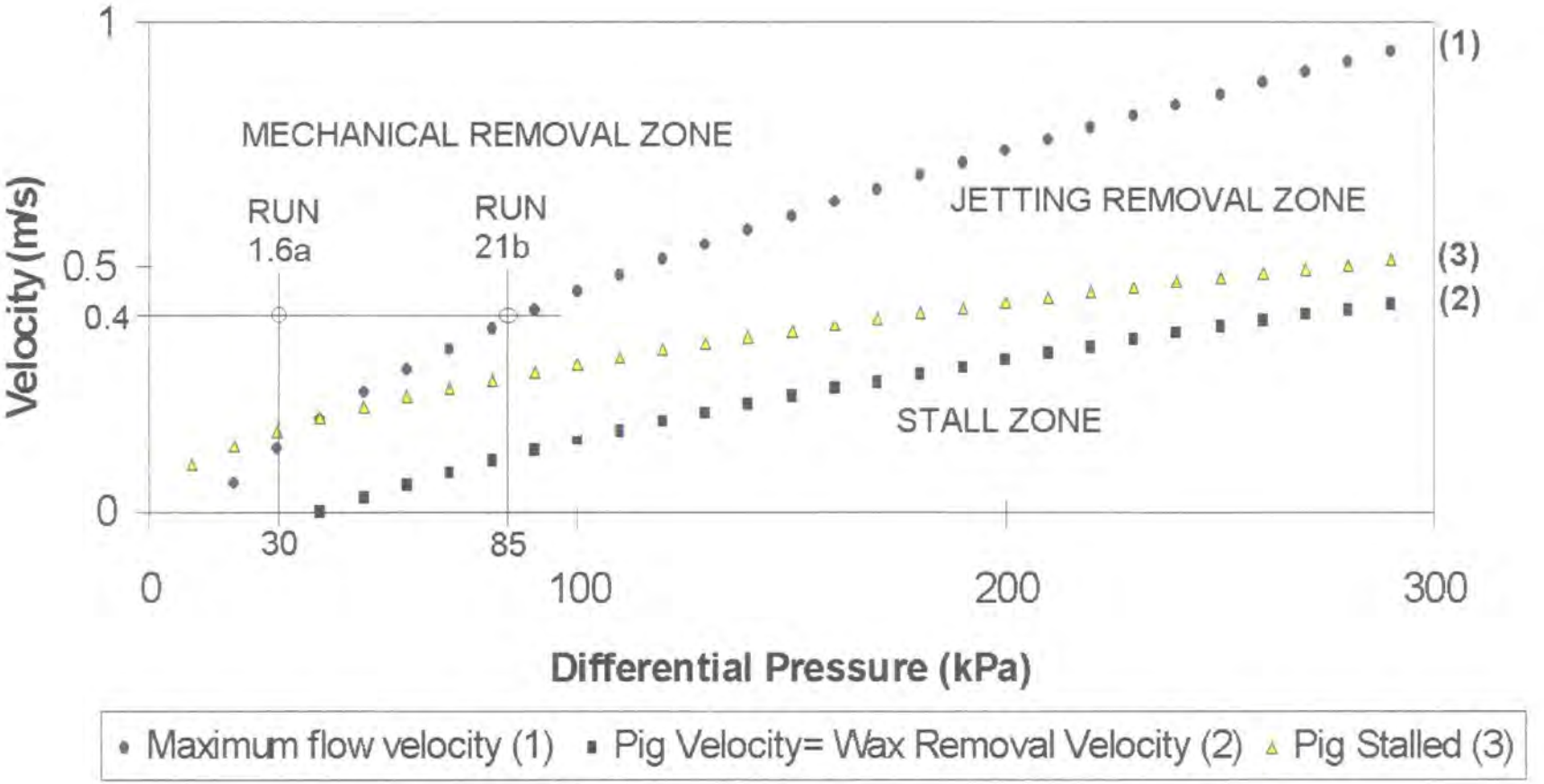

Figure 6.6 Plot of velocity against differential pressure across 12 inch pig for 30% wax sample at 5mm thick and 2mm annular gap.

occurred without plug formation, suggesting that contact did not occur between the pig's front seal and the wax deposit, or else the contact was very limited.

A more accurate evaluation of the annular bypass pig trials could be made if wax removal coefficients were available for the 5% wax, 15mm thick deposit used in the trials. It would be useful to perform a set of laboratory tests as described in chapter 5 using a deposit with characteristics to match that used in the trials. The relationship between wax thickness and removal velocity is also worthy of further investigation. Although removal velocity could be seen to decrease with increasing deposit thickness (see chapter 5, figure 5.65.3) in the laboratory tests, insufficient data exists to quantify the relationship between the two variables. At present a wax removal velocity constant is only available for a given deposit thickness. At present, the assumption of uniform deposit thickness must be made in using the annular bypass-jetting model. As deposits encountered in the field will vary in thickness due to localised conditions within the pipeline the jetting parameters should be set conservatively to ensure the largest possible 'stand-off' distance exists to reduce the risk of contact between the pig and wax deposit at particularly thick areas of deposition. Transient periods of mechanical removal may be anticipated due to the small annular gap.

While the annular bypass wax removal method worked in the trials under certain conditions, a full, non-contacting system as described in chapter 5 was unobtainable. In order to achieve this a means for lowering the pig velocity and increasing the differential pressure (and subsequent bypass) across the pig is necessary. It is clear from both the trials and the theory developed in chapter 5 that increasing the

differential pressure by creating more friction at the seals is of limited use. Eventually a point is reached where the pig merely stalls. Some test runs were also performed during the trials to test the general functionality of the pig in terms of its ability to negotiate various pipe diameters and bends. It became clear during these tests that the pigs configured to obtain high differential pressure by adding friction in the form of additional seals were prone to stalling in bends and in sections of pipe where wall thickness was increased.

For the annular bypass wax removal system to work efficiently, it is desirable to create an environment where pig velocity is not dependent on friction at the pipe wall. A slow moving pig with a small annular bypass area will produce the high bypass velocities required to remove wax deposits *and* do so with a 'stand-off' distance that can accommodate fluctuations in the strength of the deposit. This ideal set of conditions is discussed further in the following, concluding chapter.

Chapter 7 Conclusion

7.1 Evaluation of wax removal research

An understanding of wax removal from oil pipelines has been developed beyond the level of knowledge previously available. The most pertinent facts and concepts have been extracted from an array of material regarding wax deposition, allowing a qualitative understanding of the problem presented to pipe-line operators. Using this understanding, realistic models of wax deposits have been developed. This allows different removal processes to be matched to the physical characteristics of wax deposits.

The mechanical removal of wax has been analysed using the orthogonal cutting model. When applied to the wax removal process, the orthogonal cutting model accounts for the interaction between the wax deposit and the pig's scraper or seal and provides a more comprehensive description of the process than previous models used by researchers in the pigging field. Measurements of specific cutting energy, u, using the orthogonal cutting model were considerably greater than the shear strength of paraffin wax, suggesting that predictive models based on simple uni-axial load models underestimate wax removal forces for pigs. Analysis of the wax removal process using the orthogonal cutting model raises issues regarding the design of pigs and highlights the limitations of the mechanical wax removal process.

A novel non-contacting annular bypass system for the removal of soft wax deposits has been presented. An experimental procedure has been designed and tested to allow the acquisition of empirical constants for wax removal rates at different deposit

consistencies and thickness. These wax removal constants have been combined with equations describing pig dynamics to allow prediction of wax removal rates under different flow conditions. The model developed in this work allows pig velocity and wax removal rate to be balanced such that contact between the pig and wax deposit can be avoided and a fully non-contacting wax removal system used.

Full-scale trials have been conducted that point to the successful application of the annular jetting technique in the field. The trials have shown that the annular jetting system is suitable for soft, gel-like wax deposits, as predicted by the semi-empirical model developed in chapter 5 of this thesis.

7.2 Limitations of research

The experimental procedures described in this thesis represent a possible template for a standard laboratory procedure. While the results give a good qualitative indication of the process' performance, more accurate measurement and interpretation would be required for the development of a model reliable enough to allow quantitative predictions.

The wax removal rates measured for waxes containing 50% oil suggest that the annular jetting system is limited to applications involving softer, incipient deposits. Hard deposits with minimal oil content may still require mechanical removal using more traditional tools.

Testing has been performed using combinations of refined wax and oil. Real pipelines may contain non-organic deposits, such as sands, that could impinge upon the deposits behaviour under stress. The use of homogenous wax gels is, in this respect, another factor that precludes the use of the experimental data obtained in this research for anything other than a qualitative understanding of the wax removal process.

7.3 Future Work

A useful contribution by this work has stemmed from the cutting experiments. The author believes that this work is the first significant attempt to apply metal cutting theory to the mechanical removal of wax. The cutting experiments on refined paraffin wax samples have shown that the orthogonal cutting model is more useful in describing the pigging process than simple uni-axial compression. Specific cutting energies obtained in these tests were as much as ten times greater than the yield stresses that are obtained using uni-axial load models. As specific cutting energy is a function of tool geometry, more sophisticated pig tool design can offer improved performance for wax removal pigs. The observation of exaggerated specific cutting energy increases, for negative rake tools, suggests the possibility of a ploughing process occurring during orthogonal cutting of wax with tools of this geometry. Further investigation of this phenomena is recommended, as many wax removal pigs currently have a negative rake tool geometry. If ploughing is occurring, pigs may actually consolidate wax deposits rather than removing them, ultimately exacerbating the problem of wax removal.

Also worthy of further detailed investigation is the *apparent* cutting ratio obtained for wax. Cutting ratios greater than unity are not found in metal (or plastics) machining. However, the apparently high shear plane angle and *apparent* cutting ratio found in wax cutting *are* compatible with Merchant's trigonometric construction of cutting forces acting on a chip. A criticism of Merchant's model when applied to metal cutting is that it assumes the forces generated as the chip moves along the tool's rake face can be analysed using classical friction theory. This is generally not the case with metal cutting as welding and 'stiction' occur on the rake face and frictional forces therefore become proportional to contact area. It is possible that the peculiarly low forces generated when

cutting wax, and the low friction at the rake face mean that the actual cutting forces approach those predicted by Merchant's idealised model to an extent unseen in metal and plastics cutting. Further experimentation to confirm actual shear angles and cutting ratios for paraffin wax might clarify this issue and be of interest to researchers in the field of manufacturing.

In order to improve the accuracy of the annular bypass model developed in chapter 5, it is proposed that the experiments described are repeated under more stringent conditions. The tests could be performed using more accurate instrumentation and greater sample sizes. Processing of the data obtained using error analysis techniques would also improve the accuracy of the model.

During field trials of the annular bypass system it became apparent that laboratory tests parameters should precisely match those in the field to gain the most useful data. With this in mind, another series of laboratory tests could be performed using higher oil content waxes that better match the description of the deposits anticipated in the Shah Deniz pipe-line, or indeed any other pipe-line where a similar problem might be encountered.

In the experiments described within this thesis, testing has occurred on either soft or hard waxes and discrete gradations between the two. From the study of deposit aging, however, it is evident that 2 phase deposits may well establish themselves in many pipelines. Further experiments, based on those described here, could use samples of wax that have variations in property through their thickness. The manufacture of such samples would pose an interesting problem in itself. Of particular interest would be testing of the annular bypass system with gel-like deposits having a hardened surface.

Also, wax samples including sands and non-organic particulate matter might be tested to determine their effect on the removal process.

In light of the findings from this research, a number of design opportunities and challenges are raised. The comparison of the wax cutting tests described in chapter 4 with metal cutting theory suggests that broader application of metal cutting techniques may be useful for optimising wax removal using pigs. Pigs might be developed that incorporate such technology as limited contact rake face tools, vibrating tools and even onboard active tooling.

Whilst an annular bypass system appears promising for softer wax deposits, an important issue identified in this study is the need for better control of pig velocity. Because the necessary bypass flow velocity is achieved by increasing the pressure differential across the pig and slowing it down relative to the bulk flow rate of the oil, the annular bypass pig is prone to stalling. Figure 7.31 shows pig and oil velocity as a function of pipeline diameter for a constant bypass velocity and annular gap. It can be seen that the risk of stalling will diminish as pipeline diameter increases because of the reduction in pig velocity relative to the oil velocity (ΔV).

Nevertheless, as was seen in the annular bypass pig trials, where flow rates are modest, ΔV is large enough to make stalling an unacceptably high risk in the smaller flow-lines that might normally be encountered offshore. It is proposed that for the annular bypass concept to realise its full potential, pig velocity must not be dependent on pressure differential, as it is on conventional pigs. This might be achieved by using mechanical governors that are independent of pressure differential. One concept for such a device is shown in appendix G.

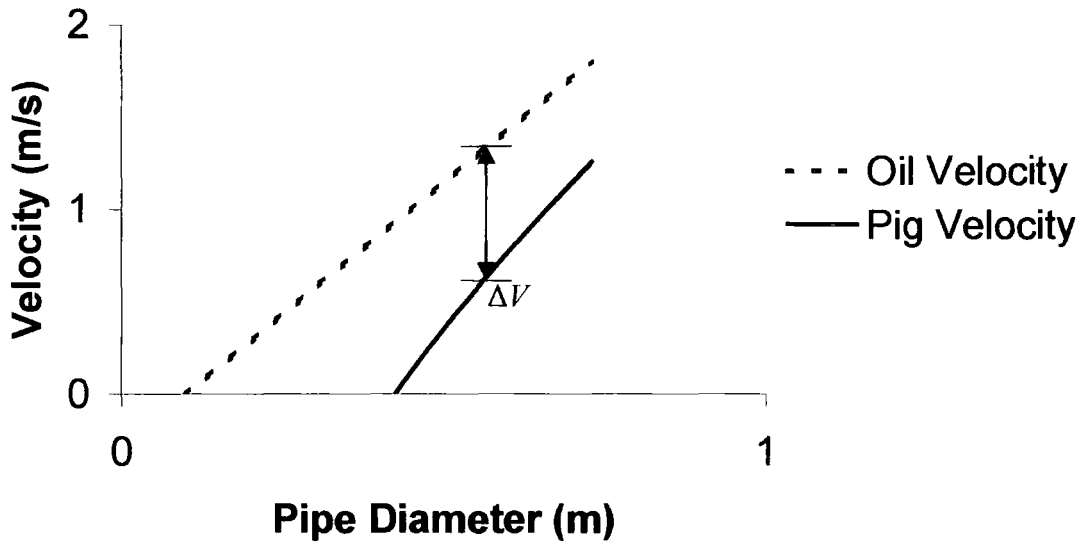

Figure 7.31. Pig and oil velocity as a function of pipeline diameter for a constant bypass velocity and annular gap

Another means of divorcing pig velocity from pressure differential is to use a powered pipeline tractor to transport an annular bypass tool through a pipeline. Such a device might maintain a sufficiently low velocity to ensure effective bypass jetting whilst posing no risk of stalling.

References

Arsecularatne, J A; Fowle, R F; Mathew, P and Oxley, P L B. Prediction of cutting forces and built-up edge formation conditions in machining with oblique nose radius tools, *Proc. Instn. Mech. Engrs*, Vol. 210, 457-469 (1996).

Atkins, A G. Modelling metal cutting using modern ductile fracture mechanics: quantitative explanations for some longstanding problems, International Journal of Mechanical Sciences 45, 373 – 396 (2002).

Azevedo, Luis Fernando A; Braga, Arthur M B; Nieckele, Angela O; Naccache, Monica F; Mendes, Paulo Roberto S and Saboya, Franciso E M. Pipeline Pigging Simulation, Internal project report, Petrobras/CENPES (1998).

Boothroyd, G. Fundamentals of Metal Machining , London, Edward Arnold Ltd (1965).

Bott, T R and Gudmundsson, J S. Deposition of Paraffin Wax from Kerosene in Cooled Heat Exchanger Tubes, The Canadian Journal of Chemical Engineering, Vol. 55, August, 381-385 (1977).

Bradley, H B. Petroleum Engineering Handbook, Society of Petroleum Engineers, USA (1992).

Brooks, J R V; Stoker, S J; Cameron T D J. Hydrocarbon exploration opportunities of the twenty-first century in the United Kingdom, American Association of Petroleum Engineers Memoir 74 (2001).

British Standards Institute, Testing concrete - method of determination of tensile splitting strength. BS 1881-117:1983 (1983)

Burger, E D; Perkins, T K; Streigler, J H. Studies of Wax Deposition in the Trans Alaska Pipeline, Journal of Petroleum Technology, June, 1075-1086 (1981).

Cordoba, A J and Schall, C A. Solvent migration in a paraffin deposit, *Fuel* Vol. 80, 1279-1284 (2001).

Cordoba, A J and Schall, C A. Application of a heat transfer method to determine wax deposition in a hydrocarbon binary mixture, *Fuel* Vol. 80, 1285-1291 (2001).

Coutinho, João A P; Edmonds, Beryl; Moorwood, Tony; Szczepanski, Richard and Zhang, Xiaohong. Reliable wax predictions for Flow Assurance, Presented at the SPE 13th European Petroleum Conference, Aberdeen, UK 29-31 October (2002).

Creek, J L; Hans, Jacob Lund; Brill, James P; Volk, Mike. Wax deposition in single phase flow, Fluid Phase Equilibria, Vol 158-160, Elsevier, 801-811 (1999).

Chanda, D et al. Combined effect of asphaltenes and flow improvers on the rheological behaviour of Indian waxy crude oil, *Fuel*, vol.77, No. 11, 1163-1167 (1998).

Department of Trade and Industry, UK: Continental Shelf Land – the state of play, Oil and Gas Directorate, p 14 (2001).

Dunstan, A E; Nash, A W; Brooks, B T; Tizard, H T, The Science Of Petroleum, Volume 1, Oxford University Press (1938).

Edwards, Lyndon and Endean, Mark, Manufacturing with Materials, Butterworth Scientific Ltd, ISBN 0408 027770 3, (1990).

Ernst, H and Merchant, M E. Chip formation, friction and high quality machined surfaces, *Surface Treatment of Metals* (American Society of Metals), 29, 299 (1941).

Fang, N .An auxiliary approach to the experimental study on chip control: A kinematically simulated test, Proceedings of the Institute of Mechanical Engineers, Vol. 212, Part B (1997).

Garcia, Maria del Carmen; Carbognani, Lante; Urbina, Argelia; Orea, Miguel. Paraffin deposition in oil production. Oil composition and paraffin inhibitors activity, Journal of Petroleum Science and Technology, Vol. 16, Issue 9-10, Oct/Nov, 1001-1021 (1998).

Garcia, Maria del Carmen; Carbognani, Lante; Urbina, Argelia; Orea, Miguel. The influence of alkane class-types on crude oil wax crystallization and inhibitors efficiency, Journal of Petroleum Science and Technology, Vol. 25 (2000).

Glauert, M B. The wall jet, Journal of Fluid Mechanics, 1, Part 5, 625-643 (1956).

Goodger, E M. Hydrocarbon fuels, Macmillan Press Ltd (1975).

Grieb. W.E. and G. Werner, Comparison of Splitting Tensile Strength of Concrete with Flexural and Compressive Strength, American Society for Testing and Materials, Proceedings, Vol 62, pp 972-995, 1962.

Hammami, Ahmed. Paraffin Deposition from crude oils: Comparison of laboratory results to field data, Paper presented at SPE Annual Technical Conference and Exhibition, San Antonio, Texas, 5th - 8th October, Paper No. SPE 38776 (1997).

Hamouda and Davidsen. An approach for simulation of paraffin deposition in pipelines as a function of flow characteristics with a reference to Teeside Oil Pipeline, Paper presented at the Society of Petroleum Engineers' International Symposium on Oilfield Chemistry, San Antonio, TX, U.S.A., 14-17 February 1995 (1995).

Hennessy, A J; Neville, A; Roberts, K J. An examination of additive-mediated wax nucleation in oil pipeline environments, Journal of Crystal Growth, 198/199, 830-837 (1999).

Hopkins, P. Time to change?, Journal of Pipeline Integrity, September, 31-55 (2002).

Hsu, Jack J C, Elphingstone, Gerald M Jr, Greenhill, Katherine L. Modelling of Wax Deposition, ASME Energy Sources Technology Conference and Exhibition, ETCE99-6674 (1999).

Irwin, G R. Analysis of stresses and strains near the end of a crack traversing a plate, Journal of Applied Mechanics, 1957, 24, 361 (1957).

Johnson, W and Sowerby, R. Plane-Strain Slip-Line Fields: Theory and Bibliography, Edward Arnold (Publishers) LTD, p22 (1970).

Jorda, R M; Shell Development Co. Paraffin Deposition and Prevention in Oil Wells, Society Of Petroleum Engineers, 1605 – 1612 (1966).

Kaufmann, K D. Development and application of "Safe Time" calculation software for high waxy crude oil pipelines on the example of the Kharyaga to Uninsk pipeline, ILF Consulting Engineers, Munich, Paper No. 1998.048, Presented at 7th UNITAR International Conference for Heavy Crude and Tar Sands, Beijing 1998 (1998).

Kinloch, A. Adhesion and Adhesives, Chapman & Hall, p.56 (1987).

Kinloch and Young. Fracture behaviour of polymers, Elsevier Applied Science Publishers LTD, ISBN 0-85334-186-9, p.115, (1988).

Kleinhans, J W; Niesen, V G and Brown, T S. Pompano paraffin calibration field trials, paper presented at the SPE Annual Technical Conference and Exhibition, Dallas, Texas, 1-4 October. Paper No. SPE 62946 (2000).

Kobayashi, Akira. Machining of Plastics, (Reprint) Krieger Publishing, NY (1981).

Lawson, J and Sathananthan, R. Effective Wax Management To Enhance Production, Paper p resented at the Flow Assurance Conference, 29th-30th October, The Café Royal, London (2002).

Lee, E H and Shaffer, B W. The theory of plasticity applied to a problem of machining, *Journal of Applied Mechanics, Trans. A.S.M.E.*, 73, 405 (1951).

Li, Mingyuan; Su, Jianguo; Wu, Zhaoliang; Yang, Yaodong; Ji, Shuling. Study of the mechanisms of wax prevention in a pipeline with glass inner layer, *Colloids and Surfaces A : Physiochemical and Engineering Aspects*, 123-124, 635-649 (1997).

Loewen, E G and Shaw, M C. Trans. Am. Soc. mech. Engrs 76, 217 (1954).

Mendes; Braga; Azevedo; Correa. Resistive Force of Wax Deposits During Pigging Operations, Journal of Energy Resources Technology, ETCE99-6671 (1998).

Merchant, M E. Journal of Applied Physics, 16, p267 (1945).

Merchant, M E and Zlatin, N. Mechanical Engineering 67, p737 (1945).

Michelbach, S. Origin, re-suspension and settling characteristics of solids transported in combined sewage, Water Science Technology, Vol. 31, No. 7, 69-76 (1995).

Mozes, G Y; Freund, M; Csikos, R; Keszthelyi, S. Paraffin Products – Properties, Technologies, Applications, Elsevier Scientific Publishing Company (1982).

Ozbayoglu, M; Demirel, B; M.V.Kok. Mathematical Modeling of Wax Deposition in Horizontal Wells, Middle East Technical University, Ankara, Turkey, International Centre for Heavy Hydrocarbons, paper No. 1998.031 (1998).

Pedersen, K S, Skovborg, P and Ronningsen, H P. Wax precipitation from North Sea crude oils. 4. Thermodynamic modelling, Energy & Fuels, **5**, 924 (1991).

Pugh, H. Mechanics of the cutting process, *Proceeds of the Conference on Technology of Engineering Manufacture*, I.Mech. E., 237 (1958).

Ragnarsson, R; Ford J L; Santangelo, C D; Bodenschatz, E. Rifts in Spreading Wax Layers, Laboratory of Atomic and Solid State Physics, Cornell University, Ithaca, New York (1995).

Sellin, R. H. J.; Hoyt, J. W.; Scrivener, O. The effect of drag-reducing additives on fluid flows and their industrial applications - 1. Basic aspects, Journal of Hydraulic Research, Volume 20, Issue No.1, 29-68 (1982).

Singh, Probjot; Venkatesan, Ramachandran; Fogler, H Scott; Nagarajan N R. Morphological Evolution of Thick Wax Deposits, AIChE Journal, Vol 47, No 1, January, 6 – 18 (2001).

Shaw, Milton C. Metal Cutting Principles, New York, Oxford University Press (1984).

Svendsen, J. Mathematical Modelling of Wax Deposition in Oil Pipeline Systems, AIChe Journal, August (1993).

Tikhomirov, R A; Babanin, V F; Petukhov, E N and Starikov, I D. High-Pressure Jetcutting, ASME Press, New York (1992).

Toms, B.A. Some observations on the flow of linear polymer solutions through straight tubes at large Reynolds numbers, Proceedings of the International Congress of Rheology, Holland, Amsterdam, 1949, Section II, 135-141 (1948).

Trent, E M. Metal Cutting, Butterworth & Co (1977).

Valer Popp, V (1998) Heavy viscous oil conditioning processes, Institute for Research and Technology, Campina, Romania, 7th UNITAR Conference on Heavy Crude and Tar Sands, published by the International Centre For Heavy Hydrocarbons, Paper No.1998.051

Venuvinod, Patri K and Jin, W L. Three-dimensional cutting force analysis based on the lower boundary of the shear zone. Part 1: Single edge oblique cutting, Int. J. Mach. Tools Manufact. Vol. 36, No.3, 307-323 (1996).

Wang, Kang-Shi; Wu, Chien-Hou; Creek, Jefferson L; Shuler, Patrick J; Tang, Yongchun. Evaluation of effects of selected wax inhibitors on paraffin deposition, Petroleum Science and Technology, Volume 21, Issue 4 (2003).

Wang and Sarica. Mechanics of Wax Removal, paper presented at the 2001 SPE Annual Technical Conference and Exhibition, New Orleans, Louisiana, 30 September-3 October (2001).

Won, K W. Thermodynamic calculation of cloud point temperatures and wax phase compositions of refined hydrocarbon mixtures, *Fluid Phase Equilibria* Volume 53, December, Pages 377-396 (1989).

Wood and Holliday. Organic Chemistry – An Introductory Text, Butterworths (1968).

Appendix A Example of flow reduction due to wax deposition

It is assumed that an operator is transporting crude from an offshore field to a reception facility on land. The pipe is 0.3m in diameter (D) and is 50km in length (L). Oil is transported at an average flow velocity (v) of 3m/s, giving a volumetric flow rate (Q) of $0.212m^3/s$. The oils density (ρ) is $900kg/m^3$and dynamic viscosity (μ) is $0.05Ns/m^2$. The pipe is new, steel un-lined pipe having a roughness value (k) of 50 microns.

Given these conditions, Reynolds number is calculated thus;

$$\mathrm{Re} = \rho\frac{vD}{\mu} \qquad \textit{equation 1}$$

$$\mathrm{Re} = 900kg/m^3\,\frac{3m/s \times 0.3m}{0.05Ns/m^2} = 1.6\times10^4 \text{ (Turbulent flow)}$$

And relative roughness;

$$\frac{k}{D} = \frac{0.05mm}{300mm} = 1.67\times10^{-4} \qquad \textit{equation 2}$$

Now applying these values to a Moody diagram, a friction factor, f, is obtained equal to 0.006. We can now use Darcy's equation to calculate the loss of pressure along the pipe.

$$p_f = 4f\frac{L}{D}\rho\frac{v^2}{2} \qquad \textit{equation 3}$$

$$p_f = 4 \times 0.006 \times \frac{5 \times 10^{-4} m}{0.3m} \times 900 kg/m^3 \frac{3m/s^2}{2} = 16.2 MPa \approx 2350 psi$$

Now let us assume a wax layer, just 5mm thick, has deposited itself along the length of the pipe. From *equation 1*, at the same rate of flow;

$$\mathrm{Re} = 900 kg/m^3 \frac{3m/s \times 0.29m}{0.05 Ns/m^2} = 1.57 \times 10^4$$

And from *equation 2*, relative roughness;

$$\frac{k}{D} = \frac{0.05mm}{290mm} = 1.72 \times 10^{-4}$$

As can be seen, given the relatively large diameter of the pipe, there is no appreciable difference in the friction factor. However, applying *equation 3*, the pressure drop becomes,

$$p_f = 4 \times 0.006 \times \frac{5 \times 10^4 m}{0.29m} \times 900kg/m^3 \frac{3m/s^2}{2} = 16.76MPa$$

This equates to an increase in pressure drop of just over 3 %. If the system cannot accommodate an increase in pressure drop, then a reduction in flow rate is the only possibility. Rearranging *equation 3* to obtain,

$$v = \sqrt{\frac{2DP}{4fL\rho}} \qquad \textit{equation 4}$$

$$v = \sqrt{\frac{2 \times 0.29m \times 16.2MPa}{4 \times 0.006 \times 5 \times 10^4 m \times 900kg/m^3}} = 2.95m/s$$

This gives a volumetric flow rate of 0.195 m^3/s, a reduction of approximately 9%.

Appendix B Heat loss from a buried pipeline

A calculation approximating temperature loss from a buried pipeline can be made using the following formulae, Dunstan [1938].

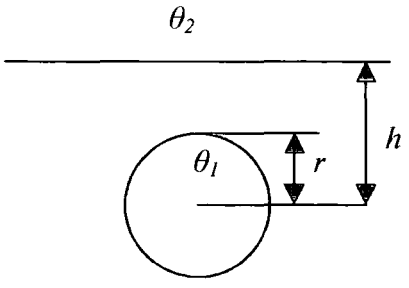

Figure 1. Heat loss from buried pipeline

$$Q = \frac{2\pi LK(\theta_1 - \theta_2)}{Log_e(2h/r)} \qquad \textit{equation 1}$$

Where

Q = Heat flow rate (Watts)

L, h, r= Length, depth, radius (metres)

K = Thermal Conductivity (W/m/°K)

Ignoring heat generated by friction within the flowing oil, the temperature of the oil at a distance l from its origin can be calculated thus;

$$\theta_l = (\theta_o - \theta_h)e^{-Fl/W} + \theta_h \qquad \textit{equation 2}$$

Where

θ_l = Temperature of oil at a distance l from origin

θ_h = Temperature of soil at a depth h

θ_o = Temperature of oil at origin (e.g. wellhead)

F = Coefficient of heat transmission per unit length of pipe

$$F = \frac{Q}{(\theta_1 - \theta_2)L} \qquad \textit{equation 3}$$

$$W = \rho AV \times C \qquad \textit{equation 4}$$

Where C is the specific heat capacity of the oil in kJ/kg/K

It is useful to consider an example of a buried pipe transporting oil produced at 90°C. The oil is being transported in an 8" pipe over a distance of 100m, buried at a depth of 2m. The soil's thermal conductivity is 2 W/m/°K and its temperature is 20°C.

From *equation 1* the heat flow rate per metre is,

$$Q = \frac{2\pi 2W/m/°K(90°C - 20°C)}{Log_e(2 \times 2m/0.1m)}$$

Q = 170 Watts per metre

Substituting this value into *equation 3*,

$$F = \frac{170W/m}{(90°C - 20°C)}$$

F = 3.4

From *equation 4*,

$$W = 750kg/m^3 \times \pi 0.1^2 \times 1.5m/s \times 2.1J/kg/K$$

$$W = 74$$

Using *equation 2* the temperature at a point 100m from the pipe's origin is,

$$\theta_l = (90°C - 20°C)e^{-3.4\times100/74} + 20°C$$

$$\theta_l = 20.5\ °C$$

Appendix C Tabulated values obtained experimentally (from quasi-static tests) for specific cutting energy (u) of pure paraffin wax.

Tool Rake	Depth of Cut (mm)	Average Force (N)	u (average) (MJ/m^3)	Peak Force (N)	u (peak) (MJ/m^3)	Predicted u (ave.) (MJ/m^3)	Predicted u (peak) (MJ/m^3)
Neutral	***1***	***157***	***6.3***	***204***	***8.2***	***6.3***	***8.2***
Neutral	2	168	3.4	206	4.1	5.5	7.1
Neutral	3	127	1.7	182	2.4	5.1	6.6
Neutral	4	107	1.1	190	0.9	4.8	6.2
45° Pos.	0.5	65	5.2	75	6	4	5.1
45° Pos.	1	81	3.2	93	3.7	3.5	4.5
45° Pos.	2	45	0.9	66	0.9	3	3.9
45° Pos.	3	63	0.8	93	1.2	2.8	3.6
45° Pos.	4	53	0.5	80	0.8	2.6	3.4
45° Pos.	6	77	0.5	132	0.9	2.4	3.2
45° Neg.	1	257	10.3	289	11.6	9.1	11.9
45° Neg.	2	315	6.3	379	7.6	8	10.4
45° Neg.	3	429	5.7	541	7.2	7.3	9.5
45° Neg.	4	292	2.9	581	5.8	6.9	9
45° Neg.	5	363	2.9	682	5.5	6.6	8.6

Note. Data obtained for 1mm cut using neutral rake tool (***bold print***) is used as baseline from which to obtain all predicted values.

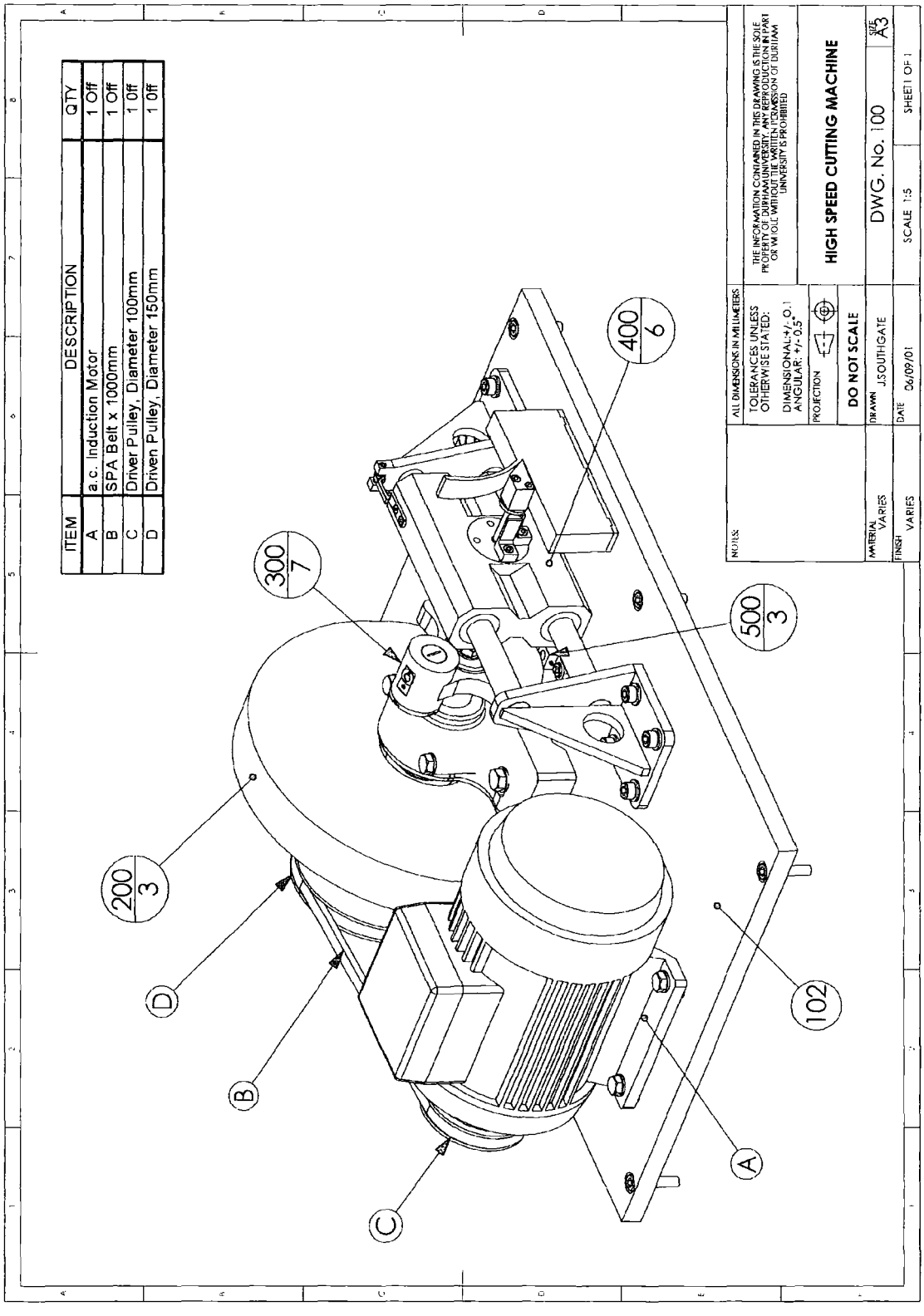
ITEM
DESCRIPTION
QTY
A
a.c. Induction Motor
1 Off
B
SPA Belt x 1000mm
1 Off
C
Driver Pulley, Diameter 100mm
1 Off
D
Driven Pulley, Diameter 150mm
1 Off
NOTES:
ALL DIMENSIONS IN MILLIMETERS
TOLERANCES UNLESS OTHERWISE STATED:
DIMENSIONAL: +/- 0.1
ANGULAR: +/- 0.5°
PROJECTION
DO NOT SCALE
THE INFORMATION CONTAINED IN THIS DRAWING IS THE SOLE PROPERTY OF DURHAM UNIVERSITY. ANY REPRODUCTION IN PART OR WHOLE WITHOUT THE WRITTEN PERMISSION OF DURHAM UNIVERSITY IS PROHIBITED
HIGH SPEED CUTTING MACHINE
MATERIAL VARIES
FINISH VARIES
DRAWN J.SOUTHGATE
DATE 06/09/01
DWG. No. 100
SCALE 1:5
SIZE A3
SHEET 1 OF 1
200/3
300/7
400/6
500/3
102
A
B
C
D

ITEM	DESCRIPTION	QTY
A	WELDIN' Adapter	1 Off
B	Taper Lock Bush 2012 (40 bore)	1 Off
C	M12 x 45 bolt, Strongback ø40 x 4 thk	1 Off
D	Plummer Block, SN509, Self Aligning	2 Off
E	M12 x 80 Hexagon head bolt	4 Off

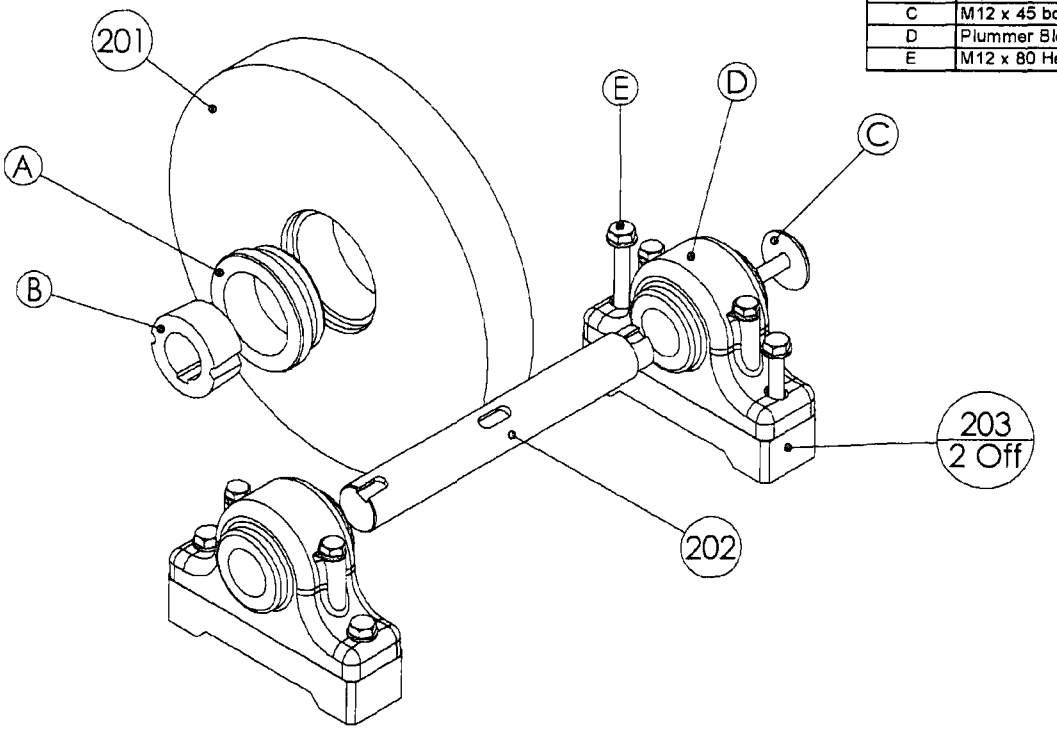

NOTES:	ALL DIMENSIONS IN MILLIMETERS	
	DO NOT SCALE	FLYWHEEL ASSY
	DRAWN J.SOUTHGATE	
MATERIAL VARIES	-	DWG. No.200 — SIZE A3
FINISH VARIES	DATE 13/09/01	SCALE 1:3 — SHEET1 OF 1

ITEM	DESCRIPTION	QTY
A	Main Spring	1 Off
B	M4 x 12mm Ch. Head Screws	4 Off
C	Detent Spring	1 Off
D	8mm Ball Bearing	1 Off
E	3mm Ball Bearing	1 Off
F	M4 x 12mm Grub Screw	1 Off

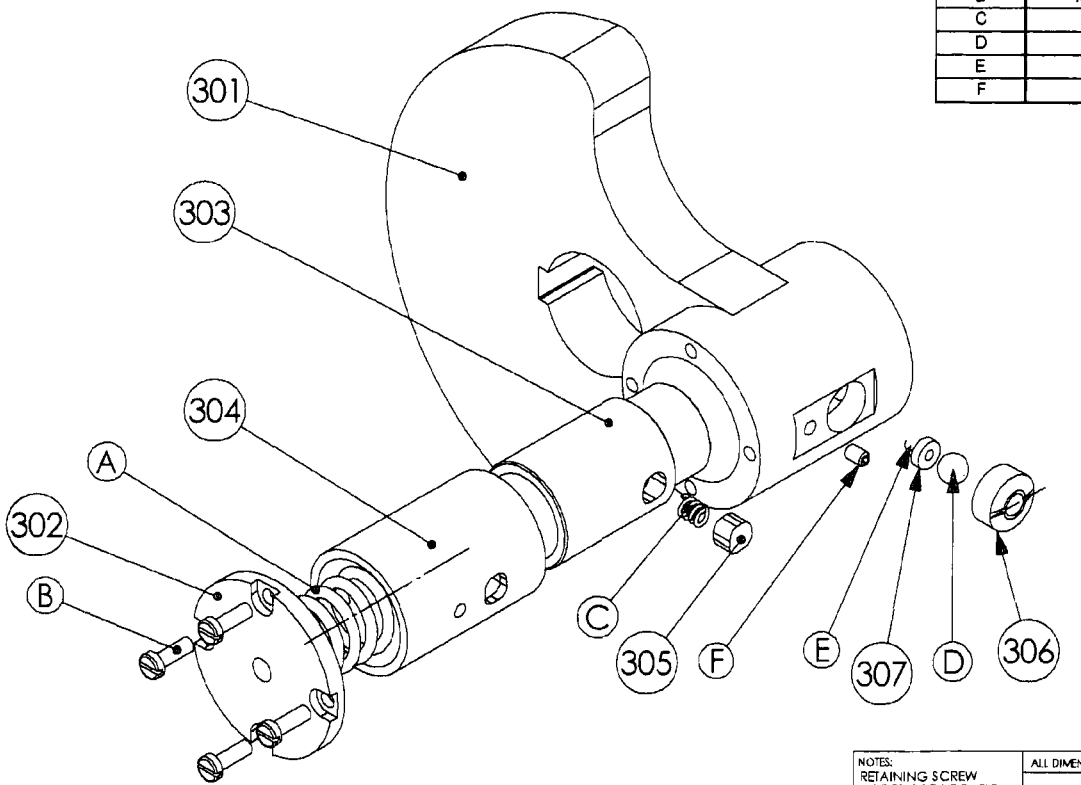

NOTES:
RETAINING SCREW ADDED FOR LOCATION OF PIN SLEEVE

ALL DIMENSIONS IN MILLIMETERS

DO NOT SCALE

DRAWN J.SOUTHGATE

MATERIAL VARIES

FINISH VARIES

2nd Issue:12/09/01

DATE 06/09/01

STRIKE PIN WHEEL

DWG. No. 300

SIZE A3

SCALE 1:1

SHEET1 OF 1

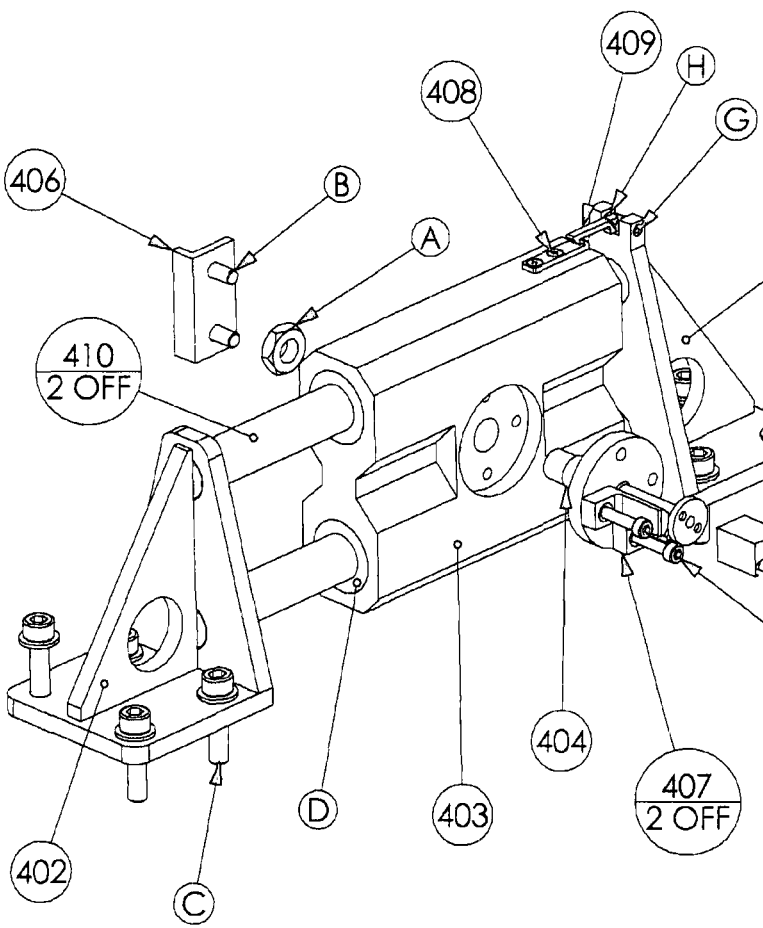

ITEM	DESCRIPTION	QTY
A	M16 Nut and Washer	1 Off
B	M8 Csk Screw x 20mm	2 Off
C	M10 Caphead Bolt x 30mm	8 Off
D	Linear Ball Bushings, 25mm ID	4 Off
E	M6 Caphead Screw x 25mm	2 Off
F	M5 Caphead x 16mm	2 Off
G	Pin, Sil.Steel,Diameter 4mm x 30mm	1 Off
H	Spacer, OD 6mm, ID 4 mm, x 4mm L	2 Off

NOTES:	ALL DIMENSIONS IN MILLIMETERS	
	TOLERANCES UNLESS OTHERWISE STATED: DIMENSIONAL:+/- 0.1 ANGULAR: +/- 0.5°	
	PROJECTION	**TOOL SLIDER ASSEMBLY**
	DO NOT SCALE	
MATERIAL VARIES	DRAWN J.SOUTHGATE	DWG. No. 400 — SIZE A3
FINISH VARIES	DATE 14/09/01	SCALE 1:2 — SHEET 1 OF 1

ITEM	DESCRIPTION	QTY
A	M8 x 20 Cap Head Bolts	2 Off
B	M3 Grub Screw	1 Off
C	Actuator Spring	1 Off

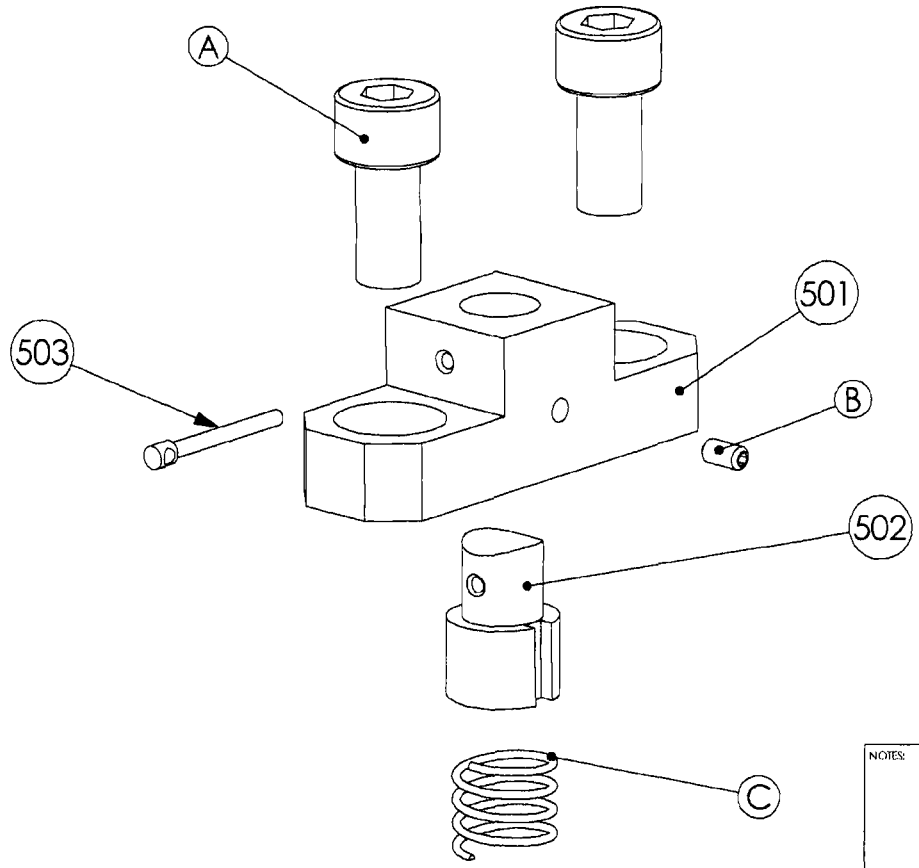

NOTES:	ALL DIMENSIONS IN MILLIMETERS	
	TOLERANCES UNLESS OTHERWISE STATED: DIMENSIONAL:+/- 0.1 ANGULAR: +/- 0.5°	THE INFORMATION CONTAINED IN THIS DRAWING IS THE SOLE PROPERTY OF DURHAM UNIVERSITY. ANY REPRODUCTION IN PART OR WHOLE WITHOUT THE WRITTEN PERMISSION OF DURHAM UNIVERSITY IS PROHIBITED
	PROJECTION **DO NOT SCALE**	**ACTUATOR ASSY**
MATERIAL VARIES	DRAWN J.SCUTHGATE	DWG. No. 500 — SIZE A3
FINISH VARIES	DATE 13/09/01	SCALE 2:1 — SHEET1 OF 1

1 Statement of Requirements

This manual sets out to record pertinent decisions in the design of a high-speed cutting machine for the orthogonal cutting of (paraffin wax) samples. Rationale and calculations are presented, but it should be born in mind that these calculations are the result of considerable iteration that cannot be practically (or indeed usefully) included.

A device is required, in order to further research the mechanical removal of paraffin wax deposits in crude oil pipelines, that will meet the following criteria;

Cutting speed range from 0.01 to 10 metres per second.
Produce a linear cut across a 100mm long, 25mm wide sample.
Allow a horizontally orientated sample.
Allow cutting depths, in increments of 1mm, from 1mm to 10mm.
Allow a 10mm deep cut without more than a 2% loss of cutting speed across the sample.

General requirements that apply to all machines must also be met, i.e. the machine must be safe to operate, etc.

2 Dynamics

2.1 Loads

The maximum load anticipated is based on data from initial experiments that gave a value for u of 8.2 MPa for paraffin wax.

The maximum load anticipated is for a 10mm cut using a negative rake tool. Under these circumstances u can be calculated thus;

$$u = 8.2MPa \times \left(\frac{145}{100}\right) \times \left(\frac{1}{10}\right)^{0.2} = 7.5MPa$$

The maximum force anticipated $F_p = ubt = 7.5 \times 25 \times 10 = 1875N$

It should be noted that up until now, actual values for u have been somewhat less than those predicted by adjusting for the 'size effect'. In light of this, a maximum load limit of 2000N has been applied to the machine.

2.2 Cutting Speed

Maximum cutting speed required is 10 m/s. Given that this linear motion will be caused by the movement of an eccentric pin through 180°, an angular velocity of π rads/0.01secconds, or 314 rads/sec, 3000 r.p.m. would be required.

This gives an average linear velocity of 10m/s, but in fact a peak velocity of r.ω.sinθ m/s, at 90° this equates to15.7 m/s. Rearranging this equation to give a *peak* linear velocity of 10 m/s, angular velocity needs to be;

$$\omega = v/r.\sin\theta \qquad \omega = 10m/s \,/0.05m \text{ x } \sin 90^\circ$$

$$\omega = 200 \text{ rads/sec}$$

$$= 1910 \text{ r.p.m.}$$

The a.c. induction motor available for use has a maximum speed of 2890 r.p.m., so a speed reduction ratio of **3:2** is required.

2.3 Flywheel Acceleration

$$\text{Radius of gyration} \quad k = \frac{r}{\sqrt{2}} = \frac{0.175m}{\sqrt{2}} = 0.1237$$

$$\text{Moment of Inertia} \quad I = mk^2 = 38kg \times 0.1237^2 = 0.582kg.m^2$$

$$\text{Angular acceleration} \quad \alpha = \frac{T}{I} = \frac{10Nm}{0.582kg.m^2} = 17.2rad/\sec^2$$

$$\text{Time to reach maximum speed} \quad t = \frac{\omega_2 - \omega_1}{\alpha} = \frac{200rad/s - 0rads/s}{17.2rads/\sec^2} = 11.6\sec onds$$

$$\text{Deceleration across sample} \quad \alpha = \frac{T}{I} = \frac{2000N \times 0.05m}{0.582kg.m^2} = 172rad/\sec^2$$

Percentage drop in angular velocity is calculated thus:

$$\omega_2^2 = \omega_1^2 + 2\alpha\theta = 200^2 - 2 \times 172 \times \pi$$
$$\omega_2 = \sqrt{38919} = 197.3rads/s$$

Percentage drop = (2.7/200) x 100 = 1.35%

2.4 Flywheel Stress

Considering the flywheel as an annular wheel, maximum tangential stress (occurring at the minor radius) and radial stress (occurring at $r = \sqrt{r_1 r_2}$) are as follows:

$$\sigma_{t\max} = \rho v^2 \frac{(3+\nu)}{4}\left(1+\frac{(1-\nu)}{(3+\nu)}\left(\frac{r_1}{r_2}\right)^2\right)$$

$$\sigma_{t\max} = 7850kg/m^3 \times 35m/s^2 \frac{(3+0.3)}{4}\left(1+\frac{(1-0.3)}{(3+0.3)}\left(\frac{0.04}{0.175}\right)^2\right)$$

$$\sigma_{t\max} = 8MPa$$

$$\sigma_{r\max} = \rho v^2 \frac{(3+\nu)}{4}\left(1-\left(\frac{r_1}{r_2}\right)^2\right)$$

$$\sigma_{r\max} = 7850kg/m^3 \times 35m/s^2 \frac{(3+0.3)}{4}\left(1-\left(\frac{0.04}{0.175}\right)^2\right)$$

$$\sigma_{r\max} = 7.5MPa$$

2.5 Bearing Loads

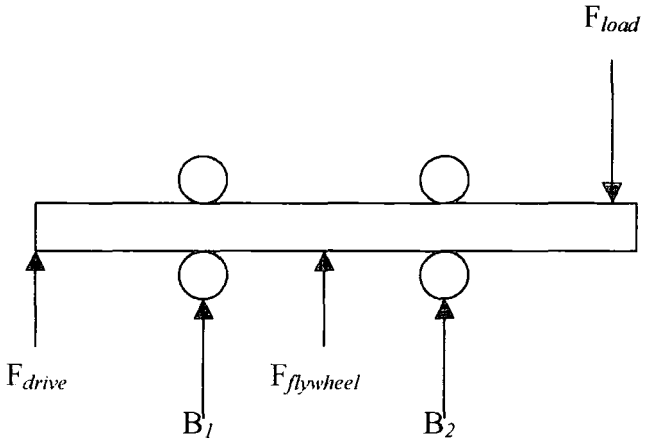

F_{drive} = Motor torque/Drive pulley radius = 15Nm/0.066m = 227N

F_{load} = Cutting force = 2000N

$F_{flywheel}$ = Torque due to deceleration/Radius of gyration = $\frac{I\alpha}{k} = \frac{0.582 \times 172}{0.1237} = 809N$

Note: External forces are not in equilibrium as system is decelerating

Taking moments around B_1;

$$(227N \times 0.079m) + (2000N \times 0.2485m) = (809N \times 0.0725m) + (B_2 \times 0.145m)$$

$$515Nm = 58.7Nm + (B_2 \times 0.145m)$$

$$515Nm - 58.7Nm/0.145m = B_2$$

$$B_2 = 3147N$$

Taking moments around B_2;

$$(2000N \times 0.1035m) = (809N \times 0.0725m) + (227 \times 0.1515) + (B_1 \times 0.145m)$$

$$207Nm = 58.7Nm + 34.4Nm + (B_1 \times 0.145m)$$

$$207 - 93.1\ Nm/0.145m = B_1$$

$$B_1 = 786N$$

Dynamic Load Rating = (Equivalent Load, 3147N) x (Life factor for 2000hrs, 1.0) x (Speed factor for 2000r.p.m.,6.0) = 18 882N.

(Self aligning ball bearings to be used have rating of 22 000N)

2.6 Maximum Shaft Torsion

Polar second moment of area for shaft ; $J = \frac{\pi}{32} 0.04m^4 = 2.51 \times 10^{-7}$

Shear stress at r=0.02m ; $\tau = \frac{T}{J} r \qquad \tau = \frac{2000N \times 0.05m}{2.51 \times 10^{-7}} 0.02m = 7.97MPa$

2.7 Drive Belt Specification

Note: From *Fenner* design manual.

a)	Speed ratio	1.5:1
b)	Service factor	1.2 (Medium duty, heavy start, less than 10hrs/day)
c)	Design Power	4kW x 1.2 = 4.8kW
d)	Belt section	SPA
e)	Minimum Pulley Ø	67mm
f)	Pulley Pitch Ø	Driver 100mm, Driven 150mm.
g)	Belt L./ Centre Dist.	1000/303, correction factor 0.85
h)	Basic power per belt	5.05
j)	Speed ratio power increment	0.92
k)	Corrected power per belt	5.05 + 0.92 = 5.97kW
l)	No. belts required	4.8/5.97 = 0.8

One SPA belt is sufficient.

2.8 Actuator Spring

The actuating pin needs to have ejected fully within ¾ of one revolution. With the pin carrier revolving at 200 rads/sec, ejection must occur within ¾ 2π/200 = 0.0236 seconds.

The pin is required to travel 0.01m to full ejection, therefore required acceleration can be calculated thus;

$$s = \frac{1}{2} at^2 \qquad a = \frac{2s}{t^2} \qquad a = \frac{0.02m}{0.0236s^2} = 36m/s^2$$

The force required to accelerate the 0.19kg pin at this rate is;

$$F = ma \qquad F = 0.19kg \times 36m/s^2 = 6.8N$$

In addition to this force, a force is required to overcome the friction between the actuator pin and its sleeve. The force exerted normal to the pin/sleeve interface is a centrifugal one and is calculated thus;

$$CF = mr\omega^2 \qquad CF = 0.19kg \times 0.05m \times 200rad/s^2 = 380N$$

The resulting frictional force to overcome is;

$$F = \mu N \qquad F = 0.2 \times 380 = 76N$$

The minimum force required to ensure timely ejection of the pin is therefore *82.8N*

If the ejector spring's rate is considered linear, then it must be exerting this force when the pin is 'half ejected' i.e. the force will be an average one.

A sample spring, from Ashfield Springs, has the following specifications;

OD	2.2mm
Free Length	38.1mm
Solid Length	21.3mm
Rate	1.09kgf/mm (10.7N/mm)

As the clearance beneath the actuating pin is 24mm closed to 34mm open, the force exerted by this spring would be 150.8N down to 43.8N fully ejected.

Therefore average force=97.3N

3 Structural

3.1 Bending Stress on Box Section Frame

Assuming a worst case whereby the entire weight of the machine is concentrated as a point load midway along one of the frame's top sections;

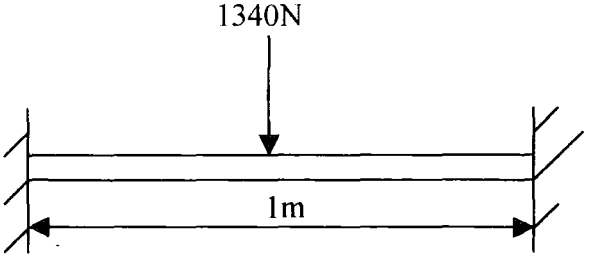

Second moment of area for hollow 80mm x 80mm box section, 2.9mm thick,
$I = 88m^4 \times 10^{-8}$

$$\text{Maximum deflection } y_m = \frac{1/192 \times 1340 \times 1^3}{207 \times 10^9 \times 88 \times 10^{-8}} = 0.04mm$$

$$\text{Maximum stress } \sigma_m = \frac{My}{I} = \frac{(1/8 \times 1340 \times 1) \times 0.04}{88 \times 10^{-8}} = 7.6MPa$$

3.2 Bending Stress on Base Plate

This empirical formula assumes a clamped edge to the plate, and a concentrated load in the centre of the plate. Carvill quotes k as 0.211 for this plate geometry.

$$\text{Maximum stress at edge of longer side } \sigma_m = kP/t^2 = \frac{0.211 \times 1340N}{0.019m^2}$$

$$\sigma_m = 0.783MPa$$

Note:
Given that this plate will contain a slot to allow fitting of flywheel, a reduction in plate thickness is inappropriate, especially considering relatively low cost of this material.

3.3 Strike Pin & Bush

The strike pin slides through and is supported by a phosphor bronze bearing such that the 'crushing' stress on the bearing, as a plain journal type, is;

$$\sigma_c = \frac{P}{bD} \qquad \sigma_c = \frac{2000N}{0.055m \times 0.03m}$$

$$\sigma_c = 1.2MPa$$

The pin itself is stepped and as such is subject to a shear stress as follows;

$$\tau = \frac{P}{A}k$$

k is the stress concentration factor applied to a stepped shaft, and in this case Carvill quotes a figure of 1.85, with a 0.5mm radius at the shoulder. Therefore;

$$\tau = \frac{2000N}{\pi 0.0125m^2} 1.85 = 7.5MPa$$

The stress imposed on the pin, however, will be due to impact. Carvill suggests a stress due to a 'suddenly applied' load is double that experienced in the steady state.

4 Dynamometer

Load range: 10N to 2000N

Cantilever tool post is 0.0675m to the centre of its load as shown.

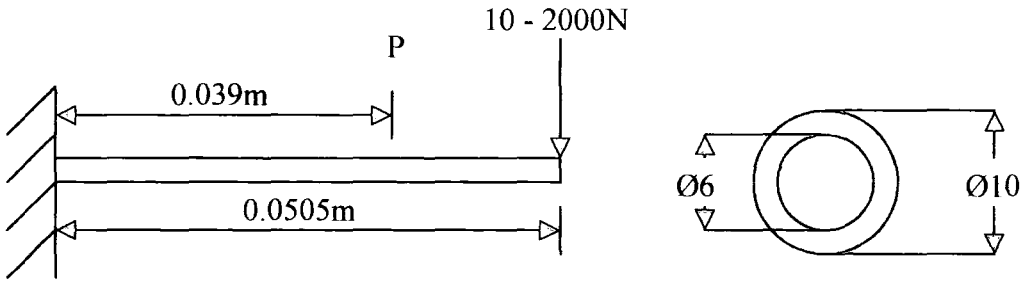

I for post;

$$I = \frac{\pi\left(D^4 - d^4\right)}{64} \qquad I = \frac{\pi\left(0.01^4 - 0.006^4\right)}{64}$$

$$\underline{I = 4.273 \text{ x } 10^{-10}}$$

Max deflection at free end;

$$y_{max} = \frac{\frac{1}{3}WL^3}{EI} \qquad y_{max} = \frac{\frac{1}{3} \times 2000 \times 0.0505^3}{\left(207 \times 10^9\right) \times \left(4.273 \text{ x } 10^{-10}\right)}$$

$$\underline{y_{max} = 0.97\text{mm}}$$

Therefore maximum deflection at point P will be from 0.97/50.5 x 39 = <u>0.75mm</u>

Min deflection at free end;

$$y_{max} = \frac{\frac{1}{3}WL^3}{EI} \qquad y_{max} = \frac{\frac{1}{3} \times 10 \times 0.0505^3}{\left(207 \times 10^9\right) \times \left(4.273 \text{ x } 10^{-10}\right)}$$

$$\underline{y_{max} = 4.9\mu\text{m}}$$

Max tensile stress;

$$\sigma_{max} = \frac{My}{I} \qquad \sigma_{max} = \frac{101 \times 0.00097}{4.273 \times 10^{-10}}$$

$$\underline{\sigma_{max} = 229 \text{ MPa}}$$

Set against the cantilever post at point P are 2 beams normal to the post vertically and horizontally. Strain gauges set into the centre of the beams will measure strain produced by bending moment in these beams and this measurement will produce a signal for an oscilloscope.

5 Approximate Weights.

The weight to be supported by the frame is as follows;

Flywheel	38 kg
Base Plate	54 kg
Motor	24 kg
Main Shaft	3 kg
Slide Shafts x 2	3 kg
Plummer Blocks x 2	6 kg
Slide Assy.Brackets x 2	3 kg
Dynamometer Assy.	3 kg
Miscellaneous Fittings	2 kg
Total	136 kg
(Frame	86kg)

6 Material Properties

	UTS ($N\ mm^{-2}$)	E ($GN\ m^{-2}$)	ρ ($kg\ m^{-3}$)	υ
Steel BS 970 070M20	430	207	7850	0.3
Steel BS 970 080M40	510	207	7850	0.3
Aluminium NS4	170	70	2700	0.32

7 Dynamometer Calibration

Measurement of the deflection of the beams acting on the dynamometer's 'cantilever tool post' was achieved using electrical strain gauges. It was therefore necessary to calibrate the output from a strain gauge amplifier to the load acting on the post in the horizontal and vertical planes (representing cutting and thrust forces respectively during the wax cutting tests).

The dynamometer post was loaded by attaching a pulley to the high-speed rig's machine bed that would allow weights to be hung from the post such that the forces generated were normal to the horizontal plane of the tool. To calibrate the dynamometer post in the vertical plane (i.e. the direction measuring thrust forces) a hole was drilled through the machine bed beneath the dynamometer such that weights could be hung from the post to generate a force normal to the vertical plane of the tool.

The dynamometer was initially calibrated by loading it in the horizontal and vertical planes separately. Loads were applied in approximate increments of 10 kg up to a maximum of 50 kg. Output from the strain gauge amplifier is shown plotted against load for the calibration of strain gauge 'A' (horizontal load) in figure D1. Similarly, output from the strain gauge amplifier is shown plotted against load for the calibration of strain gauge 'B' (vertical load) in figure D2. Note that loads were applied incrementally to a maximum value and then down to a minimum value. This cycle was repeated three times to give an average value and to ensure 'bedding in' of the strain gauges.

Once the individual strain gauges had been calibrated a check was made for 'cross-talk'. This phenomenon occurs if there is any deviation of the tool post's movement from the

vertical and horizontal planes. 'Cross-talk' would manifest itself in a slight increase or decrease in measured loads perpendicular to the plane of action under scrutiny caused by such deviation. To check for 'cross-talk' loads were asynchronously applied to both gauges as can be seen in figures D3 and D4.

Figure D1. Dynamometer Calibration14/01/02 Gauge 'A'

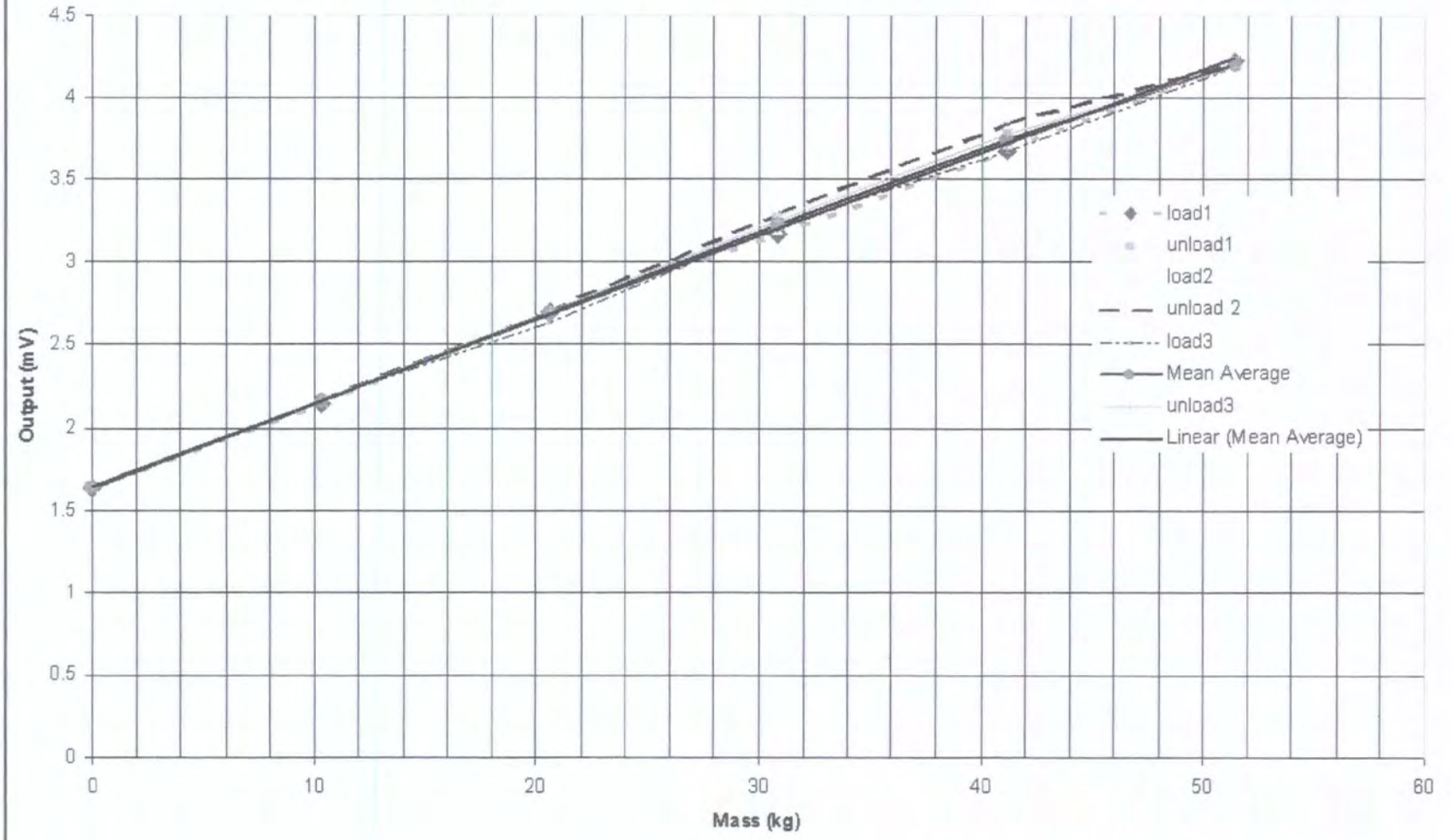

Figure D2. Dynamometer Calibration14/01/02 Gauge 'B'

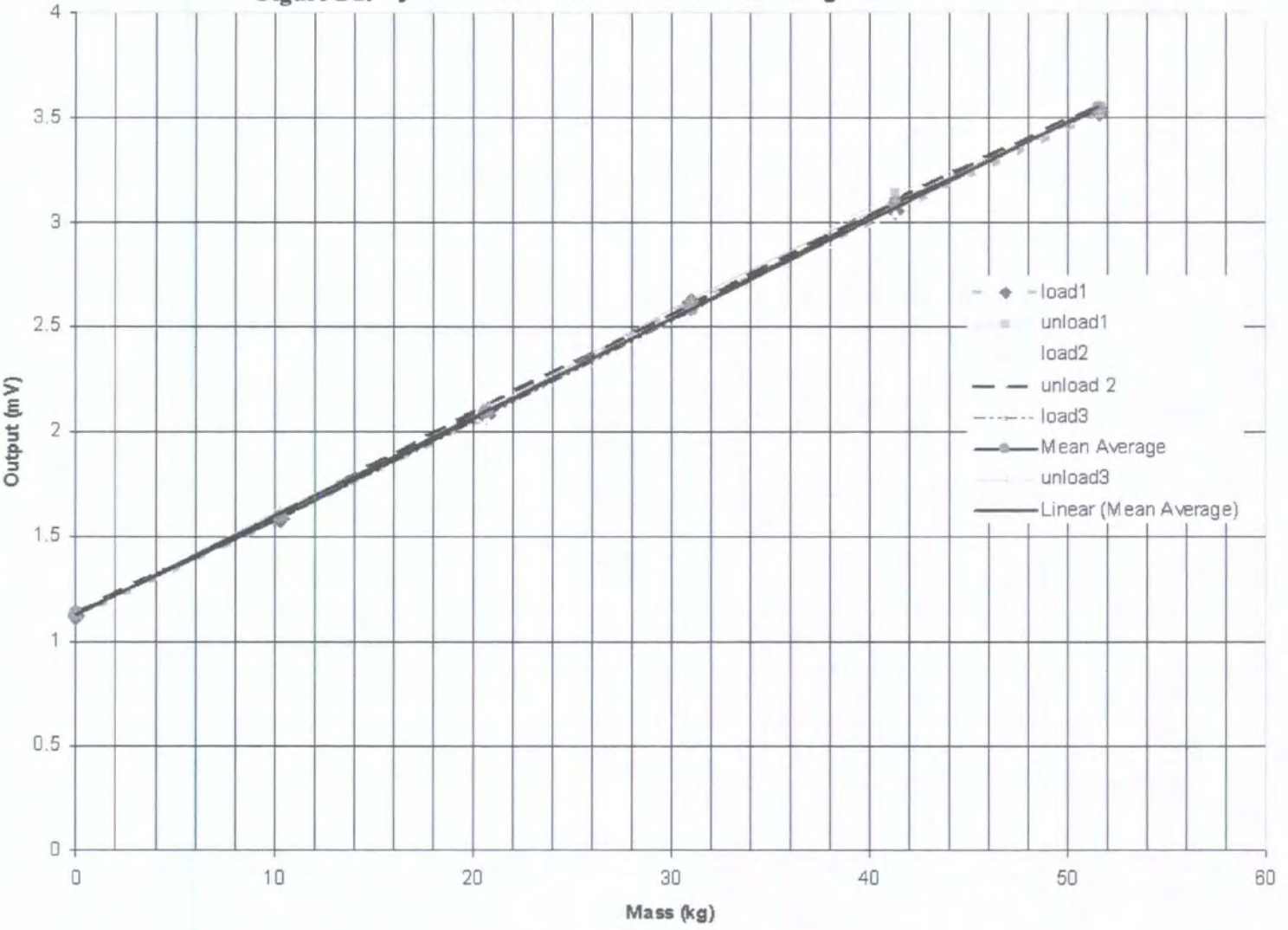

Figure D3. Cross-Talk, Output from gage 'B'

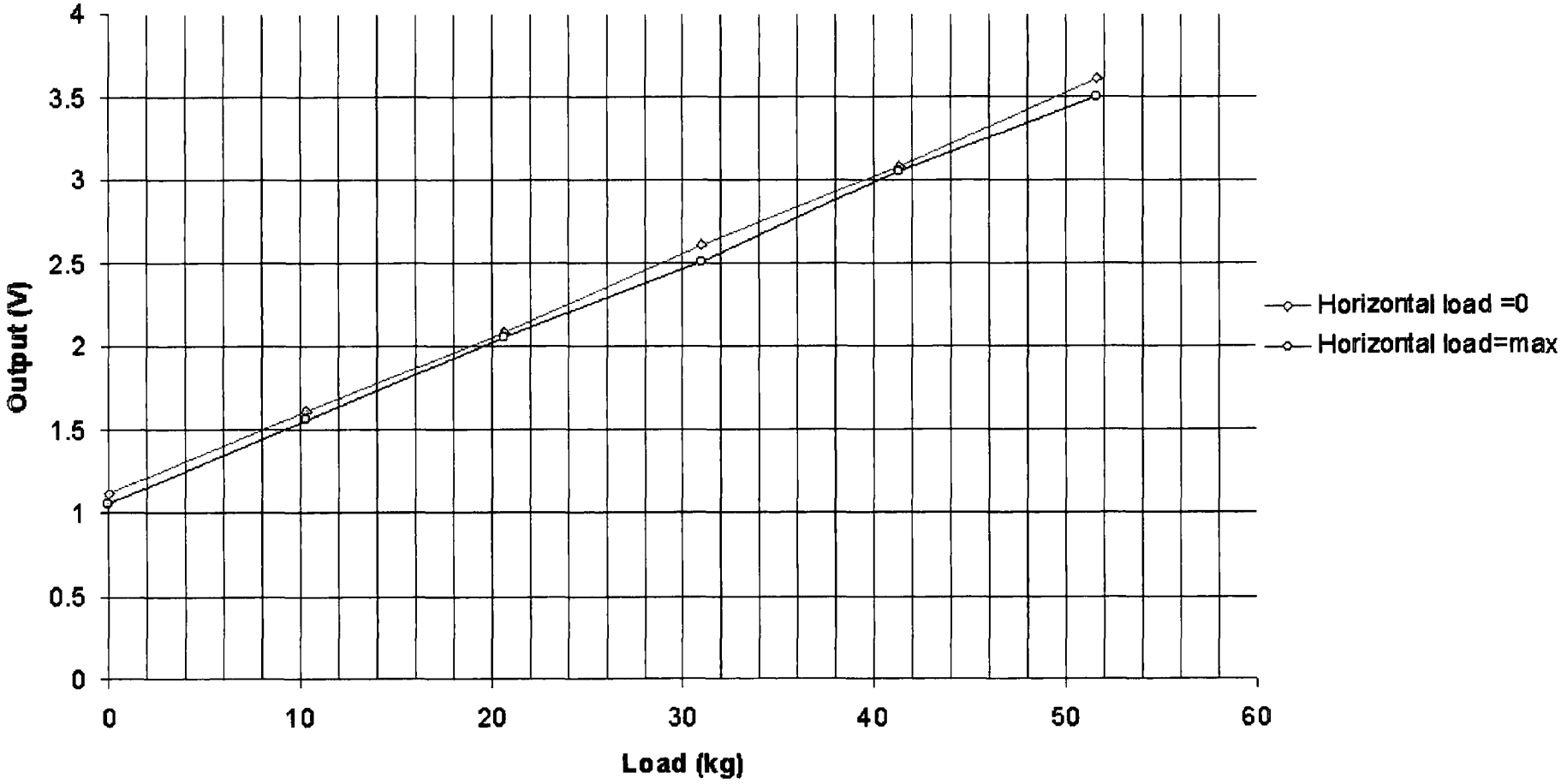

Figure D4. Cross-Talk, Output from gage 'A'

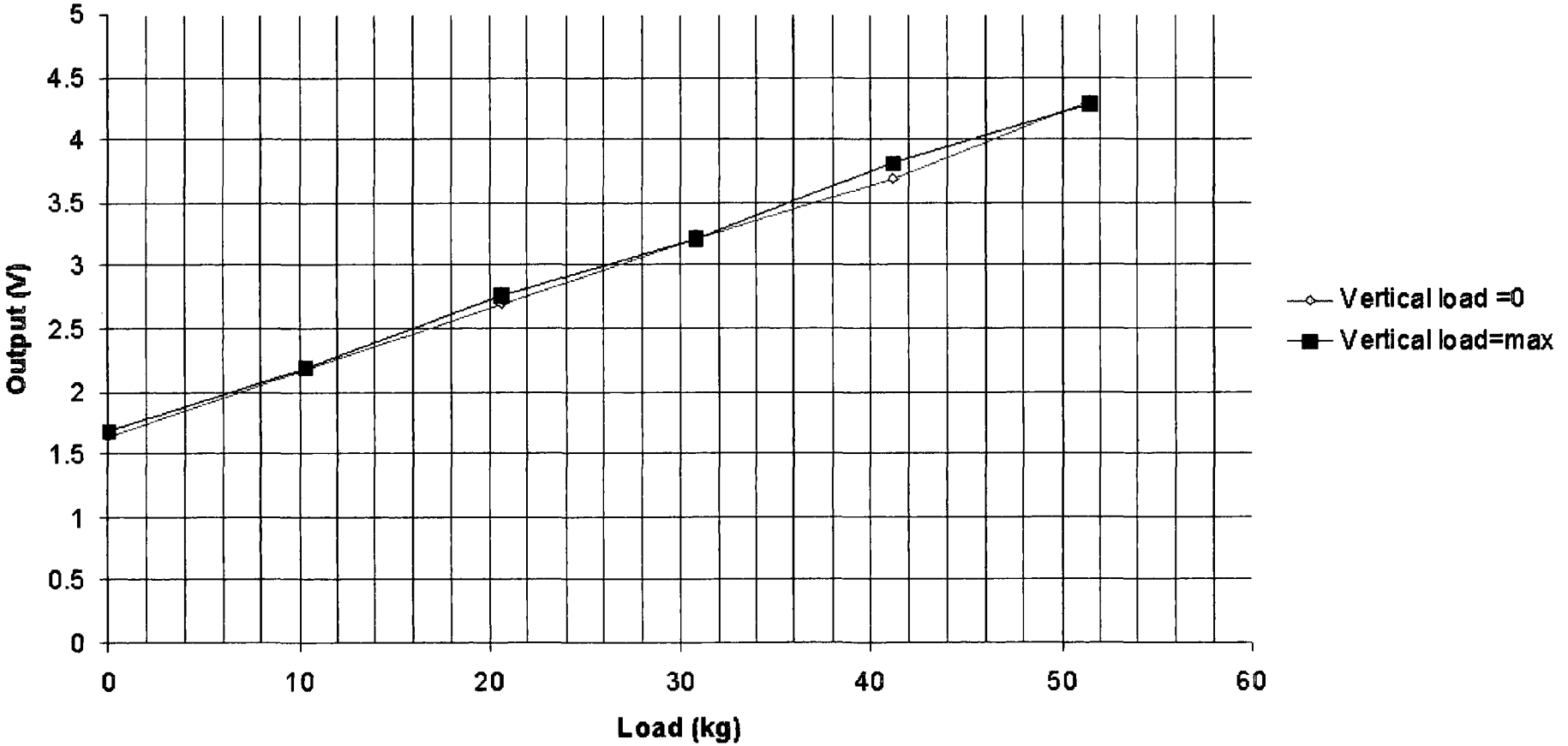

Appendix E Trial Test Procedure

I. SUPPLIER DOCUMENT FRONT SHEET

Shah Deniz Gas Export Project

SUPPLIERS FRONT SHEET (FOR A4/A3 DOCUMENTS ONLY)

DOCUMEN TITLE	Test Loop Procedure

TOTAL No. OF PAGES	19
SUPPLIERS ORDER No.	A9149

SUPPLIERS OWN DOCUMENT No.	REV NO.	DATE	SUPPLIERS APPROVAL NAME
A91491406	1	11/08/03	Mike Sowa
	2	2/10/03	Blake Vaughan

SUBMITTED FOR : ☐ INFO ☑ REVIEW

REVIEW DOES NOT CONSTITUTE ACCEPTANCE OF DESIGN DETAILS, CALCULATIONS, TEST METHODS OR MATERIALS DEVELOPED OR SELECTED BY SUPPLIER, NOR DOES IT RELIEVE SUPPLIER FROM FULL COMPLIANCE WITH CONTRACTURAL OR OTHER OBLIGATIONS

☐ 1. ACCEPTED.

☐ 2. ACCEPTED. PROCEED WITH WORK AND INCORPORATE COMMENTS AND RESUBMIT.

☐ 3. NOT ACCEPTED. WORK MAY NOT PROCEED. REVISE AND RESUBMIT

☐ 4. FOR INFORMATION - NO SIGNATURE REQUIRED

NAME: ..... DATE: .....

Shah Deniz Gas Export Project

SUPPLIER NAME:- Pipeline Engineering

PACKAGE DESCRIPTION :- Pipeline Pigs

TAG NOS :-	MODEL TYPE NOS :-
NA	NA

TOTAL NO. SHEETS:-	SDRL PRIME CODE :-
14	H05

PURCHASE ORDER NO.	SDRL.CAT.	SEQUENCE NO.	REV
BPSD-SHAH-PSPL26A	H	0008	2

Pipeline

Shah Deniz Gas Export Project
Low Flow Pig Development
Wax Removal and General Piggability Trial
Test Procedure

II. REVISION HISTORY

Revision	Date	Description	Originated		Reviewed		Internal Approval		Client Approval
1	25/07/03	Issued for client approval	KW		MS		BV		
2	19/09/03	Client comments added	KW		MS		BV		

PE DOCUMENT NUMBER	**A9149-14-01-A**
CLIENT DOCUMENT NUMBER	BPSD-SHAH-PSPL26A H0008 01

COMMENT

CONTENTS

1.0 INTRODUCTION

- 1.1 General
- 1.2 Pigging Operations
- 1.3 Test Rig Information
- 1.4 Driving Medium
- 1.5 Related Documents
- 1.6 Abbreviations

2.0 HEALTH, SAFETY AND ENVIRONMENT (HSE)

- 2.1 General
- 2.2 Responsible Persons
- 2.3 Safety Meetings
- 2.4 Safety Precautions

3.0 TEST RIG HYDROTEST PROCEDURE

- 3.1 General
- 3.2 Hydrotest
- 3.3 Cleaning

4.0 WAX MIXING AND APPLICATION

- 4.1 De-waxing Testing
- 4.2 Wax Mixing and Application - General
- 4.3 Mixing
- 4.4 Application

5.0 DE-WAXING TEST PROCEDURE

- 5.1 Scope 1 – De-waxing Tests
- 5.2 Scope 2 – General Piggability
- 5.3 Foam Pig Rescue

6.0 WAX DISPOSAL

7.0 REPORTING, COMMUNICATION AND RECORDING

- 7.1 Reporting
- 7.2 Records
- 7.3 Instrument Calibration

8.0 TEMPORARY RIG DRAWINGS

- 8.1 Test Loop Schematic
- 8.2 Test Rig General Arrangement.

9.0 DAILY TEST REPORT PROFORMA.

1.0 INTRODUCTION

1.1 General

The proposed Shah Deniz pipeline will transport single-phase waxy condensate, via a 94km, 12" pipeline, from the Shah Deniz field in the South Caspian Sea to the Sangachal Terminal near Baku in Azerbaijan.

A substantial build-up of wax is expected, with up to a 5 mm per day coating being deposited on the internal pipewall over the first 40km. The wax is relatively soft in nature having a high percentage of entrapped liquid. Over a three day period up to 110m^3 of soft wax, or 19m^3 of solid wax, could accumulate in the line. Management of this wax build up is a key concern for BP Azerbaijan.

1.2 Pigging Operations

During normal flow velocities (~1.2 m/s) it will be possible to have bypass through the pig, which can be used to keep the wax in front of the pig in suspension and produce a slurry. During the turndown scenario (flow velocity ~0.4m/s) it may not be possible to have by-pass flow through the pig. Bypass at low velocities could cause the pig to stall. However, without bypass, there is a concern that the wax will build up in front of the pig, cause it to stall and a line blockage to occur.

Pipeline Engineering have been invited to develop a system, which will allow by-pass through the pig, which in turn will 'cut' wax from the pipewall, thereby ensuring that the wax in front of the pig will remain in suspension during all flow conditions.

1.3 Test Rig Information

The rig has been designed to simulate a build up of wax on an actual pipeline. The visual rig section is made from high impact Perspex. The rig also incorporates pipe and fitting features as will be encountered in the actual pipeline.

This will include as follows-:

Item	Description	Details	Connections
1.	16" x 12" Launcher	Overall length 2400 mm Major barrel I/D 381mm Neck pipe I/D 303 mm	2 x ½" Instrument Connection 1 x 4" Kicker Connection 1 x 4" Drain Connection 1 x Signaller Connection - A
2.	12 " Spool 1	Overall length 20 M I/D 291.3 mm	1 x ½" Instrument Connection 2 x Signaller Connection – B and C
3.	12" Barred Tee	Overall length 563 mm I/D 286.5 mm	12" Blinded Branch
4.	12" Spool 2	Overall length 1000 mm I/D 276.3 mm	1 x Signaller Connection – D
5.	12" Bend	Overall length 2544 mm I/D 269.9 mm	1 x ½" Instrument Connection
6.	12" Spool 3	Overall length 1000 mm I/D 291.3 mm	None
7.	12" Spool 4 (Perspex)	Overall length 1000 mm I/D 291.3 mm	None
8.	12" Spool 5	Overall length 12 M I/D 282.7 mm	1 x ½" Instrument Connection 1 x Signaller Connection – E
9.	16" x 12" Receiver	Overall length 2400 mm Major barrel I/D 381mm Neck pipe I/D 303 mm	2 x ½" Instrument Connection 1 x 4" Return Connection 1 x 4" Drain Connection 1 x Signaller Connection - F

1.31 Test Medium

Potable water pumped from break tank and recovered via return/drain hose.

1.4 Related Documents

Document Number	Description
59/16/09	PE HSE Plan
A9149/03/01	PE QC Plan
PE A914980-3134/GN	PE Risk Assessment
DOCUMENT NO. 59/01/01	PE General Hydrotest Practices and Procedures

1.5 Abbreviations

HSE: Health Safety and Environment
PPE: Personal Protective Equipment
PE: Pipeline Engineering

2.0 HEALTH, SAFETY AND ENVIRONMENT (HSE)

2.1 General

Pipeline Engineering recognise that the health and safety of personnel and its assets, the protection of the environment are an integral part of successful operations. Procedures and activities shall not be allowed which would violate this concept.

All safety precautions shall comply with statutory and other relevant regulations.

2.2 Responsible Persons

The PE Test Supervisor shall have overall responsibility for the operational safety during testing operations. The PE Test Supervisor will be the point of contact for the onsite Client representatives.

2.3 Safety Meetings

Prior to tests commencing, a safety meeting / toolbox talk will be convened to introduce all personnel and advise all Safety Procedures and the PE Permit to Work System. All personnel engaged upon the testing operations shall be made aware of the possible consequences of fitting or hose failure under pressure conditions and the hazards associated with the energy stored within systems under pressure, specifically the subtleties between hydraulic and pneumatic energy.

2.4 Safety Precautions

The following safety precautions shall be adopted during the testing operations:

a. The area in which the tests are taking place will be cordoned off with barrier tape and signs indicating testing operations are ongoing will be displayed. PA announcements shall be made warning of the impending operations. Announcements shall be made prior to, during and on completion of operations.

b. All personnel involved with the testing operations shall wear as a minimum, protective headgear, protective footwear, eye protection and coveralls. Ear protection will be required to be worn at times when appropriate or as required by PE test supervisor.

3.0 TEST RIG HYDROTEST PROCEDURE

3.1 General.

The test rig is to be set up on firm level ground in the test area of the PE fabrication department (Factory 2). Pressure transducers will be fitted to the four ports on the rig. These in turn will be connected to a four-channel data logger, to give real time recording during the pigging runs. On commencement of pigging tests, the return hose from the rig will be piped via an open filter to strain out the wax cuttings. A steel 'dummy spool' will be fitted in place of the Perspex section for the cleaning stage to avoid causing any damage.

3.2 Hydrotest.

1. Attach calibrated gauge via hose to vent connection on launcher.
2. Attach air hydro test pump to pigging connection on receiver.
3. Completely fill the rig with clean potable water.
4. Vent any air from the highest port on the rig. Attach suitable plug.
5. Connect dry lubricated air supply to air hydro pump.
6. Slowly stroke the pump until 5 bar is reached, hold for 15 minutes. Visually check for leaks.
7. Continue to raise the pressure until 10 bar is reached. Visually check for leaks.
8. Hold for 15 minutes.
9. Check and adjust channel settings on the data logger so as they all read the same pressure and are reading 10 bar.
9. After the hold period, slowly release the test pressure via the valve on the pump.
10. Drain the test rig and remove the test equipment.

3.3 Cleaning

1. Open launcher door and insert 12" Medium Density PE RB Foam Pig.
2. Close the door and gravity fill behind the pig via the pigging hose.
3. Ensure the launcher is completely full and all air has been expelled via the vent.
4. Start the pigging pump and run idle for 5 minutes to warm the engine.
5. Close the by-pass valve and open the pigging valve.
6. Increase the pump revs to launch the pig.
7. Check the pig passage by noting the signaller flags.
8. Once the pig has tripped the signaller on the receiver, increase the revs on the pump to ensure the pig is fully into the receiving trap.
9. Close the pigging valve and open the drain valve.
10. Attach air supply to vent valve and push the water back to the break tank. Ensure the air pressure does not rise above 1 bar.
11. Fully vent any pressure from the rig.
12. Open the receiver door and recover the pig.
13. Close the receiver door.
14. Check for any damage to the pig.
15. Repeat as necessary.
16. Re-fit Perspex spool.

4.0 SCOPE OF TESTING

4.1 De-waxing Testing

Rig to be configured as per Drawing No PES 608 Scope 1 – De-waxing.

Test 1 – Setting flows and pigging speeds.

This set of initial testing will be to set pump revs and valve settings on the rig and by-pass on the pig to be used during other tests.

1. Set the iris plate on the rear of the pig to the predetermined mark where applicable. This mark is the initial starting point and has been calculated to give a flow of 5 litres per second at a pressure of 0.1 bar pigging pressure.
2. Open the closure door and insert the pig. Push with pig pusher pole on fork truck to seal in neck pipe.
3. Close the door and gravity fill behind the pig via the pigging hose.
4. Ensure the launcher is completely full and all air has been expelled via the vent. Close the pigging valve to ensure the pig is not allowed to be pushed backwards during filling of the rig.
5. Start the pigging pump and run idle for 5 minutes to warm the engine.
6. Gravity fill the rig in front of the pig by opening the drain valve on the receiver. Allow all air to be expelled via the vent on the receiver.
7. Start the data recorder.
8. Close the by-pass valve and open the pigging valve.
9. Increase the pump revs to launch the pig and set the required flow rate.
10. Check the pig passage by noting the signaller flags.
11. Once the pig has tripped signaller B, with a stopwatch, time the passage until the pig trips signaller C. This is a measured 10 M length and will indicate the pigging speed and flowrate.
12. Note the jetting action as the pig passes through the Perspex section. Use video capture for each run.
13. Once the pig has tripped the signaller on the receiver, increase the revs on the pump to ensure the pig is fully into the receiving trap.
14. Close the pigging valve and open the drain valve.
15. Attach air supply to vent valve and push the water back to the break tank. Ensure the air pressure does not rise above 1 bar.
16. Fully vent any pressure from the rig.
17. Open the receiver door and recover the pig.
18. Close the receiver door.
19. Check for any damage to the pig.

The above should be repeated until the pigging speed, the by-pass on the pig is correct and all operators are familiar with the operation.

Remove the Perspex section (Item 7) in preparation for wax application

4.2 Wax Mixing and Application – General

The wax will be formed by mixing a micro-crystalline wax with a macro-crystalline paraffin wax. This is then added to a light white paraffin based oil. The oil will be heated to an approximate temperature of 80° C. The micro and macro crystalline mixture will then be added to form the wax mixture. Once the mixture is fully liquefied, the heat will be removed and the mixture will then be allowed to cool to around 60° C before being applied to the internal pipewall of the Perspex tube and steel spool section. This will

then solidify as the mixture cools, leaving an even coating of 'wax' in preparation for the de-waxing test.

Varying viscosities of the 'wax' will be tried by adjusting the amount of wax mixture added to the oil.

In all tests the thickness of wax applied to the tube will be approximately 15mm. The length of tube coated will be 900 to1000mm.

Prior to mixing and applying the wax mixture, the Perspex spool will be set up on powered rollers and with polyurethane discs fitted 900 to 1000mm apart as per the sketch Figure 1 below.

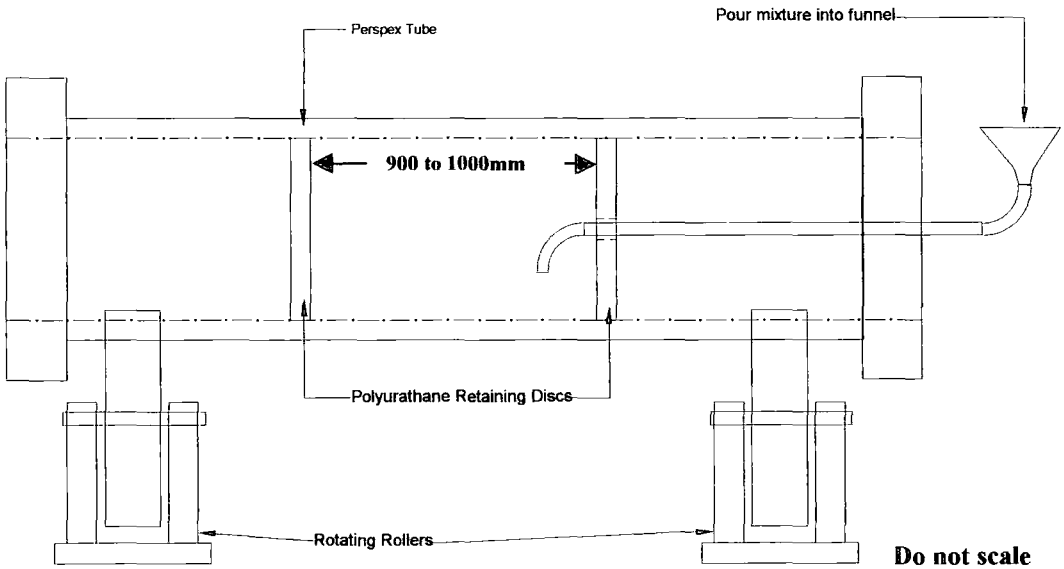

Figure 1

The discs have a slight interference fit on the inside of the Perspex tube. The filling hose, which passes through the hole in the disc, may be rubber or plastic.

4.3 Mixing – Change ratios for more or less viscous mixtures.

1. Add 0.92 ltr per 100mm of 291.3mm I/D pipe to be coated, to a large clean metallic container.
2. Heat the oil to 80° C.
3. Mix 0.19 ltr macro-crystalline paraffin wax and 0.19 ltr micro-crystalline wax and add this to the oil.
4. Once the wax has fully dissolved, stir well and remove the mixture from the heat
5. Allow the mixture to cool to 60° C before proceeding to the application.

The above gives a 70/30 mixture. This is the base case.

4.4 Application

1. Start the motor on the powered rollers. The rotation speed is 12 RPM.
2. Slowly pour the mixture into the annulus via the funnel and the hose.
3. Once all the mixture has been poured into the annulus, remove the funnel and hose.
4. The mixture will start to solidify at around 40° C.
5. Allow the tube to turn on the rollers until the liquid has fully solidified.

6. Once the mixture has set. Pour cold water onto the outside of the tube in the area of the wax deposit to fully harden and cool the wax.
7. Stop the rotation and remove the spool from the roller assembly.
8. Carefully remove the polyurethane retaining discs from the inside of the tube.
9. Leave for a further 30 minutes prior to using.
10. Re-fit to the main test rig

5.0 De-waxing Test Procedure

5.1 Scope 1 - De-waxing Test

Test 2 – Observation of de-waxing in Perspex spool.

1. Check the iris plate on the rear of the pig is set to the predetermined mark where applicable.
2. Open the closure door and insert the pig. Push with pig pusher pole on fork truck to seal in neck pipe.
3. Close the door and gravity fill behind the pig via the pigging hose.
4. Ensure the launcher is completely full and all air has been expelled via the vent. Close the pigging valve to ensure the pig is not allowed to be pushed backwards during filling of the rig.
5. Start the pigging pump and run idle for 5 minutes to warm the engine.
6. Gravity fill the rig in front of the pig by opening the drain valve on the receiver. Allow all air to be expelled via the vent on the receiver.
7. Start the data recorder.
8. Close the by-pass valve and open the pigging valve.
9. Increase the pump revs to launch the pig.
10. Check the pig passage by noting the signaller flags.
11. Once the pig has tripped signaller B, with a stopwatch, time the passage until the pig trips signaller C. This is a measured 10 M length and will ensure the pigging speed is correct.
12. Note the jetting action and the removal of the wax as the pig passes through the Perspex section. Video capture each run.
13. Once the pig has tripped the signaller on the receiver, increase the revs on the pump to ensure the pig is fully into the receiving trap.
14. Close the pigging valve and open the drain valve.
15. Attach air supply to vent valve and push the water back to the break tank. Ensure the air pressure does not rise above 1 bar.
16. Fully vent any pressure from the rig.
17. Open the receiver door and recover the pig.
18. Close the receiver door.
19. Check for any damage to the pig.

Repeat as necessary with differing profiled jetting discs and through body by-pass rates.

Test 3 – De-waxing in steel spool observation of wax suspension.

Remove spool Item 6. Apply wax as for the Perspex section.

Re-fit the spool in the rig.

1. Check the iris plate on the rear of the pig is set to the predetermined mark where applicable.
2. Open the closure door and insert the pig. Push with pig pusher pole on fork truck to seal in neck pipe.
3. Close the door and gravity fill behind the pig via the pigging hose.
4. Ensure the launcher is completely full and all air has been expelled via the vent. Close the pigging valve to ensure the pig is not allowed to be pushed backwards during filling of the rig.
5. Start the pigging pump and run idle for 5 minutes to warm the engine.
6. Gravity fill the rig in front of the pig by opening the drain valve on the receiver. Allow all air to be expelled via the vent on the receiver.
7. Start the data recorder.
8. Close the by-pass valve and open the pigging valve.
9. Increase the pump revs to launch the pig.
10. Check the pig passage by noting the signaller flags.
11. Once the pig has tripped signaller B, with a stopwatch, time the passage until the pig trips signaller C. This is a measured 10 M length and will ensure the pigging speed is correct.
12. Note the jetting action and the wax in suspension, which has been removed from the previous spool (Item 6) as the pig passes through the Perspex section.
13. Once the pig has tripped the signaller on the receiver, increase the revs on the pump to ensure the pig is fully into the receiving trap.
14. Close the pigging valve and open the drain valve.
15. Attach air supply to vent valve and push the water back to the break tank. Ensure the air pressure does not rise above 1 bar.
16. Fully vent any pressure from the rig.
17. Open the receiver door and recover the pig.
18. Close the receiver door.
19. Check for any damage to the pig.

Repeat any or all of the above as necessary.

5.2 Scope 2 – General Piggability.

Rig to be configured as per Drawing No PES 608 Scope 2 – General Piggability.

To test for pigging pressures in the varying internal diameters and de-waxing in the largest internal diameter.

After re-configuring the rig, carry out hydro-test and a cleaning run as in 3.0 above. Then continue on to-:

Test 4 – General Piggability.

1. Check the iris plate on the rear of the pig is set to the predetermined mark where applicable.
2. Open the closure door and insert the pig. Push with pig pusher pole on fork truck to seal in neck pipe.
3. Close the door and gravity fill behind the pig via the pigging hose.
4. Ensure the launcher is completely full and all air has been expelled via the vent. Close the pigging valve to ensure the pig is not allowed to be pushed backwards during filling of the rig.
5. Start the pigging pump and run idle for 5 minutes to warm the engine.
6. Gravity fill the rig in front of the pig by opening the drain valve on the receiver. Allow all air to be expelled via the vent on the receiver.
7. Start the data recorder.
8. Close the by-pass valve and open the pigging valve.
9. Increase the pump revs to launch the pig.
10. Check the pig passage by noting the signaller flags.
11. Once the pig has tripped the signaller on the receiver, increase the revs on the pump to ensure the pig is fully into the receiving trap.
12. Close the pigging valve and open the drain valve.
13. Attach air supply to vent valve and push the water back to the break tank. Ensure the air pressure does not rise above 1 bar.
14. Fully vent any pressure from the rig.
15. Open the receiver door and recover the pig.
16. Close the receiver door.
17. Note the differing pressures as the pig has passed through the differing I/D's.

Check for any damage to the pig

Repeat as necessary.

Test 5 – Large volume wax removal.

Remove the 12 M spool (Item 8) and set up on rollers as for wax application. Set one end slightly higher and then pour in the liquid wax. The spool should be at ambient air temperature, so the wax starts to set on contact with the pipe wall. As much wax as possible should be applied along the complete length of the spool. Re-assemble into the rig.

Configure the hose system so as to launch the pig from the receiver. So then the launcher becomes the receiver. This is so that the wax in suspension can be seen in the Perspex spool which is directly after the 12 M spool.

1. Check the iris plate on the rear of the pig is set to the predetermined mark where applicable.
2. Open the closure door and insert the pig. Push with pig pusher pole on fork truck to seal in neck pipe.

3. Close the door and gravity fill behind the pig via the pigging hose.
4. Ensure the launcher is completely full and all air has been expelled via the vent. Close the pigging valve to ensure the pig is not allowed to be pushed backwards during filling of the rig.
5. Start the pigging pump and run idle for 5 minutes to warm the engine.
6. Gravity fill the rig in front of the pig by opening the drain valve on the receiver. Allow all air to be expelled via the vent on the receiver.
7. Start the data recorder.
8. Close the by-pass valve and open the pigging valve.
9. Increase the pump revs to launch the pig.
10. Check the pig passage by noting the signaller flags.
11. Once the pig has tripped signaller B, with a stopwatch, time the passage until the pig trips signaller C. This is a measured 10 M length and will ensure the pigging speed is correct.
12. Note the jetting action and the wax in suspension, which has been removed from the previous spool (Item 8) as the pig passes through the Perspex section.
13. Once the pig has tripped the signaller on the receiver, increase the revs on the pump to ensure the pig is fully into the receiving trap.
14. Close the pigging valve and open the drain valve.
15. Attach air supply to vent valve and push the water back to the break tank. Ensure the air pressure does not rise above 1 bar.
16. Fully vent any pressure from the rig.
17. Open the receiver door and recover the pig.
18. Close the receiver door.

Repeat as necessary.

Check for any damage to the pig.

5.3 Foam Pig Rescue

Test 6 – Foam pig rescue

Re-configure the hose system as for the initial tests ie Launcher is launcher etc.

Recover as much of the wax debris as possible from the filter basket and push this into the launcher and first spool. This is to simulate a wax plug in front of the rescued pig attempting to create a realistic wax build up scenario. This applies to the standard pig and the low flow wax removal pig.

1. Check the iris plate on the rear of the pig is set to the predetermined mark. Where applicable.
2. Open the closure door and insert the pig. Push with pig pusher pole on fork truck as far as possible into spool Item 2.
3. Insert the ribbed foam pig and push with the pig pusher pole on the fork truck to seal in the neck pipe.
4. Close the door and gravity fill behind the foam pig via the pigging hose.
5. Ensure the launcher is completely full and all air has been expelled via the vent. Close the pigging valve to ensure the foam pig is not allowed to be pushed backwards during filling of the rig.
6. Start the pigging pump and run idle for 5 minutes to warm the engine.
7. Gravity fill the rig in front of the pig by opening the drain valve on the receiver. Allow all air to be expelled via the vent on the receiver.
8. Start the data recorder.
9. Close the by-pass valve and open the pigging valve.
10. Increase the pump revs to launch the foam pig.

11. Check the pig passage by noting the signaller flags.
12. Once the pig has tripped signaller B, with a stopwatch, time the passage until the pig trips signaller C. This may differ from previous as the train is now two pigs and a large amount of wax.
13. Note the position of the foam pig as it pushes the wax removal pig and note if the wax is in suspension in front of the wax removal pig which has been removed from spool (Item 2) as the pig passes through the Perspex section.
14. Once the pig has tripped the signaller on the receiver, increase the revs on the pump to ensure the pig train is fully into the receiving trap.
15. Close the pigging valve and open the drain valve.
16. Attach air supply to vent valve and push the water back to the break tank. Ensure the air pressure does not rise above 1 bar.
17. Fully vent any pressure from the rig.
18. Open the receiver door and recover the pigs.
19. Close the receiver door.

Check for any damage to either of the pigs

Repeat as necessary.

6.0 WAX DISPOSAL

The wax will be filtered out of the flow before the return flow enters the break tank. This will be via an open filter, so as the wax cuttings may be inspected to check on cut angles etc. After the wax cuttings have been removed from the filter/strainer, they will be placed in barrels for disposal. The waste is un-controlled and has been classed as non-hazardous.

7.0 REPORTING, COMMUNICATIONS AND RECORDS

7.1 Reporting

The PE Test Supervisor will produce a report. The report covering the operation will be submitted to KBR for review.

7.2 Records

All records will be witnessed and signed, as a minimum by the Client Representative.

A Daily Operations Log will be maintained and will be used to record events relevant to the tests taking place. (Appendix 1)

These logs will form part of the PE report and will be included in the final report.

7.3 Instrument Calibration

For all instruments used during the hydrotest and tests, copies of their calibration certificates will be available to KBR. These shall be calibrated within 6 months prior to use.

8.0 TEMPORARY RIG DRAWINGS

8.1 Test Rig General Arrangement

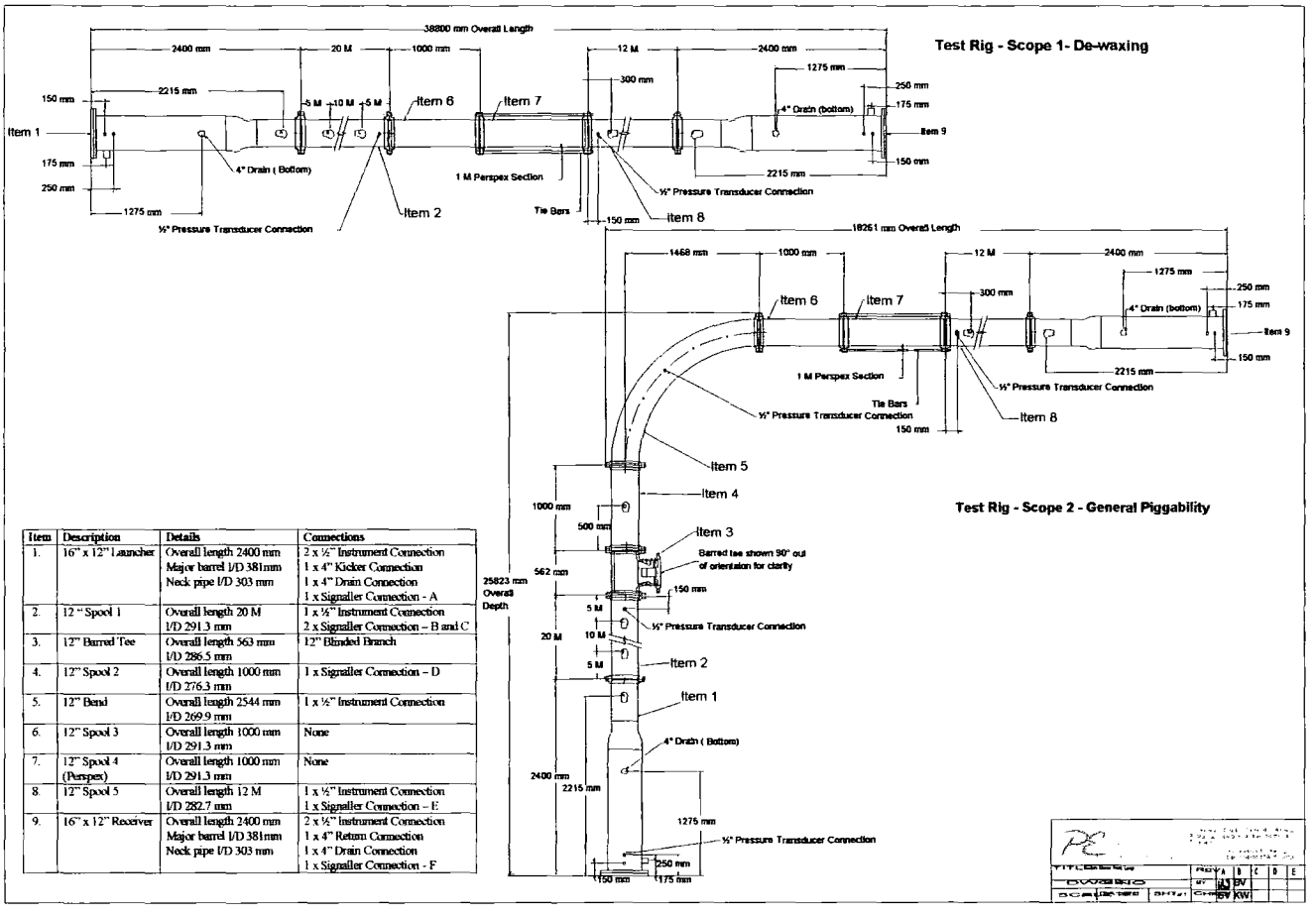

Item	Description	Details	Connections
1.	16" x 12" Launcher	Overall length 2400 mm Major barrel I/D 381mm Neck pipe I/D 303 mm	2 x ½" Instrument Connection 1 x 4" Kicker Connection 1 x 4" Drain Connection 1 x Signaller Connection - A
2.	12 " Spool 1	Overall length 20 M I/D 291.3 mm	1 x ½" Instrument Connection 2 x Signaller Connection – B and C
3.	12" Barred Tee	Overall length 563 mm I/D 286.5 mm	12" Blinded Branch
4.	12" Spool 2	Overall length 1000 mm I/D 276.3 mm	1 x Signaller Connection – D
5.	12" Bend	Overall length 2544 mm I/D 269.9 mm	1 x ½" Instrument Connection
6.	12" Spool 3	Overall length 1000 mm I/D 291.3 mm	None
7.	12" Spool 4 (Perspex)	Overall length 1000 mm I/D 291.3 mm	None
8.	12" Spool 5	Overall length 12 M I/D 282.7 mm	1 x ½" Instrument Connection 1 x Signaller Connection – E
9.	16" x 12" Receiver	Overall length 2400 mm Major barrel I/D 381mm Neck pipe I/D 303 mm	2 x ½" Instrument Connection 1 x 4" Return Connection 1 x 4" Drain Connection 1 x Signaller Connection - F

8.2 Test Loop Schematic

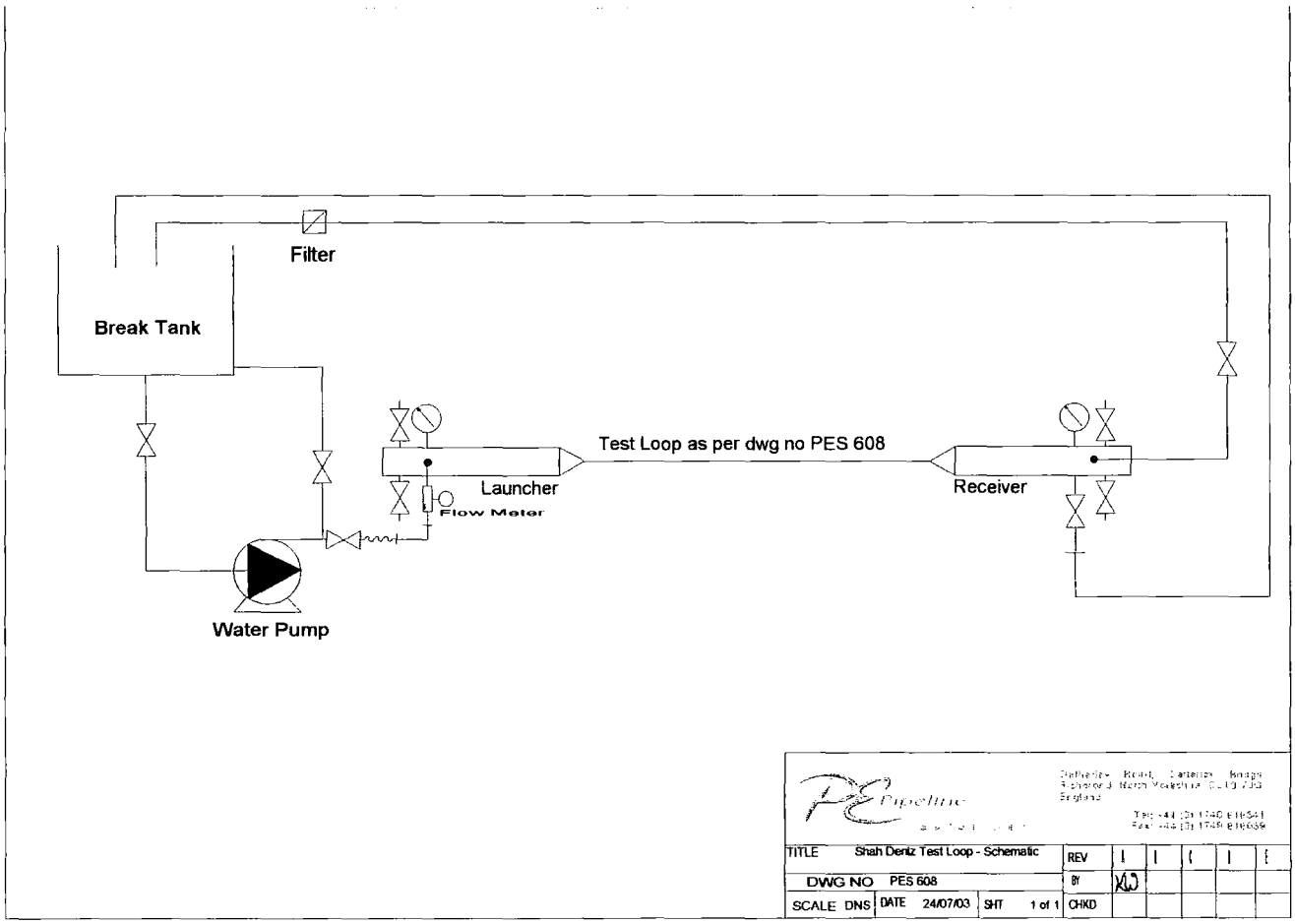

10.0 Daily Test Report Proforma.

Pipeline Engineering – Daily Report			**Client-:**	
Report No-:		**Operator Name-:**		
Date-:		**III.** SITE-INSTALLATION-:		
Local Weather	**AM**		**PM**	
Signature – Please sign.			PE Operator	
Client			Position	

Appendix F. Pitot tube measurements

1 Objectives

The aim of the Pitot tube measurements was to obtain a velocity profile for the wall jet used to remove wax in the tests described in chapter 5. Most importantly, it was necessary to quantify the rate of deceleration of the jet close to the pipe wall, where it would impinge on the wax deposit.

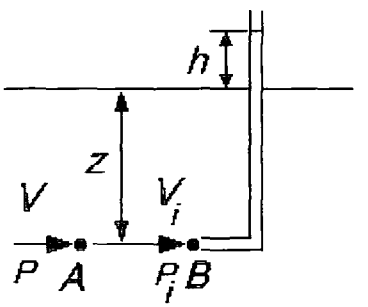

Figure 1.Pitot tube

A Pitot tube is an 'L' shaped tube that is inserted into a fluid stream such that the 'impact hole' at the end faces the oncoming flow. If V and P are the velocity and pressure of the fluid at point A in a fluid stream (figure 1) then V_i and P_i are the velocity and pressure of the same fluid at point B (the 'impact hole') where it is brought to rest. At point B, the velocity of the fluid is zero and the pressure in the Pitot tube is increased. In theory, no energy is lost and applying Bernoulli's equation,

$$\frac{V^2}{2g}+\frac{P}{\rho g}=\frac{V_i^2}{2g}+\frac{P_i}{\rho g} \qquad \textit{equation 1}$$

The velocity at point B is zero, therefore,

$$\frac{P_i}{\rho g} = \frac{V^2}{2g} + \frac{P}{\rho g} \qquad \textit{equation 2}$$

$$\frac{V^2}{2g} = \frac{P_i - P}{\rho g} = h \qquad \textit{equation 3}$$

The velocity at point A is therefore,

$$V = \sqrt{2gh} \qquad \textit{equation 4}$$

2 Experimental Equipment and Procedure

The rectangular pipe section, described in section 5, was modified to allow the insertion of a 5mm diameter Pitot tube through a two-part brass gland and 'o' ring. The 'o' ring was held within the gland in the same manner as an 'olive' in a compression fitting, sealing against the pitot tube and holding it in position. This arrangement allowed the Pitot tube to slide in the vertical plane with the gland unlocked. Pressure readings were taken from the Pitot tube using an aneroid pressure gauge. An identical gauge was used to take pressure readings at a tapping flush to the pipe wall and vertically aligned to the mouth of the Pitot tube. Measurements of pressure were taken at horizontal increments of 50mm and vertical increments of 5mm, as indicated by the node points in figure 1.

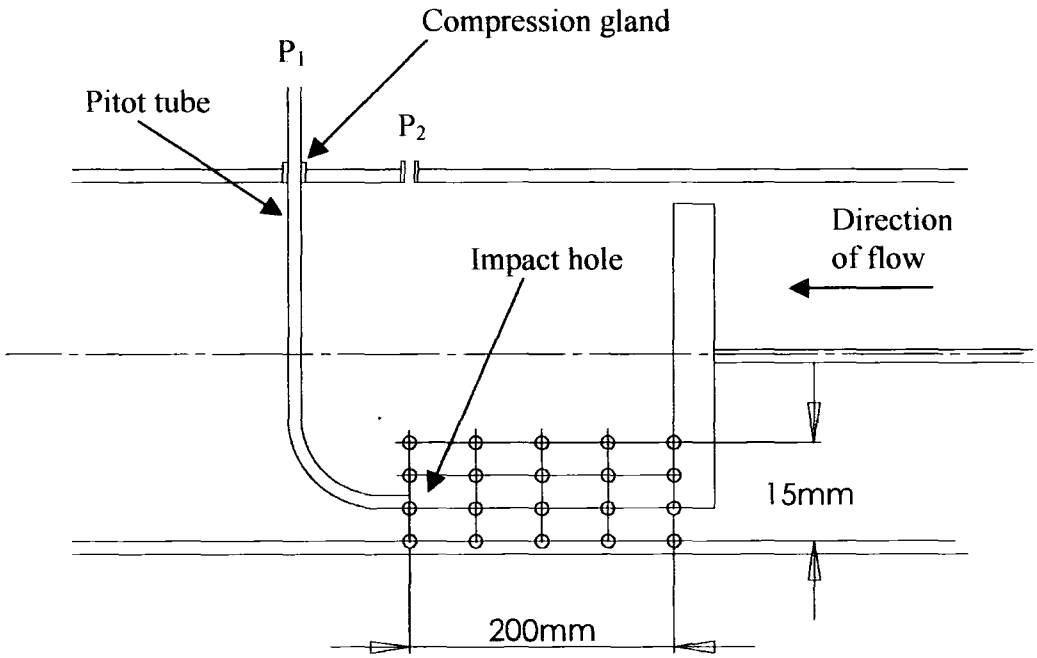

Figure 1. Arrangement of pitot tube and test plate.

1.3 Results of Pitot Tube Measurements

The results of the Pitot tube measurements are shown in graphical form in figure 5.65.5 (Page 167) in chapter 5.

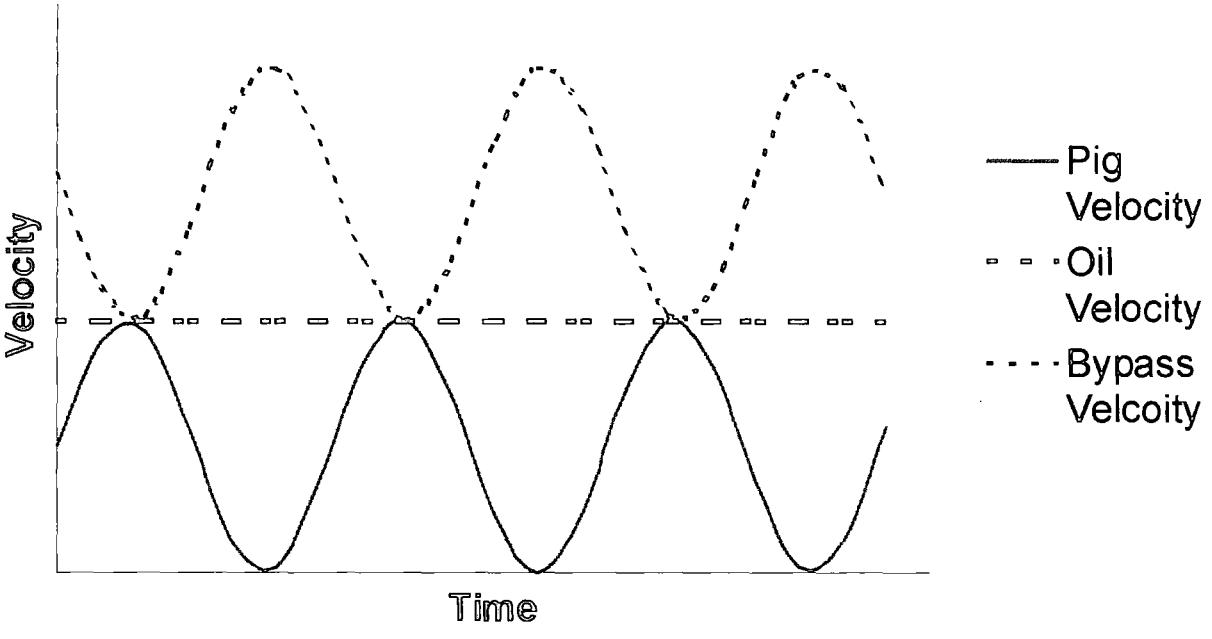

Figure 1. Pig, Oil and Bypass velocity plotted against time.

The development of a passive speed governor for a pressure driven pig that is not reliant on bypass might greatly improve the general applicability of the jetting system. Perhaps the most promising concept for such a device would employ intermittent bypass allowing the pig to 'nibble' its way along a pipe without ever actually contacting the wax deposit. An annular bypass pig that could alternate between the conditions of 100% bypass and zero bypass might achieve this 'nibbling' action. The performance of such a system is illustrated by figure 1, a plot of pig velocity against time. While the pig has no bypass, it travels with the mean velocity of the oil in the pipeline. As the pig has a high differential pressure across it due to friction, it rapidly decelerates when the annular bypass opens. At this point the ratio of bypass velocity to pig velocity is very high and conditions are favourable for wax removal by the annular bypass jet. When the bypass

closes again and the pig begins to accelerate, it is moving into a region of pipe that it has just cleared of wax, thus avoiding the risk of contact between the pig and the deposit.

A possible design for a pig that produces intermittent annular bypass is shown in figure 2. The pig uses a bypass shut-off system that is essentially a 'poppet' valve. Unlike the poppet valves used to open the ports of an internal combustion engine however, it is envisaged that a configuration would be used that would encourage oscillation or 'bounce' of the valve. In this way the pig would be a passive device that alternated between states of bypass and no bypass as it progressed along a pipe. Figure 2 shows the pig in its open, bypassing stage (A) and its closed, no bypass state (B). Such a device would have an added advantage in that the central shaft varying the valve stopper would be automatically closed on impact with a high strength deposit allowing the pig full drive from the pipe-line fluid.

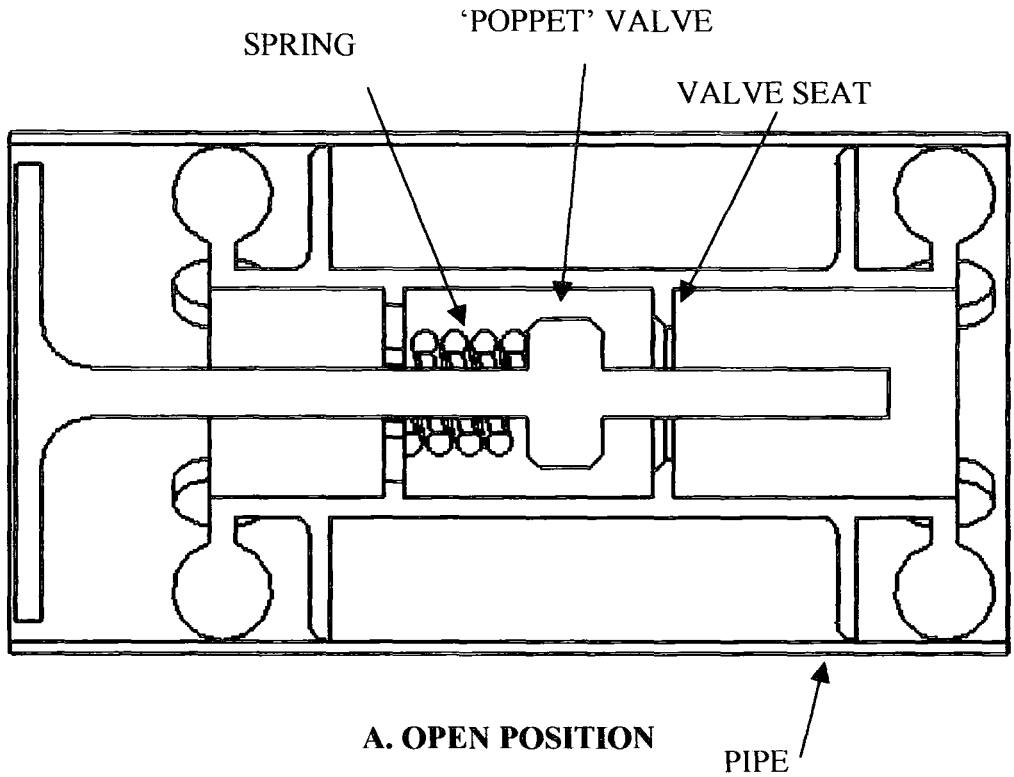

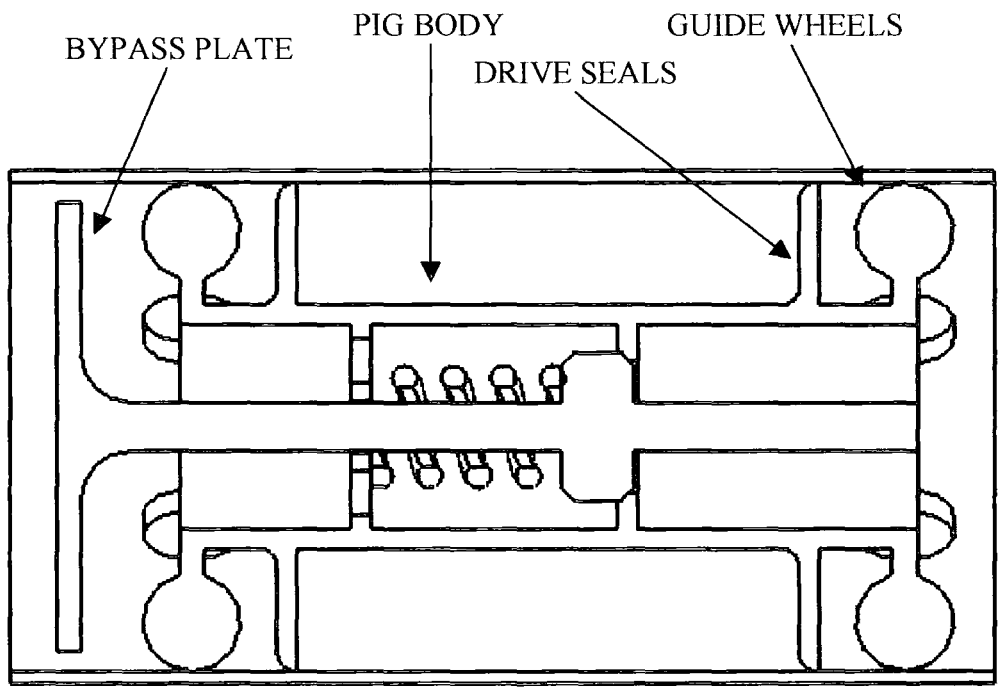

Figure 2. Intermittent annular bypass concept pig shown in open (A) and closed positions (B)

Appendix H

Shell Vitrea Oils

Premium quality industrial oils

Shell Vitrea Oils are premium quality, solvent refined, high viscosity index mineral oils specially chosen for their ability to provide superior lubrication in a wide range of industrial applications.

Applications

- Plain and rolling element bearings
- Enclosed spur, helical, bevel & worm gear-boxes where a non-additive mineral oil is approved by the gear manufacturer
- Machine tool circulatory systems
- High-speed spindle lubricant (Shell Vitrea Oil 9)

Shell Vitrea Oils may be used in industrial applications where loadings and temperatures are moderate

Performance Features

- Good oxidation and thermal stability
  Natural resistance to the formation of sludge and other harmful products of oxidation. Long oil life
- High viscosity index
  Minimal change of oil viscosity over the operating temperature range. (Shell Vitrea Oil 9 is a naphthenic oil with a low viscosity index)
- Water shedding properties
  Shell Vitrea Oils have excellent water separation properties. Excess water can be drained easily from lubrication systems. (Water can greatly accelerate surface fatigue on gear and bearing interfaces and promote ferrous corrosion on all internal surfaces. Water contamination should be avoided or removed as quickly as possible after the occurrence.)

Performance Specifications

Morgan Construction Co. - Morgoil roll neck bearings

Seal Compatibility

Shell Vitrea Oils are compatible with all normal mineral oil seal materials. This includes Nitrile and Butyl rubbers, Neoprene, Viton etc., where minimal swell and hardness are required in service

Health & Safety

Shell Vitrea Oils are unlikely to present any significant health or safety hazard when properly used in the recommended application, and good standards of industrial and personal hygiene are maintained.

For further guidance on Product Health & Safety refer to the appropriate Shell Product Safety Data Sheet. This can be obtained from your own internal Health & Safety focal point. In the event of any queries contact your local Shell Business Development Manager or:

Normal Office Hours
Shell UK Oil Products Ltd
Delta House
Wavell Road
Wythenshawe
Manchester M22 5SB
Tel: 0161 499 4000

Emergencies
Shell UK Oil Products Ltd
Shell Centre
London
SE1 7NA

Tel: 020 7934 1234

Advice

Advice on applications not covered in this leaflet may be obtained from your Shell Business Development Manager.

Typical Physical Characteristics

Shell Vitrea Oil	**9**	**22**	**32**	**46**	**68**	**M100**	**M150**	**M220**	**M320**	**M460**	**M570**	**M680**
Viscosity Grade	9	22	32	46	68	100	150	220	320	460	570	680
(ISO 3448)												
Kinematic Viscosity												
@ 40 °C cSt	8.3	22	32	46	68	100	150	220	320	460	570	680
100 °C cSt	2.2	4.2	5.4	6.8	8.8	11.2	14.8	19.2	24.6	31.0	32.0	37.0
(IP 71)												
Viscosity Index												
(IP 226)	53	80	100	100	95	95	95	95	95	95	80	80
Density @ 15 °C kg/l												
(IP 365)	0.869	0.866	0.868	0.873	0.881	0.877	0.882	0.887	0.891	0.896	0.902	0.910
Pour Point °C	-39	-18	-12	-9	-9	-9	-6	-6	-6	-6	-6	-6
(IP 15)												
Flash Point °C												
(PMCC)	141	204	222	228	223	225	243	249	255	260	265	270
(IP 34)												

These characteristics are typical of current production. Whilst future production will conform to Shell's specification, variations in these characteristics may occur.

(Published by Shell Oils, Delta House, Wavell Road, Wythenshawe, MANCHESTER M22 5SB)